



**Intrinsic and extrinsic regulation
of receptor tyrosine kinase signaling
for axon growth and guidance**

Dissertation zur Erlangung des Doktorgrades

Der Naturwissenschaften

an der Fakultät für Biologie

der Ludwig-Maximilians-Universität München

Graziana Gatto

Intrinsic and extrinsic regulation
of receptor tyrosine kinase signaling
for axon growth and guidance

**Dissertation zur Erlangung des Doktorgrades
Der Naturwissenschaften**

der Fakultät für Biologie der Ludwig-Maximilians-Universität
München

Graziana Gatto

1. Gutachter: Prof. Dr. Rüdiger Klein
2. Gutachter: Prof. Dr. Barbara Conradt

Tag der Einreichung: 16.04.2013

Tag der mündlichen Prüfung: 18.09.2013

The work presented in this dissertation was performed in the laboratory of Prof. Dr. Rüdiger Klein, Department of Molecules – Signaling – Development, Max-Planck-Institute of Neurobiology, Martinsried, Germany.

Eidesstattliche Erklärung

Ich versichere hiermit an Eides Statt, dass die vorgelegte Dissertation von mir selbständig und ohne unerlaubte Hilfe angefertigt ist.

München, den 16.04.2013

Graziana Gatto

Erklärung

Hiermit erkläre ich, dass die Dissertation nicht ganz oder in wesentlichen Teilen einer anderen Prüfungskommission vorgelegt worden ist und ich mich anderweitig einer Doktorprüfung ohne Erfolg nicht unterzogen habe.

München, den 16.04.2013

Graziana Gatto

Publications from the work presented in this dissertation

Gatto G, Dudanova I, Suetterlin P, Davies AM, Drescher U, Bixby JL, Klein R

Protein Tyrosine Phosphatase Receptor Type O Inhibits Trigeminal Axon Growth and Branching by Repressing TrkB and Ret Signaling

J.Neurosci 2013 March 20; 33(12):5399-410

Dudanova I, Gatto G, Klein R

GDNF acts as a chemoattractant to support ephrinA-induced repulsion of limb motor axons

Current Biology 2010 December 7; 20(23): 2150-6

To my dear grandmother Graziella in loving memory

*"It is the rule rather than the exception
in research that new leads come
from accidental findings and these leads,
when followed, would channel
the investigation into a new direction."*

(cit. Rita Levi-Montalcini)

Acknowledgements

First I would like to thank my supervisor Ruediger Klein for giving me the opportunity to work in such a great scientific environment, and for giving me the freedom to develop my own ideas. Thank you for your constant and unreserved support and for helping me to mature as a scientist.

Ringrazio i miei genitori e le mie nonne per il sostegno e la fiducia che mi hanno dato e continueranno a darmi, e soprattutto perché tutto ciò che ho e che sono diventata lo devo a loro.

I am grateful to Alun Davies for kindly teaching me how to culture trigeminal neurons, and to Philipp Suetterlin and Uwe Drescher for performing the retinotopic tracings. I thank the members of my thesis advisory committee: Andrea Huber and Takashi Suzuki, for their support, their intellectual input and their continuous interest in my work.

I would like to thank Irina Dudanova for introducing me to the motor neuron world patiently teaching me all the related techniques, and for our great collaboration over the years; and Sónia Paixão for introducing me to the spinal cord and adult brain world, and for the effort to teach me in Italian the related techniques.

My special thanks go to Ilona Kadow, Archana Mishra, Dani del Toro, Irina Dudanova, Sónia Paixão, Falko Hampel, Laura Loschek, Alessandro Filosa, Thomas Gaitanos, Pontus Klein, Daniel Nagel and Jingyi Gong for their support, their input, for teaching me several techniques and for all the critical discussions. I would like to thank Louise Gaitanos, Pilar Alcalá and Jana Lindner for their help and for keeping the lab an organized and functional place; Daria Marinescu, Stephanie Krinner and Diana Haba-Schneider for helping me handle the mouse colony. I wish to thank Irina Dudanova and Louise Gaitanos for critically reading my thesis. I would also like to acknowledge the IMPRS coordination office, for their continuous support. Finally, I would like to thank all the present and past members of the Klein lab for the nice and stimulating working atmosphere.

My sincerest thanks go to Børk, for being the patient target of my quotidian sarcasm; to Dr. Leidenschaft for being my personal driver and my PR; to God and his wife, for introducing me to the joy of Pizza Hawaii; to Fragile Flower for constantly improving his

six pack; to Don Falcone, for showing me that is possible to be happy every single day of your PhD; to the Hulk, for competing with me in G&T consumption; to BamBamDonia, for being such beautiful people; to the Belgian for rocking the dance floor; and to Pizzeria Europa, for feeding me and Dr. Leidenschaft every Thursday night. Finally I would like to thank all the friends with whom I shared happy, sad, complaining, funny or silly moments over the last few years.

Table of Contents

Abbreviations.....	VI
List of Figures.....	X
Abstract.....	XII
1. Introduction.....	1
1.1. Receptor Tyrosine Kinases: an overview	2
1.1.1. Neurotrophin/Trk receptor signaling.....	3
1.1.1.1. Neurotrophin/Trk signaling for neuron survival	6
1.1.1.2. Other neurotrophin/Trk functions in the central and peripheral nervous system.....	8
1.1.2. Ret/GDNF signaling.....	10
1.1.2.1. GDNF, Ret and GFR α 1: mouse models.....	12
1.1.2.2. GDNF, Ret and GFR α 1 functions in the central and peripheral nervous systems	13
1.1.2.3. GDNF and Ret can signal independently of each other	15
1.1.3. Eph/ephrin signaling.....	16
1.1.3.1. Distinctive features of Eph signaling	19
1.1.3.2. Eph receptor functions during embryonic development and in adulthood.....	22
1.2. Neuron development: Axon growth and guidance	27
1.2.1. Trigeminal neurons.....	28
1.2.2. Motor neurons of the lateral motor columns	31
1.3. Intrinsic mechanisms to regulate RTKs signaling	34
1.3.1. Keeping the phosphotyrosine balance: RPTPs versus RTKs	36
1.3.1.1. PTPRO regulation of Trk and Eph receptors	38
1.3.2. Shedding regulates receptor expression and signaling.....	39
1.3.3. Cooperation of guidance cues and receptor cross-talk.....	42
1.4. Purpose of thesis project.....	44
2. Results.....	45
2.1. PTPRO's role during development.....	45
2.1.1. PTPRO's developmental expression pattern.....	45
2.1.2. E11.5 and E12.5 <i>PTPRO</i> ^{-/-} embryos have bigger and more complex TG arbors.....	51

2.1.3. Cultured E12.5 <i>PTPRO</i> ^{-/-} TG neurons display increased sensitivity to BDNF and GDNF, but not NGF.....	54
2.1.4. Cultured P1 <i>PTPRO</i> ^{-/-} TG neurons do not display increased sensitivity to BDNF and GDNF.....	58
2.1.5. The exuberant growth and branching observed in <i>PTPRO</i> ^{-/-} embryos and neurons are not due to alterations in cell fate or survival.	60
2.1.6. PTPRO regulates TrkB and Ret signaling.....	63
2.1.7. PTPRO does not regulate Eph receptors in the developing TG ganglion.....	68
2.1.8. PTPRO is dispensable as Eph-regulator in LMC axon guidance.....	69
2.1.9. PTPRO is not required for retinotectal mapping in mouse.....	72
2.1.10. The chick but not the mouse isoform of PTPRO can dephosphorylate EphA4.....	73
2.2. Role of EphA4 cleavage during development.....	74
2.2.1. EphA4 is cleaved in Hela and HEK293 cells, independently of ligand stimulation.....	74
2.2.2. EphA4 shedding during embryonic development is temporally and spatially regulated.....	77
2.2.3. Identification of the EphA4 cleavage site.....	80
2.2.4. <i>In vitro</i> characterization of the EphA4 ^{CR} mutant.....	82
2.2.5. Generation of the EphA4 ^{CR} knock-in mouse.....	84
2.2.6. EphA4 expression in <i>EphA4</i> ^{CR/CR} embryos.....	86
2.2.7. EphA4 shedding is required for LMC _L neuron axon guidance.....	89
2.2.8. EphA4 shedding is dispensable for dorsal funiculus and anterior commissure formation.....	91
2.3. Receptor cross-talk during development.....	93
2.3.1. EphA4 and Ret do not interact in LMC neurons.....	93
2.3.2. EphA4 signaling is not impaired in <i>Ret</i> ^{-/-} mice.....	96
2.3.3. GDNF and ephrinAs cooperate in Motor Axon Turning.....	98
3. Discussion.....	99
3.1. Roles of RPTPs during development.....	100
3.1.1. Regulation and specificity of the phosphatase activity.....	101
3.1.2. Non cell-autonomous role of PTPRO.....	103
3.1.3. PTPRO as a potential therapeutic target.....	105
3.2. How does receptor cleavage regulate axon guidance decisions?.....	106
3.2.1. Potential molecular mechanisms leading to LMC _L misguidance in <i>EphA4</i> ^{CR/CR} embryos.....	109

3.2.2. What triggers EphA4 cleavage?	112
3.2.3. EphA4 cleavage in neurodegenerative diseases	113
3.3. Guidance cue integration	115
3.3.1. Additive and non-additive effects of guidance cues	115
4. Materials and Methods.....	117
4.1. Chemicals and drugs.....	117
4.2. Reagents.....	117
4.2.1. Plasmids.....	117
4.2.2. Oligonucleotides.....	118
4.2.3. Cloning primers.....	118
4.2.4. Genotyping primers.....	119
4.2.5. Primary antibodies.....	120
4.2.6. Secondary antibodies.....	121
4.2.7. Cell lines.....	121
4.2.8. Media.....	122
4.2.8.1. Luria-Bertani (LB) medium	122
4.2.8.2. LB plates.....	122
4.2.8.3. Cell culture media	122
4.2.9. Primary culture reagents.....	122
4.2.10. Primary culture media	123
4.2.11. Buffers and Solutions	124
4.2.12. Mouse lines.....	128
4.3. Methods.....	129
4.3.1. Molecular Biology.....	129
4.3.1.1. Preparation of plasmid DNA.....	129
4.3.1.2. Transformation of competent <i>E. coli</i> by electroporation	129
4.3.1.3. Site-direct mutagenesis.....	129
4.3.1.4. TOPO cloning.....	130
4.3.1.5. Tail DNA preparation and genotyping using PCR.....	130
4.3.1.6. Agarose gel electrophoresis.....	131
4.3.2. Cell culture.....	132
4.3.2.1. Propagation, thawing and freezing of mammalian cells	132
4.3.2.2. Transfection of cell lines using Lipofectamine	132
4.3.2.3. Primary culture of dissociated mouse trigeminal neurons	133

4.3.2.4. Explant of trigeminal neurons	134
4.3.2.5. Primary culture of dissociated mouse motor neurons	134
4.3.2.6. Explant culture of mouse motor neurons	135
4.3.2.7. Primary culture of dissociated cortical neurons	136
4.3.3. Biochemistry	136
4.3.3.1. Cell lysis and immunoprecipitation of proteins	136
4.3.3.2. Immunoblotting.....	137
4.3.4. Immunofluorescence	137
4.3.5. Mouse work.....	138
4.3.6. Histology.....	138
4.3.6.1. Cryostat sections.....	138
4.3.6.2. Whole mount Neurofilament staining	139
4.3.6.3. Staining of tissue sections	139
4.3.6.4. Labeling of explant cultures and dissociated motor neurons	140
4.3.6.5. Motor neuron retrograde tracings.....	140
4.3.7. Generating <i>EphA4</i> ^{CR/CR} knock-in mouse	141
4.3.7.1. Cloning.....	141
4.3.7.2. ES cells culture and DNA electroporation	141
4.3.7.3. DNA extraction	142
4.3.7.4. Southern Blot.....	142
5. Bibliography.....	144
6. Curriculum vitae.....	173



Abbreviations

°C	degree Celsius
aAC	anterior AC
AC	anterior commissure
ADAM	A disintegrin and metalloprotease
APP	amyloid precursor protein
APS	ammonium persulfate
ARTN	artemin
Bax	Bcl-2 associated X protein
BDNF	brain derived neurotrophic factor
BSA	bovine serum albumin
C	cysteine-rich domain
Cad	cadherin-like domain
cAMP	cyclic adenosine monophosphate
cGMP	cyclic guanosine monophosphate
CGRP	calcitonin gene related peptide
CIN	commissural interneuron
CM	cutaneous maximus
CMB	cell mask blue
CNS	central nervous system
CNTF	ciliary neurotrophic factor
CPG	central pattern generator
CPSG	chondroitin sulfate proteoglycan
CR	cysteine-rich cluster
CST	corticospinal tract
DCC	deleted in colorectal carcinoma
DF	dorsal funiculus
DiI	1,1'-dioctadecyl-3,3,3'-tetramethylindocarbocyanine perchlorate
DIV	days in vitro
DMEM	Dulbecco's modified Eagle's medium
DMSO	dimethyl sulfoxide
DNA	deoxyribonucleic acid
dNTP	deoxyribonucleotide
Dok	docking protein
DREZ	dorsal root entry zone
DRG	dorsal root ganglia
DTT	dithiothreitol
E	embryonic day
ECD	extracellular domain

Abbreviations

ECL	enhanced chemiluminescence
EDTA	ethylenediaminetetraacetic acid
ENC	enteric neural crest
Eph	erythropoietin-producing hepatoma
EphA4 ^{CR}	EphA4 cleavage resistant
EphA4-GFP	EphA4 with the intracellular domain replaced by GFP
EphA4 ^{KD}	EphA4 kinase-dead
EphA4Δ15	EphA4 lacking the external juxtamembrane region
EphA4ΔFN3	EphA4 lacking the fibronectin domains
EphA4ΔLBD	EphA4 lacking the ligand binding domain
EphA4ΔN	EphA4 lacking the extracellular domain
Ephexin	Eph interacting exchange protein
ERK	extracellular signal-regulated kinase
ES	embryonic stem
FBS	fetal bovine serum
FLRT	fibronectin-and-leucine-rich-transmembrane protein
FMTC	familial medullary thyroid carcinoma
FN	fibronectin like domain
FRS2	fibroblast growth factor receptor substrate 2
Gab	Grb-associated-binding protein
GAP	GTPase-activating protein
GDNF	glial cell line-derived neurotrophic factor
GEF	guanine exchange factor
GFL	GDNF-family ligand
GFP	green fluorescent protein
GFR α	GDNF family receptors alpha protein
GPCR	G-protein coupled receptor
GPI	glycosylphosphatidylinositol
Grb	growth factor receptor-bound protein
GTP	guanosine-5'-triphosphate
HBSS	Hank's balanced salt solution
HEPES	4-(2-hydroxyethyl)-1-piperazineethanesulfonic acid
HGF	hepatocyte growth factor
HRP	horse radish peroxidase
ICD	intracellular domain
Ig	immunoglobulin-like
Ig-CAMs	immunoglobulin family cell adhesion molecules
INL	inner nuclear layer
IP3	phosphatidylinositol-(1,4,5) triphosphate
IRS	insulin receptor substrate

JNK	c-Jun N-terminal kinase
kDa	kilo Dalton
LAR	leukocyte common antigen-related
LB	Luria-Bertani
LD	latissimus dorsi
LMC	lateral motor column
LMC _L	lateral LMC
LMC _M	medial LMC
LRR	leucine-rich repeat
LTD	long term depression
LTP	long term potentiation
MAPK	mitogen activated protein kinase
MEN2	multiple endocrine neoplasia type 2
MMP	matrix metalloprotease
mRNA	messenger RNA
NCS	newborn calf serum
NF- κ B	nuclear factor kappa-light-chain-enhancer of activated B cells
NGF	nerve growth factor
NRTN	neurturin
NT-3	neurotrophin-3
NT-4/5	neurotrophin-4/5
ONL	outer nuclear layer
P	post-natal
p140 ^{NCAM}	p140 neural cell adhesion molecule
p75 ^{NTR}	neurotrophin receptor p75
pAC	posterior AC
PAGE	polyacrylamide –gel –electrophoresis
PBM	PDZ binding motif
PBS	phosphate buffered saline
PCR	polymerase chain reaction
PI3K	phosphoinositide-3-kinase
PLC γ	phospholipase C gamma
PS	presenilin
PSPN	persephin
PTB	phospho-tyrosine binding
PTP	protein tyrosine phosphatase
PTPRO	receptor protein tyrosine phosphatases type O
pTyr	phosphotyrosine
pY1062	phosphotyrosine1062
RBD	receptor binding domain

Abbreviations

RD	rhodamine dextran
Ret	rearranged during transfection
RGC	retinal ganglion cell
RNA	ribonucleic acid
Robo	roundabout
RPTP	receptor protein tyrosine phosphatases
RTK	receptor tyrosine kinase
RTK	room temperature
SAM	sterile- α -motif
SC	superior colliculus
SCF	stem cell factor
SCG	superior cervical ganglia
SDS	sodium dodecyl sulfate
SEM	standard error of the mean
Sema	semaphorin
SH2	src homology 2
Shc	Src homologous and collagen-like
SHH	sonic hedgehog
SP	substance P
STAT	signal transducer and activator of transcription
TCL	total cell lysates
TEMED	tetramethylethylenediamine
TG	trigeminal ganglion
TGF- β	transforming growth factor- β
Tris	tris(hydroxymethyl)aminomethane
Trk	tropomyosin-related kinase
TZ	termination zone
VEGF	vascular endothelial growth factor
Wnt	wingless integration
Wt	wild-type
μ	Micro

List of Figures

- Figure 1-1 Structure of Trk receptors and p75
- Figure 1-2 BDNF/TrkB signaling cascade
- Figure 1-3 Structure of Ret, GFR α s and GFLs
- Figure 1-4 GDNF/GFR α 1/Ret signaling complex
- Figure 1-5 Structure of Eph receptor and ephrins
- Figure 1-6 Eph/ephrin forward signaling
- Figure 1-7 Eph/ephrin reverse signaling
- Figure 1-8 EphA/ephrinA signaling in the retinotopic mapping
- Figure 1-9 EphB/ephrinB signaling in retinotopic mapping
- Figure 1-10 Sensory neuron guidance in the trigeminal ganglion
- Figure 1-11 LMC guidance in the limb
- Figure 1-12 Axon guidance at the spinal cord midline
- Figure 2-1 Specificity of the anti-PTPRO antibody
- Figure 2-2 PTPRO expression pattern in LMC neurons
- Figure 2-3 PTPRO expression pattern during TG development
- Figure 2-4 PTPRO expression in a subset of TG neurons
- Figure 2-5 PTPRO expression in a subset of DRG neurons
- Figure 2-6 PTPRO expression at the spinal cord midline
- Figure 2-7 PTPRO expression in the retina
- Figure 2-8 E11.5 *PTPRO*^{-/-} embryos have a more complex ophthalmic arbor
- Figure 2-9 E12.5 *PTPRO*^{-/-} embryos show exuberant arborization of the ophthalmic branch of the TG nerve
- Figure 2-10 E12.5 *PTPRO*^{-/-} embryos show defasciculation of the maxillary branch
- Figure 2-11 E12.5 *PTPRO*^{-/-} TG neurons are more sensitive to BDNF and GDNF
- Figure 2-12 E12.5 *PTPRO*^{-/-} TG neurons are more sensitive to BDNF and GDNF, but not NGF stimulation
- Figure 2-13 P1 *PTPRO*^{-/-} TG neurons do not show increased sensitivity to neurotrophins and GDNF
- Figure 2-14 *PTPRO*^{-/-} embryos do not have defects in TG neuron differentiation
- Figure 2-15 *PTPRO*^{-/-} embryos do not have defects in DRG neuron differentiation
- Figure 2-16 Loss of TrkA⁺ and TrkC⁺ neurons in newborn *PTPRO*^{-/-} mice
- Figure 2-17 Regulation of TrkB signaling by PTPRO in transfected cells
- Figure 2-18 Regulation of Ret51 signaling by PTPRO in transfected cells
- Figure 2-19 PTPRO does not regulate TrkB and Ret 51 surface expression
- Figure 2-20 *PTPRO*^{-/-} TG explants do not show increased sensitivity to ephrinAs
- Figure 2-21 Neurofilament staining on whole-mount *PTPRO*^{-/-} embryos does not show any guidance defects
- Figure 2-22 *PTPRO*^{-/-} motor neurons are not more sensitive toward ephrin stimulation

- Figure 2-23 *PTPRO*^{-/-} mice do not show misguidance or aberrant branching in the retinocollicular map
- Figure 2-24 The chick but not the mouse isoform of PTPRO can dephosphorylate EphA4
- Figure 2-25 EphA4 is cleaved in HeLa and HEK293 cells
- Figure 2-26 EphA4 cleavage is proportional to EphA4 expression levels
- Figure 2-27 EphA4 cleavage is independent of ligand stimulation
- Figure 2-28 EphA4 is cleaved in E16.5 cortical neurons and cleavage regulates receptor levels in culture
- Figure 2-29 EphA4 is cleaved *in vivo*
- Figure 2-30 EphA4 cleavage is spatially and temporally regulated
- Figure 2-31 EphA4 cleavage has a peak between E12.5 and E15.5
- Figure 2-32 Eph receptor cleavage
- Figure 2-33 EphA4Δ15 is still cleaved with low efficiency
- Figure 2-34 EphA4^{CR} is cleavage resistant
- Figure 2-35 EphA4^{CR} is expressed on the cell surface and it is phosphorylated upon ephrinA5 stimulation
- Figure 2-36 EphA4^{CR} shows increased trans-endocytosis into ephrin expressing cells
- Figure 2-37 Generation of the EphA4^{CR} knock-in mouse
- Figure 2-38 EphA4^{CR} mutation is sufficient to abolish receptor cleavage *in vivo*
- Figure 2-39 *EphA4*^{CR/CR} has increased levels of EphA4 full-length protein
- Figure 2-40 In *EphA4*^{CR/CR} embryos full-length EphA4 is up-regulated in the hindlimb mesenchyme but not on motor axons
- Figure 2-41 In *EphA4*^{CR/CR} embryos full-length EphA4 is up-regulated in the dorsal spinal cord but not on motor neurons
- Figure 2-42 Hindlimb retrograde tracings show misguidance of LMC_L neurons in *EphA4*^{CR/CR} embryos
- Figure 2-43 Dorsal funiculus morphology and anterior commissure formation are not affected in *EphA4*^{CR/CR} mice
- Figure 2-44 Characterization of dissociated LMC cultures
- Figure 2-45 Specificity of Ret and EphA4 antibodies
- Figure 2-46 Ret and EphA4 do not directly interact in motor axons
- Figure 2-47 EphA4 phosphorylation and shedding are not altered in E12.5 *Ret*^{-/-} embryos
- Figure 2-48 EphA4-induced growth cone collapse is not affected in *Ret*^{-/-} embryos
- Figure 2-49 Cooperation between GDNF and ephrinA5 in motor axon turning
- Figure 3-1 Models for the regulation of RPTP phosphatase activity
- Figure 3-2 Hypothetical molecular mechanisms leading to LMC_L misguidance in *EphA4*^{CR/CR} mice

Abstract

Axons are equipped with an exploratory tip, the growth cone, to navigate and sense the cues presented by the surrounding environment. Several families of ligands are present along the axonal pathways, while their receptors are expressed on the growth cone and allow different axons to follow a great variety of trajectories. However, the number of molecules involved could be considered relatively small if compared to the diversity of trajectories, speed of growth and arborization patterns present in developed organisms. The fine tuning and the integration of different guidance cues represent good mechanisms to amplify and diversify the outputs of a relatively small number of ligand/receptor systems. The molecular players taking part in the modulation and integration of different signaling are not yet fully elucidated. In this study I focused on three intrinsic mechanisms to modulate receptor tyrosine kinase signaling: dephosphorylation by receptor protein tyrosine phosphatases (RPTPs), receptor cleavage and receptor cross-talk.

First, I analyzed TrkB, Ret and Eph receptor interaction with RPTP type O (PTPRO) in trigeminal and motor neurons. PTPRO is expressed mainly in TrkB⁺ and Ret⁺ mechanoreceptors within the TG during embryogenesis. In *PTPRO* mutant mice, the maxillary and ophthalmic branches of the trigeminal ganglion grow more complex arbors than in littermate controls. Cultured *PTPRO*^{-/-} TG neurons display enhanced axonal outgrowth and branching in response to BDNF and GDNF compared to control neurons, indicating that PTPRO negatively controls the activity of BDNF/TrkB and GDNF/Ret signaling. Mouse PTPRO fails to regulate Eph signaling in retinocollicular development,

in hindlimb motor axon guidance, and in transfected heterologous cells, suggesting that chick and mouse PTPRO have different substrate specificities.

On a second approach to identify intrinsic mechanisms to regulate receptor signaling, I analyzed how receptor cleavage regulates EphA4 signaling during development. Upon characterizing EphA4 cleavage *in vitro*, I generated a knock-in mouse carrying a mutation that made the EphA4 receptor cleavage resistant (*EphA4^{CR}*). Abolishing EphA4 cleavage led to an increased expression of the full-length protein in hindlimb mesenchyme and in dorsal spinal cord, but not on motor neuron soma or axons. Moreover, in *EphA4^{CR}* embryos, LMC_L neurons were aberrantly rerouted to the ventral mesenchyme, similarly to the guidance defects observed in *EphA4^{-/-}* embryos. Interestingly, two other phenotypes present in *EphA4^{-/-}* mice, the shallowing of the dorsal funiculus and the loss of the anterior commissure, were not present in *EphA4^{CR}* mice, suggesting that cleavage is only required for certain EphA4 functions.

Finally, I studied, in collaboration with Dr. Irina Dudanova, the molecular mechanisms underlying EphA4 and Ret cooperation in motor axon guidance at the sciatic plexus. We demonstrated that the two signaling systems act in parallel and independently to guide LMC_L axons in the dorsal mesenchyme of the hindlimb. When presented as opposing gradients, GDNF and ephrinAs cooperated and triggered a stronger turning response, suggesting that Ret and EphA4 exert different effects on the same growth cone. The *in vitro* results were consistent with the *in vivo* expression of the two proteins, where GDNF expressed dorsally to the choice point attracts LMC_L axons, and ephrinAs expressed ventrally repel them. This represents the first example of two opposing cues

acting in an additive manner to promote the same guidance choice at an intermediate target.

Taken together these data provide new insights in understanding the regulation of receptor signaling by modulatory proteins or by other receptors.

1. Introduction

During embryonic development neurons need to find their appropriate synaptic targets among many possible. Each axon terminates with an exploratory tip, the growth cone, which is equipped with several receptors to sense different cues in the surrounding environment. These cues can be either membrane-bound or soluble, and can provide trophic or tropic support. Several families of receptors/ligands are expressed on growth cones and in their target tissues and allow different axons to follow a great variety of trajectories. Neurons receive support for their outgrowth, branching and survival from neurotrophic factors and guidance direction from several families of axon guidance molecules [1].

In the last decades, four conserved families of axon guidance molecules have been identified: ephrins, netrins, semaphorins and Slits. In addition to these well characterized families, further guidance factors have more recently been described, e.g. morphogens such as Wnts and sonic hedgehog (SHH), growth factors such as hepatocyte growth factor (HGF), glial cell line-derived neurotrophic factor (GDNF), immunoglobulin family cell adhesion molecules (Ig-CAMs), and protocadherin family (reviewed in [2]). However, the numbers of ligand/receptor systems can be considered relatively small if compared to the complexity of the nervous system. Nonetheless, regulation and integration of guidance cues may represent mechanisms by which only a few molecules are sufficient to ensure the correct formation of a great variety of structures in the nervous system (as well as in other tissues). Work over the past years has identified several means of yielding diverse outcomes from the same ligand/receptor system: firstly, the controlled regulation of the molecule's expression (by alternative splicing,

microRNAs, etc.); secondly, the intrinsic (neuron type-specific) or extrinsic regulation of the signal transduction pathways; lastly, the interaction with other receptors [3].

1.1. Receptor Tyrosine Kinases: an overview

Cells express on their surface a plethora of receptors to transduce a great variety of extracellular stimuli. There are three main classes of receptors: G-protein coupled receptors (GPCRs), ion channels and enzyme-coupled receptors. The latter can either act as an enzyme upon ligand binding or be associated with an enzyme. Among the enzyme-coupled receptors having their own catalytic activity, the most prominent family is the receptor tyrosine kinase family (RTKs) [4].

In humans there are 20 subfamilies of RTKs, which share similar structures. The mechanism of activation and the downstream pathways are conserved from nematode to humans. Mutations that affect RTK activity, abundance, cellular localization or tissue expression are associated with numerous diseases, including inflammation, cancer, diabetes, and arteriosclerosis [5].

Generally, RTKs are activated by dimerization and act on common downstream pathways: mitogen activated protein kinase (MAPK), Akt, phospholipase C gamma (PLC γ) and nuclear factor kappa-light-chain-enhancer of activated B cells (NF- κ B). The first substrates of the kinase activity are the tyrosine residues present on the receptor, which then act as docking sites for adaptor proteins containing Src Homology 2 (SH2) and Phospho Tyrosine Binding (PTB) domains. In the absence of a ligand, kinase activity is often blocked by an auto-inhibitory mechanism, which can vary among different RTKs. For example, in the insulin receptor the auto-inhibitory tyrosine is in the kinase loop, whereas in the MuSK receptor the auto-inhibitory tyrosines are located in the

juxtamembrane region. Moreover, when not bound to their ligands, receptors can be kept in a dephosphorylated state by interaction with protein tyrosine phosphatases (PTPs). Pharmacological blockade of PTPs results in a general increase of RTK activation [5]. Once the receptor has been activated, it can receive positive and negative feedbacks, which can modulate the strength and the duration of the signaling output [5]. Amongst others, two families of transmembrane proteins have been characterized as RTK regulators: the receptor protein tyrosine phosphatase (RPTP) family and the LIG family of leucine-rich repeat (LRR) and immunoglobulin proteins.

In the following paragraphs I will focus on three RTK subfamilies that play a well-established role in neuron growth and guidance: Trk, Ret and Eph receptors.

1.1.1. Neurotrophin/Trk receptor signaling

The neurotrophin family, in mammals, has four members: nerve growth factor (NGF), brain derived neurotrophic factor (BDNF), neurotrophin-3 (NT-3) and neurotrophin-4/5 (NT-4/5). Neurotrophins act as dimers and are secreted as precursors (pro-neurotrophins). Pro-neurotrophins can be cleaved intracellularly (in the trans-Golgi network) by furin and other pro-hormone convertases, or extracellularly by plasmin. Neurotrophins bind to two classes of receptors: the tropomyosin-related kinase (Trk) receptor family and neurotrophin receptor p75 (p75NTR), a member of the tumor necrosis receptor superfamily. p75NTR is a common receptor for all neurotrophins, and although it lacks a catalytic domain, it regulates neuronal survival and differentiation through interaction with other receptors. p75NTR can also act as a co-receptor for the Trk receptors, increasing their affinity for the ligand [6, 7].

In mammals, the Trk receptor family has only three members: TrkA, TrkB and TrkC. Each receptor is characterized by the presence of two cysteine-rich clusters, three leucine-rich repeats and two immunoglobulin-like domains in the extracellular region, a transmembrane domain and an intracellular kinase domain (Figure 1-1). The membrane-proximal immunoglobulin domain has been described as important for the binding of neurotrophins [8]. Trk receptors undergo alternative splicing generating several isoforms, which can either differ by a few amino acids within or around the immunoglobulin domain, or be truncated versions of the receptors, lacking portions of the intracellular domain. Differences in the immunoglobulin domain modify the affinity of Trk receptors to specific neurotrophins, generally to the non-preferred ligands [9, 10]. The truncated receptors have different functions than their full-length counterparts: they can either initiate their own signaling cascade or act as dominant negative regulators of Trk signaling [11, 12].

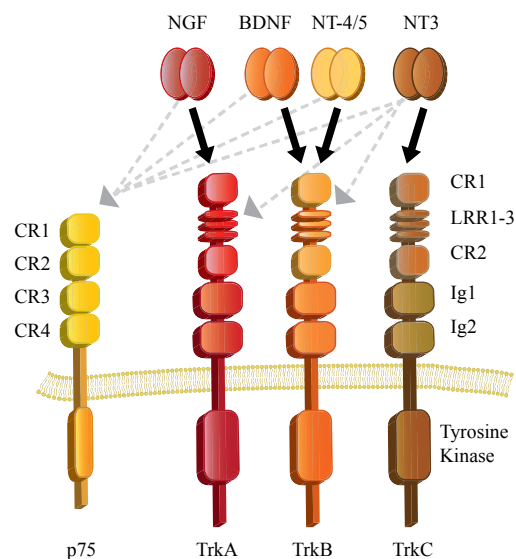


Figure 1-1. Structure of Trk receptors and p75

Schematic drawing of Trk receptors. The Trk extracellular region contains two cysteine-rich clusters (C1-2), three leucine-rich repeats (LRR1-3) and two immunoglobulin-like domains (Ig1-2). The intracellular region has a tyrosine kinase domain. p75 has four cysteine-rich clusters (CR1-4) and an intracellular domain lacking kinase activity. NGF is TrkA ligand, BDNF and NT-4/5 are TrkB ligands, and NT-3 is the ligand for TrkC (black arrows). p75 binds all neurotrophins with low affinity (grey arrows).

TrkA, TrkB and TrkC bind with high affinity to NGF, BDNF and NT-3, respectively. TrkB can also bind NT-4/5 (Figure 1-1). Upon ligand binding these receptors dimerize, trans-phosphorylate the tyrosine residues in their intracellular domains, and activate several signaling pathways. In vertebrates, Trk receptors have 10 conserved tyrosine residues that can be phosphorylated upon ligand binding. Three of these tyrosines are present in the autoregulatory loop of the kinase domain, thereby controlling receptor activation [13].

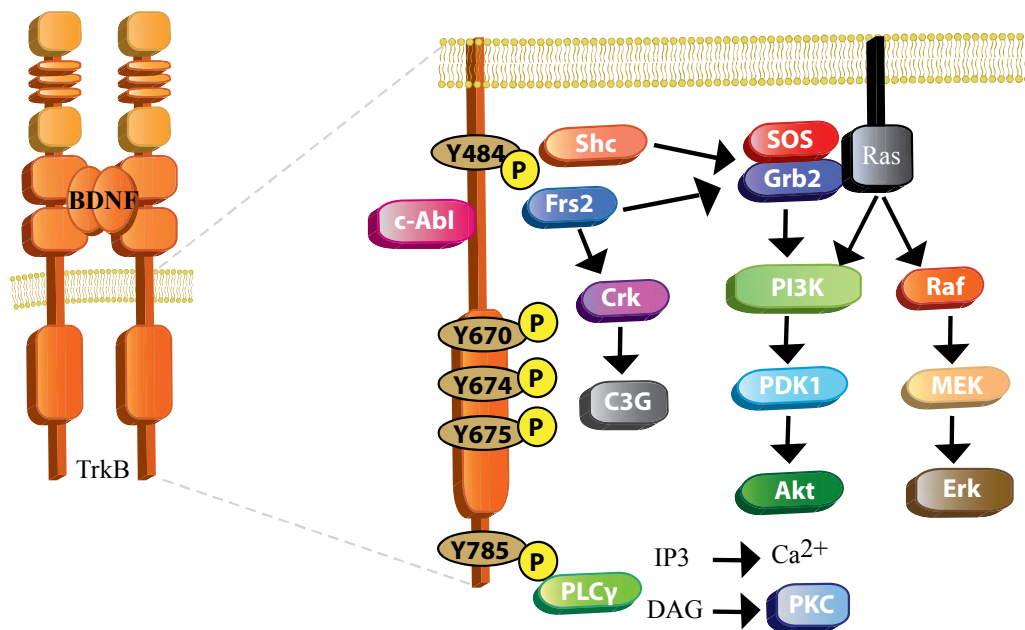


Figure 1-2. BDNF/TrkB signaling cascade

Schematic drawing of TrkB signaling. Upon BDNF binding TrkB forms dimers and several of its intracellular tyrosines become autophosphorylated. The phospho-residues act as docking sites for few adaptor proteins, which activate several downstream pathways, like MAPK/ERK, PI3K, PLCγ.

In TrkA the two main phospho-tyrosines are tyrosine 490 (tyrosine 484 in TrkB) and tyrosine 785 [14]. Tyrosine 490 acts as a docking site for Src homologous and collagen-like (Shc) and fibroblast growth factor receptor substrate 2 (FRS2), and tyrosine 785 for PLCγ. Shc triggers the transient activation of Ras, which then starts the phosphoinositide-3-kinase (PI3K) and MAPK/ERK signaling pathways; FRS2 recruits Crk, which binds the guanine nucleotide exchange factor, C3G [15-17]. Recruitment and phosphorylation

of PLC γ leads to formation of phosphatidylinositol-(1,4,5) triphosphate (IP₃), which stimulates the release of calcium from intracellular storage compartments, and diacyl glycerol (DAG), which activates protein kinase C (PKC) [8]. Although tyrosines 490 and 785 are the main phosphorylation sites, knock-in mice in which these tyrosines have been converted to phenylalanine do not show major abnormalities, suggesting that there is a redundancy of phospho-tyrosines that can start the downstream signaling pathways [18-20]. Finally, the tyrosines in the autoregulatory loop can recruit growth factor receptor-bound protein 2 (Grb2) [21, 22], and c-Abl can also bind to non-phosphotyrosine residues [23, 24] (Figure 1-2).

1.1.1.1. Neurotrophin/Trk signaling for neuron survival

According to the neurotrophic factor hypothesis, between embryonic day 13 (E13) and 18 (E18) neurons generated in excess during development undergo programmed cell death, because they compete for limited amount of neurotrophic factors present in the target tissues [25, 26]. Genetic ablation of neurotrophin and Trk genes in most of the cases, with the exception of NT-4/5, affects mouse viability and the survival of several populations of peripheral neurons [13]. Although *in vitro* neurotrophins promote survival of several populations of neurons, *in vivo* their role seems to be restricted to specific populations [8].

NGF and TrkA knockout mice display loss of neurons in superior cervical ganglia (SCG), dorsal root ganglia (DRG) and trigeminal ganglia (TG). In the DRG there is a loss of calcitonin gene related peptide positive (CGRP⁺), IB4 positive (IB4⁺) and substance P positive (SP⁺) neurons, and in the spinal cord, projections to lamina I and II (nociceptive fibers) are lost. As a consequence of this loss of nociceptive neurons, knockout mice are

less sensitive to pain. Moreover, these mutant mice have a reduced number of low-threshold mechanoreceptor [27-30]. In the central nervous system (CNS), TrkA and NGF knockouts show loss of cholinergic projections, although the number of neurons is not affected [30].

TrkB and BDNF knockout mice display loss of SCG, TG, vestibular, nodose, trigeminal mesencephalic nucleus and DRG neurons. The DRG neurons lost in these knockouts are a subset of the cutaneous mechanoreceptors. NT-4/5 knockout mice have a reduced number of nodose and geniculate neurons, and this phenotype is enhanced in *NT-4/5^{-/-};BDNF^{-/-}* mice [31-35].

Based on their expression patterns, TrkC and NT-3 have been associated with neurons responsible for proprioception. Consistent with this observation, mutant mice for either the ligand or the receptor are impaired in movements and have abnormal postures. NT-3 and TrkC mice display loss of neurons in the SCG, in the TG, in the nodose ganglion, in the cochlear ganglion and in DRGs. Sensory projections connecting to motor pools in the spinal cord (Ia projections, proprioceptive axons) are missing. Moreover, in these mice Golgi tendon organs, muscle spindles and sensory peripheral innervation are absent. NT-3 mutant mice show a more severe phenotype than the TrkC knockouts, suggesting that NT-3 may have additional receptors [36-41].

Interestingly, a recent paper showed that TrkA and TrkC, but not TrkB are able to signal independently of neurotrophin binding. Over-expression of these receptors is sufficient to trigger cell death in absence of the ligand, and if NGF or NT-3 are added to the neurons, cell death is rescued [42]. This data further prove the hypothesis that TrkA and TrkC act as dependence receptors. Dependence receptors are receptors able to initiate

two signaling cascades: one in the presence of ligand, leading to survival, differentiation or migration; and another one in the absence of the ligand, which triggers or amplifies signaling, leading to programmed cell death [43].

1.1.1.2. Other neurotrophin/Trk functions in the central and peripheral nervous system

In addition to their well-established roles in neuron survival, neurotrophins and Trk receptors have been implicated in differentiation, modulation of axonal and dendrite outgrowth and guidance, and in the regulation of synaptic plasticity [13].

In vivo, it has been possible to uncover additional functions of neurotrophin signaling only upon crossing neurotrophin and neurotrophin receptor mutants with Bcl-2 associated X protein (Bax) knockouts. Removing Bax prevents apoptosis, and allows the uncoupling of neurotrophin effects on survival from those on specification. *TrkA/Bax* and *NGF/Bax* double knockouts show a milder loss of neurons compared to *TrkA* or *NGF* single knockouts. In *NGF*^{-/-}, *TrkA*⁺ neurons are unable to differentiate into *CGRP*⁺, *Ret*⁺ and *SP*⁺ neurons [44]. This *in vivo* data are supported by the ability of NGF to induce neuropeptide expression in cultured embryonic DRG neurons [44].

A role for neurotrophins as guidance molecules has been speculated since the discovery of NGF-induced neurite outgrowth in cultures [45]. All neurotrophins trigger neurite outgrowth in embryonic sensory neuron cultures [46, 47]. The *in vivo* relevance of TrkA signaling in supporting neurite outgrowth was assessed, as described before for TrkA role in differentiation, in *TrkA/Bax* knockouts. In these mice spinal cord innervation is unaffected, but cutaneous innervation is disrupted, suggesting that NGF/TrkA signaling is required for peripheral innervation, and the absence of projections in the spinal cord of

NGF or *TrkA* knockouts is secondary to cell death [44]. Mice over-expressing NGF or BDNF in the dermis provide further evidence for a role of neurotrophins in regulating peripheral innervation. since these transgenic mice display hyper-innervation of the whisker pad and the dermis [48]. In addition to their trophic functions, neurotrophins can act as attractive guidance cues for mouse DRG neurons and *Xenopus* spinal neurons when presented in a gradient [47, 49]. Surprisingly, neurotrophins can also act as chemorepellents when cyclic adenosine monophosphate (cAMP) and cyclic guanosine monophosphate (cGMP) are inhibited [49]. Although *in vitro* neurotrophins are able to steer the growth cones of several types of neurons, *in vivo* data support a role for neurotrophins in regulating outgrowth, branching and target innervation of several neuronal populations, but not axon pathfinding [50].

A role for neurotrophins in regulating synaptic plasticity is shown by several lines of evidence, including the regulation of their secretion by neuronal activity and their ability to potentiate synaptic transmission [51]. Neurotrophins are also able to induce structural changes, i.e. regulate the size of dendritic arbors of pyramidal neurons, and to enhance short- and long-term synaptic transmission. BDNF and TrkB mutants show severe impairment of LTP, although basal synaptic transmission is not affected [52, 53]. Consistently with impairment in LTP, neurotrophin mutant mice have several behavioral abnormalities when performing tasks to assess their ability to learn or memorize. The conditional knockout approach allowed the investigation of behavioral defects in mice where TrkB was specifically removed from the hippocampus: this resulted in abnormal memory acquisition and consolidation in hippocampus-dependent learning tasks [53].

Similarly to *BDNF*^{-/-} mice, reduction of NGF levels (NGF heterozygous mice) caused impairment in the formation and retention of memory [54].

1.1.2. *Ret/GDNF signaling*

GDNF-family ligands (GFLs) belong to the transforming growth factor- β (TGF- β) super-family. They are characterized by the presence of six cysteine residues regularly spaced to form 3 disulfide bonds (cysteine knot). They are secreted as precursors (preproGFLs), and after being activated by proteolytic cleavage, function as homodimers [55]. The four GFLs - GDNF, neurturin (NRTN), artemin (ARTN) and persephin (PSPN) - signal via Ret, a transmembrane receptor tyrosine kinase, and one of the four GPI-anchored GDNF family receptors alpha proteins (GFR α 1-4) [56] (Figure1-3).

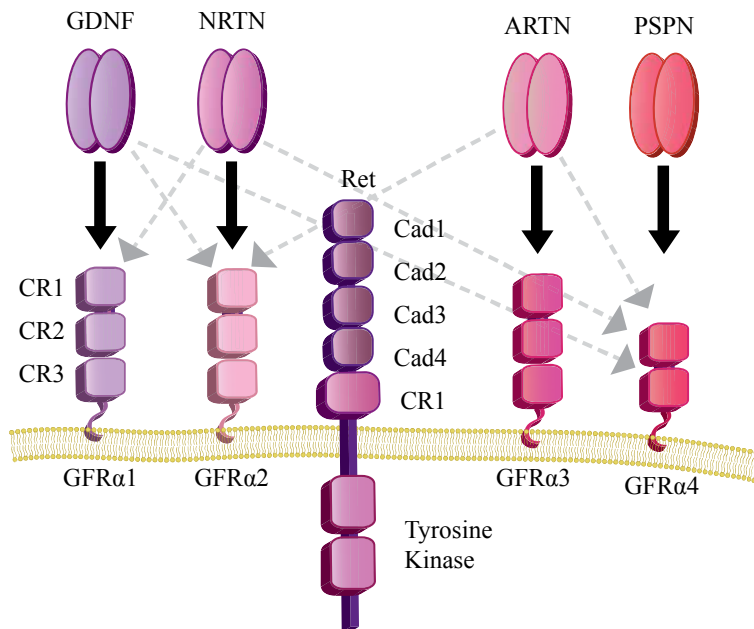


Figure 1-3. Structure of Ret, GFR α s and GFLs

Schematic drawing of Ret receptors, GFR α co-receptors and GFLs. The extracellular region of Ret contains four cadherin-like domains (Cad1-4) and one cysteine-rich domain (C1). The intracellular region has a large intercalated tyrosine kinase domain. GFR α 1, GFR α 2 and GFR α 3 have three cysteine-rich clusters (CR1-3), whereas GFR α 4 has only two. GFLs act as dimers. All GFLs bind to Ret, but using different co-receptors. GDNF binds with high affinity (black arrow) to GFR α 1, and low affinity (grey arrows) to GFR α 2 and GFR α 4. Neurturin (NRTN) binds with high affinity to GFR α 2, and low affinity to GFR α 1 and GFR α 4. Artemin (ARTN) binds mainly to GFR α 3, and with low affinity to GFR α 2 and GFR α 4. Persephin (PSPN) specifically binds GFR α 4.

Human Ret exists in three isoforms: Ret9, Ret43 and Ret51, which are generated by alternative splicing of the 3' terminus and which differ in the length of their C-terminal domains [57]. The Ret43 isoform is the less characterized and the less evolutionarily conserved. Genetic studies have shown that Ret9 has a major role *in vivo*, indeed removing only this isoform is enough to reproduce most of the Ret full knockout phenotypes [58]. Ret has four cadherin-like domains and a cysteine-rich region in its extracellular part, a single transmembrane domain and a large intercalated intracellular kinase domain [59] (Figure 1-3).

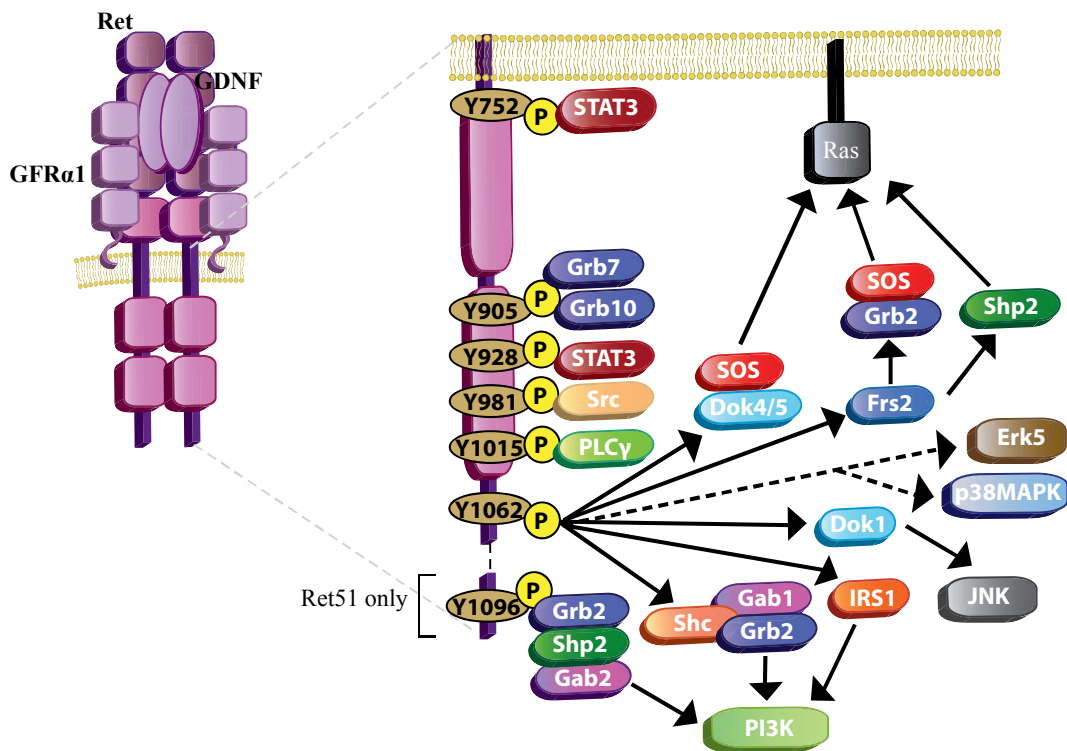


Figure 1-4. GDNF/GFRα1/Ret signaling complex

Schematic drawing of Ret downstream signaling upon GDNF activation. GDNF, as a homodimer, binds to two molecules of GFRα1 and two molecules of Ret. This ternary complex starts a signaling cascade, upon phosphorylation of several tyrosine residues in the Ret intracellular domain. Ret51 isoform has an additional tyrosine (Y1096). Via the recruitment of several adaptor proteins, Ret activates different signaling pathways: Ras, PI3K, JNK, p38MAPK, Erk5, STAT3, PLCγ.

Upon ligand binding a ternary complex (GDNF-Ret-GFRα1) is formed and several tyrosines in the intracellular domain of Ret are phosphorylated [60, 61]. GDNF induces

phosphorylation of several tyrosines [in human Ret residues 752, 905, 928, 981, 1015, 1062 and 1096 (the last one is only present in the Ret51 isoform)], but tyrosine 1062 has a pivotal role in Ret signaling, representing the main docking site for several downstream effectors [62, 63]. Growth factor bound proteins 7 and 10 (Grb7 and Grb10) are recruited to tyrosine 905, Src to tyrosine 981, signal transducer and activator of transcription 3 (STAT3) to tyrosine 752 and 928, and PLC γ to tyrosine 1015. Tyrosine 1062 activates the Ras-Erk pathway by recruiting FRS2 or docking protein (Dok) 4/5, the JNK pathway via Dok1, the PI3K pathway via the Shc/Grb2/Grb-associated-binding protein 1 (Gab1) complex, or via insulin receptor substrate (IRS) binding. Moreover, tyrosine 1062 can initiate the ERK5 and p38 MAPK pathway although the downstream adaptor is not known yet. The two Ret isoforms, although sharing most downstream effectors, have some specific interactors: Shank3 binds to the PDZ domain of Ret9, and Grb2 is recruited to the tyrosine 1096, which is only present in Ret51 [64] (Figure 1-4).

1.1.2.1. GDNF, Ret and GFR α 1: mouse models

GDNF, Ret and GFR α 1 knockout mice die after birth due to hypodysplasia or aplasia of the kidneys and to severe loss of enteric innervation [65-70]. Kidneys, in mammals, develop due to a reciprocal interaction of the ureteric bud and the metanephric mesenchyme. The ureteric bud, expressing Ret and GFR α 1, is activated by GDNF secreted by the metanephric mesenchyme. In the absence of GDNF/Ret signaling components, the ureteric bud fails to grow and branch, leading to renal agenesis [71-73]. Enteric neural crest (ENC) cells give rise to the majority of enteric neurons and glia. ENC precursor cells migrate rostro-caudally to reach the enteric wall. The intestinal aganglionosis in GDNF, Ret and GFR α 1 knockouts is a consequence of aberrant

migration and differentiation of the ENC cells [66, 74]. In humans, Ret mutations are associated with Hirschsprung's disease, characterized by the absence of enteric ganglia in the colon [75].

In contrast to loss of function approaches, knock-in mice carrying mutations that constitutively activate Ret, display several neural crest-derived and endocrine tumors. In humans, Ret gain-of-function mutations are associated with multiple endocrine neoplasia type 2A or 2B (MEN2A or MEN2B) and familial medullary thyroid carcinoma (FMTC). In MEN2A, a mutation in one of the extracellular cysteines causes the formation of inter-molecular disulfide bonds instead of intra-molecular ones, leading to the constitutive dimerization (and therefore activation) of Ret. In MEN2B, mutations are localized in the intracellular domain of Ret and cause changes in the kinase activity and the specificity of substrates [76].

1.1.2.2. GDNF, Ret and GFR α 1 functions in the central and peripheral nervous systems

GDNF was originally identified as a dopaminergic neuron survival factor *in vitro* [77], however GDNF/Ret signaling *in vivo* is dispensable for their embryonic development. In certain animal models of Parkinson disease GDNF/Ret signaling prevents dopaminergic neuron loss and promotes functional recovery [78, 79].

Work over recent decades has identified GDNF as a neurotrophic factor for several other types of neurons, including petrosal and motor neurons [80-84]. In addition to its survival effects on motor neurons *in vivo* and *in vitro*, GDNF/Ret signaling is important for motor neuron specification. At E12.5, motor neurons of the cutaneous maximus (CM) and latissimus dorsi (LD) pools are misplaced in the spinal cord of GDNF knockout

mice, although their survival is not affected. This misplacement is phenocopied in PEA3 knockouts. PEA3 is a transcriptional factor of the ETS family required for cell body positioning, muscle innervation dendrite morphology and afferent synapse formation of the CM and LD motor pools. Work by Haase *et al.* showed that GDNF/Ret signaling is required to induce PEA3 expression in the CM and LD motor pools [85]. The role of GDNF/Ret signaling in motor neuron axon guidance will be further discussed later in this thesis.

Another role of GDNF is the regulation of cell migration and peripheral innervation [55]. GDNF, Ret and GFR α 1 knockout mice show, already in embryonic stages, loss of the otic and sphenopalatine ganglia, two parasympathetic ganglia. GDNF is expressed within or around the parasympathetic precursor cells, which express Ret and GFR α 1, and is required for their migration and proliferation [86]. Although GDNF/Ret signaling is dispensable for DRG and TG neurons during embryonic development, it may be required postnatally for survival and target innervation. For example, in postnatal stages, there is a loss of myelinated mechanoreceptors in GDNF heterozygous mice and local hyper-innervation in mice over-expressing GDNF [87, 88].

Ret expression labels two classes of sensory neurons. Most Ret-expressing neurons in the DRGs are small to medium diameter non-peptidergic nociceptors and express TrkA in the early stages of development and Ret only after E15. GDNF/Ret signaling has a central role in their maturation and cutaneous innervation [89]. The second class of neurons consists of large-soma neurons, which express Ret prior to E11.5 and do not express TrkA. GDNF/Ret signaling is required here for the formation of neural circuits underlying touch perception [90].

1.1.2.3. GDNF and Ret can signal independently of each other

In the nervous system, GFR α family members are more widely expressed than Ret, suggesting that they can have diverse roles, probably interacting with other transmembrane receptors or in a homophilic manner. Indeed, Ret-independent GDNF signaling has been implicated in cell migration and synapse formation through interaction with the p140 neural cell adhesion molecule (p140^{NCAM}) and GFR α 1 [91, 92]. *In vitro*, the formation of a ternary complex GDNF/GFR α 1/NCAM reduces homophilic interaction between NCAM molecules. *Ex vivo*, GDNF/NCAM signaling induces Schwann cell migration and cortical and hippocampal neuron outgrowth. NCAM knockout mice have a reduced olfactory bulb, due to the aberrant migration of neuron precursor cells in the rostral migratory system [92].

Another role for NCAM-dependent GDNF signaling is the guidance of commissural neurons across the spinal cord midline. GDNF signaling promotes the expression of PlexinA1 on commissural axons that reached the midline, by inhibiting the calpain-dependent proteolytic processing of the receptor. The increased expression of the PlexinA1 makes commissural axons more sensitive to Sema3B expressed at the floor plate. Sema3B repulsion enables these axons to grow away from the spinal cord midline in order to reach their final synaptic targets [93].

Interestingly, GDNF-mediated GFR α 1 homophilic binding has been implicated in synapse formation, and was the first example described of ligand-induced cell adhesion molecule interaction. GDNF promotes the homophilic interaction of two GFR α 1 molecules expressed *in trans* on the presynaptic and post-synaptic termini of hippocampal neurons. GDNF/GFR α 1 signaling is sufficient to promote pre-synaptic

differentiation *in vitro*, and consistently GDNF mutant mice have decreased presynaptic puncta and decreased synaptic localization of pre-synaptic molecules *in vivo* [91].

Not only GDNF can signal independently of Ret, but also Ret can signal independently of GDNF. In sympathetic neurons *in vivo* and *in vitro*, Ret can be phosphorylated by TrkA in post-natal stages, independently of both GFLs and GFRas. TrkA-induced Ret phosphorylation results in increased growth, metabolism and gene expression [94]. Ret over-expression in some cell lines induces apoptosis, through a fragment of the receptor intracellular domain, produced after caspase cleavage. Interestingly, application of GDNF stops Ret pro-apoptotic activity, suggesting that Ret could act, similarly to TrkA and TrkC, as a dependence receptor [95].

1.1.3. Eph/ephrin signaling

Eph receptors are the largest family of RTKs and are divided into A-type (EphA) and B-type receptors (EphB), based on their preference for ephrinA or ephrinB ligands. However, EphA4 and EphB2 can bind both ephrinAs and ephrinBs. In mammals, there are fourteen Eph receptors (nine EphAs and five EphBs) and eight ligands (five ephrinAs and three ephrinBs). Eph receptors have a cysteine-rich domain (CRD) and two fibronectin-like domains (FN) in their extracellular region; a kinase domain, a sterile- α -motif (SAM) and a PDZ binding motif (PBM) in their intracellular region. EphrinAs are GPI-anchored proteins, characterized by the presence of a globular receptor binding domain (RBD). EphrinBs are transmembrane proteins, characterized by the presence of an extracellular RBD and intracellular PBM and five conserved tyrosine residues [96] (Figure 1-5).

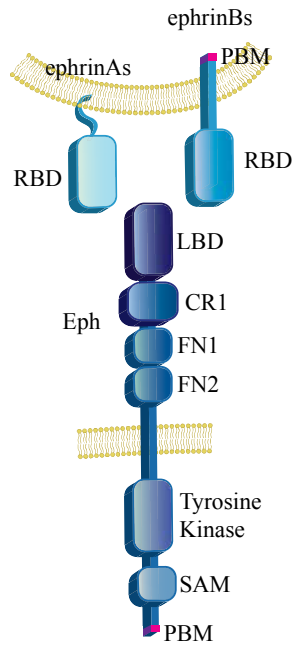


Figure 1-5. Structure of Eph receptor and ephrins

Schematic drawing of Eph/ephrin structures. The extracellular region of Eph receptors contains a ligand binding domain (LBD), a cysteine-rich domain (C1) and two fibronectin-like domains (FN1-2). The intracellular region has a tyrosine kinase domain, a SAM domain and a PDZ binding motif (PBM). EphrinAs are GPI-anchored proteins, with a Receptor Binding Domain (RBD), and ephrinBs are transmembrane proteins with a RBD and an intracellular PBM.

Similarly to other RTKs, upon binding to their ligand, Eph receptors undergo auto-phosphorylation in their juxtamembrane tyrosines, which leads to the phosphorylation of additional tyrosine residues and the complete activation of the kinase domain. Once the receptors are activated, adaptor proteins bind to them and activate downstream effectors, enhancing cytoskeletal rearrangements [96]. The major downstream effectors of Eph signaling are members of the Rho family of GTPases, namely RhoA, Cdc42 and Rac. Rho GTPases can shuttle between two conformational states: active (GTP-bound) and inactive (GDP-bound) [97]. The shuttling between the two states can be regulated by other families of proteins: guanine exchange factors (GEFs), which promote the binding to GTP and the release of GDP, whereas GTPase-activating proteins (GAPs) promote the release of GTP.

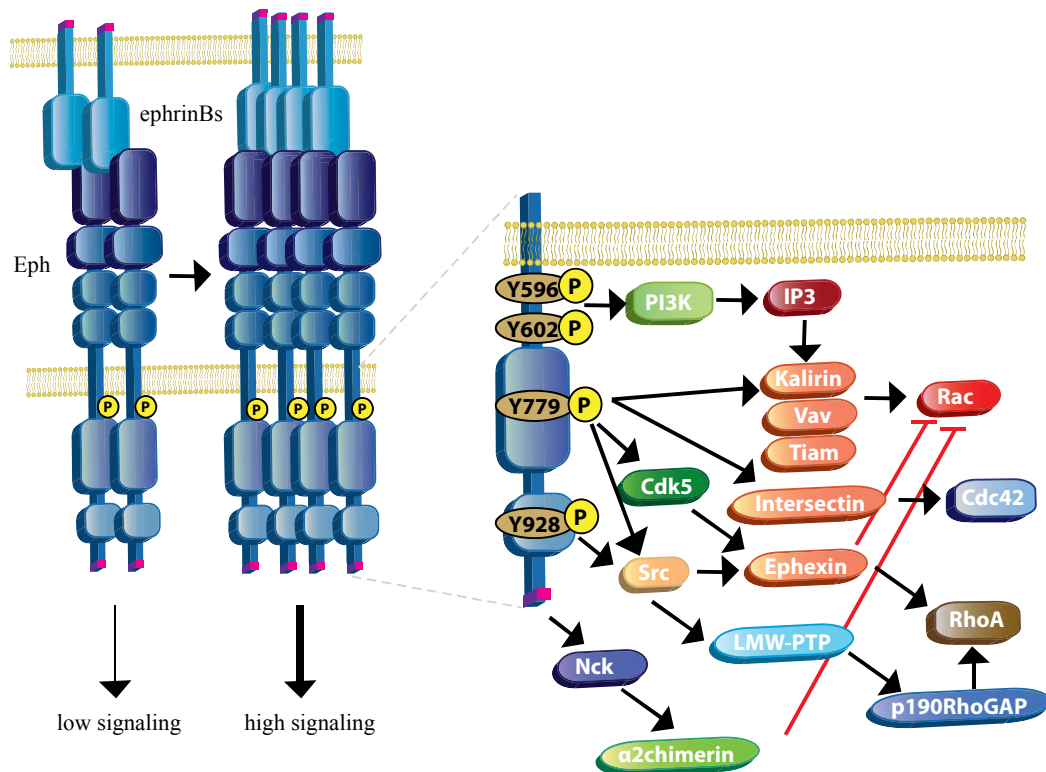


Figure 1-6. Eph/ephrin forward signaling

Schematic drawing of Eph signaling. Upon ligand binding, Eph receptors form dimers, and then oligomers. Several tyrosines in Eph receptor intracellular domain become phosphorylated and act as docking sites for different adaptor proteins, which lead to the activation of GEF proteins (pink ellipses). The main outcome of Eph activation is the remodeling of the actin cytoskeleton, through the differential activation of Rac, RhoA and Cdc42. The tyrosine residue numbers are referred to EphA4 sequence, in other Eph receptors the same tyrosine may occupy a different position.

Eph receptors trigger Rho GTPase signaling, mainly through activation of GEFs. Eph interacting exchange protein (Ephexin) is constitutively bound to EphAs, and in its dephosphorylated state triggers the activation of RhoA, Rac1 and Cdc42. Upon ligand binding, EphAs phosphorylate ephexin, probably via Src, and this leads to the preferential activation of RhoA, which in neurons promotes growth cone collapse [98, 99]. Remarkably, α -chimaerin and Nck1/Nck2 knockout mice have similar defects in cortical and spinal circuit assembly compared to EphA4 knockouts, demonstrating their role as essential downstream effectors [100, 101]. Vav2, a common molecule downstream of EphAs and EphBs, activates Rac1-dependent endocytosis of Eph/ephrin

complexes, enabling cell-cell repulsion [102]. Other downstream effectors are intersectin-1, Kalirin-7 and Tiam [103] (Figure 1-6).

1.1.3.1. Distinctive features of Eph signaling

Eph/ephrin signaling shows some distinctive features: high-order clustering, bi-directional signaling and endocytosis, receptor and ligand cleavage, and *cis*-interactions [96].

Contrary to other RTKs, Eph receptors form oligomers upon activation. After initial receptor/ligand binding, more molecules of Eph and ephrin are recruited, via intracellular and extracellular interactions, to generate high-order clusters. The CRD of EphA3 plays an important role in the lateral expansion of these clusters, whereas the SAM domain of EphA4 and EphB2 may be required for the stabilization of oligomers [104-106]. In the absence of ligand, EphA2 ectodomains form array-like networks due to parallel staggered (LBD-sushi domain) interactions. Upon ephrinA5 binding, in-register arrays are formed due to LBD-LBD and sushi domain-sushi domain interactions [107]. Once the high-order clusters are generated additional Eph receptors (hetero-oligomerization) or other transmembrane proteins (i.e. metalloproteases or Ryk) can be recruited [108-111].

One of the most intriguing aspects of Eph/ephrin interaction between two opposing cells is bi-directional signaling: one signaling pathway is triggered in the Eph-expressing cell (forward signaling) and one in the ephrin-expressing cell (reverse signaling). EphrinAs and ephrinBs use different strategies to transduce reverse signaling. EphrinAs, as mentioned previously, lack an intracellular domain, hence they often require a co-receptor to initiate a signaling cascade. For example, in the retina ephrinA5 interacts with p75, phosphorylating Fyn and starting a signaling cascade, which trigger cytoskeletal

rearrangement and ultimately causes repulsion [112]. Moreover, ephrinA5 binds TrkB to regulate axon branching and synapse formation in retinal ganglion cells (RGCs) and hippocampal neurons [113]. Upon Eph-induced ephrinB clustering, Src family kinases bind to ephrinB cytoplasmic domain and phosphorylate specific tyrosine residues. These phosphorylated residues recruit SH2-containing adaptor proteins, such as Grb4, in order to promote actin cytoskeleton rearrangements, changes in focal adhesion, pruning and spine maturation in neurons [114-116] (Figure 1-7).

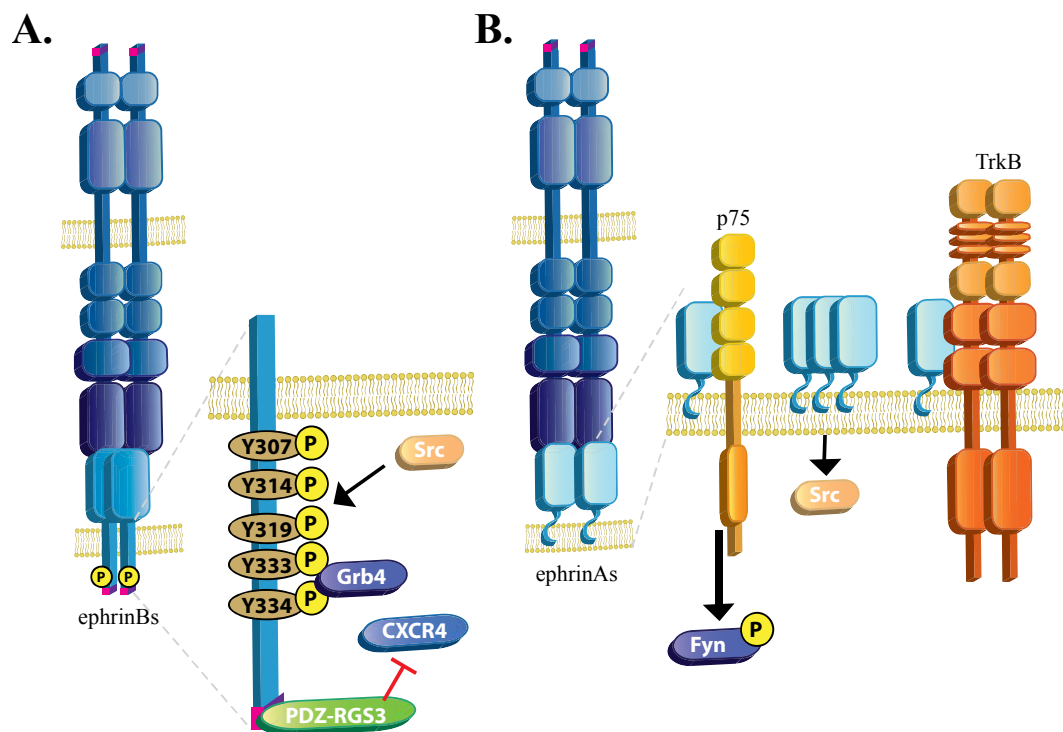


Figure 1-7. Eph/ephrin reverse signaling

Schematic drawing of ephrin signaling. (A) Eph stimulation triggers the phosphorylation of the five conserved intracellular tyrosines of ephrinBs, probably via Src activation. The tyrosine residue numbers are referred to ephrinB2 sequence, in other ephrinBs the tyrosines may occupy different positions. Phosphotyrosines recruit Grb4 and start the reverse signaling. The PBM recruits PDZ-RGS3, which prevents CXCR4 activation. (B) ephrinAs, being GPI-anchored protein, need a co-receptor to transduce the signal, i.e. p75 or TrkB. ephrinAs activation recruits Src in the lipid rafts, by an unknown mechanism.

Interestingly, lymphatic vessel remodeling is more affected in knock-in mice carrying a mutation in the ephrinB2 PDZ domain than in mice where the five intracellular tyrosine residues of ephrinB2 have been mutated [117]. The PDZ domain can act as a docking site

for adaptor proteins, like GRIPs or PDZ-RGS3 [118, 119]. The interaction with the latter prevents its binding to CXCR4, a G-coupled receptor, leading to inhibition of CXCR4-mediated chemoattraction [119].

The interaction between Eph receptors and ephrins represents an interesting paradox: despite initial high-affinity binding, signaling then leads to cell-cell repulsion. Two mechanisms have been shown to promote cell-cell detachment after the initial adhesion: bi-directional endocytosis and receptor or ligand cleavage by metalloproteases [96]. Both EphB receptors and ephrinB ligands undergo bi-directional endocytosis, in order to remove the EphB/ephrinB complexes from cell contact sites. To date, the identity of the molecular pathways involved in endocytosis in the Eph expressing cell (forward endocytosis) and in the ephrin expressing cell (reverse endocytosis) are still poorly characterized [120, 121]. In addition to bi-directional endocytosis, EphBs promote repulsion from ephrinB expressing cells, by cleavage of the receptors or the ligand. HEK293 cells or hippocampal neurons expressing mutant EphB2, unable to be cleaved, are no longer able to detach from ephrinB-expressing cells [122]. The relative importance of shedding and endocytosis for repulsion *in vivo* has not been addressed to date. So far the only mechanism proposed for EphA mediated cell-cell repulsion is the cleavage of the ephrinA GPI-anchor. EphA3, upon binding to ephrinA5, activates ADAM proteases that cleave the ephrinA5 GPI-anchor and allow the two cells to detach [110]. Whether ADAM cleaves ephrinAs *in cis* [123] or *in trans* [110] and if cleavage plays an essential role in *in vivo* guidance is still debated. *In vitro* it has been shown that EphA4 activates bi-directional endocytosis, but whether this is required for repulsion to occur has not been shown [121].

Finally, Ephs and ephrins can be expressed either in a complementary pattern or be coexpressed in the same cell, suggesting that the receptor/ligand system can have *trans* or *cis* interactions. Early evidence for *cis* interaction came from work done in the retinotectal system, where ephrinAs negatively regulate the response of coexpressed EphAs. Interactions *in cis* can be LBD-dependent or -independent, and result in a reduced receptor phosphorylation, and therefore reduced sensitivity to *trans* ephrin stimulation. The relative expression levels of the two molecules titrate their *cis* versus *trans* interactions [124-127]. This last aspect will be further discussed in the motor neuron guidance paragraph.

1.1.3.2. Eph receptor functions during embryonic development and in adulthood

Eph/ephrin signaling plays a pivotal role in embryonic development and in maintaining the homeostasis in adult organisms. It is required in a wide range of biological functions, such as axon guidance, cell sorting and positioning, vascular and lymphatic development, and synaptic plasticity. Consistent with their versatile functions during development, disruption of Eph/ephrin signaling is associated with the onset and the progression of several human diseases, e.g. cancer [128].

Eph receptors play an important role in several guidance systems, where axons are presented either with a gradient or a bimodal choice. The best characterized example of ephrins expressed in a gradient is the retinotopic map [129-131]. Axons from the retina project either to the superior colliculus (SC) (optic tectum in chick) or to the thalamus, where they synapse on neurons that project to the visual cortex [132, 133].

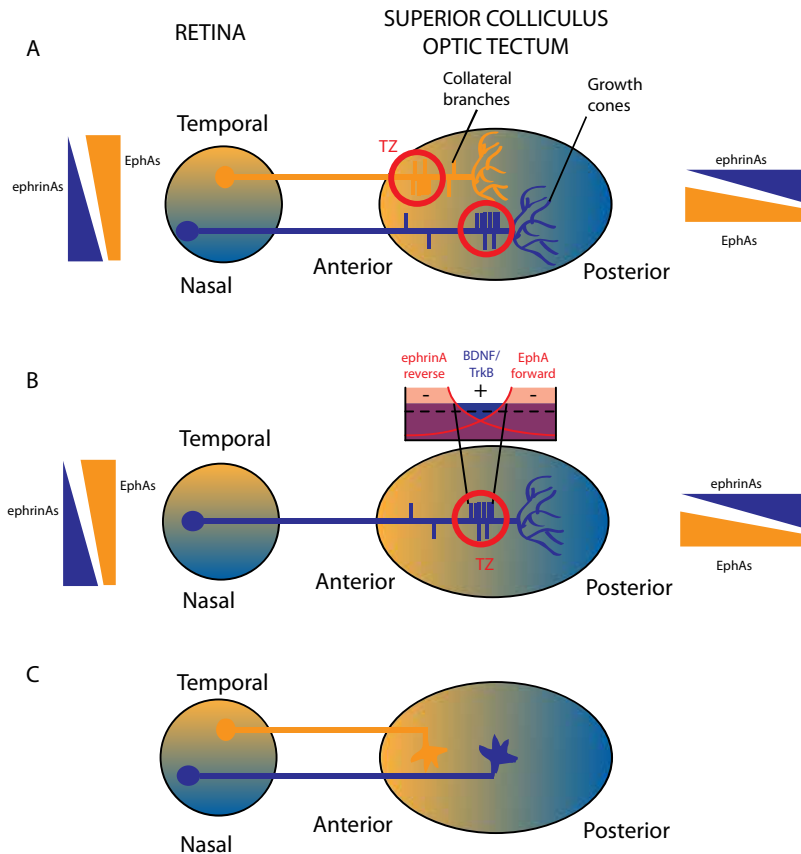


Figure 1-8. EphA/ephrinA signaling in the retinotopic mapping

(A,C) Eph receptors and ephrins, expressed in a gradient on both the RGCs and in the superior colliculus, play a pivotal role in the formation of the retinotopic map. In mouse and chick, RGCs overshoot their future termination zone (TZ), but branching in the correct topographic location refines the projections and the posterior axon is eliminated by pruning. Nasal RGCs, expressing low levels of EphAs, project to the posterior region of the superior colliculus, expressing high levels of ephrinAs, whereas temporal RGCs, expressing high level of EphAs, terminate in the anterior part, where ephrinA expression is low. (B) Interstitial branching is prevented by ephrinA reverse signaling anterior to the TZ, and by EphA forward signaling posterior to the TZ. The branching is promoted by BDNF/TrkB signaling. The overlap of these three activities defines the TZ.

In the SC each point is unequivocally defined by the graded expression of guidance molecules along its two axes, and retinal ganglion cells (RGCs) are equipped with the required set of receptors to find their appropriate termination zone. The RGCs enter the anterior part of the SC and overshoot their termination zone (TZ). After entering the SC, interstitial branches start forming on the axon shaft, preferentially in the future TZ, and they grow along the medio-lateral axis. At this point, the projections are refined by pruning of the axon posterior to the TZ and elimination of the ectopic branches and

arbors [134]. EphrinAs are expressed in a low to high gradient along the antero-posterior axis of the SC and along the temporo-nasal axis in the retina. EphAs are expressed in an opposing gradient in both SC and retina [130, 135-139]. Hence, nasal RGCs terminate in the posterior region of the SC, whereas temporal RGCs project to the anterior SC (Figure 1-8). Knockout and knock-in mice have confirmed a role for EphA5, EphA3, ephrinA2, ephrinA3 and ephrinA5 in retinotopic mapping [135, 136, 140]. Interestingly, it has been shown that it is not the absolute but the relative expression level of Eph receptors in RGCs that is critical for the correct formation of the map [135]. The other interesting aspect is how the peak of interstitial branching is precisely located at the future TZ. One model suggests that branching is prevented by ephrinA reverse signaling anterior to the TZ and by EphA forward signaling posterior to the TZ [112, 141-144]. BDNF/TrkB signaling promotes RGC branching [145]. The TZ is defined by the area where branch promotion by BDNF/TrkB signaling is stronger than the Eph-mediated branch-inhibition [134] (Figure 1-8).

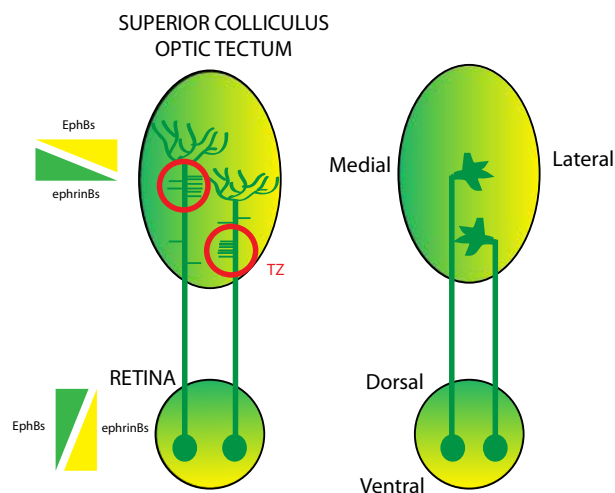


Figure 1-9. EphB/ephrinB signaling in retinotopic mapping

EphB/ephrinB signaling guides RGCs along the dorsal/ventral axis. High levels of ephrinBs repel branches of RGCs that are formed medially to the TZ. Low levels of ephrinBs act as attractive cues for branches formed by RGCs located laterally to the TZ.

EphB/ephrinB signaling controls dorsal/ventral mapping of RGCs, and according to their relative expression levels, they can have either attractive or repulsive activities. EphrinBs are expressed in a low to high medio-lateral gradient in the SC, and in a high to low dorsal/ventral gradient in RGCs. EphB receptors are expressed in an opposing fashion. RGCs positioned lateral to their TZ form branches in response to an attractive ephrinB signal, whereas branches of RGCs positioned medial to their TZ are repelled by high levels of ephrinBs (Figure 1-9) [146, 147]. How these two signaling outputs are achieved has not been completely clarified to date. Reverse signaling has been proven to be important in *Xenopus laevis*, but does not seem to be conserved in mice [146, 148].

Another example of Eph-mediated axon guidance is represented by the spinal cord midline. Here alteration of EphA4 signaling leads to misprojections of two populations of neurons. The corticospinal tract (CST), the major descending motor pathway controlling voluntary movements, originates from neurons in layer V of the cortex and navigates through the forebrain, midbrain and hindbrain to reach the spinal cord. In the medulla, CST axons decussate (cross the midline), and descend the spinal cord in a structure, called the dorsal funiculus (DF). Synaptic targets of CST fibers are usually interneurons in the dorsal spinal cord, contralateral to the neurons originating in the cortex and ipsilateral to the fibers after the decussation [149]. CST axons express EphA4, whereas ephrinB3 is expressed at the spinal cord midline. In wild-type animals, ephrinB3 prevents EphA4-expressing axons from aberrantly recrossing to the contralateral side. In EphA4 or ephrinB3 knockouts, corticospinal axons aberrantly traverse the midline [150-152]. In these mutants not only the axons are misguided but also the anatomical structure containing them is altered. In EphA4 or ephrinB3 knockout mice the dorsal funiculus

appears shallower, already at P0, when CST axons have not yet invaded the spinal cord [150-152]. Thus, the alteration in the morphology of the DF, although dependent on EphA4, seems independent of the CST tract misguidance. The molecular mechanisms underlying these phenotypes are to date unknown, although it is known that EphA4 kinase activity is required [152]. In addition to being expressed on CST axons, EphA4 is expressed by excitatory commissural interneurons (CINs) in the spinal cord [151, 153]. Upon removal of either EphA4 or ephrinB3, similarly to as has been described for CST axons, CINs fibers aberrantly cross the midline [151]. This leads to altered innervation of the locomotor central pattern generator (CPG). Locomotor CPGs are spinal networks of neurons, which generate a rhythmic activity and coordinate left-right and flexor-extensor alternations. The behavioral consequence of this aberrant innervation is a hopping gait: EphA4 and ephrinB3 knockouts do not show alternate limb movement but move left and right limbs synchronously (rabbit-like gait). Both excitatory and inhibitory CINs are implicated in left-right alternation [154]. Since in *EphA4*^{-/-} and *ephrinB3*^{-/-} excitatory axons form ectopic synapses on the contralateral CPGs, they override the commissural inhibition and abolish left-right coordination [150-153].

An example of Eph receptors required as ligands during development is the formation of the anterior commissure (AC), a large forebrain tract. It consists of an anterior (aAC) and posterior branch (pAC), which connect the two lobes of the olfactory bulbs and the medial temporal cortical areas of the two hemispheres, respectively. EphA4 is required for the formation of the aAC and pAC, and EphB2 for the formation of the pAC [150, 152, 155]. EphA4 is not expressed on the aAC tract but on the surrounding cells [152, 156]. In *EphA4*^{-/-} mice the aAC and pAC are not formed, however in *EphA4*^{KD} (kinase-

dead knock-in) mice the phenotype is rescued, suggesting that the kinase activity, and thus the forward signaling, are not required [150, 152].

Eph and ephrin expression is maintained in the adult brain, mainly in areas where there is active remodeling of neuronal circuits upon environmental changes. In the hippocampus, Eph receptors play an important role in learning and memory, through the modulation of LTP and long term depression (LTD). EphA4 and EphB2 knockout mice have reduced LTP and LTD, although basal synaptic transmission is not impaired. LTP and LTD defects were rescued in knock-in mice expressing EphA4 lacking the intracellular domain, suggesting that this function is dependent on reverse signaling [157-161]. Work from our laboratory showed that EphA4, expressed post-synaptically in hippocampal neurons, activates ephrinA3, expressed on perisynaptic astrocytes, and via reverse signaling regulates the levels of glial glutamate transporters. EphA4 and ephrinA3 knockout mice have more glutamate transporters on the astrocyte and less glutamate in the synaptic cleft, causing impairment in LTP [158].

1.2. Neuron development: Axon growth and guidance

To reach their appropriate synaptic targets neurons navigate the environment supported by trophic factors and oriented by guidance molecules. Trk, Ret and Eph receptors play key roles in development orchestrating the growth rate and the growth direction of several populations of neurons.

In my thesis I focused on two different populations of neurons - trigeminal and motor neurons - and analyzed their development, their growth and branching in response to ephrins and neurotrophic factors.

1.2.1. Trigeminal neurons

The trigeminal ganglion (TG) is one of the cranial sensory ganglia. It is composed of nociceptive, proprioceptive and mechanoreceptive neurons, and provides sensory innervation to the face, the oral and the nasal cavities. Trigeminal neurons are pseudounipolar.

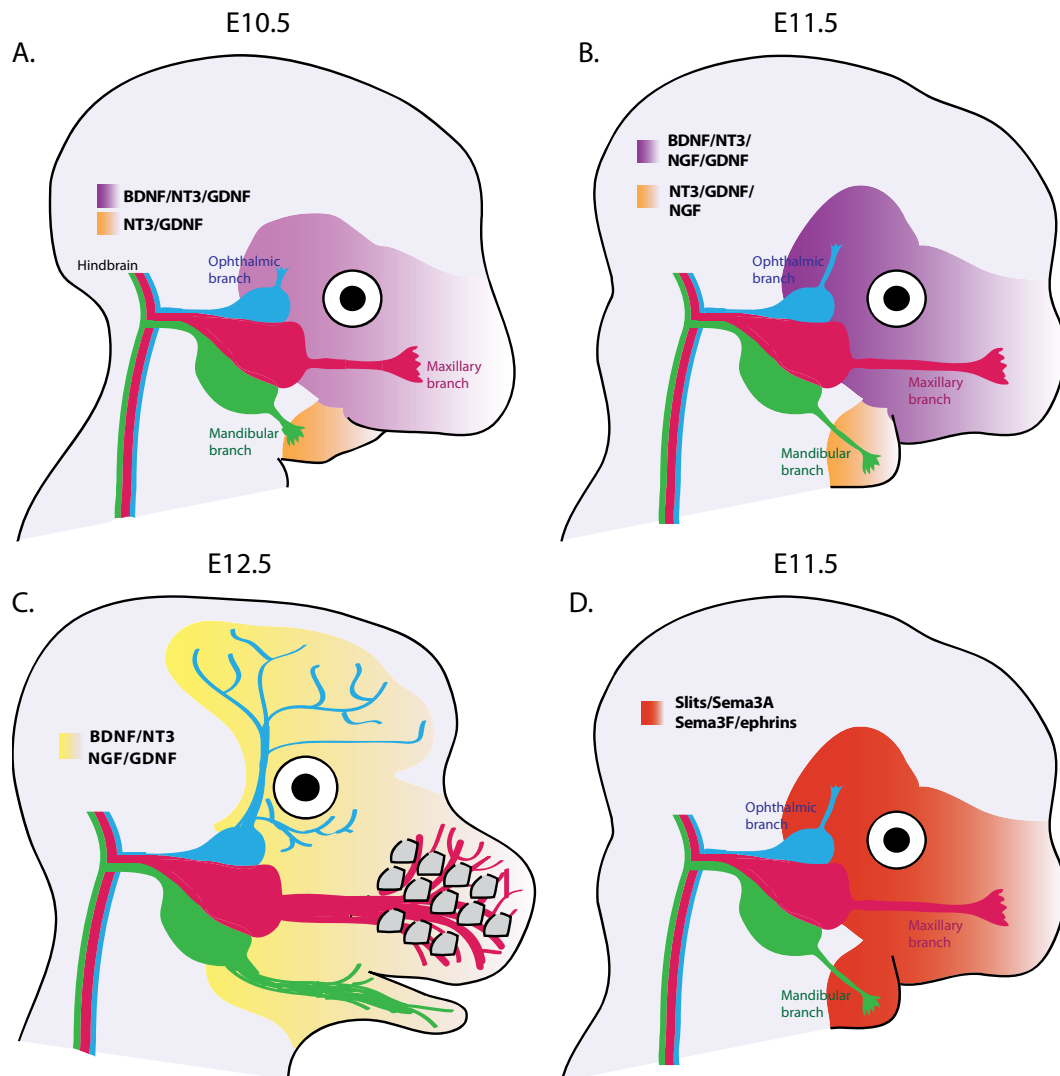


Figure 1-10. Sensory neuron guidance in the trigeminal ganglion

Scheme of sensory neuron development in the trigeminal ganglion. (A) At E10.5 pioneering axons emerge separated into the three branches of the trigeminal ganglion – ophthalmic (blue), maxillary (fuchsia), mandibular (green). Target tissues support their growth by secreting BDNF, NT3 and GDNF. (B) At E11.5, NGF expression starts to be up-regulated in the target tissues, and axons start invading the target tissues. (C) The three branches grow further in the periphery, and their arbors increase in complexity. (D) Trigeminal axons are guided towards their targets by the repulsive signaling of Sema3A/Neuropilin1 and Sema3F/Neuropilin2. The arborization of the three branches is regulated by the Slit/Robo signaling.

The two axons emerge from the opposite sites of the soma: one grows toward the periphery, the other enters the hindbrain. In the periphery the TG has three main branches: the maxillary, the mandibular and the ophthalmic. Since they emerge from the ganglion, axons are separated into three independent routes, each one corresponding to one of the peripheral branches (Figure 1-10). In the periphery axons gradually leave the nerve to form branched terminal plexi, whereas as soon as they enter the brainstem, they bifurcate to form the ascending and descending projections of the trigeminal tract [162]. Pioneering axons leave the ganglion at E9.5 reaching the mandibular epithelium by E10.5 and the maxillary one by E11. The last axons reach their target tissue by E15. The number of neurons in the ganglion peaks at E13, and programmed cell death peaks at E14 [163]. *In vitro* and *in vivo* studies have shown that trigeminal neurons have three phases: first they are neurotrophin independent (earlier than E10), then their survival is BDNF and NT-3-dependent (E10-E13), later it becomes NGF-dependent [163-165].

Lack of TrkA/NGF signaling causes a postnatal loss of trigeminal neurons, whereas lack of TrkB/BDNF signaling reduces the number of neurons already at E14, reflecting the different timing of their requirement for survival. The switch between BDNF and NGF happens around E12, when TrkB signaling is inhibited. This inhibition could be partially explained by the reduction of TrkB expression, but to date has not been fully elucidated [165]. According to their growth rate, trigeminal neurons can be divided into slow and fast growing, although these two populations have not been molecularly characterized [166]. Consistent with their role in survival, BDNF and NT-3 mRNA are detected in the target tissue before the arrival of pioneering axons, whereas NGF is detectable only upon target tissue innervation [164, 167-169]. Neurotrophins are poorly

expressed in the brainstem, suggesting that survival of trigeminal neurons is mainly dependent on peripheral sources [164]. Neurotrophins are also able to modulate the growth and arborization of trigeminal neurons during development. In slice culture, NGF stimulation leads to increases in axon elongation of both central and peripheral trigeminal axons, whereas NT-3 promotes excessive axon branching of these tracts [170].

Ret is also expressed in developing trigeminal neurons and GDNF is present in the target tissue [171-173]. *In vitro* GDNF is a trophic factor for a subset of trigeminal neurons, however *Ret*^{-/-} and *GDNF*^{-/-} mice do not show a loss of trigeminal neurons [55]. In *GDNF* knockout mice there are no GFR α 1-positive neurons, and *GDNF* heterozygous mice have less myelinated axons and their associated terminals [87, 173]. To date the *in vivo* extent of GDNF/Ret signaling in supporting trigeminal neuron growth and branching has not been fully elucidated.

Trigeminal neurons express several guidance receptors, including neuropilins, Robos and Eph receptors. Neuropilin1/Sema3A and neuropilin2/Sema3F signaling are essential for the migration of cranial neural crest cells and the formation of the trigeminal ganglion. Semaphorins secreted by the target tissues, i.e. cornea or tongue, prevent the premature innervation by trigeminal axons [174]. Neuropilin1 and Sema3A mutants show normal TG size and positioning, however axon trajectories are severely disorganized. The trigeminal arbors are extremely defasciculated and widely spread, and the ophthalmic nerve overshoots its termination area [175, 176]. Robo/Slit signaling is required for correct development of the peripheral arbors of the ophthalmic branch [177]. Eph receptors and ephrins are expressed both in the target tissue and on the trigeminal neurons [178]. So far, the only phenotype reported is impairment of vibrissa innervation in

EphA4^{-/-} embryos due to the lack of reverse signaling [179]. In addition to classical guidance cues, p75NTR plays a role in determining the arborization of the ophthalmic branch. In *p75NTR* knockouts the ophthalmic branch shows a reduced arbor size, partially due to defects in neurite elongation, which is partially due to impaired Schwann cell migration [180].

Although in the mouse some of the receptor tyrosine kinases influencing the growth, guidance and survival of trigeminal neurons have been well described, the fine-tuning mechanisms that allow axons to extend following a great variety of trajectories and with different growth rate have not yet been elucidated.

1.2.2. Motor neurons of the lateral motor columns

Motor neurons in the spinal cord are organized in pools according to their position and their target muscles. Pools of motor neurons vary at different levels of the spinal cord. Lateral motor column (LMC) motor neurons are present at the brachial and lumbar levels of the spinal cord, and are further subdivided in medial (LMC_M) and lateral (LMC_L) (Figure 1-11). In vertebrates, LMC axons emerge from the spinal cord at E10.5. In the hindlimb, LMC axons from the lumbar segment L3-5 follow a common trajectory (sciatic nerve) until E11.5, when they reach the sciatic plexus at the base of the hindlimb. At the sciatic plexus, the sciatic nerve divides into a ventral (tibial nerve) and dorsal branch (peroneal nerve), formed by LMC_M and LMC_L axons, respectively [181, 182]. LMC_M neurons express the transcription factor *Islet1*, which induces the expression of *EphBs*, whereas LMC_L express *Lim1*, which enhances the expression of *EphA4* [183, 184]. LMC_L, expressing high levels of *EphA4*, are repelled by the ventral mesenchyme, enriched in ephrinAs; and LMC_M, expressing high levels of *EphBs*, are repelled by the

dorsal mesenchyme, enriched in ephrinBs (Figure 1-11). *Lim1*^{-/-} mice show randomization of this dorsal/ventral choice [185]. In *Epha4* knockouts, a subpopulation of LMC_L axons project ventrally, whereas in the triple *EphB* knockouts or *ephrinB1* knockouts certain LMC_M axons project dorsally [183, 184, 186, 187].

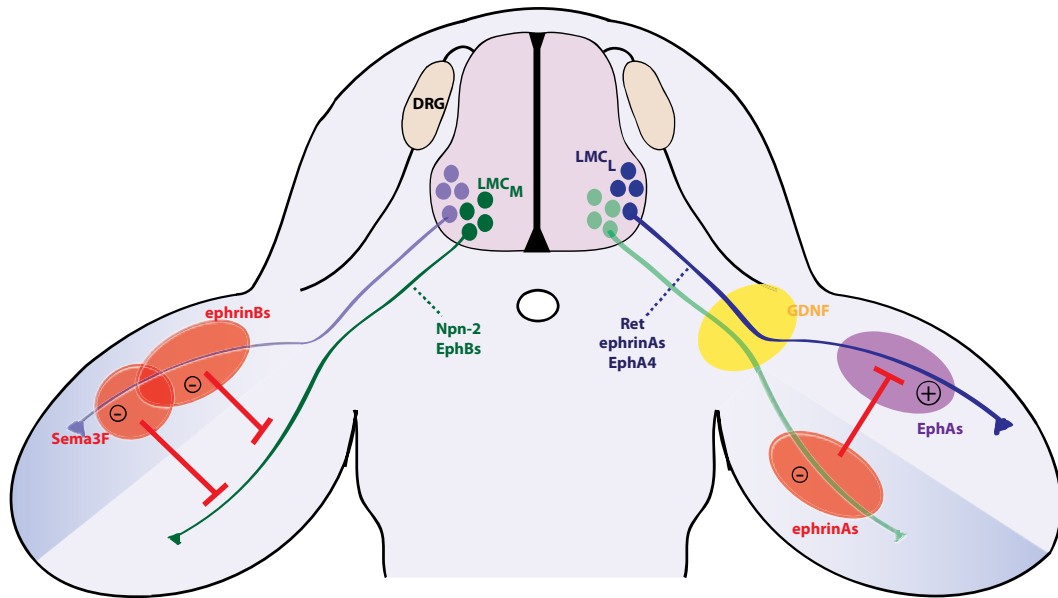


Figure 1-11. LMC guidance in the limb

Scheme of a limb horizontal cross-section at E12.5. LMC_L neurons express high levels of EphA4, Ret and ephrinAs. LMC_M neurons express high levels of EphBs and Neuropilin2 (Npn-2). The ventral mesenchyme expresses ephrinAs, and the dorsal Sema3F, ephrinBs and EphAs. GDNF is expressed slightly dorsally at the sciatic plexus. EphA4/ephrinA repulsive signaling (forward signaling) prevents LMC_L axons (blue) from entering the ventral mesenchyme, whereas ephrinA/EphA attractive signaling (reverse signaling) pulls them in the dorsal region. Ret/GDNF signaling cooperates with Eph receptors in guiding LMC_L axons (green) in the dorsal mesenchyme. EphB/ephrinB and Sema3F/Neuropilin2 repulsive signaling prevent LMC_M from entering the dorsal region.

EphA4/ephrinA signaling has had a controversial role in hindlimb axon guidance since both ligands and receptor are expressed on the nerve and in the target tissue [188-190]. EphA4 can act as a receptor on the nerve, but can also act as a ligand in the mesenchyme. Work by Sam Pfaff's group showed that ephrinAs and EphAs can be localized in different membrane patches, from where they can signal independently. EphA4 forward signal mediates repulsion, whereas ephrinA reverse signaling mediates growth cone spreading, an *in vitro* correlate of axon attraction [190]. A conditional

knockout approach showed that both reverse and forward signaling cooperate to refine the axonal trajectories. However, removing EphA4 from only the hindlimb mesenchyme is not sufficient to cause LMC misprojections, probably because the loss of EphA4 is compensated by the presence of EphA7 and EphA3 [191]. Although the importance of Eph-mediated attraction and repulsion are well established, it is still unclear how the axons become insensitive to Eph-mediated attraction and grow away from this intermediate target (sciatic plexus). Since both EphA7 and EphA4 can be cleaved, two scenarios are possible: either they act as soluble ligands or cleavage enables the axons to detach from the Eph-expressing cells and to grow further into the limb mesenchyme [192, 193].

Another level of complexity is added by the ability of Eph receptor and ephrins to interact both *in cis* and *in trans*. The availability of Eph receptors to bind ephrins *in trans* is titrated by the levels of co-expressed ephrins. Low expression of ephrins on LMC axons, favors Eph/ephrin *trans*-interactions, and axons are repelled by the ephrin-expressing mesenchyme. High expression of ephrins favors Eph/ephrin *cis*-interactions, preventing Eph-mediated repulsion. Knock-down or over-expression of ephrinA5 or ephrinB2 in chick results in LMC_M or LMC_L misguidance, due to changes in Eph receptor availability for *trans* interactions [126].

The fidelity of this dorsal/ventral choice is also enhanced by the presence of other guidance systems [194]. In addition to known guidance molecules, two neurotrophic factors, HGF and GDNF, are also involved. *In vitro* HGF is a very strong chemoattractant for motor neurons, although its *in vivo* role is not yet well characterized [195]. GDNF is expressed dorsally to the sciatic plexus, and Ret is highly expressed on LMC_L axons.

Genetic ablation of Ret or GDNF causes misguidance of a subset of LMC_L axons, which grow erroneously in the ventral mesenchyme of the hindlimb. Interestingly, *Ret* and *GDNF* knockouts phenocopy *EphA4* mutants. More interestingly, *EphA4* and *Ret* double knockouts show a more severe phenotype than the single knockouts, hinting for a genetic interaction of the two signaling pathways [196]. Similarly, in chick, over-expression of EphA4 or Ret on LMC_M neurons is sufficient to re-route a subset of their axons to the dorsal mesenchyme [186, 196]. Thus, EphA4 and Ret are likely to cooperate in guiding LMC_L neurons, although the molecular mechanisms of this cooperation are still unclear. Another class of receptors and ligands involved in this dorsal/ventral choice is the semaphorin/neuropilin family. At brachial level, the repulsive interaction of Sema3F and neuropilin2 contributes to LMC_L guidance. Sema3A-neuropilin1 regulates fasciculation, outgrowth and bifurcation of both LMC populations [197].

Work over the last years has also started to identify potential downstream effectors required for LMC guidance. Src and Fyn are expressed in both populations of LMC neurons. Knock-down and over-expression experiments in chick, complemented by analysis of knockout mice, have shown a requirement for Src and Fyn in axon guidance downstream of Eph receptors. Interestingly, LMC_M neurons rely more on Src activity for their pathfinding than LMC_L [198]. If Src and Fyn act only downstream of Eph receptors or if they can be common to signaling cascades initiated by different receptors is still unknown.

1.3. Intrinsic mechanisms to regulate RTKs signaling

As mentioned above neurons evolved several mechanisms to regulate axon growth and guidance. To ensure the proper connection with the right synaptic target several

events must take place: 1) receptors and ligands must be complementarily expressed in neurons and target tissues; 2) receptors must have the right cellular localization (axon, dendrite, soma or growth cones) and soluble guidance cues must be properly distributed in the extracellular environment; 3) signaling from different receptors must be transduced and integrated; 4) signaling must be modulated and terminated. Each step introduces a different level of regulation, and suggests the presence of several families of intrinsic regulators of receptor signaling [199].

Levels and location of ligands and receptors can be regulated transcriptionally (i.e. Lim1-induced EphA4 expression in LMC_L neurons) or post-translationally (cleavage of pro-neurotrophins by furin and metalloproteases) [183, 200]. Mis-expression of a receptor or a ligand can result in guidance, outgrowth or branching defects. For example, ectopic expression of Ret in LMC_M neurons is sufficient to re-route some of them into the dorsal shank of the hindlimb [196]. Over-expression of neurotrophins in the target tissues causes hyper-innervation by sensory neurons [48].

Sub-cellular localization can be regulated either by local translation or by interaction with co-receptors or scaffolding proteins. Disrupting ephrinA and EphA4 cellular localization in motor neurons, dramatically changes the *cis* versus *trans* interaction, impairing both reverse and forward signaling [190]. Interestingly, a series of studies demonstrated that RTKs can signal either from the plasma membrane or from intracellular compartments (i.e. endosomes) [201]. Hence, endocytosis not only regulates the abundance of receptor molecules available on the plasma membrane but also modulates the signal cascades initiated upon ligand binding.

The activation of common downstream effectors is one way to integrate signaling. Different receptors can converge on the same pathway, i.e. actin cytoskeletal remodeling, and differentially regulate some of the pathway components. In *C. elegans* for example, three different receptor/ligand systems – netrin/DCC, Slit/Robo and ephrin/Eph - regulate actin-nucleation via the WAVE/SCAR complex during embryonic morphogenesis. The three receptors have distinct effects on F-actin, that once integrated, ensure correct level and polarization of the actin cytoskeleton during morphogenesis [202].

RTKs can interact with different classes of transmembrane proteins which can positively or negatively regulate their signaling. Interaction with RPTPs, provides an inhibitory mechanism in the absence of the ligand, but also determines the strength and the duration of the signaling cascade after ligand stimulation. Another class of RTK regulators is the LIG family of leucine-rich repeat and immunoglobulin proteins. Linx1 enhances BDNF- and GDNF-mediated growth, guidance and branching [203]. On the other hand Lrig1 can negatively regulate GDNF-induced neurite outgrowth, partially by preventing GDNF binding to Ret [204].

In the next paragraphs, I will delve into the role of RPTPs in RTK signaling modulation and termination; the role of proteolytic cleavage in regulating receptor expression and signaling; and finally, the cooperation of different families of guidance cues and receptor cross-talk.

1.3.1. Keeping the phosphotyrosine balance: RPTPs versus RTKs

Several signaling cascades, based on tyrosine phosphorylation, regulate different aspects of development, including cell proliferation, differentiation and axon guidance. Work over the last decades has defined a clear role for kinases in the development of the

nervous system, however the role, function and substrate of phosphatases has not been fully elucidated. In the human genome there are 107 known phosphatases, and 21 of these belong to the RPTP family. RPTPs are a family of transmembrane phosphatases, involved in axon guidance, regeneration and synapse formation [205]. In vertebrates RPTPs are organized into eight subfamilies, according to their extracellular structure and number of phosphatase domains. The extracellular domain contains several motifs, common to the CAM family. The intracellular domain contains either one or two phosphatase domains. In the molecules with two phosphatase domains, i.e. LAR, the first phosphatase domain is responsible for 99% of the catalytic activity [206, 207]. The cysteine in the phosphatase domain is the key residue for enzymatic activity [208].

In *Drosophila*, all the RPTPs expressed are involved in axon growth and guidance of motor neurons, photoreceptors, and neurons in the mushroom body, and in the antennal and optic lobes. They have been shown to act both as negative and positive regulators. In vertebrates, the regulation of growth and guidance is conserved for class II and III RPTPs. Among these two classes the best studied are type II RPTPs, which include LAR, PTP σ and PTP δ [205].

To date, several RTKs have been shown as *in vitro* substrates of RPTPs. However, in most of the cases the *in vitro* data are not supported by an *in vivo* interaction. Few RPTPs have been proposed as regulators of Trk and Eph receptor signaling, but to date there is no RPTP shown to regulate Ret signaling. TrkB is a substrate for LAR and PTP σ , although the former acts as a positive and the latter as a negative regulator [209, 210]. PTP σ has been previously shown to dephosphorylate TrkA and TrkC specifically when coexpressed in HEK293 cells, and later to be able to dephosphorylate TrkB in primary

hippocampal cultures upon chondroitin sulfate proteoglycan (CPSG) activation [209, 211]. PTP σ activation by CPSGs leads to a reduction of BDNF-induced spines [211]. LAR enhances TrkB phosphorylation and *LAR*^{-/-} hippocampal neurons display a reduction of TrkB signaling and diminished BDNF-induced survival [210]. However, in both *LAR*^{-/-} and *PTP σ* ^{-/-} mice the observed phenotypes are not compatible with a loss or gain of function of TrkB [212, 213]. Finally, RPTPZ can dephosphorylate TrkA and reduce NGF-dependent outgrowth in sensory neurons [214].

EphB2 activity can be regulated by LAR, a type II RPTP. FGFR1 activation can increase EphB2 phosphorylation in the absence of ligand, via the inhibition of LAR [215]. Interestingly, in *C. elegans*, *ptp3* (LAR ortholog) and VAB-1 (Eph ortholog) have synergistic effects in epidermal morphogenesis, suggesting redundant functions for the two proteins, rather than LAR acting as a negative regulator of Eph receptor [216].

1.3.1.1. PTPRO regulation of Trk and Eph receptors

PTPRO is a type III RPTP, with eight fibronectin-like domains in the extracellular region, a transmembrane domain and one intracellular phosphatase domain. The extracellular domain has been shown to act as a repulsive guidance cue for RGCs in chick [217]. In mouse, PTPRO has been reported as a regulator of nociceptive (TrkA⁺) and proprioceptive (TrkC⁺) fiber guidance [218] and, in chick, as a regulator of motor and retinal axon guidance [219]. PTPRO knockout mice are less sensitive to thermal stimulation, as a consequence of missing CGRP⁺ DRG neurons and nociceptive fibers in the dorsal horn of the spinal cord. Additionally, in these mutants, parvalbumin-positive (PV⁺) neurons terminate before reaching their synaptic target (motor neurons), and cause a minor impairment in hindlimb placement and rotarod performance [218]. However, the

molecular mechanisms of these guidance defects have not been elucidated. *In vitro*, PTPRO when over-expressed in heterologous cells, is able to dephosphorylate TrkC, but this interaction has never been confirmed *in vivo* [220].

In chick, PTPRO knock-down causes the absence of a secondary branch of the peroneal nerve in the hindlimb [221]. This phenotype is partially rescued by knocking down a type II RPTP, suggesting that these two classes of RPTPs might balance each other's signaling. As for the DRG projections, the potential PTPRO substrates, ligands or interactors have not been identified.

In the chick retina, PTPRO knock-down or over-expression causes aberrant projections of RGCs. This phenotype is due to PTPRO-dependent regulation of Eph receptor phosphorylation. Over-expression of wild type PTPRO diminishes Eph receptor phosphorylation and makes retinal axons less sensitive to ephrin stimulation. Similarly, over-expression of a dominant negative form of PTPRO enhances Eph phosphorylation and makes axons more sensitive to ephrin stimulation. Since PTPRO dephosphorylates Ephs in two conserved juxtamembrane tyrosines, it can act as a phosphatase for both EphA and EphB receptors [219]. In mouse, PTPRO's function as a potential Eph regulator and its tissue-specificity have not been addressed.

1.3.2. Shedding regulates receptor expression and signaling

Several different post-translational modifications regulate receptor availability at the plasma membrane, including regulated endocytosis, receptor trafficking, mRNA transport and receptor cleavage. Interestingly, cleavage not only regulates receptor expression, but can also modulate its signaling properties. In humans, there are more than 500 proteases, constituting 1.5% of the protein-coding genes [222]. Among them, metalloproteases

represent a large family of Zinc-dependent proteases, comprising secreted (ADAMTSs, MMPs, and Pappalysins), membrane-bound (ACEs, ADAMs, and MT-MMPs), and cytosolic proteins (Insulysin, Neprilysins, and THOP1) [223]. Pioneering studies on the role of metalloproteases in axon guidance were done in Marc Tessier-Lavigne's laboratory showing that the inhibition of DCC ectodomain shedding potentiates axon outgrowth in response to Netrin stimulation [224].

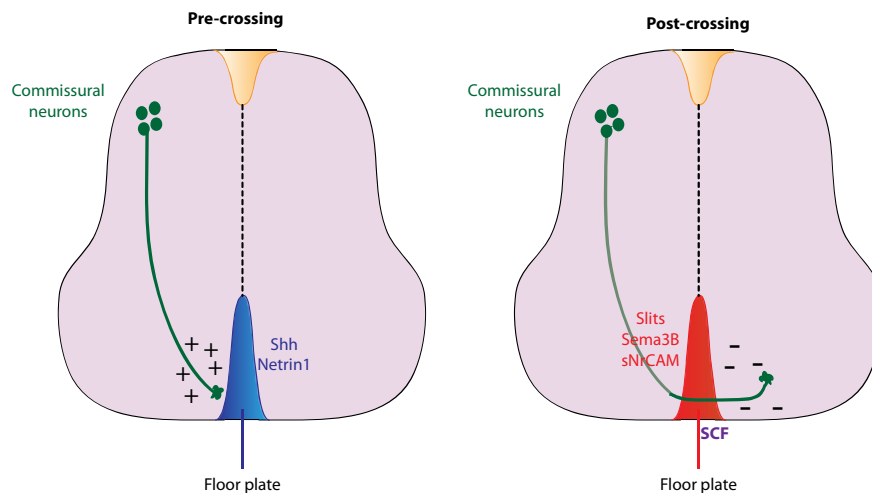


Figure 1-12. Axon guidance at the spinal cord midline

Scheme of commissural neuron guidance in the spinal cord illustrating guidance cues acting on the axons before (left) and after (right) crossing. Pre-crossing axons are attracted toward the midline by Netrin1, Shh and VEGF. At the floor plate Netrin attraction is silenced by Robo1/Slit, and plexinA1 expression on the axons is increased via NrCAM- and GDNF-mediated inhibition of its proteolytic cleavage by calpain. Sema3B and Slit drive axons away from the midline, while SCF provides trophic support.

Commissural neuron guidance represents an elegant example of how receptor cleavage regulates receptor expression and allows axons to respond to different cues. Commissural neurons, located in the dorsal spinal cord, extend their axons towards the floor plate in response to an attractive gradient of Netrin. After reaching the floor plate the axons are repelled by the midline, and start growing along the longitudinal tract. This switch between attraction and repulsion is achieved through the regulation of the receptors present on the growth cone of commissural axons [225]. For example, PlexinA1 expression is up-regulated at the growth cone after crossing the midline through the

inhibition of the calpain-dependent degradation of the receptor. PlexinA1 up-regulation sensitizes these axons to the repulsive Sema3B expressed at the midline [93, 226] (Figure 1-12).

In addition to regulating receptor expression levels, ectodomain shedding can also reduce the availability of ligand, further limiting the extent of receptor activation. For example, Met receptor cleavage releases the Met ectodomain, which acts as a decoy, binding to HGF and preventing its action on the full length receptor [227].

Cleavage is also an important component of Eph/ephrin signaling: it represents a mechanism to promote cell-cell repulsion upon the initial binding and the released fragments can initiate an independent signaling cascade [122, 192, 228]. EphB2 cleavage can be triggered by two different mechanisms: one ligand-dependent and one induced by calcium influx. The ligand-dependent pathway triggers EphB2 ubiquitination, internalization and endosomal processing of the receptor. Upon ligand binding the receptor is cleaved, independently of metalloproteases and the released carboxiterminal fragments are degraded by the proteasome [228]. And probably, this inhibition of ligand-dependent EphB2 cleavage is what prevents cell-cell detachment [122]. Calcium-induced cleavage happens at the plasma membrane and requires metalloproteases and γ -secretase. NMDA receptor activation enhances receptor cleavage, via the calcium influx pathway [228]. In addition to EphB2, another member of the Eph receptor family undergoes proteolytic processing: EphA4. EphA4 is cleaved in two consecutive steps by metalloproteases and γ -secretase. This leads to the release of a shed ectodomain (EphA4-ECD), with an yet unidentified function, and of an intracellular fragment (EphA4-ICD), which preferentially activates Rac1. In transfected hippocampal neurons, EphA4-ICD

induces the formation of spines. Interestingly, EphA4 cleavage is not induced by ligand but by synaptic activity [192]. “What is the *in vivo* function of EphA4 shedding?”, “In which tissues EphA4 is cleaved?” and “Is EphA4 shedding a developmentally regulated process?” are still unexplored questions.

1.3.3. Cooperation of guidance cues and receptor cross-talk

Once all the major families of axon guidance and growth molecules have been discovered, the big challenge is to understand how they cooperate to progressively instruct the growth of neurons towards their synaptic targets. To date there are several reported examples of sets of guidance cues that act simultaneously or in subsequent steps on the same neuron population.

The best studied example is the spinal cord midline where different families of guidance cues cooperate in consecutive steps. Netrin, Shh and Vascular endothelial growth factor (VEGF) cooperate to guide the axons toward the floor plate; Slit, Semaphorins and stem cell factor (SCF) cooperate to push axons away from the midline (Figure 1-12). The phenotypes observed in the knockout mice reflect the different requirements during guidance: the commissural axons in netrin, Shh and VEGF signaling mutants terminate before the floor plate; in Slit, Robo1, Sema3B and PlexinA1 mutants axons reach the floor plate but either they stall at the midline or they recross to the ipsilateral side; and in *SCF* knockouts axons stall after crossing the floor plate [199, 225, 229-233]. At the molecular level the switch from attraction to repulsion is achieved by regulating receptor dynamics at the surface, either as previously described by cleavage of the receptors or by receptor cross-talk. Robo can, indeed, silence the attractive effect of Netrin, by binding to its receptor DCC [233].

In the hindlimb, multiple signaling systems cooperate to ensure that motor axons follow the appropriate trajectories [194]. In contrast to the spinal cord midline, in the hindlimb these signaling pathways act in parallel. *Ret* and *GDNF* knockouts display misguidance of LMC_L neurons, similarly to what is observed in *EphA4* mutants [196]. The molecular mechanisms underlying *Ret* function in the LMC_L guidance choice are not yet clarified. Although GDNF/*Ret* signaling has a well established growth-promoting function, emerging evidence suggests that GDNF can act as a chemoattractant [55]. Which aspect of GDNF/*Ret* signaling is necessary to support this dorsal/ventral choice has not been addressed. Intriguingly, *EphA4/Ret* double knockout mice have a stronger phenotype than the single mutants, suggesting that the two receptors cooperate in guiding LMC_L axons in the dorsal mesenchyme of the hindlimb. However, the two receptors do not influence each other's expression levels. Indeed in *Ret*^{-/-} or *GDNF*^{-/-}, although rerouted to the ventral mesenchyme, LMC_L axons keep expressing higher levels of *EphA4* than LMC_M fibers. Similarly, in *EphA4*^{-/-} embryos, *Ret* expression was maintained on the misguided LMC_L axons [196]. If the two receptors cooperate at the molecular level is still unknown, although a few mechanisms can be speculated. The two receptors could influence each other's signaling (cross-talk) or converge on common downstream effectors, such as ephexin or Src kinases, to amplify the signaling output. *Ret* could enhance *EphA4*-mediated repulsion, hence in the absence of *Ret*, *EphA4*⁺ LMC_L axons would no longer be able to be repelled by the ventral region of the hindlimb. Similarly, *EphA4* could positively modulate *Ret* signaling, thus in *EphA4* knockouts *Ret*⁺ LMC_L axons would no longer be responsive to GDNF present at the choice point. Alternatively, as has been described for SCF at the midline [234], GDNF can provide trophic support to

enable LMC_L axons to leave the intermediate target upon being repelled by ephrinAs. Another alternative is that EphA4 and Ret act in parallel, exerting opposite effects on the growth cones.

1.4. Purpose of thesis project

As mentioned in the previous paragraphs, molecular mechanisms to fine tune and integrate different guidance cues are still not fully elucidated. In my thesis I focused on two different guidance systems: trigeminal and motor neurons, and three potential mechanisms to regulate receptor signaling: interaction with RPTPs, proteolytic processing and cooperation with other guidance cues.

Growth promoting signals required for trigeminal neuron growth and branching are well known, however how the same receptors can regulate a great variety of trajectories and how axons expressing the same Trk receptor can grow at different speeds has not yet been clarified. I analyzed the trigeminal projections at two developmental stages and observed an enhanced complexity of the maxillary and ophthalmic arbors. To define the underlying molecular mechanism, I examined the potential interaction of PTPRO with Trk receptors and Ret. In parallel, I studied whether PTPRO's role as a specific Eph receptor phosphatase was conserved between chick and mice.

The roles of receptor cleavage during development have not been well characterized. In particular, nothing is known about the *in vivo* relevance of Eph receptor cleavage and its impact on Eph-dependent guidance decisions. To address this question I generated a knock-in mouse carrying a mutation to abolish EphA4 receptor cleavage. I analyzed three of the most prominent phenotypes observed in *EphA4* knockout mice: motor neuron axon guidance at the sciatic plexus, dorsal funiculus and anterior commissure formation.

Finally, I focused on if and how two RTKs, EphA4 and Ret cooperate in guiding LMC_L neurons. Although the genetic interaction of Ret/GDNF and EphA4/ephrinAs has already been described, the underlying molecular mechanism has been poorly elucidated. To shed light on the potential cross-talk between the two receptors, I studied their sub-cellular localization in motor neuron growth cones. Moreover, in collaboration with Dr. Irina Dudanova, we addressed whether Ret signaling was dependent on EphA4 and vice versa.

2. Results

2.1. PTPRO's role during development

2.1.1. PTPRO's developmental expression pattern

To address the function of PTPRO in axon growth and guidance of sensory and motor neurons I analyzed its temporal expression pattern between E10.5 and post-natal day 0 (P0). The specificity of the PTPRO antibody was tested on different tissues derived from PTPRO knockout embryos (Figure 2-1) (see also [235]).

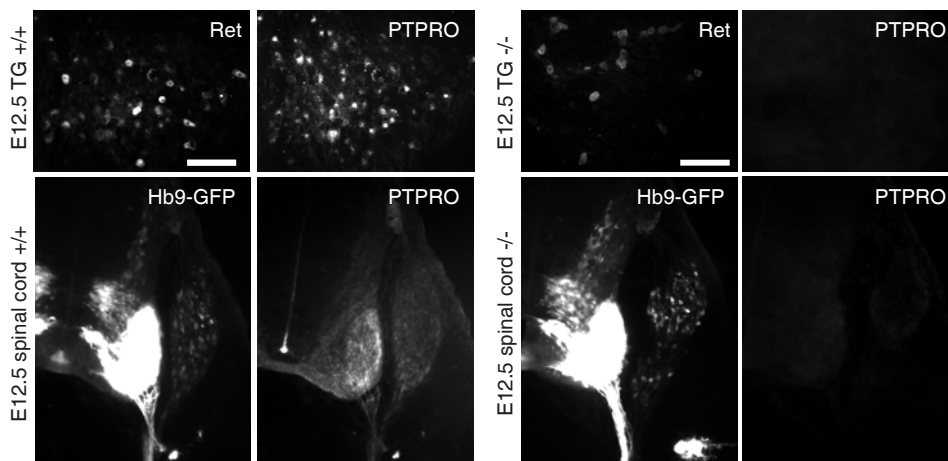


Figure 2-1. Specificity of the anti-PTPRO antibody

Top panels show cross sections of the trigeminal ganglion (TG) from wild-type and *PTPRO*^{-/-} E12.5 embryos stained with anti-PTPRO and anti-Ret (as control) antibodies. Lower panels show cross sections of the spinal cord from wild-type and *PTPRO*^{-/-} E12.5 embryos crossed with a transgenic line expressing GFP under the Hb9 promoter (Hb9-GFP) stained with anti-PTPRO antibody. Scale bar is 50µm.

In particular, I analyzed PTPRO expression pattern in lateral motor column (LMC), trigeminal (TG), dorsal root ganglia (DRG) and RGC neurons. I prepared cryosections from E12.5 embryos and performed co-immunostaining of PTPRO with Lim1 and Islet1, to label LMC_L and LMC_M neurons, respectively. At E12.5, PTPRO was not specifically localized to either of the two populations but seemed evenly distributed in both (Figure 2-2). The expression in both classes of neurons was consistent with the idea that PTPRO interacts with both EphA and EphB receptors, which are enriched in the LMC_L and LMC_M populations, respectively.

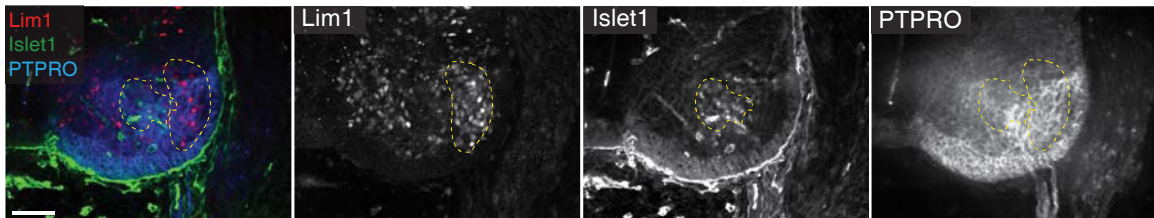


Figure 2-2. PTPRO expression pattern in LMC neurons

Cross sections from E12.5 lumbar spinal cord were stained with anti-PTPRO, anti-Is11 and anti-Lim1 antibodies. LMC_L and LMC_M populations were defined by Lim1 and Islet1 expression, respectively. PTPRO co-localizes with both markers. Scale bar is 50 μ m.

Regarding the sensory system, I analyzed two different types of peripheral sensory ganglia: trigeminal and lumbar DRG. I prepared cryosections from wild-type E10.5, E11.5, E12.5 embryos and stained them for PTPRO and the axonal marker Tuj1. At E10.5, PTPRO was barely detectable in trigeminal neurons, but by E11.5 was seen on trigeminal cell bodies and axons, both labeled by Tuj1 staining. PTPRO expression was maintained through all later embryonic stages of development and in newborns (Figures 2-3 and 2-4). The expression pattern on trigeminal cell bodies suggested that PTPRO expression might be restricted to a subset of trigeminal neurons. Trigeminal neurons are divided into four populations, according to the expression of TrkA, TrkB, TrkC and Ret. TrkA labels nociceptive neurons, TrkB and Ret (at early stages) mechanoceptive. Later in

development, TrkA^+ neurons further differentiate into peptidergic and non-peptidergic, and start expressing Ret [236].

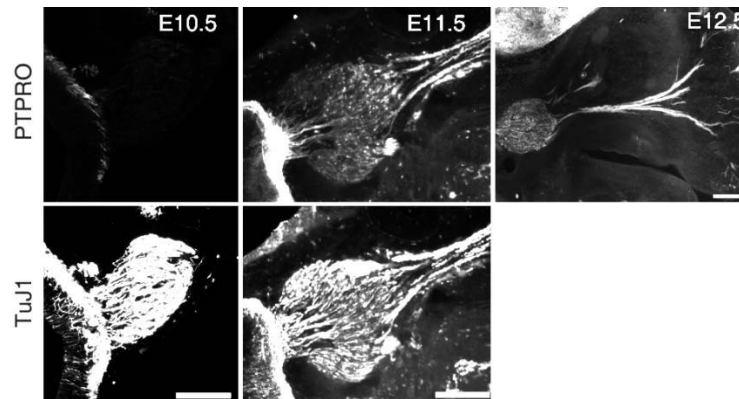


Figure 2-3. PTPRO expression pattern during TG development

Trigeminal ganglion cross sections were stained with anti-PTPRO and anti-Tuj1 antibodies. PTPRO expression was analyzed at three developmental stages E10.5, E11.5 and E12.5. Scale bar is 250 μm .

To verify in which populations PTPRO was expressed, I prepared co-immunostainings with TrkA, TrkB, TrkC and Ret at three different developmental stages: E12.5 (time of axon elongation), E15.5 (time of axon arborization), and P0 [162]. At E12.5 PTPRO was expressed in roughly half of TrkB^+ and Ret^+ , in a small population of TrkC^+ , but rarely in TrkA^+ neurons (Figure 2-4). At E15.5, and similarly at P0, PTPRO expression decreased significantly in TrkB^+ but remained high in Ret^+ neurons, and did not increase in the other two populations (Figure 2-4). The expression pattern showed that PTPRO is localized in mechanoreceptive neurons in the early phases of their development. Since at E16.5 PTPRO is reportedly expressed mainly in E16.5 TrkA^+ and TrkC^+ DRG neurons [237], I repeated the expression analysis in the DRG looking at three developmental stages. Consistent with the trigeminal data at E12.5, PTPRO was expressed in roughly half of the TrkB^+ , in a tenth of TrkC^+ , and rarely in TrkA^+ neurons. In contrast to the TG, PTPRO was expressed only in a third of Ret^+ DRG neurons.

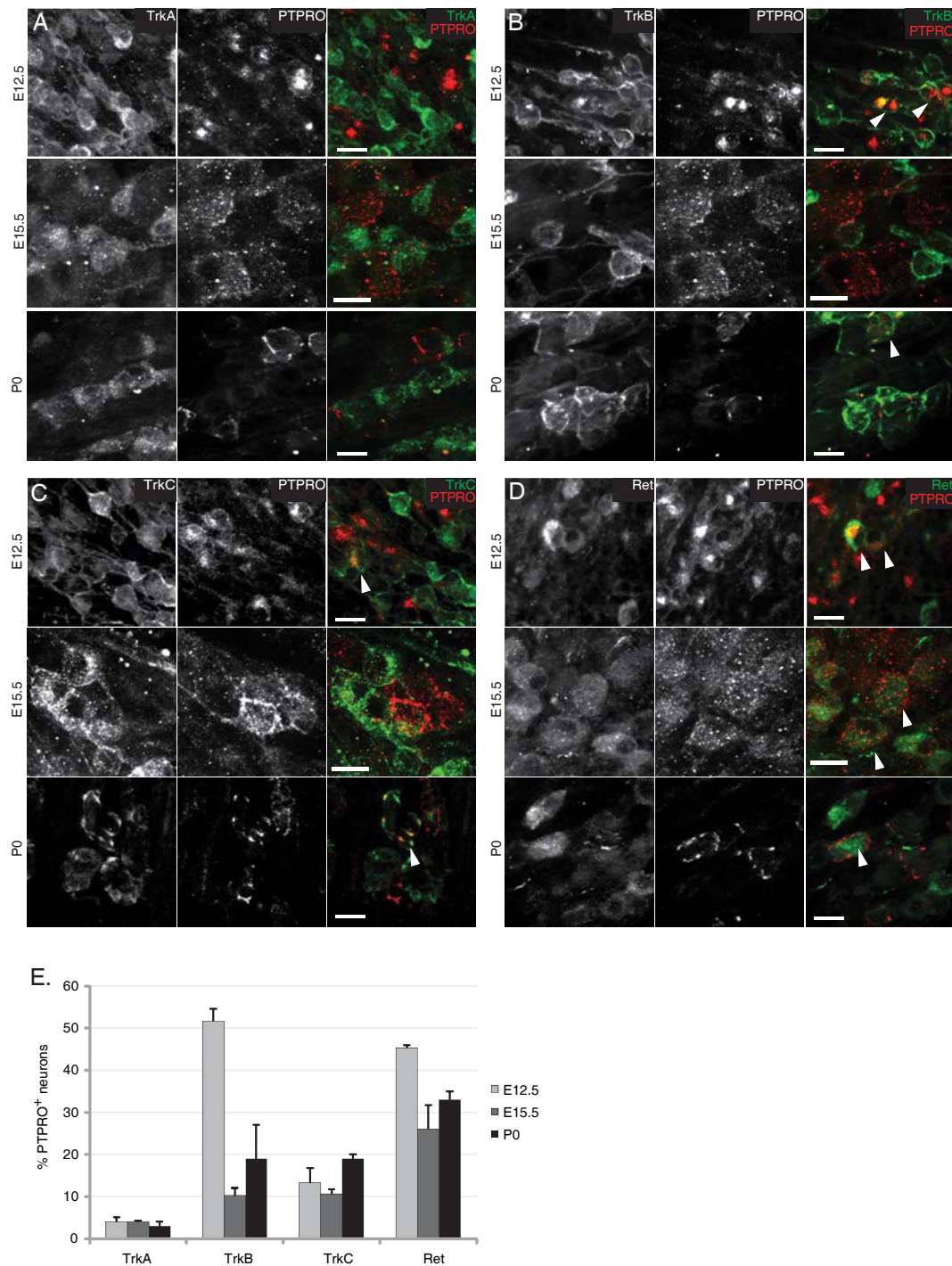


Figure 2-4. PTPRO expression in a subset of TG neurons
 (A-D) Confocal images showing colocalization of PTPRO with TrkA (A), TrkB (B), TrkC (C) and Ret (D) in E12.5, E15.5 and P0 trigeminal ganglia. Scale bar is 100 μ m. Arrowheads point to neurons coexpressing PTPRO and either Trks or Ret. (E) Graph shows mean \pm SEM of the percentage of TrkA⁺, TrkB⁺, TrkC⁺ and Ret⁺ neurons expressing PTPRO at E12.5 and P0. For each data point N=3 embryos (9 images/embryo). For each group (TrkA, TrkB, TrkC and Ret) the percentages of neurons expressing PTPRO at different developmental stages were compared using one-way ANOVA followed by Bonferroni's post-hoc comparison test (*p<0.05, **p<0.01).

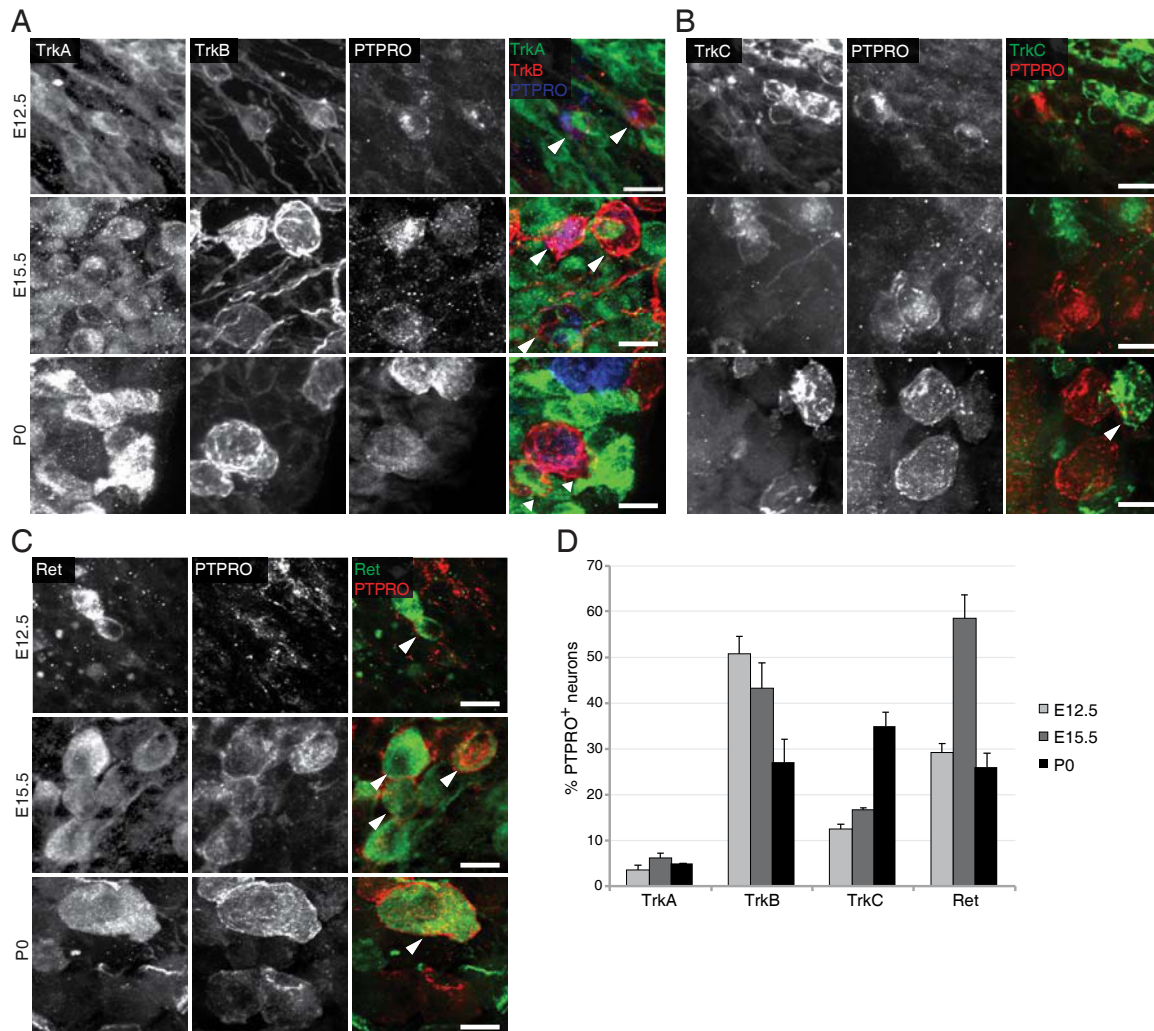


Figure 2-5. PTPRO expression in a subset of DRG neurons

(A-C) Confocal images showing colocalization of PTPRO with TrkA and TrkB (A), TrkC (B) and Ret (C) in E12.5, E15.5 and P0 lumbar DRGs. Scale bar is 25 μ m. Arrowheads point to neurons coexpressing PTPRO and either Trks or Ret. (D) Graph shows mean \pm SEM of the percentage of TrkA⁺, TrkB⁺, TrkC⁺ and Ret⁺ neurons expressing PTPRO at E12.5, E15.5 and P0. For each data point N=3 embryos (9 images/embryo).

At E15.5, no differences were observed between TG and DRG regarding PTPRO expression in TrkA⁺ and TrkC⁺ neurons. In contrast to what I described in the TG, in the DRG PTPRO expression in TrkB⁺ and Ret⁺ neurons remained high at this developmental stage. At P0, as has been observed for the TG, phosphatase expression decreased in Ret⁺ and TrkB⁺, and did not increase in TrkA⁺ neurons, but in contrast to the TG, the percentage of neurons coexpressing PTPRO and TrkC increased (Figure 2-5).

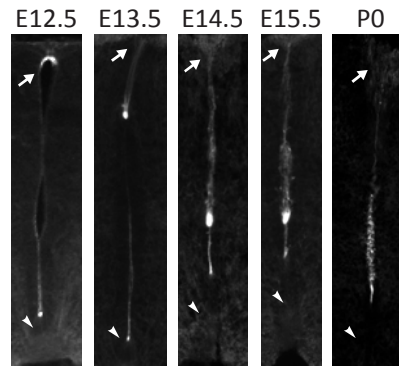


Figure 2-6. PTPRO expression at the spinal cord midline

Cross sections of E12.5, E13.5, E14.5, E15.5 and P0 lumbar spinal cord were stained with anti-PTPRO antibody. PTPRO is expressed at the spinal cord midline. Arrows point to the roof plate, and arrowheads to the floor plate.

The differences in PTPRO expression between TG and DRG could reflect a different requirement of the molecule in the development of these two populations of sensory neurons. While PTPRO was not expressed in the peripheral target region of TG and DRG neurons, i.e. whisker pad and hindlimb, it was expressed in the central target region of the DRG axons, the spinal cord. I detected PTPRO expression at the spinal cord midline and at the dorsal root entry zone (DREZ). PTPRO expression at the midline was quite interesting since it resembled the expression pattern of a midline marker, like ephrinB3 (Figure 2-6).

Finally, since PTPRO was required for Eph-dependent retinotectal projection in chick, I performed immunostaining on the retina of newborn mice. Consistent with the data from chick, PTPRO was expressed in the inner nuclear layer (INL) of the retina (Figure 2-7).

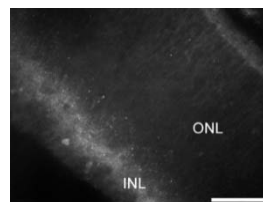


Figure 2-7. PTPRO expression in the retina

PTPRO immunostaining on sagittal sections of P0 retina. Scale bar is 200 μ m. ONL – outer nuclear layer, INL – inner nuclear layer.

2.1.2. E11.5 and E12.5 *PTPRO*^{-/-} embryos have bigger and more complex TG arbors

To investigate a possible requirement of PTPRO for the outgrowth of sensory axons *in vivo*, I examined *PTPRO*^{-/-} embryos at two different stages of development. I performed neurofilament immunostaining on whole embryos to analyze the trajectories of sensory axons and the formation of peripheral arbors. At both developmental stages, there were no major changes in the mandibular branch, but I observed defects in the maxillary branch and in one of the arbors of the ophthalmic branch. This arbor starts to grow at E10.5, forms a complex branch above the eye at E12.5, and is fully developed by E13.5.

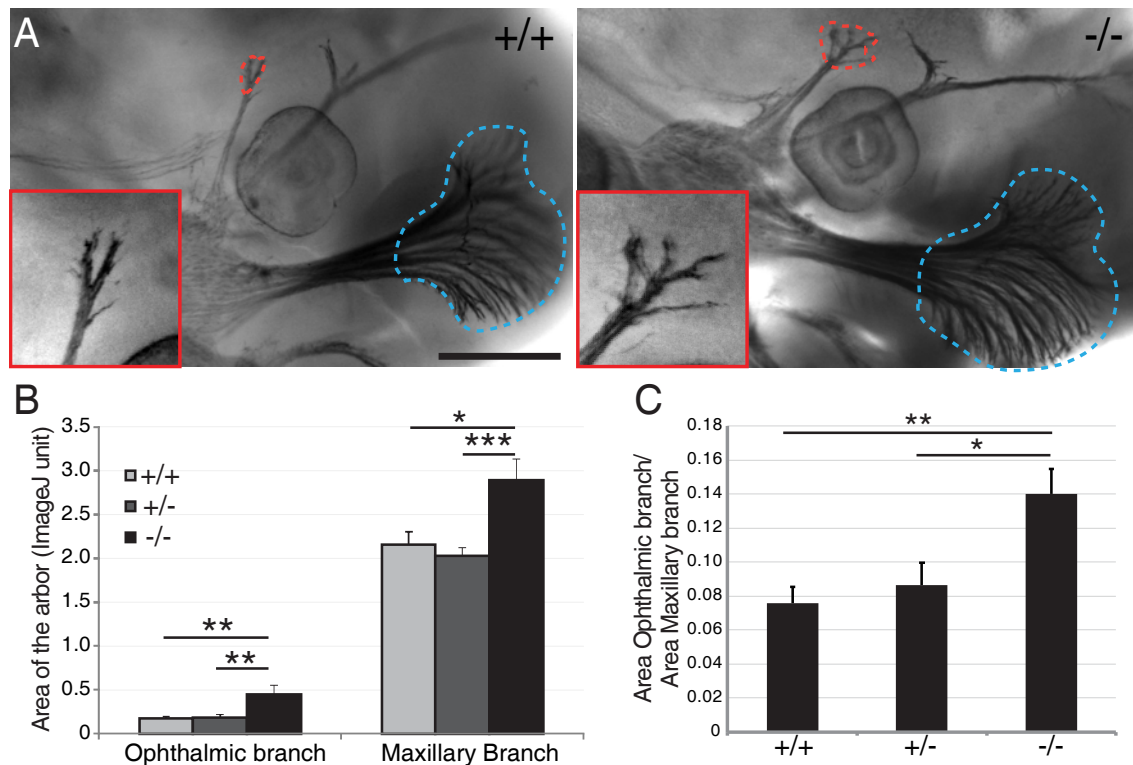


Figure 2-8. E11.5 *PTPRO*^{-/-} embryos have a more complex ophthalmic arbor

(A) Representative pictures of TG nerve branches from whole-mount neurofilament stained E11.5 wild-type and *PTPRO*^{-/-} embryos. Red and blue dashed lines encircle the area of ophthalmic and maxillary arbors, respectively. The inset shows a higher magnification of the arbor of the ophthalmic branch that was analyzed. (B) Graph represents the mean±SEM area of 18 wild-type, 21 *PTPRO*^{+/-} and 15 *PTPRO*^{-/-} TG arbors. Statistical analysis was done using two-tailed Student's t-test (*p<0.05, **p<0.01, ***p<0.001). Scale bar is 500µm.

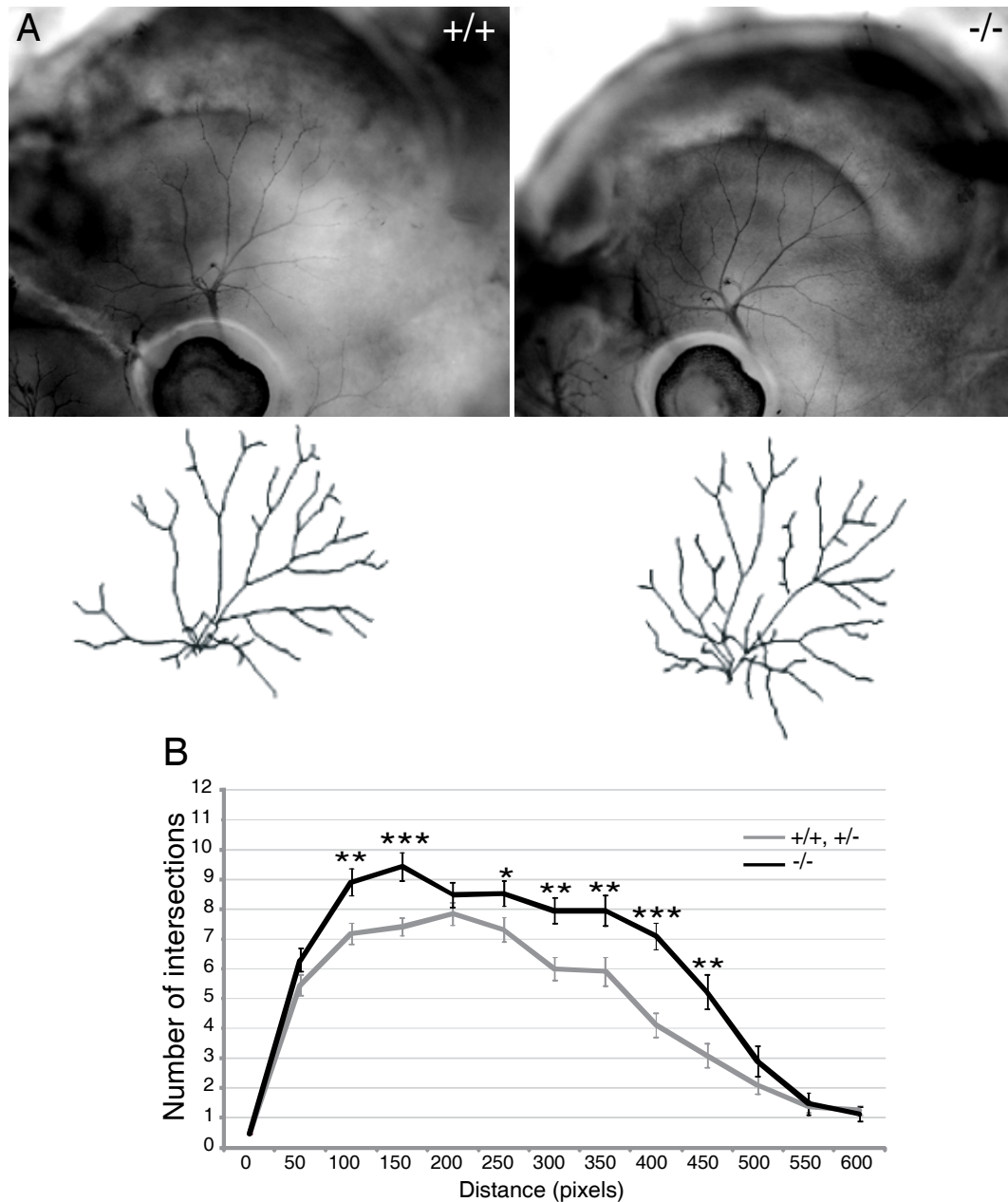


Figure 2-9. E12.5 *PTPRO*^{-/-} embryos show exuberant arborization of the ophthalmic branch of the TG nerve

(A) Representative pictures of TG nerve branches from whole-mount neurofilament stained E12.5 wild-type and *PTPRO*^{-/-} embryos. Lower panels in A show tracings of the ophthalmic arbors. (B) Sholl analysis of the ophthalmic arbor at E12.5 was done on 32 wild-type and *PTPRO*^{+/-}, and 24 *PTPRO*^{-/-} TG ganglia. Statistical analysis was done as for Figure 2-8.

In E11.5 wild-type embryos, the arbor had two main axon bundles, whereas in stage-matched *PTPRO*^{-/-} embryos the two bundles were longer and presented collateral branching (Figure 2-8). Similarly, the maxillary arbor covered a bigger area in *PTPRO*^{-/-}

embryos (Figure 2-8). The difference in the ophthalmic branch was, however, greater than in the maxillary branch. Hence, the ratio measurement (ophthalmic/maxillary branch) also showed a significant difference and normalized the data to compensate for eventual small developmental differences (Figure 2-8). No difference was observed between wild-type and heterozygous *PTPRO*^{+/-} embryos (Figure 2-8). At E12.5 I analyzed the ophthalmic arbor by Sholl analysis, and found an increased complexity in *PTPRO*^{-/-} embryos compared to wild-type controls (Figure 2-9). Taken together, these data support a role for PTPRO as an outgrowth or branching inhibitor.

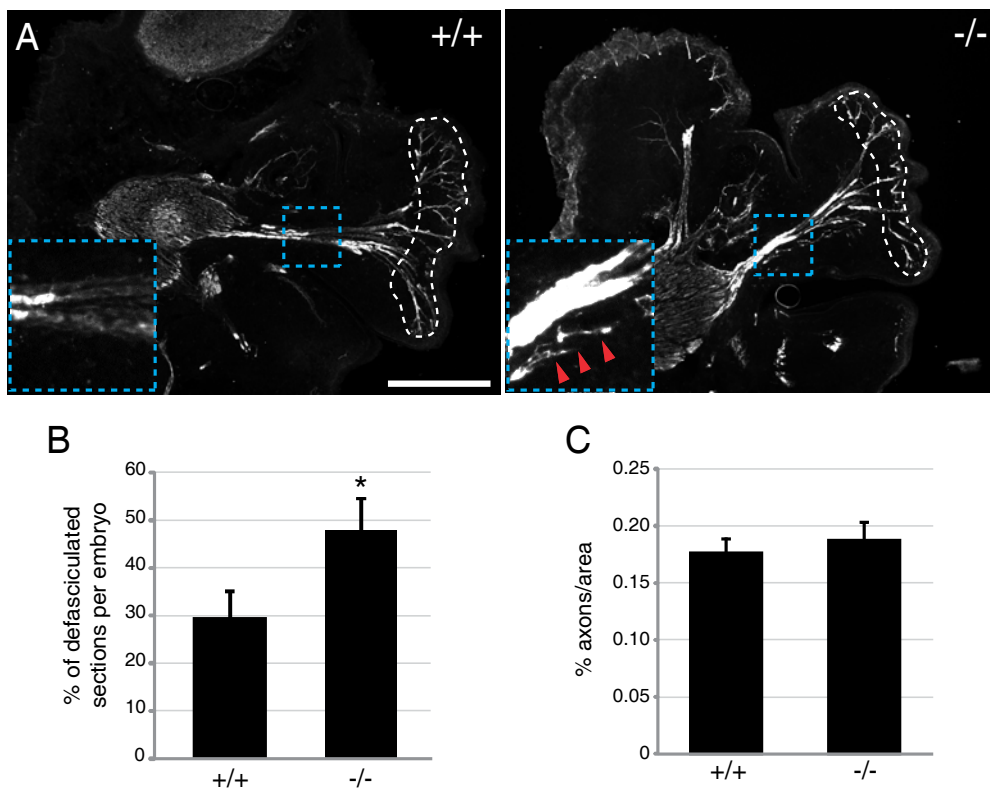


Figure 2-10. E12.5 *PTPRO*^{-/-} embryos show defasciculation of the maxillary branch
 (A) TuJ1 immunostaining on sagittal sections of E12.5 wild-type and *PTPRO*^{-/-} TG ganglia. The inset displays a higher magnification of the maxillary nerve. Red arrowheads point to defasciculated axons. Scale bar is 500µm. The dashed white lines depict the areas analyzed for terminal branching (B) Graph represents the percentage of sections with defasciculated axons (mean±SEM, N=16 embryos per genotype). (C) Graph represents the percentage of tissue area covered by axons in the terminal region of the maxillary arbor (mean±SEM, N=16 embryos per genotype). Statistical analysis was done as for Figure 2-8.

I then prepared cryosections of E12.5 embryonic head and further analyzed the complexity of the maxillary branch to complement the quantification in the whole-mount configuration. Immunostaining for the axon marker Tuj1 showed more numerous areas of defasciculation in *PTPRO*^{-/-} embryos than in wild-type littermates (Figure 2-10), possibly due to enhanced branching or defasciculation of these neurons. The areas of defasciculation were seen mainly in the proximal region of the nerve; more distal terminal arborizations were not affected (Figure 2-10). To assess the terminal arborization pattern, I determined the percentage of the maxillary arbor terminal area covered by axons, and did not see any difference between *PTPRO*^{-/-} and wild-type embryos (Figure 2-10).

2.1.3. Cultured E12.5 PTPRO^{-/-} TG neurons display increased sensitivity to BDNF and GDNF, but not NGF

The observed phenotypes suggested either impaired axon bundling or enhanced outgrowth of certain axons. To better understand PTPRO's role in developing TG neurons I prepared primary TG neuron cultures and stimulated them with different neurotrophic factors. E12.5 neurons were incubated for 18 hours with 10ng/ml NGF, alone or in combination with 5ng/ml BDNF or 5ng/ml GDNF (Figure 2-11). Since PTPRO is mainly expressed in TrkB⁺ and Ret⁺ neurons, I expected an effect on the growth and branching only in presence of BDNF and GDNF. Indeed, stimulation with NGF alone did not elicit any difference in outgrowth or branching between wild-type and *PTPRO*^{-/-} neurons. In contrast, in the presence of BDNF and GDNF, *PTPRO*^{-/-} neurons had longer neurites than the wild-type controls (Figure 2-11). Although E12.5 neurons were mainly bipolar, BDNF stimulation triggered a significant increase in the mean

number of primary branch points (Figure 2-11). BDNF stimulation increased the number of branching points to the same extent in wild-type and *PTPRO*^{-/-} neurons, whereas GDNF stimulation enhanced branching only in *PTPRO*^{-/-} neurons (Figure 2-11). To further study their neurite arbors, I performed Sholl analysis on these neurons [238]. In all conditions, I observed an increased complexity of the arbors in *PTPRO*^{-/-} cultures, but this effect was stronger for BDNF and GDNF as compared to NGF (Figure 2-11).

To better uncouple PTPRO's effects on axon growth from those on cell survival, and to exclude a possible synergistic effect of BDNF and GDNF with NGF, I performed a dose-response analysis for neurotrophins and GDNF in the presence of caspase inhibitors. Interestingly, in the absence of any neurotrophic stimulation *PTPRO*^{-/-} axons were already longer than wild-type controls (Figure 2-12). Consistent with the previous experiment, stimulation with NGF, except at high doses (100ng/ml), did not show significant differences between wild-type and *PTPRO*^{-/-} neurons (Figure 2-12). However, since at this concentration NGF is reported to exert TrkA-independent growth inhibiting effects, these data are still consistent with PTPRO not being coexpressed with TrkA [239]. Stimulation with 1ng/ml of BDNF or GDNF was sufficient to keep the *PTPRO*^{-/-} neurons growing more than controls. Responses generally plateaued by 10ng/ml of neurotrophic factor (Figure 2-12). The shift in sensitivity was more evident when data were plotted as a logarithm of the concentration of neurotrophins on the x-axis versus the axon length on the y-axis, and could be fitted to a sigmoid dose-response curve by nonlinear regression. Since logarithm of 0 is infinity, I assigned to the condition with no neurotrophin stimulation the arbitrary value of -3.

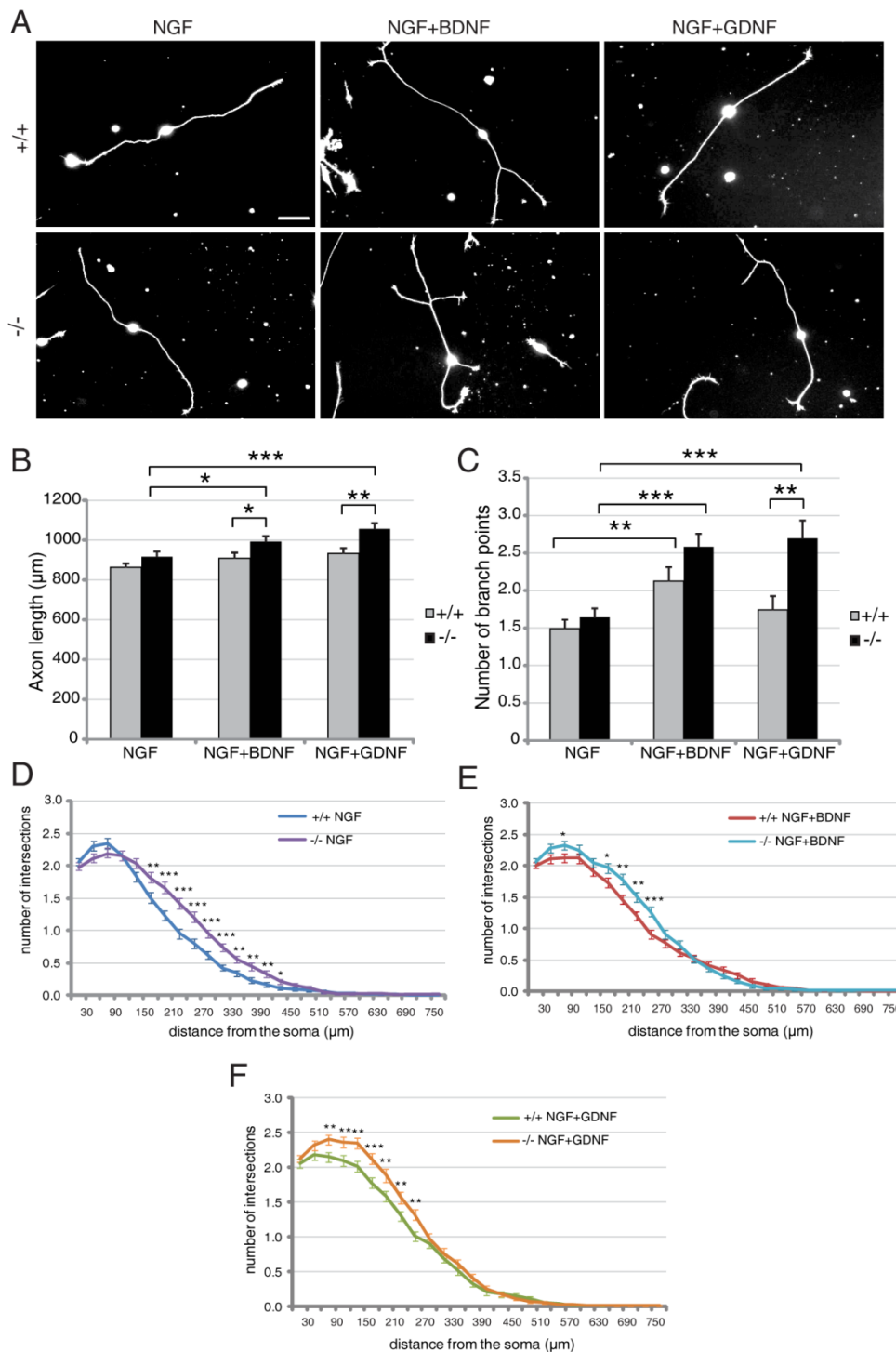


Figure 2-11. E12.5 *PTPRO*^{-/-} TG neurons are more sensitive to BDNF and GDNF

(A) Representative pictures of E12.5 TG neurons, stimulated with growth factors as indicated. Scale bar, 100µm. Quantification of the length of the axons (B) or the number of branch points (C) of neurons stimulated as indicated on the x-axis. (D-F) Sholl analysis of cultured primary TG neurons from E12.5 wild-type and *PTPRO*^{-/-} embryos, stimulated with NGF (D), BDNF (E) and GDNF (F). Graphs represent mean±SEM. Numbers of TG neurons analyzed from at least 3 independent cultures: for NGF stimulation 200 neurons (wild-type) and 195 neurons (*PTPRO*^{-/-}), for BDNF and GDNF stimulation 150 neurons per genotype. Statistical analysis was done as for Figure 2-8.

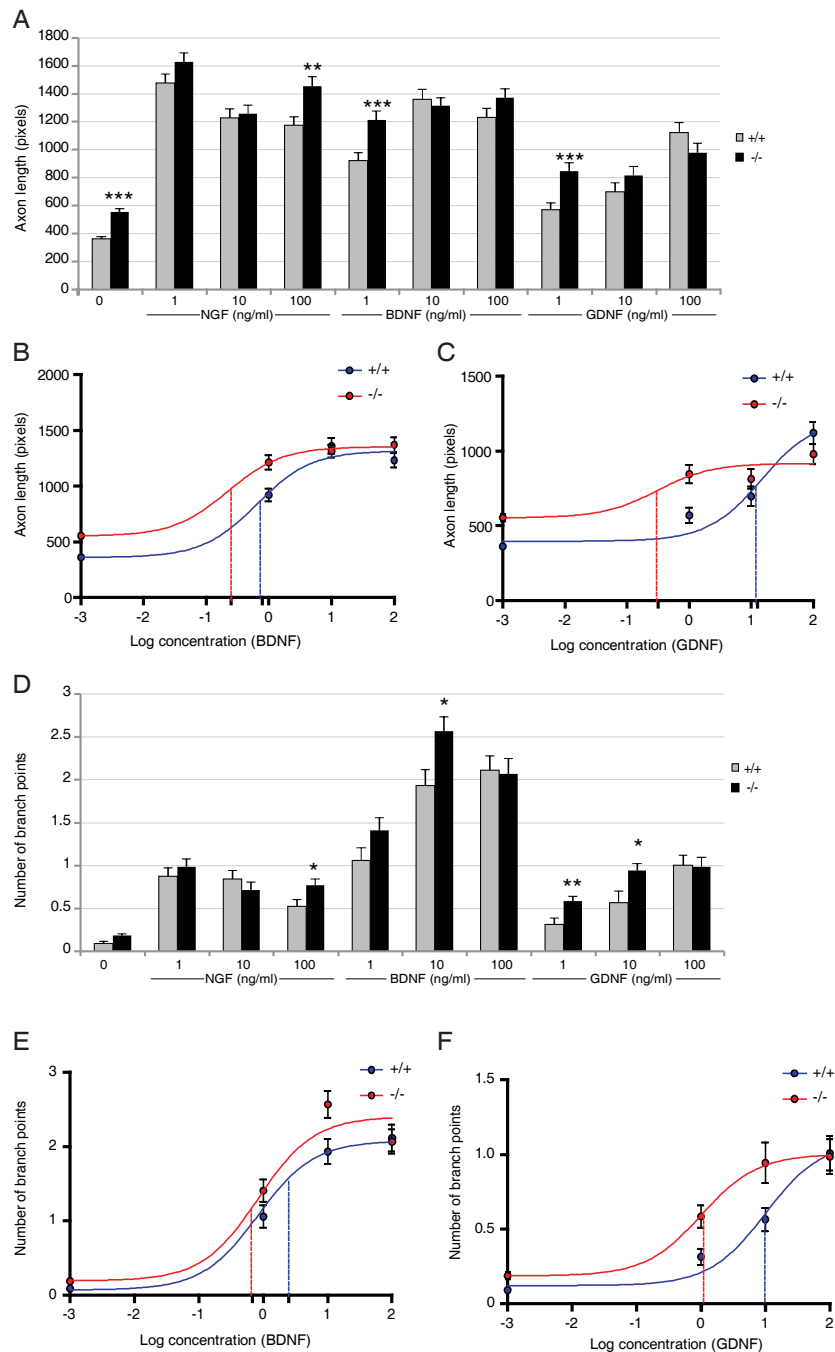


Figure 2-12. E12.5 *PTPRO*^{-/-} TG neurons are more sensitive to BDNF and GDNF, but not NGF stimulation

(A,D) Quantification of the length (A) and branching (D) of the TG axons from wild-type and *PTPRO*^{-/-} E12.5 embryos stimulated with increasing concentration of NGF, BDNF or GDNF in the presence of caspase inhibitors. Graphs represent mean±SEM. Numbers of TG neurons analyzed from at least 3 independent cultures: for no stimulation 542 (wild-type) and 550 (*PTPRO*^{-/-}) neurons, for NGF stimulation 200 neurons (wild-type) and 195 neurons (*PTPRO*^{-/-}), for BDNF and GDNF stimulation 150 neurons per genotype. Statistical analysis was done as for Figure 2-8. (B-C) Nonlinear regression representation of the dose-response curves for BDNF (B,E) and GDNF (C,F). Dashed blue and red lines indicate EC50 of wild-type and *PTPRO*^{-/-} response, respectively.

The nonlinear regression allows the calculation of half of the maximal response (EC50), and although this is not an absolute value, since I assigned an arbitrary value to the lowest concentration, it still gives a relative indication of sensitivity to neurotrophins. For both BDNF and GDNF the EC50 values were significantly lower in the *PTPRO*^{-/-} curves (Figure 2-12) compared to controls.

Axon branching was not affected in *PTPRO*^{-/-} neurons stimulated with NGF except at very high doses (100ng/ml) (Figure 2-12). BDNF stimulation had the biggest effect on branching for both wild-type and *PTPRO*^{-/-} neurons. For both BDNF and GDNF I observed a strong difference for intermediate concentrations of neurotrophic factor (10ng/ml) and the response generally plateaued by 100ng/ml (Figure 2-12). Analyzing the data as a nonlinear regression showed a difference in EC50 for GDNF but not BDNF stimulation (Figure 2-12).

Taken together, these results indicate that embryonic *PTPRO*^{-/-} neurons are more responsive to BDNF and GDNF, consistent with the expression of PTPRO in TrkB⁺ and Ret⁺ neurons.

2.1.4. Cultured P1 PTPRO^{-/-} TG neurons do not display increased sensitivity to BDNF and GDNF

To further investigate the role of PTPRO in TG neuron branching and growth, I prepared primary TG neuron cultures from P1 wild-type and *PTPRO*^{-/-} pups. At this stage of development primary cultured TG neurons display several branch points and a very complex structure. As done for E12.5 cultures, neurons were kept in 10ng/ml NGF or 10ng/ml NGF plus 5ng/ml BDNF or GDNF.

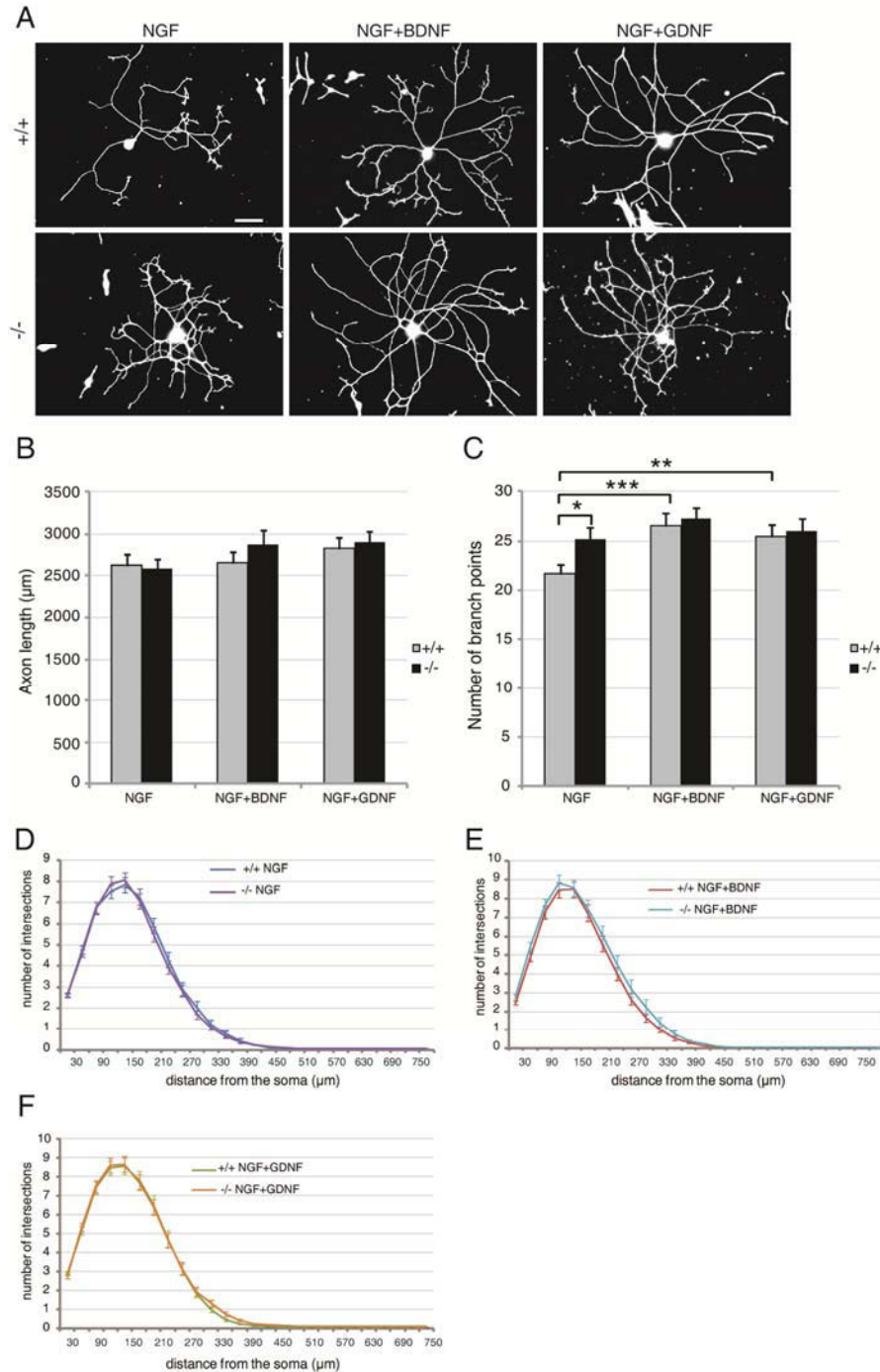


Figure 2-13. P1 *PTPRO*^{-/-} TG neurons do not show increased sensitivity to neurotrophins and GDNF

(A) Representative pictures of P1 TG neurons, stimulated with growth factors as indicated. Scale bar, 100µm. Quantification of the length of the axons (B) or the number of branch points (C) of neurons stimulated as indicated on the x-axis. (D-F) Sholl analysis of cultured primary TG neurons from P1 wild-type and *PTPRO*^{-/-} embryos, stimulated with NGF (D), BDNF (E) and GDNF (F). Graphs represent mean±SEM. Numbers of TG neurons analyzed from at least 3 independent cultures: for NGF stimulation 230 neurons (wild-type) and 234 neurons (*PTPRO*^{-/-}), for BDNF 176 neurons (wild-type) and 190 neurons (*PTPRO*^{-/-}) and for GDNF 232 neurons (wild-type) and 216 neurons (*PTPRO*^{-/-}). Statistical analysis was done as for Figure 2-8.

In contrast to the results obtained with E12.5 neurons, *PTPRO*^{-/-} neurons from newborn mice were not more branched or longer than controls. The only significant difference observed was the decreased number of branch points in *PTPRO*^{-/-} after NGF treatment (Figure 2-13). Interestingly, BDNF and GDNF were able to further stimulate branching in wild-type but not *PTPRO*^{-/-} neurons, suggesting that these two signaling pathways might be already activated in the absence of stimulation in knockout neurons. The lack of a differential response in the knockout neurons could be due to the decreased expression of PTPRO in TrkB⁺ and Ret⁺ neurons observed at E15.5 and P0.

2.1.5. The exuberant growth and branching observed in PTPRO^{-/-} embryos and neurons are not due to alterations in cell fate or survival.

Since cranial sensory neurons display intrinsic differences in growth rates [166], the enhanced growth and arborization of a sensory nerve branch may also result from a relative increase in the numbers of fast versus slow growing neurons. The observed phenotype could be secondary to changes in cell fate or absence of a selective population. To test this hypothesis, I counted the number of TrkA⁺, TrkB⁺, TrkC⁺, Ret⁺ and NeuN⁺ neurons at E12.5. At this developmental stage, TG neurons were NGF-dependent and expressed mainly TrkA, and the other three populations accounted for less than half of the overall contingent (Figure 2-14) [240]. I did not detect any difference in the number of neurons (Figure 2-14), suggesting that the absence of PTPRO does not affect the cell fate of TG neurons. Consistent with this observation, I did not observe changes in any of the populations in E12.5 *PTPRO*^{-/-} DRGs (Figure 2-15).

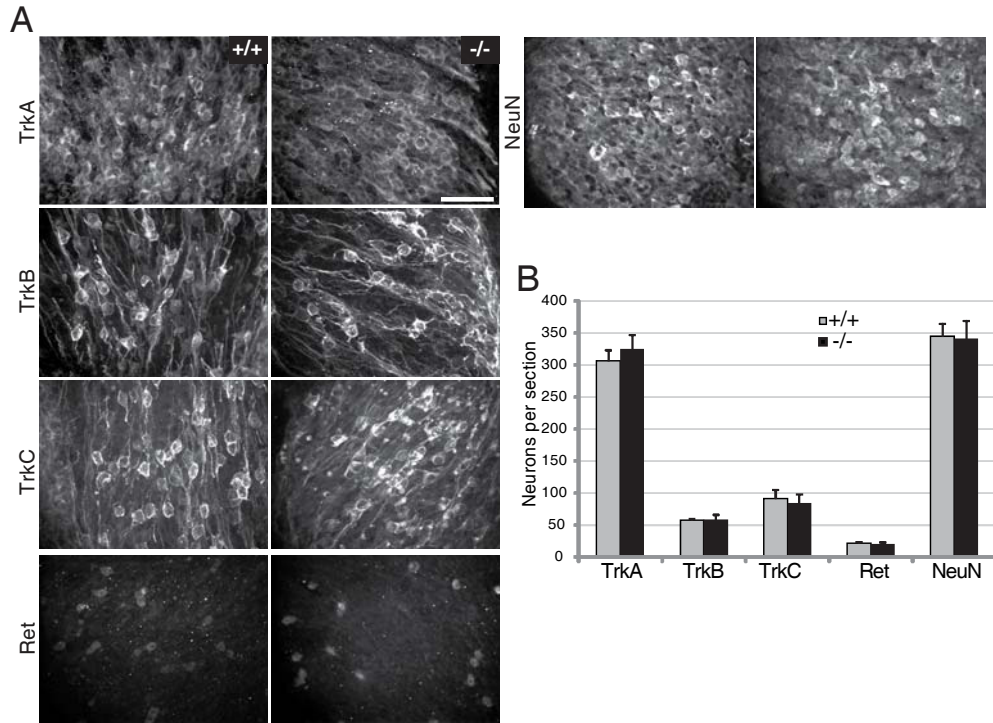


Figure 2-14. *PTPRO*^{-/-} embryos do not have defects in TG neuron differentiation

(A) Immunostainings for TrkA, TrkB, TrkC, Ret and NeuN on TG ganglia cryosections from E12.5 wild-type and *PTPRO*^{-/-} embryos. Scale bar is 50 μ m. (B) Graph represents the average number (mean \pm SEM, N=3, 9 images/embryo) of TrkA⁺, TrkB⁺, TrkC⁺, Ret⁺ and NeuN⁺ neurons per section. Statistical analysis was done as for Figure 2-8.

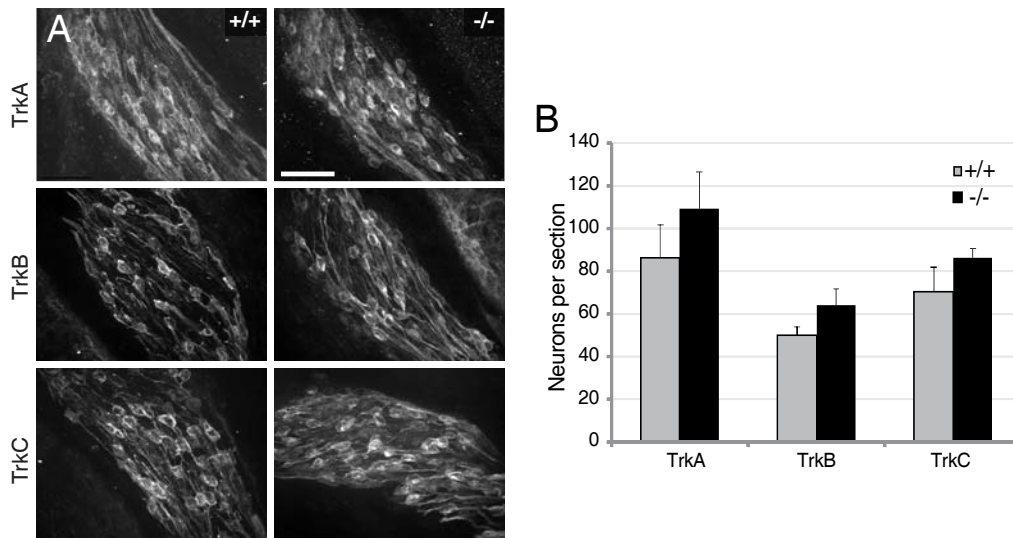


Figure 2-15. *PTPRO*^{-/-} embryos do not have defects in DRG neuron differentiation

(A) Immunostainings for TrkA, TrkB and TrkC on lumbar DRG cryosections from E12.5 wild-type and *PTPRO*^{-/-} embryos. Scale bar is 50 μ m. (B) Graph represents the average number (mean \pm SEM, N=3, 9 images/embryo) of TrkA⁺, TrkB⁺ and TrkC⁺ neurons per section. Statistical analysis was done as for Figure 2-8.

At P0, TrkA⁺ neurons were still the largest subpopulation, although reduced in number compared to E12.5; TrkB⁺ neurons were unchanged in number compared to E12.5; TrkC⁺ neurons were slightly reduced, and the Ret⁺ population had increased (Figure 2-16) [241]. I counted the number of TrkA⁺, TrkB⁺, TrkC⁺, Ret⁺ and NeuN⁺ neurons at P0 (Figure 2-16), and did not observe a reduction in the number of TrkB⁺ and Ret⁺, but there was a significant loss of TrkA⁺ and TrkC⁺ neurons (Figure 2-16). The loss of TrkA⁺ neurons in the TG is also consistent with the data shown for the DRGs at P0 by the Bixby laboratory [218]. Since PTPRO shows very little colocalization with TrkA, the loss of TrkA⁺ neurons could be due to a non-cell autonomous role of PTPRO.

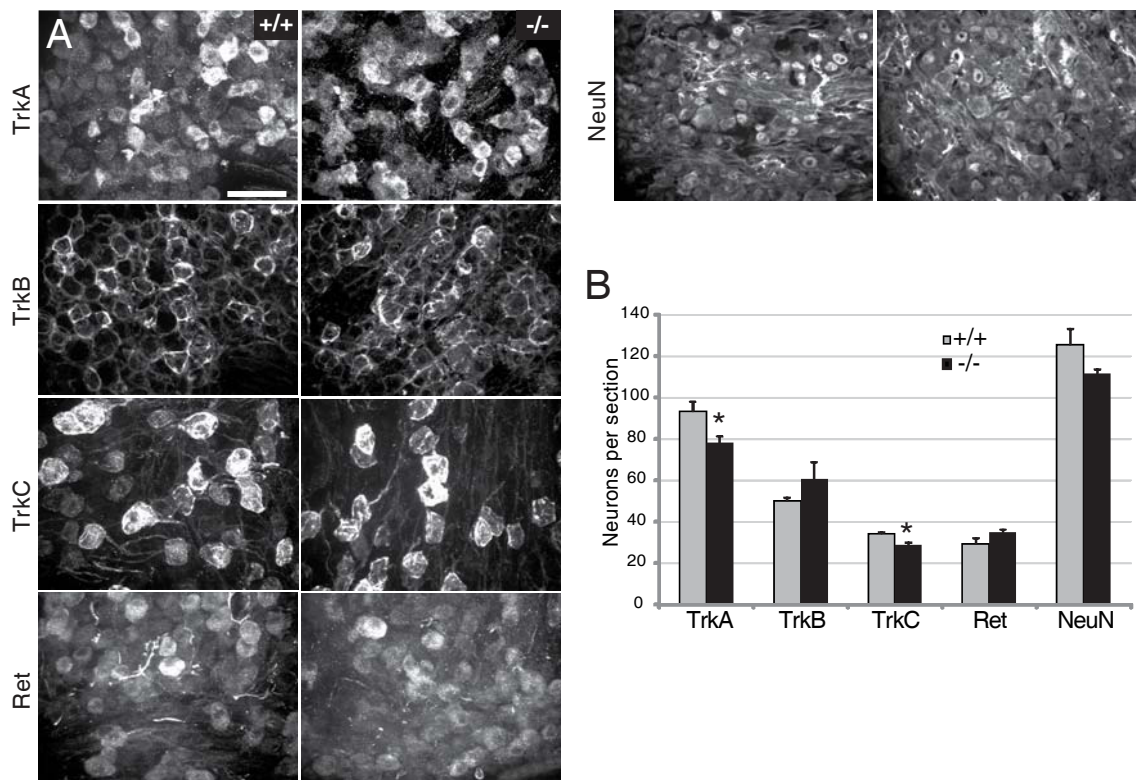


Figure 2-16. Loss of TrkA⁺ and TrkC⁺ neurons in newborn *PTPRO*^{-/-} mice

(A) Immunostainings for TrkA, TrkB, TrkC, Ret and NeuN on TG cryosections from newborn wild-type and *PTPRO*^{-/-} embryos. Scale bar is 50 μ m. (B) Graphs represent the average number (mean \pm SEM, N=3-4, 9-20 images/pup) of TrkA⁺, TrkB⁺, TrkC⁺, Ret⁺ and NeuN⁺ neurons per section. Statistical analysis was done as for Figure 2-8.

PTPRO is localized in 10% of TrkC⁺ neurons, suggesting that it could cell autonomously cause the loss. Interestingly, staining for the general neuronal marker “NeuN” did not reveal changes in the total numbers of neurons, suggesting a role of PTPRO in regulating TG neuronal differentiation more than survival (Figure 2-16).

Together these results suggest that changes in cell fate and survival do not contribute significantly to the exuberant growth and branching of E12.5 embryonic TG axons *in vivo* and *in vitro*.

2.1.6. PTPRO regulates TrkB and Ret signaling

Next I tested whether PTPRO directly regulates TrkB and Ret signaling, and whether it inhibits growth by suppressing TrkB and Ret kinase activity. I tried to examine colocalization of PTPRO with RTKs in cultured neurons, but was unable to detect PTPRO with sufficient subcellular resolution using the available antibodies. As an alternative, I investigated colocalization and activation of these proteins in heterologous cell culture, over-expressing the mouse isoform of PTPRO with a Flag-tag (mPTPRO). Over-expression of TrkB in Hela cells led to ligand-independent activation [214], as shown by anti-phosphotyrosine immunostaining (Figure 2-17). When TrkB and mPTPRO were coexpressed, the intensity of phosphotyrosine staining was markedly reduced (Figure 2-17). I repeated the experiment in HEK293 cells to complement the immunostaining data with biochemical evidence. Stimulation of TrkB-transfected cells with 50ng/ml BDNF for 5 or 20 minutes increased the levels of receptor phosphorylation and led to the activation of downstream effectors, e.g. phosphoERK. When TrkB and mPTPRO were coexpressed in HEK293 cells, BDNF-induced TrkB autophosphorylation and ERK1/2 phosphorylation were strongly suppressed (Figure 2-17).

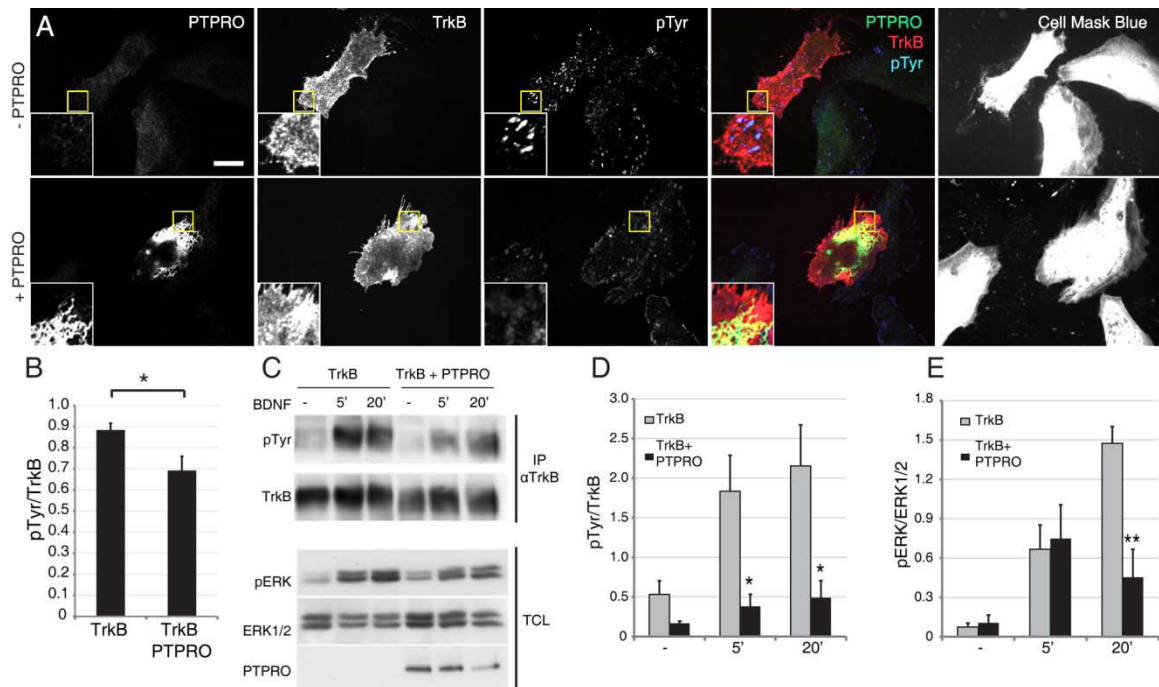


Figure 2-17. Regulation of TrkB signaling by PTPRO in transfected cells

(A) HeLa cells transfected with TrkB, with or without PTPRO, stimulated with BDNF and immunostained for PTPRO, TrkB, and phosphotyrosine (pTyr). Cells outlines are labeled with Cell Mask Blue. Insets are higher magnification images of the areas marked with a box. Scale bar is 20 μ m. (B) Graph represents the intensity of phosphotyrosine (pTyr) staining normalized to the intensity of TrkB staining (mean \pm SEM). Number of cells analyzed: 26 cells for TrkB and 29 cells for TrkB and PTPRO from 3 independent experiments. (C) Western blots of HEK293 cells transfected with TrkB with or without PTPRO-flag and stimulated as indicated. Total cell lysates (TCL) were probed against phosphoERK (pERK), ERK1/2 and Flag (PTPRO). Immunoprecipitates of TrkB (IP α TrkB) were probed against pTyr and TrkB. (D,E) Graphs represent TrkB autophosphorylation levels (D) and ERK phosphorylation (E). Three independent experiments were performed and the intensities of the phospho bands were quantified using ImageJ and normalized to the total levels of the proteins. Statistical analysis was done as for Figure 2-8.

Since the two Ret isoforms - Ret9 and Ret51 - elicit similar response to GDNF stimulation in sympathetic neurons [242], for the following *in vitro* experiments I used only the Ret51 isoform. I transfected HeLa cells with Ret51 and stimulated them for 5 minutes with 50ng/ml GDNF and soluble GFR α 1. Stimulation increased the intensity of phosphotyrosine staining and this increase was suppressed when Ret was coexpressed with PTPRO (Figure 2-18). As for TrkB, I assessed by Western Blot Ret signaling in presence and absence of PTPRO. In transfected HEK293 cells, basal Ret autophosphorylation, which was visualized by immunoblotting with anti-phosphotyrosine

(pTyr) and anti-phosphotyrosine1062 (pY1062) antibodies, was high and was not increased by GDNF stimulation.

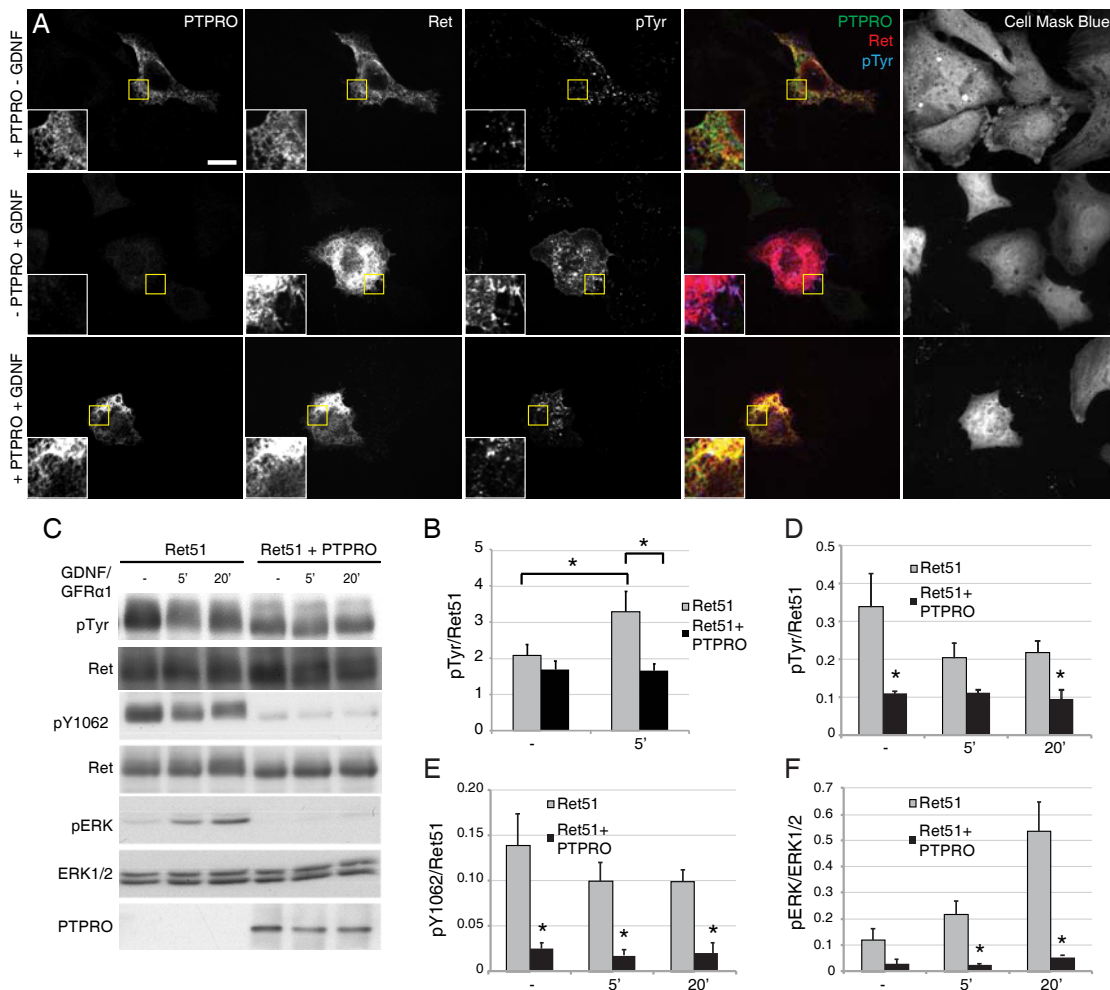


Figure 2-18. Regulation of Ret51 signaling by PTPRO in transfected cells
 (A) HeLa cells transfected with Ret51, with or without PTPRO, and stimulated as indicated. Fixed cells were stained with anti-Flag (PTPRO), anti-Ret and pTyr antibodies and marked with Cell Mask Blue. Scale bar is 20µm. (B) Graph represents pTyr staining intensity normalized to the intensity of Ret staining (mean±SEM). Numbers of cells analyzed: 48 cells before and 26 cells after stimulation for Ret alone, and 36 cells before and 26 cells after stimulation for Ret and PTPRO, from at least 3 independent experiments. (C) Western blots of HEK293 cells transfected with Ret, with or without PTPRO, and stimulated as indicated. TCL were probed against Ret phosphotyrosine 1062 (Ret pY1062), Ret, pERK, ERK1/2, and Flag. (D-F) Graphs represent Ret autophosphorylation levels (D,E) or ERK phosphorylation (F). Three independent experiments were performed and the intensities of the phospho bands were quantified using ImageJ and normalized to the total levels of the proteins. Statistical analysis was done as for Figure 2-8.

When PTPRO and Ret were co-transfected, Ret phosphorylation was strongly suppressed (Figure 2-18). However, PTPRO-induced dephosphorylation was more evident using the pY1062 than the pTyr antibody, suggesting that PTPRO might target only some of the

tyrosine residues present on the receptor (Figure 2-18). Although stimulation with GDNF and soluble GFR α 1 did not increase the levels of Ret phosphorylation, it led to a significant increase in the levels of phosphoERK. PTPRO coexpression was sufficient to abolish this GDNF-induced ERK phosphorylation (Figure 2-18).

Finally, I analyzed whether the phosphatase directly interacted with the two RTKs. I was not able to co-immunoprecipitate either of the two RTKs and PTPRO, but in transfected Hela cells I observed nice colocalization. To examine the degree of colocalization I tested the colocalization staining for the total pools of receptor and phosphatase (cells were permeabilized), or I restricted the analysis to only the cell surface. To restrict the colocalization analysis to the cell surface, I did not permeabilize the cells and I used an antibody raised against the extracellular domain of PTPRO. When PTPRO and TrkB were coexpressed in Hela cells and cells were permeabilized and stained, I observed 40% of the puncta to be colocalized. Stimulation with BDNF did not increase the percentage of TrkB/PTPRO colocalizing puncta (Figures 2-17 and 2-19). Surface staining for PTPRO and TrkB showed a higher degree of colocalization of the two proteins compared to total staining, and this percentage was not affected by BDNF stimulation (Figure 2-19). Ret colocalization with PTPRO, upon total staining, was stronger compared to TrkB (60% of Ret⁺ puncta co-localized with PTPRO) and the degree of colocalization in transfected Hela cells was enhanced by stimulation with GDNF and soluble GFR α 1 (Figures 2-18 and 2-19). This increase, however, was only detectable when cells were permeabilized but not when only the surface staining was considered, suggesting that upon stimulation mPTPRO and Ret may co-localize in intracellular compartments, e.g. endosomes (Figure 2-19).

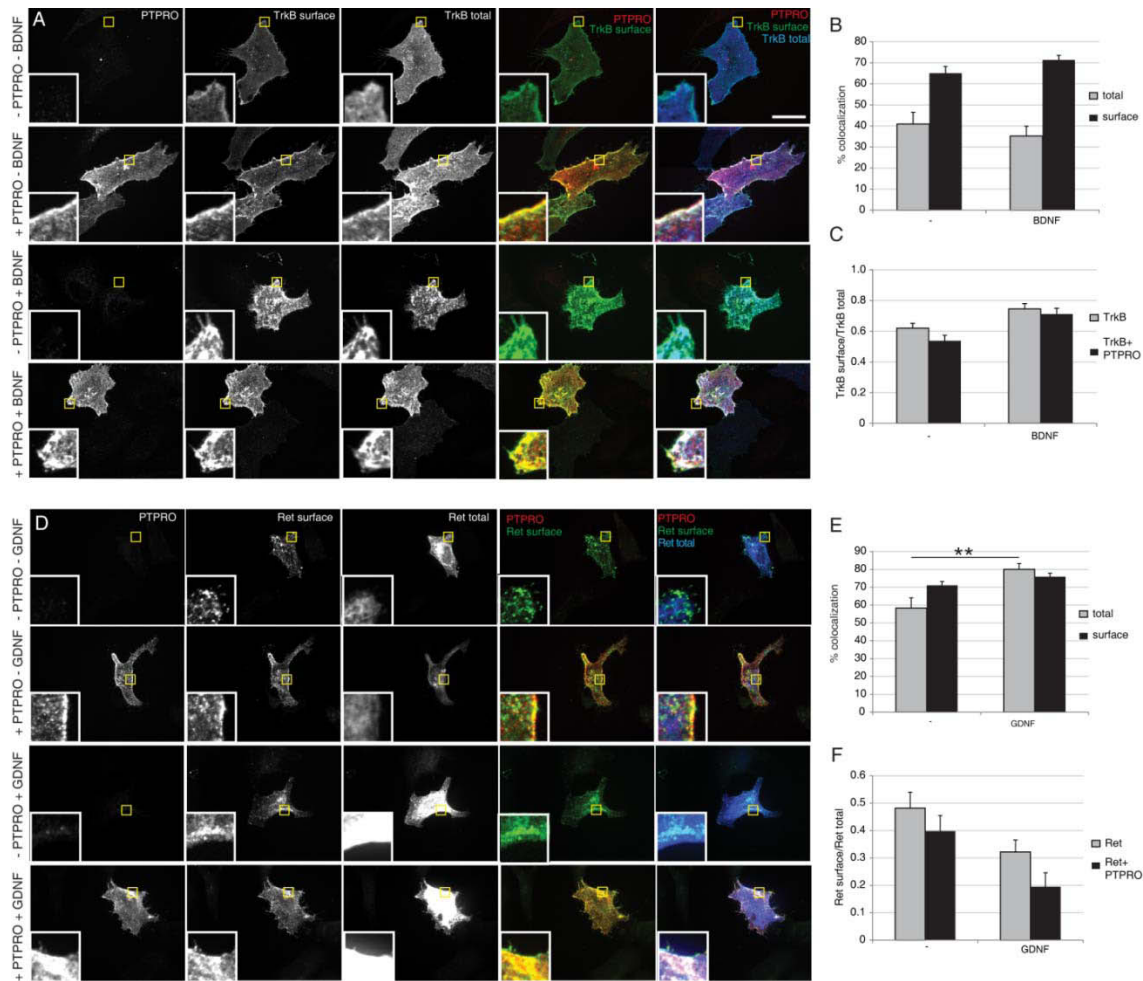


Figure 2-19. PTPRO does not regulate TrkB and Ret 51 surface expression (A,D) HeLa cells transfected with TrkB (A) or Ret51 (D) with or without PTPRO, and stimulated as indicated. Cells were stained to detect surface expression of PTPRO (PTPRO surface) and TrkB or Ret (TrkB or Ret surface) and total expression of TrkB or Ret (TrkB or Ret total). Scale bar is 20 μ m. (B,E) Graphs represent the degree of colocalization of TrkB (B) or Ret (E) and PTPRO (mean \pm SEM) before and after stimulation, with (total) or without (surface) cell permeabilization. % of colocalization was normalized to PTPRO staining. 14-23 cells analyzed from at least 3 independent experiments. (C,F) Graph represents the ratio of surface and total intensities of TrkB (C) and Ret (F) staining (mean \pm SEM). 14-23 cells analyzed from at least 3 independent experiments. Statistical analysis was done as for Figure 2-8.

I then checked whether PTPRO coexpression influenced surface levels of Ret and TrkB in presence and absence of their ligands. I stained the fixed cells for TrkB and Ret before and after permeabilization in order to detect the surface and the total expression of the receptors. In absence of stimulation the surface levels of TrkB were unaffected by PTPRO coexpression. Upon stimulation with BDNF for 5 minutes, TrkB expression on the surface slightly increased and no differences were observed if PTPRO was

coexpressed (Figure 2-19). Without GDNF, Ret expression on the surface was unaltered by coexpression of PTPRO. Upon stimulation with GDNF, Ret was internalized. Also in this case, I did not observe significant differences in Ret distribution when PTPRO was coexpressed (Figure 2-19).

Together, these results revealed that PTPRO regulates TrkB and Ret kinase activity and signaling, supporting the role of PTPRO as a negative regulator of BDNF- and GDNF-induced axon growth and branching.

2.1.7. PTPRO does not regulate Eph receptors in the developing TG ganglion

Since PTPRO was shown to be a regulator of Eph signaling [219] and several members of the Eph family are expressed in the TG [178] I decided to investigate whether Eph signaling was affected and contributed to the *in vivo* phenotype. Firstly, I assessed whether TG explants were responsive to ephrin stimulation, so I prepared explants from different stages of development and stimulated them with Fc (as a negative control) or ephrinA5-Fc (human ephrinA5-fused to Fc portion of IgG) for 30 minutes. To visualize the growth cones, I performed a staining using an anti-phalloidin antibody. As expected, I observed an increase in the growth cone collapse rate after stimulation with ephrinA5-Fc (Figure 2-20). At E12.5, axons showed less variability in their response to Fc and ephrinA5 (smaller standard deviation and higher p value) and the effect was not maximal, leaving a bigger window for assessing differences upon PTPRO removal. I then performed the same experiment using wild-type and *PTPRO*^{-/-} TG explants, and found that knockout explants were equally sensitive as wild-type to ephrin stimulation (Figure 2-20). Stimulation with a higher dose of pre-clustered ephrinA5 did not elicit an increase in growth cone collapse, neither in wild-type nor in knockout explants (Figure 2-20).

Therefore, these results suggest that during TG development, genetic removal of PTPRO does not affect Eph signaling.

To explore whether in *PTPRO*^{-/-} mice Eph signaling was at all affected, I analyzed two different axon guidance systems: LMC motor axon guidance at the sciatic plexus and retinotectal mapping, where Eph receptors have been proven to play a pivotal role. I complemented the *in vivo* approach with *in vitro* experiments, to assess sensitivity to ephrins.

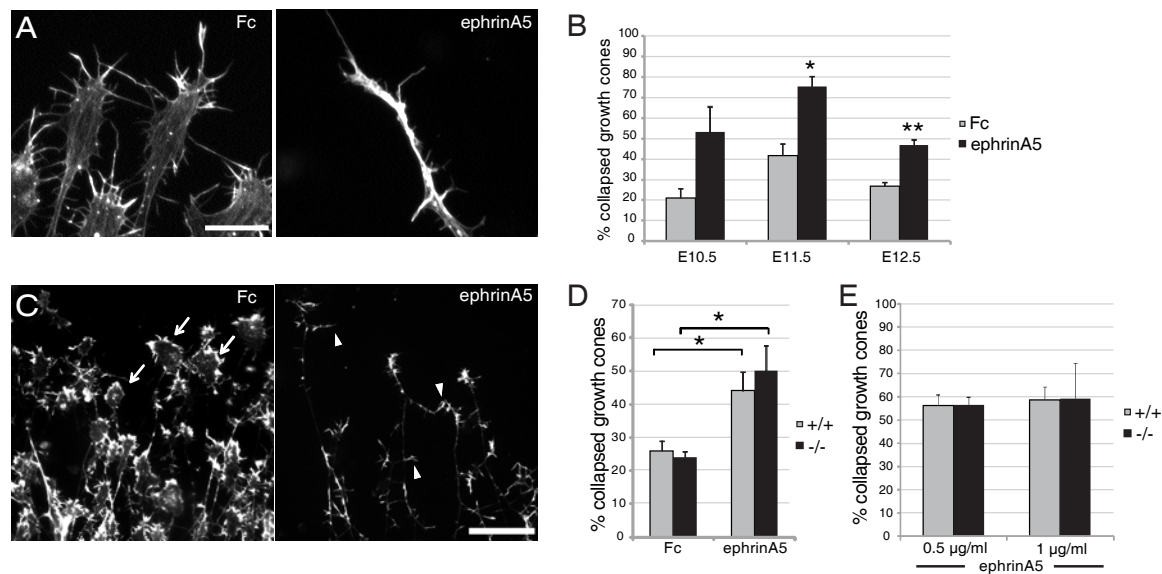


Figure 2-20. *PTPRO*^{-/-} TG explants do not show increased sensitivity to ephrinAs
 (A) Representative pictures of E11.5 TG growth cones stimulated with 0.5 µg/ml pre-clustered Fc (negative control) or pre-clustered ephrinA5. Explants were stained with Phalloidin-568. Scale bar is 50µm. (B) Graph represents mean±SEM of the percentage of collapsed growth cones at three developmental stages. Analysis was done on four to six explants per condition from at least 2 independent cultures. (C) Representative pictures of E12.5 TG neuron explant cultures stimulated with 0.5µg/ml pre-clustered Fc (negative control) or pre-clustered ephrinA5. Arrows point to non-collapsed growth cones and arrowheads show collapsed growth cones. Scale bar is 100µm. (D,E) Graphs represent mean±SEM of the percentage of collapsed growth cones at E12.5. Three to six explants per condition were analyzed from 3 embryos per genotype. Statistical analysis was done as for Figure 2-8.

2.1.8. *PTPRO* is dispensable as Eph-regulator in LMC axon guidance

Over-expression of Eph receptors in chick or genetic deletion of Ephs in mice have resulted, amongst other phenotypes, in misguided projections at the sciatic plexus. EphA4 guides LMC_L axons into the dorsal mesenchyme of the hindlimb, whereas EphBs guide

LMC_M axons into the ventral mesenchyme. LMC_L and LMC_M axons form the peroneal and tibial nerve, respectively. Since PTPRO is expressed in both populations of LMC neurons and it has been shown to act on both types of Eph receptors, I analyzed both LMC_L and LMC_M projections. I performed neurofilament staining of the whole embryo at E11.5 and E12.5 (Figure 2-21).

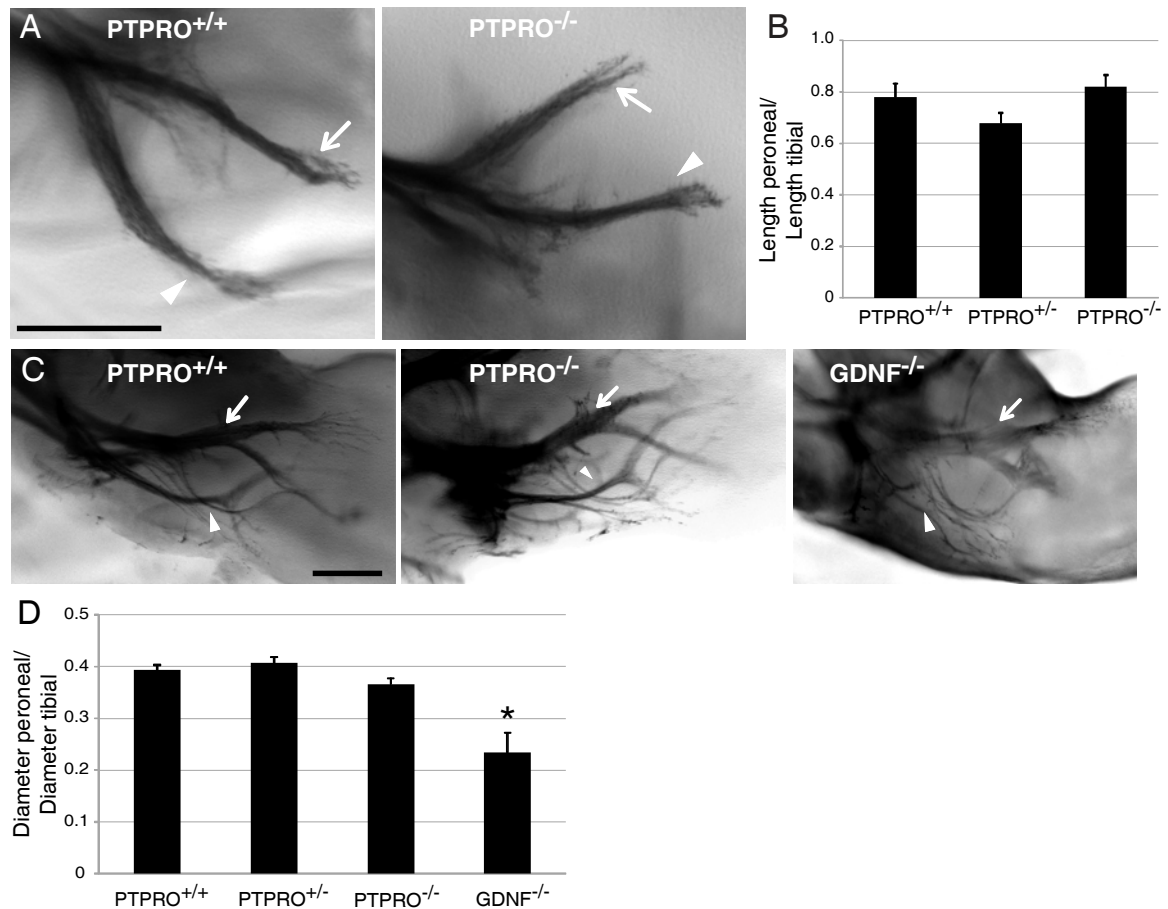


Figure 2-21. Neurofilament staining on whole-mount *PTPRO*^{-/-} embryos does not show any guidance defects

(A) Representative pictures of neurofilament stained E11.5 whole-mount embryos. (B) Graph represents the ratios between the length of the peroneal and the tibial nerves of 19 wild-type, 12 *PTPRO*^{+/-}, and 16 *PTPRO*^{-/-} hindlimbs (mean±SEM). (C) Representative pictures of neurofilament stained E12.5 whole-mount embryos of the indicated genotypes. *GDNF*^{-/-} were used as positive controls for LMCL misguidance [196]. (D) Graph represents the ratios between the diameter of the peroneal and the tibial nerves of 16 wild-type, 12 *PTPRO*^{+/-}, 15 *PTPRO*^{-/-} and 3 *GDNF*^{-/-} hindlimbs (mean±SEM). Arrowheads point to the peroneal nerve; arrows point to the tibial nerve. Scale bar is 250µm. Statistical analysis was done as for Figure 2-8.

At E11.5 the peroneal and the tibial nerve had the same length in wild-type and *PTPRO* knockout embryos, and at E12.5 the ratio of their diameters was not changed. As

expected, at E12.5 *GDNF*^{-/-} embryos (used as positive controls for the technique) displayed an increase in the diameter of the tibial nerve and a decrease in the diameter of the peroneal nerve (Figure 2-21). Since whole-mount staining is not a very sensitive technique and does not allow distinction between sensory and motor neurons, Dr. Irina Dudanova performed retrograde tracings from the ventral and dorsal hindlimb. For the dorsal tracing she injected Rhodamine Dextran (RD) in the dorsal shank of the hindlimb, which should be innervated only by LMC_L (Lim⁺ neurons), and counted the number of Isl1⁺ neurons labeled with the dye (data not shown). The number of cells labeled was similar in wild-type and *PTPRO*^{-/-} E12.5 embryos (data not shown). Additionally, she injected RD in the ventral shank, which should be innervated only by LMC_M (Isl1⁺ neurons), and counted the number of neurons labeled with RD and Lim1 (data not shown). As before, she did not observe any misprojections, suggesting that Eph-mediated motor neuron axon guidance is not affected *in vivo* in *PTPRO*^{-/-} embryos.

To exclude a potential *in vivo* compensation by other guidance systems, I assessed the response of MN explant culture to ephrin stimulation. I cultured explants of lumbar motor columns from *Hb9-GPF*⁺ transgenic embryos [243] for 18 hours and stimulated them for 30 minutes with 0.1µg/ml or 0.5µg/ml clustered Fc, ephrinA2/A5 (mixed 1:1) or ephrinB2 (Figure 2-22), to assess response of EphA and EphB receptors, respectively. I used ephrinA2 and ephrinA5 in a 1:1 mix, since this resembled the *in vivo* expression [188]. Consistent with the results of growth cone collapse with TG explants, I did not observe an increased sensitivity towards ephrin stimulation in *PTPRO*^{-/-} motor neurons (Figure 2-22).

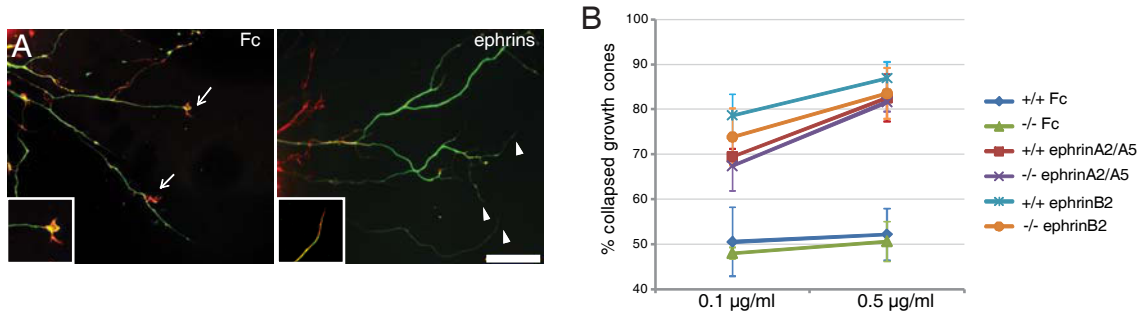


Figure 2-22. *PTPRO*^{-/-} motor neurons are not more sensitive toward ephrin stimulation

(A) Representative pictures of motor neuron explant cultures stimulated with Fc (as a control) or ephrins. Arrows and arrowheads point to non-collapsed and collapsed growth cones, respectively. In green is the Hb9-GFP and in red the Phalloidin-568 staining. Insets show a higher magnification of non-collapsed and collapsed growth cones. Scale bar is 200µm. (B) Graph represents the percentage of collapsed growth cones. Three to six explants per condition were analyzed from 4 embryos per genotype. Compared to the respective controls, all the ephrinA2/A5 and ephrinB2 stimulated explants show a statistically significant increase in the percentage of growth cone collapse (0.1µg/ml ephrinA2/A5-Fc on wild-type cultures, $p=0.038$; 0.5µg/ml on wild-type, $p=0.009$; 0.1µg/ml on *PTPRO*^{-/-}, $p=0.007$; 0.5µg/ml on *PTPRO*^{-/-}, $p=0.002$; 0.1µg/ml ephrinB2-Fc on wild-type cultures, $p=0.015$; 0.5µg/ml on wild-type, $p=0.001$; 0.1µg/ml on *PTPRO*^{-/-}, $p=0.009$; 0.5µg/ml on *PTPRO*^{-/-}, $p=0.001$). Statistical analysis was done as for Figure 2-8.

Taken together these data argue against a role of PTPRO in regulating Eph receptor signaling in LMC axon guidance.

2.1.9. *PTPRO* is not required for retinotectal mapping in mouse

Since ephrins in the hindlimb are presented as a bimodal choice, it is possible that there is no requirement for a fine-tuning of Eph phosphorylation. Conversely, the fine tuning of phosphorylation levels is more likely to be required in the retinotectal system, where Ephs and ephrins are expressed in gradients. In line with this hypothesis, the initial study on PTPRO-mediated Eph regulation showed a critical role for the phosphatase in the retinotectal mapping [219]. On these bases, we collaborated with Dr. Philipp Suetterlin and Prof. Uwe Drescher to perform retinocollicular tracings in *PTPRO*^{-/-} mice at P8. They did not observe misguidance defects or ectopic branching in *PTPRO*^{-/-} mice (Figure 2-23), suggesting that PTPRO is dispensable for development of the mouse retinocollicular map.

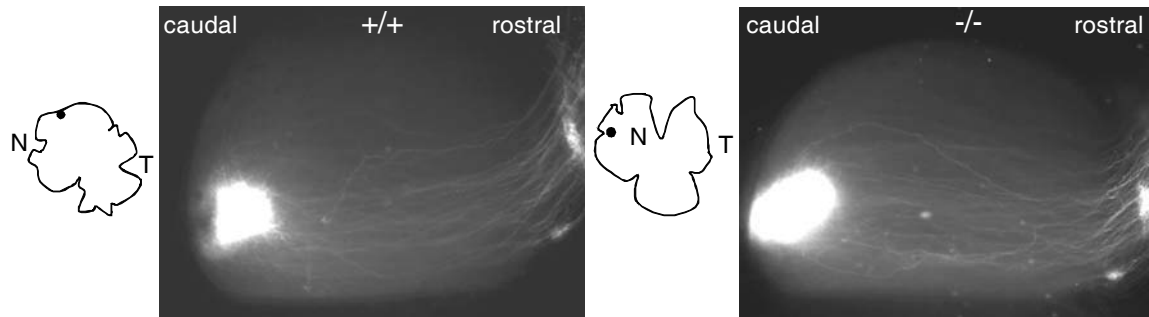


Figure 2-23. *PTPRO*^{-/-} mice do not show misguidance or aberrant branching in the retinocollicular map (in collaboration with Dr. Philipp Suetterlin and Prof. Uwe Drescher)

Representative pictures for the analysis of the retinocollicular projection in wild-type and *PTPRO*^{-/-} mice at P8. Injection of DiI into a small area of nasal retina (drawings on left side) result in labelling of topographically appropriate termination zones in the caudal part of the superior colliculus. Numbers of animals analyzed for the termination zone were: 7 wild-type, 12 *PTPRO*^{+/-} and 5 *PTPRO*^{-/-}. Numbers of animals analyzed for ectopic branching were: 3 wild-type, 4 *PTPRO*^{+/-} and 4 *PTPRO*^{-/-}.

2.1.10. The chick but not the mouse isoform of *PTPRO* can dephosphorylate *EphA4*

The lack of Eph-related phenotypes in *PTPRO*^{-/-} mice could be due to functional redundancy of PTPRO with another Eph phosphatase or to an evolutionary divergence of the mouse (mPTPRO) and chick (cPTPRO) isoforms of PTPRO. To distinguish between these two possibilities, I over-expressed in HEK293 cells EphA4 together with either mPTPRO or cPTPRO. The day after transfection cells were stimulated with 1 µg/ml pre-clustered Fc (as a control) or ephrinA4 for 30 minutes. As expected, ephrinA4 stimulation increased EphA4 phosphorylation levels. When EphA4 was coexpressed with cPTPRO, the receptor was significantly less phosphorylated upon stimulation (Figure 2-24). When EphA4 was coexpressed with mPTPRO, receptor phosphorylation was significantly higher than in presence of cPTPRO and not significantly different from the receptor expressed alone (Figure 2-24). These results indicate that mPTPRO does not regulate Eph signaling and suggest that mPTPRO and cPTPRO have different substrate specificities.

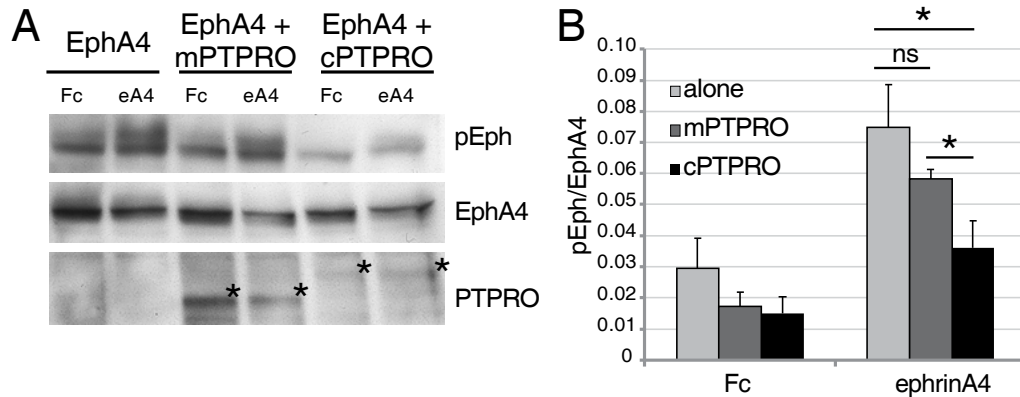


Figure 2-24. The chick but not the mouse isoform of PTPRO can dephosphorylate EphA4

(A) Western blots of HEK293 cells co-transfected with EphA4 and mouse (mPTPRO) or chick (cPTPRO) isoforms of PTPRO-Flag and stimulated as indicated. Total cell lysates (TCL) were probed against phospho- and total EphA4 and Flag (PTPRO). Asterisks indicate PTPRO bands; mPTPRO runs at 140 kDa and cPTPRO at 160 kDa. (B) Graph represents the levels of EphA4 autophosphorylation (mean \pm SEM) after control Fc and ephrinA4-Fc stimulation. The experiment was done in triplicate and the intensities of the phospho bands were quantified using ImageJ and normalized to the total level of the proteins. Statistical analysis was done as for Figure 2-8.

2.2. Role of EphA4 cleavage during development

2.2.1. EphA4 is cleaved in HeLa and HEK293 cells, independently of ligand stimulation

EphA4 has previously been shown to undergo two consecutive proteolytic cleavages, first by a still unknown metalloprotease in its extracellular region, and then by γ -secretase in its transmembrane domain [192]. To assess whether EphA4 cleavage could be modulated by kinase activity or ligand binding, I over-expressed EphA4 with an extracellular Flag-tag (EphA4-Flag) in two cell lines, HeLa and HEK293 cells. I then collected the supernatant and prepared total cell lysates (TCL) 24 hours after transfection. To detect the shed ectodomain (EphA4-ECD) I probed the membrane with an antibody against the Flag-tag. Although in HEK293 cells EphA4 and EphA4-ECD were expressed at higher levels than in HeLa cells (Figure 2-25), both cell lines represented a valid and reliable model to assess receptor shedding.

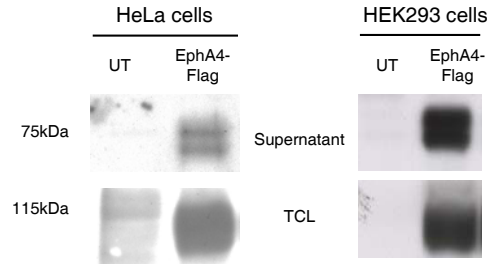


Figure 2-25. EphA4 is cleaved in HeLa and HEK293 cells

Western blots of HeLa and HEK293 cells transfected with EphA4 carrying a Flag tag in its extracellular domain (EphA4-Flag). Total cell lysates (TCL) and supernatants were probed against Flag.

Having characterized the cell lines, I compared two differently tagged EphA4 constructs. In addition to the Flag-tagged construct, where the Flag was positioned at the beginning of the extracellular domain (N-term), I used a construct where mCherry was inserted in the juxtamembrane region of the receptor (EphA4-mCherry). HEK293 cells transfected with EphA4-mCherry, showed again the release of the EphA4-ECD in the supernatant (Figure 2-26).

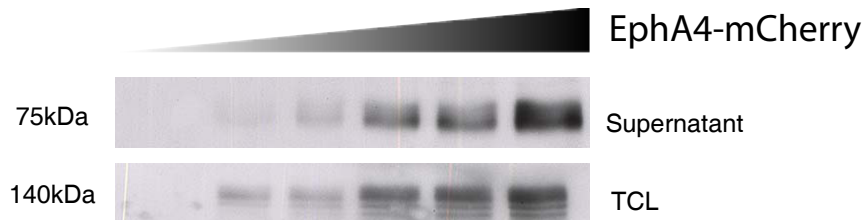


Figure 2-26. EphA4 cleavage is proportional to EphA4 expression levels

Western blots of HEK293 cells transfected with 0.1, 0.2, 0.5, 1, 5µg of EphA4 carrying an mCherry tag in its intracellular domain (EphA4-mCherry). Total cell lysates (TCL) were immunoprecipitated and probed with an antibody against GFP. Supernatant was probed with EphA4-SEK.

I then decided to test several antibodies against different intracellular and extracellular domains of EphA4 to detect the intracellular fragment (EphA4-ICD) and the EphA4-ECD, to recognize the endogenous protein and its fragments in *ex vivo* experiments. To detect the EphA4-ECD I used an antibody produced by BD Bioscience (referred to EphA4-SEK in the following experiments) (Figure 2-26). For EphA4-ICD detection, I obtained the best results with the antibody produced by Zymed (referred to

EphA4-Zymed in following experiments) (Figures 2-27) and one produced by Santa-Cruz (referred to EphA4-S20 in the following paragraphs).

I transfected HEK293 cells with increasing amounts of EphA4-mCherry, and 24 hours after transfection I collected the supernatant and prepared total lysates. EphA4 shedding positively correlated with EphA4 expression levels, suggesting that cleavage could be an intrinsic cell mechanism to control the receptor expression on the surface (Figure 2-26).

I then examined whether the stimulation with soluble ligand had an effect on EphA4 cleavage by over-expressing EphA4-Flag in HEK293 cells and stimulating either with 1 μ g/ml of pre-clustered Fc (as control) or ephrinA4. Stimulation with ephrinA4 induced EphA4 phosphorylation. The EphA4-ICD was also phosphorylated upon stimulation, but its expression was not increased (Figure 2-27). These results were consistent with the reported results showing that EphA4 cleavage in hippocampal cultured neurons is ligand-independent [192].

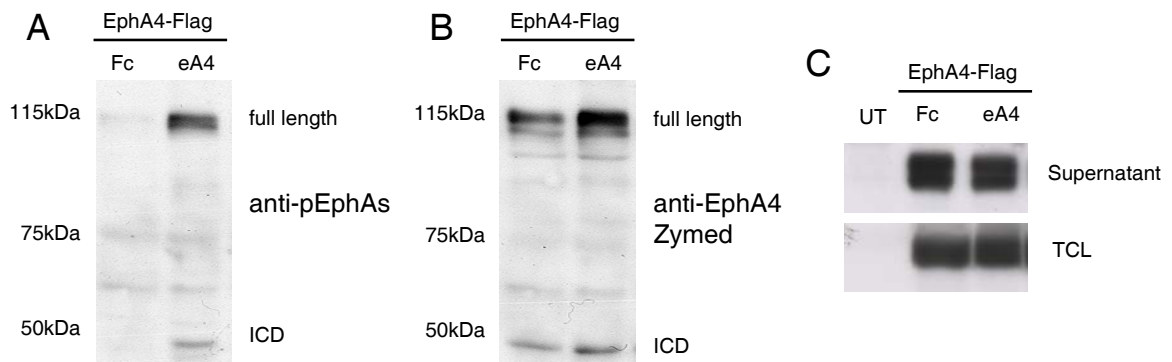


Figure 2-27. EphA4 cleavage is independent of ligand stimulation

(A-B) Western blots of HEK293 cells transfected with EphA4-Flag stimulated with 1 μ g/ml pre-clustered Fc or ephrinA4. TCLs were probed against phospho- (A) and total (B) EphA4 (EphA4-Zymed antibody). The two bands visible correspond to EphA4 full length and the EphA4-ICD (ICD). (C) Western blots of HEK293 cells transfected with EphA4-Flag stimulated with 1 μ g/ml pre-clustered Fc or ephrinA2/A5 (1:1 mix). TCLs and supernatant were probed with EphA4-SEK antibody.

2.2.2. *EphA4* shedding during embryonic development is temporally and spatially regulated

To complement the cell culture data, I prepared E16.5 cortical neuron dissociated cultures from wild-type and *EphA4* knockout mice. I kept neurons in culture for 14 hours, then collected the supernatant and harvested the cells. Since EphA4 is a glycosylated protein, I immunoprecipitated the proteins present in the supernatant by lectin pull-down.

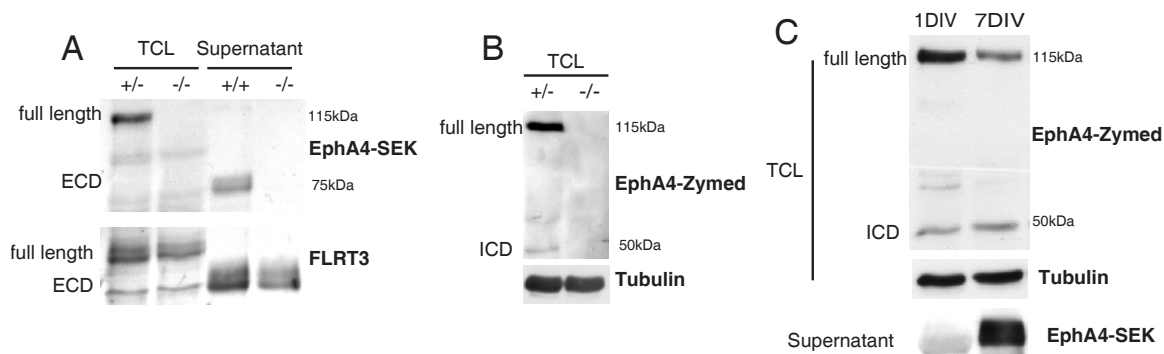


Figure 2-28. EphA4 is cleaved in E16.5 cortical neurons and cleavage regulates receptor levels in culture

(A-B) Western blots of E16.5 cortical neurons from wild-type and *EphA4*^{-/-} embryos. Samples were probed with EphA4SEK and FLRT3 (as control) antibodies (A), and with EphA4-Zymed and tubulin antibodies (B). (C) Western blots of wild-type E16.5 cortical neurons kept in culture for one (1DIV) or seven days (7DIV). TCLs were probed with EphA4-Zymed and tubulin antibodies. Supernatants were probed with EphA4-SEK antibody.

Using Western Blot I showed that the EphA4-ECD was detected only in the wild-type supernatant, whereas the EphA4-ICD was present only in the wild-type TCL (Figure 2-28). As a control, FLRT3-ECD (a known cleaved protein [244]) was detected in the supernatant of both wild-type and *EphA4*^{-/-} cortical neuron cultures. Interestingly, after 7 days in culture, cortical neurons showed decreased expression of full length EphA4, and EphA4-ECD was accumulated in the supernatant. No differences were observed in the levels of EphA4-ICD, suggesting the presence of an intracellular regulatory mechanism in maintaining its constant expression, e.g. proteasome degradation (Figure 2-28). These

data confirmed the *ex vivo* cleavage of EphA4, and reinforced the idea that EphA4 shedding could be a way of regulating EphA4 expression.

Although I showed cleavage in transfected cells and neuronal cultures, it was still unclear if cleavage was happening *in vivo* or was a culture artifact. Thus, I prepared spinal cord and hindlimb lysates from E12.5 wild-type and *EphA4*^{-/-} embryos and probed the membranes with the EphA4-SEK antibody. The antibody recognized two bands in both tissues, one corresponding to the full length protein and one to the EphA4-ECD (Figure 2-29). Interestingly, EphA4-ECD was in a 1:1 ratio with the full length EphA4 in the hindlimb, and in a 1:2 ratio in the spinal cord, suggesting that the extent of cleavage might be tissue-specific.

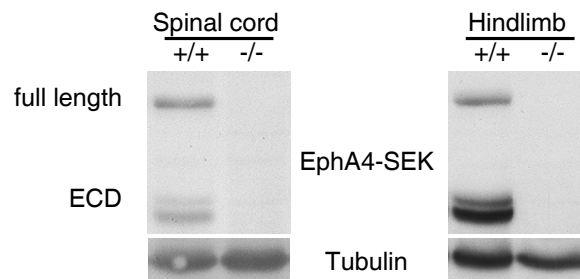


Figure 2-29. EphA4 is cleaved *in vivo*

Western blots of E12.5 spinal cord and hindlimb lysates from wild-type and *EphA4*^{-/-} embryos. Samples were probed with EphA4SEK and tubulin antibodies.

To further characterize the space and time regulation of EphA4 cleavage during development I prepared lysates from three different tissues - spinal cord, hindlimb and forebrain – at several developmental stages. EphA4-ICD and EphA4-ECD showed a similar regulation (quantified as percentage of full-length protein) in all the tissues and at every developmental stage (Figures 2-30 and 2-31).

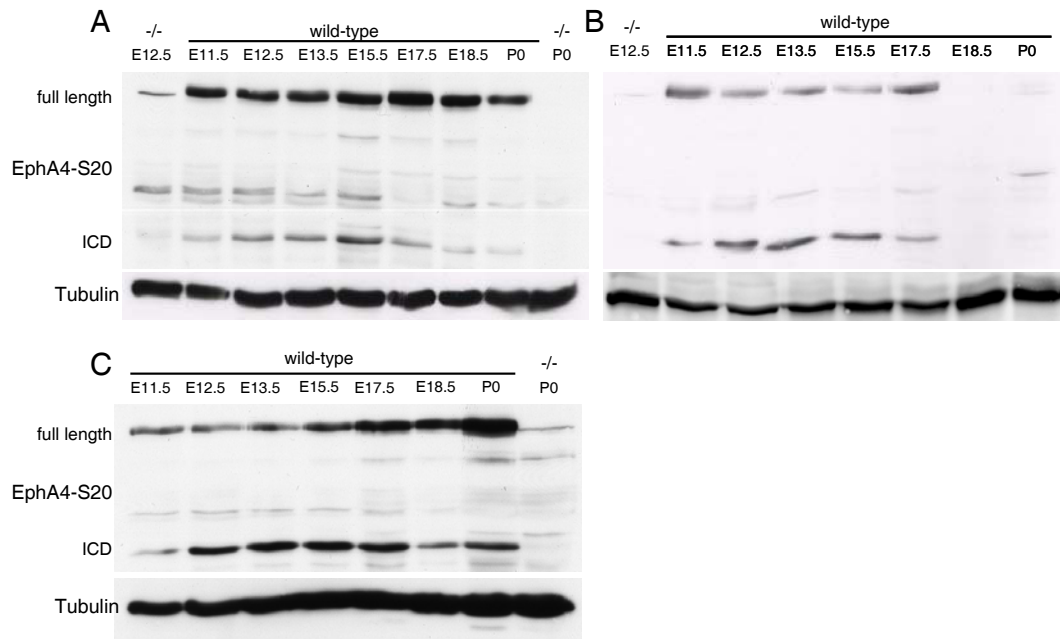


Figure 2-30. EphA4 cleavage is spatially and temporally regulated
 (A-C) Western blots of wild-type and *EphA4*^{-/-} spinal cord (A), hindlimb (B) and forebrain (C) lysates prepared from several developmental stages probed with EphA4-S20 and tubulin antibodies.

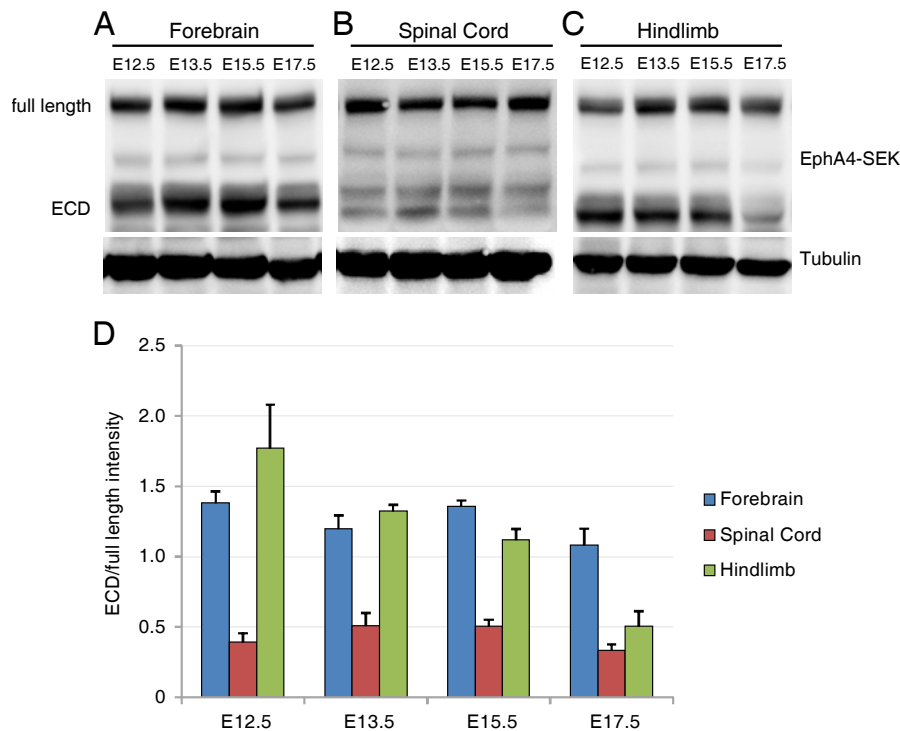


Figure 2-31. EphA4 cleavage has a peak between E12.5 and E15.5
 (A-C) Western blots of wild-type spinal cord (A), hindlimb (B) and forebrain (C) lysates prepared from several developmental stages probed with EphA4-SEK and tubulin antibodies. (D) Graph showing quantification of the cleavage, calculated as the intensity of the EphA4-ECD band divided by the intensity of the full length EphA4 band, at different developmental stages in different tissues (mean±SEM).

In the spinal cord, although it was possible to observe a peak between E13.5 and E15.5, at all stages EphA4-ECD represented a minimal percentage of the total EphA4 expression (Figures 2-30 and 2-31). In the hindlimb, EphA4 cleavage peaked at E12.5 and decreased by E17.5 (Figures 2-30 and 2-31). In the forebrain EphA4-ICD was highly expressed across all the developmental stages, although decreasing in post-natal stages (Figures 2-30 and 2-31). Taken together these data suggest that EphA4 shedding is a temporally and spatially limited process. Interestingly, the temporal regulation of EphA4 cleavage and the extent of cleavage differ in the three tissues analyzed, implying a tissue-specific regulation, probably due to the presence of specific proteases.

2.2.3. Identification of the EphA4 cleavage site

To identify the cleavage site in the receptor, I transfected HeLa cells with different EphA4 mutants, carrying deletions of the whole extracellular domain (EphA4 Δ N), or of the two fibronectin domains (EphA4 Δ FN3) or of the ligand binding domain (EphA4 Δ LBD), and an EphA4 mutant, in which the intracellular domain was replaced by GFP (EphA4-GFP). All these mutants had an N-terminal Flag tag. As additional controls, I used two other receptors belonging to the Eph family, EphB2 and EphA3, both carrying a Flag-tag in their extracellular domain. EphB2 was already reported to be shed [122, 228], but nothing was known about EphA3. This experiment gave three important lines of evidences. First, it strengthened the concept that shedding is independent of the kinase activity, since the EphA4-GFP, although lacking completely the kinase domain, was cleaved to the same extent as wild-type EphA4 (Figure 2-32). Second, it showed that not all the Eph receptors undergo cleavage, since EphA3 was not shed (Figure 2-32). Finally,

it suggested that the cleavage site was not in one of the previously known domains of EphA4, since all the EphA4 mutants, except the EphA4 Δ N, were shed (Figure 2-32).

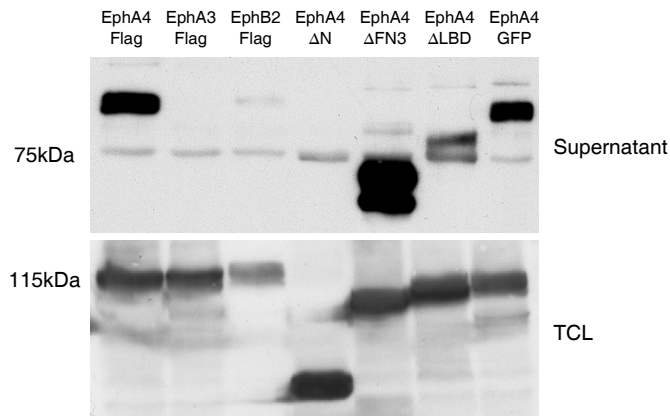


Figure 2-32. Eph receptor cleavage

Western blots of total cell lysates (TCL) and supernatant of HeLa cells transfected with EphA4 wt (EphA4-Flag), EphA3, EphB2 and different constructs carrying deletion in the extracellular or intracellular region of EphA4. Blots were probed with an antibody against Flag. The weak band seen at 75kDa is an unspecific band.

The only portion of the protein not affected by the deletions was a stretch of 15 amino acids in the extracellular juxtamembrane region. Deleting these amino acids (EphA4 Δ 15, carrying an N-terminal Flag tag) led to a strong decrease of EphA4 cleavage, although still did not completely abolish shedding (Figure 2-33). EphA4 Δ 15 cleavage released a smaller EphA4-ECD, implying that the deletion either abolished a glycosylation site or unmasked a different cleavage site.

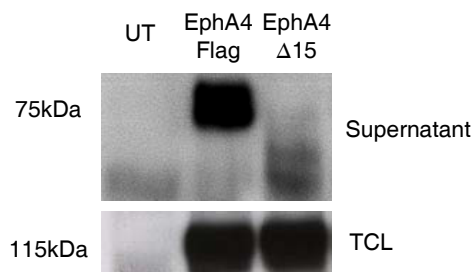


Figure 2-33. EphA4 Δ 15 is still cleaved with low efficiency

Western blots of total cell lysates (TCL) and supernatant of HeLa cells transfected with EphA4 wt (EphA4-Flag) and EphA4 Δ 15. Blots were probed with an antibody against Flag.

Since deleting the extracellular juxtamembrane region was not sufficient to fully abolish receptor shedding, I decided to use a different approach and do site-directed

mutagenesis to alter this stretch of amino acids. Since EphA3 was not cleaved (see Figure 2-32) I performed site-directed mutagenesis to convert the 15 amino acids in the extracellular juxtamembrane region of EphA4 to the corresponding 13 amino acids of EphA3. The reduction of shedding was proportional to how much the mutated sequence resembled EphA3. The complete exchange of these amino acids (EphA4^{CR}, where CR stands for Cleavage Resistant) completely abolished EphA4 shedding. EphA4-ECD and EphA4-ICD were no longer detected in the supernatant and TCL, respectively (Figure 2-34).

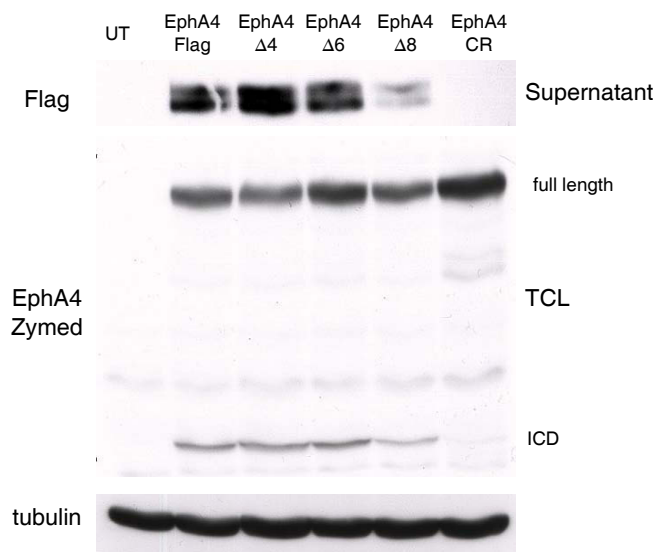


Figure 2-34. EphA4^{CR} is cleavage resistant

Western blots of total cell lysates (TCL) and supernatant of HeLa cells transfected with EphA4 wt (EphA4-Flag) and several EphA4 mutants obtained by site-direct mutagenesis.

2.2.4. *In vitro* characterization of the EphA4^{CR} mutant

Before generating a knock-in mouse carrying the CR mutation, I characterized EphA4^{CR} in selected *in vitro* assays. Flag staining of HeLa cells transfected with EphA4^{CR} confirmed that the protein was expressed normally at the cell surface (Figure 2-35). Moreover, activation of the receptor upon stimulation with increasing amounts of ephrinA5 was not changed (Figure 2-35).

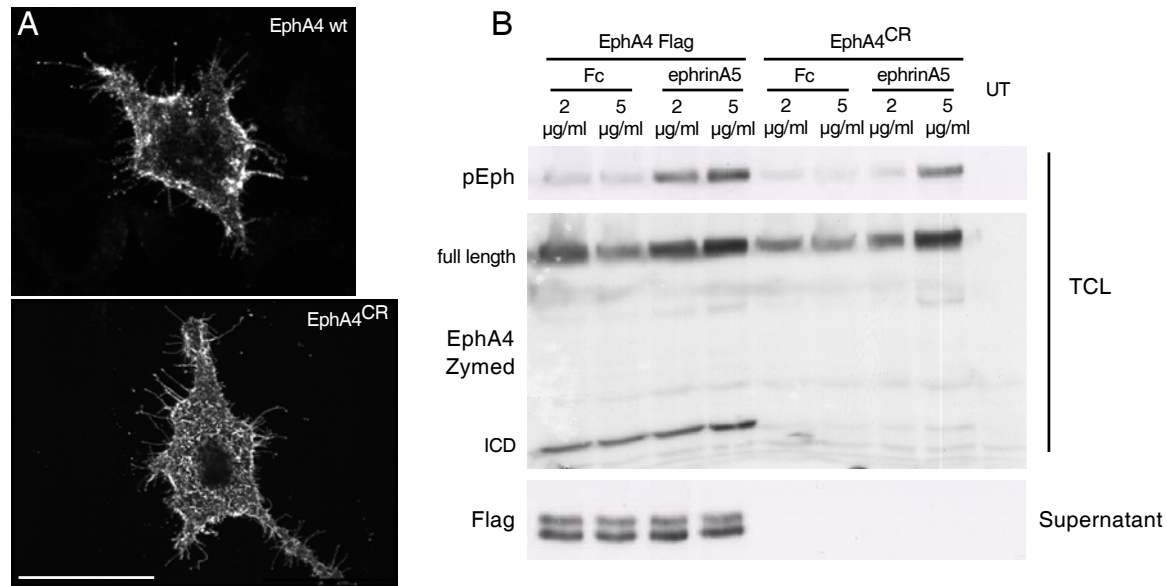


Figure 2-35. EphA4^{CR} is expressed on the cell surface and it is phosphorylated upon ephrinA5 stimulation

(A) HeLa cells transfected with EphA4wt-Flag and EphA4^{CR}-Flag were stained with Flag antibody to detect surface expression. Scale bar is 50μm. (B) Western blots of total cell lysates (TCL) of HeLa cells transfected with EphA4-Flag and EphA4^{CR} and stimulated as indicated. EphA4 phosphorylation was assessed using an anti-phosphoEphA antibody. Full-length protein and EphA4-ICD were detected using the EphA4-Zymed antibody. Anti-Flag staining showed the EphA4-ECD in the supernatant.

As already mentioned, Eph receptors undergo bi-directional endocytosis, so I decided to assess whether impairing cleavage would affect the trans-endocytosis rate by co-culturing EphA4-transfected HeLa cells with SKN-TG2 cells. SKN-TG2 cells are stably expressing histone2B-mCherry, and endogenously express ephrinAs and ephrinBs. As a negative control I used HeLa cells expressing EphA4ΔLBD since it does not bind to ephrins. I seeded the SKN-TG2 cells on top of the HeLa-transfected cells and after 1 hour and 30 minutes I fixed cells. I performed immunostaining before and after permeabilization to detect the surface and total expression of EphA4. In the case of wild-type EphA4 it was possible to detect the receptor inside the SKN-TG2 cells, suggesting that the molecule was trans-endocytosed into the ephrin-expressing cells. EphA4ΔLBD was not present in the SKN-TG2 cells, showing that impairing ligand-receptor binding blocks trans-endocytosis (Figure 2-36). EphA4^{CR} was trans-endocytosed into the ephrin expressing

SKN-TG2 (Figure 2-36) more than the wild-type receptor, suggesting that endocytosis could counteract the absence of cleavage.

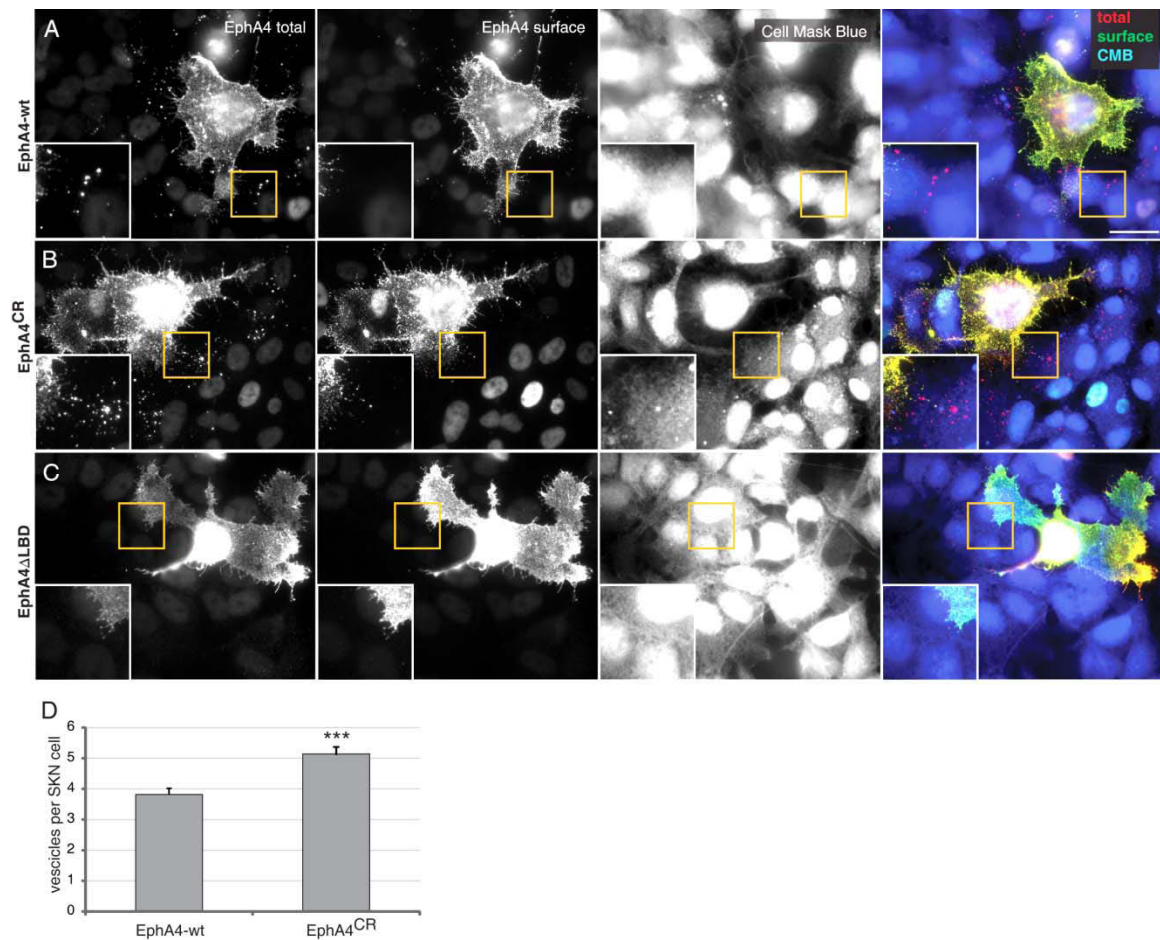


Figure 2-36. EphA4^{CR} shows increased trans-endocytosis into ephrin expressing cells
 (A-C) HeLa cells transfected with EphA4 wild-type (A), EphA4^{CR} (B) and EphA4 Δ LBD (C) co-cultures with SKN-TG2 cells. Cells were stained with anti-Flag antibody before and after permeabilization to detect surface and total expression of EphA4. Cell outlines were labeled by Cell Mask Blue (CMB) staining. Insets show higher magnification of the cells. (D) Graph represents the number of vesicles internalized per SKN cells (mean \pm SEM). 5 SKN cells in the surrounding of each transfected HeLa cell were analyzed. N=344 cells for EphA4 wild-type and 365 cells for EphA4^{CR} from 4 independent experiments. Scale bar is 10 μ m. Statistical analysis was done as for Figure 2-8.

2.2.5. Generation of the EphA4^{CR} knock-in mouse

To address how the impairment of receptor cleavage would affect EphA4 signaling during development, I generated a knock-in mouse carrying the mutation. I inserted the mutated EphA4 cDNA in frame in the exon 3 of the EphA4 gene. The targeting vector carried a gene for resistance to neomycin, so embryonic stem (ES) cells were selected by

antibiotic resistance and then screened by Southern Blot for the mutation. For screening by Southern Blot I digested genomic DNA with BamHI and used a probe that annealed in the 5' region of the EphA4 locus and to confirm the positive clones, I used a probe for the 3' region of the locus (see Figure 2-37 for the targeting strategy). If the clones carried the mutation an additional BamHI site was created, generating an additional band on the Southern Blot with the 3' probe (running at ~5kb). Out of 338 clones screened 5 clones were positive for the insertion (Figure 2-37). Three clones were used for blastocyst injections and all gave rise to chimaeric mice. Chimaeric mice were then crossed with *PGK-Cre*⁺ mice to remove the neo cassette, and bred for three generations.

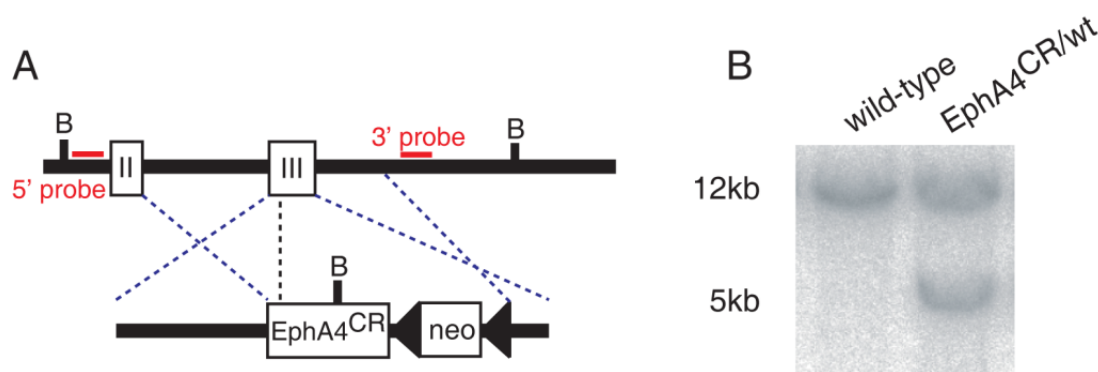


Figure 2-37. Generation of the EphA4^{CR} knock-in mouse.

(A) Scheme representing the knock-in strategy. B indicates BamHI restriction sites. II and III indicate EphA4 gene exons. Blue dashed lines show the long and short arm of recombination. (B) Southern Blot of wild-type and heterozygous *EphA4*^{CR/wt} ES cells. Samples were probed with a radioactively labeled 3' probe.

Before starting phenotypic analysis, I checked that the mutation was sufficient to abolish cleavage *in vivo*. I prepared lysates from different tissues of E12.5 embryos and performed a Western Blot to detect EphA4 cleavage and expression. In *EphA4*^{CR/CR} embryos the EphA4-ICD and the EphA4-ECD were no longer detected in any of the tissues (Figure 2-38).

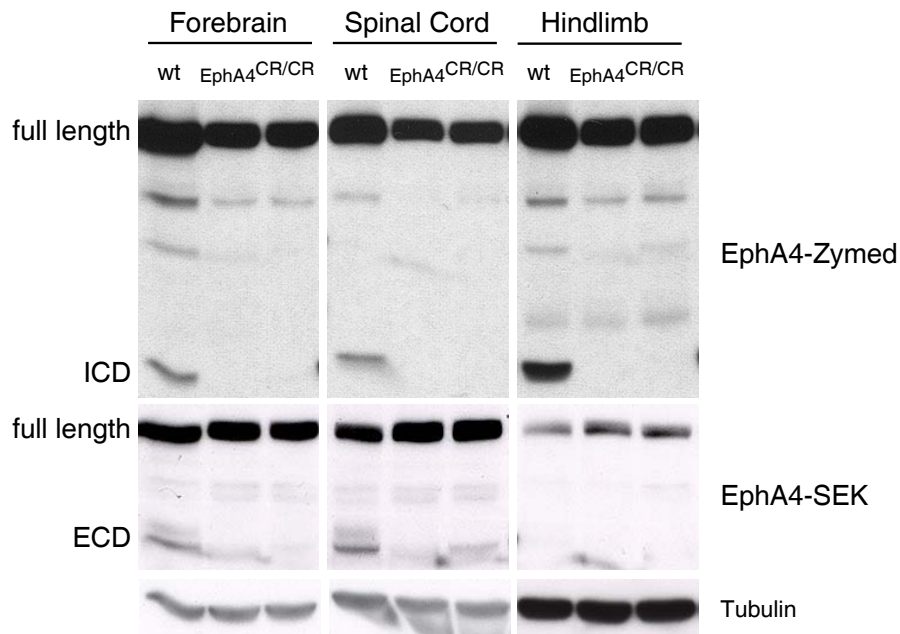


Figure 2-38. EphA4^{CR} mutation is sufficient to abolish receptor cleavage *in vivo*. Western blots of E12.5 wild-type and samples from two different *EphA4^{CR/CR}* embryos, forebrain, spinal cord and hindlimb probed with EphA4-Zymed, EphA4-SEK and tubulin antibodies.

2.2.6. *EphA4* expression in *EphA4^{CR/CR}* embryos

Data from cortical primary culture and transfected cells hinted that the cleavage might regulate EphA4 expression. Thus, I investigated whether genetically blocking EphA4 cleavage *in vivo* would affect the expression of the full length protein. Western Blot performed at E12.5 and E13.5 showed an increase in the amount of full length EphA4 in *EphA4^{CR/CR}* hindlimb, spinal cord and forebrain lysates as compared to controls (Figure 2-39). At E12.5 the increase was more dramatic in the forebrain and in the hindlimb where EphA4 was cleaved to a greater extent. In the heterozygous *EphA4^{wl/CR}* spinal cords, the mutation increased the full length expression as much as in *EphA4^{CR/CR}* embryos. At E13.5 the expression of EphA4 was higher still, although the difference between wild-type and mutant was less evident, suggesting the presence of additional mechanisms regulating full length protein expression.

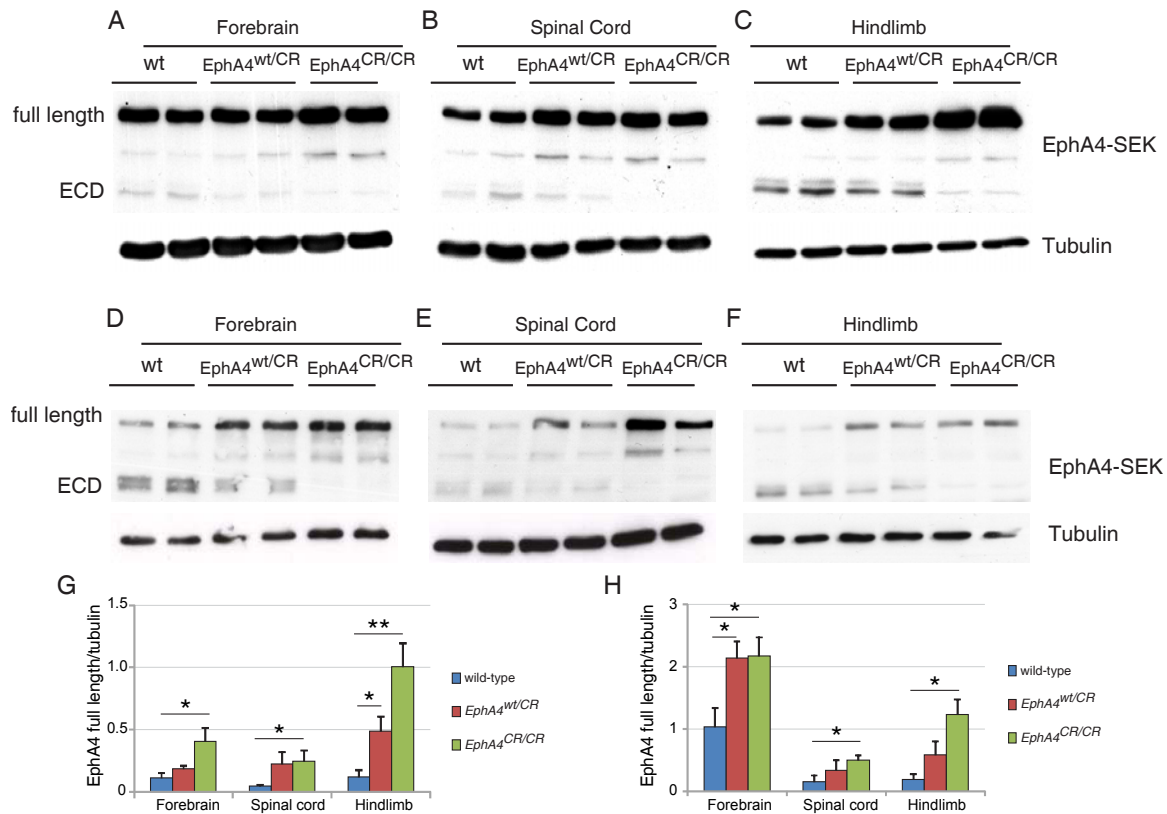


Figure 2-39. *EphA4*^{CR/CR} has increased levels of EphA4 full-length protein.

(A-C) Western blots of E12.5 wild-type, *EphA4*^{wt/CR} and *EphA4*^{CR/CR} forebrain (A), spinal cord (B) and hindlimb (C) probed with EphA4-Zymed and tubulin antibodies. (D-F) Western blots of E13.5 wild-type, *EphA4*^{wt/CR} and *EphA4*^{CR/CR} forebrain (D), spinal cord (E) and hindlimb (F) probed with EphA4-Zymed and tubulin antibodies. (G,H) Graphs representing full-length EphA4 expression, normalized to tubulin, at E12.5 (G) and E13.5 (H) in wild-type, *EphA4*^{wt/CR} and *EphA4*^{CR/CR} tissues.

To complement the Western Blot analysis and to identify whether the increase in full length protein expression was ubiquitous or limited to specific cell populations, I prepared cryosections of E12.5 embryos and performed immunostaining using an EphA4 antibody. In the hindlimb there are two sources of EphA4 expression: the hindlimb mesenchyme and the motor axons. EphA4 is expressed at higher levels on the peroneal nerve, which innervates the dorsal mesenchyme, and at lower levels on the tibial nerve, which provides innervation to the ventral mesenchyme [187, 188, 196]. In *EphA4*^{CR/CR} embryos EphA4 expression did not increase on either of the two nerves and the ratio of peroneal and tibial expression remained unaffected (Figure 2-40). In the hindlimb EphA4

is widely expressed in the mesenchyme, although at higher levels in the dorsal region. In *EphA4^{CR/CR}* embryos I observed an increase in EphA4 expression in both the dorsal and the ventral part of the hindlimb mesenchyme (Figure 2-40), although the ratio between the two was not changed. These data suggest that abolishing cleavage is sufficient to up-regulate EphA4 expression in the mesenchyme but not on the growing axons. Moreover, I showed that inhibiting cleavage does not change the relative expression of the protein, indeed, the dorsal/ventral ratio is conserved.

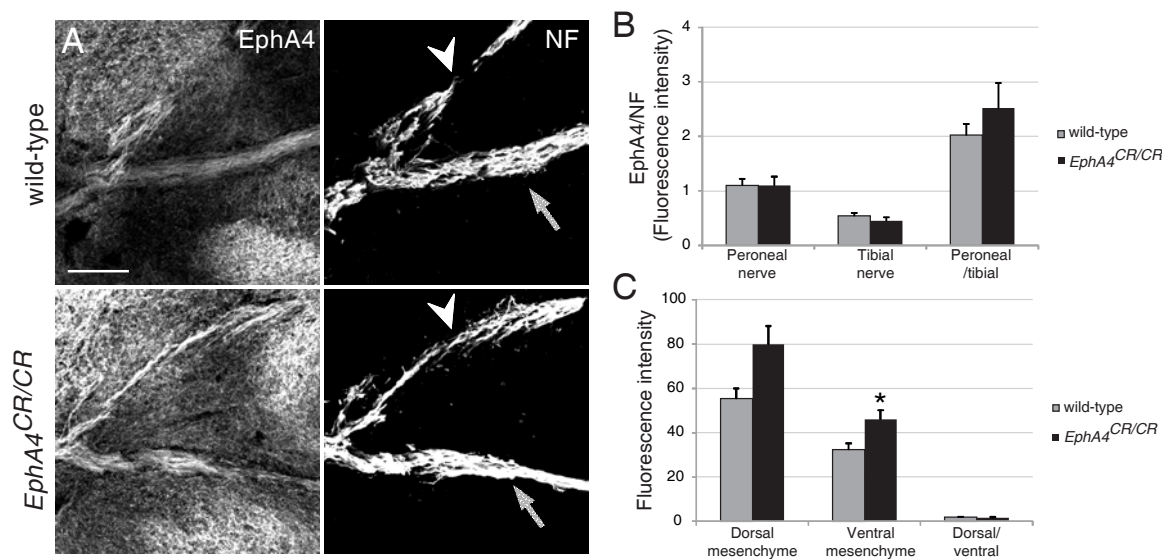


Figure 2-40. In *EphA4^{CR/CR}* embryos full-length EphA4 is up-regulated in the hindlimb mesenchyme but not on motor axons.

(A) Immunostaining of E12.5 wild-type and *EphA4^{CR/CR}* hindlimb with EphA4-S20 and neurofilament (NF) antibodies. Arrowheads point to the peroneal nerve, and arrows to the tibial. Scale bar is 100µm. (B) Graph representing mean±SEM of EphA4 staining intensity on the peroneal and tibial nerves, normalized to neurofilament (N=3 embryos per genotype). (C) Graph representing mean±SEM of EphA4 staining intensity on the dorsal and ventral mesenchyme (N=3 embryos per genotype). Statistical analysis was done as for Figure 2-8.

At E12.5 EphA4 is expressed in several neuronal populations within the spinal cord, although most strongly in motor neurons. I prepared cryosections of E12.5 embryos and stained them with EphA4 and neurofilament antibodies. I identified the motor neurons by their position in the spinal cord and measured EphA4 expression, normalizing to the intensity of neurofilament staining. In the *EphA4^{CR/CR}* spinal cord, EphA4 was not up-

regulated on motor neuron cell bodies as compared to wild-type littermates (Figure 2-41). When I compared the levels of EphA4 between the dorsal and ventral regions of the spinal cord, I made the surprising observation that in *EphA4*^{CR/CR} embryos the protein is expressed at higher levels in the dorsal part. Taken together these data suggest that in the spinal cord the up-regulation of EphA4 expression is restricted to the dorsal spinal cord.

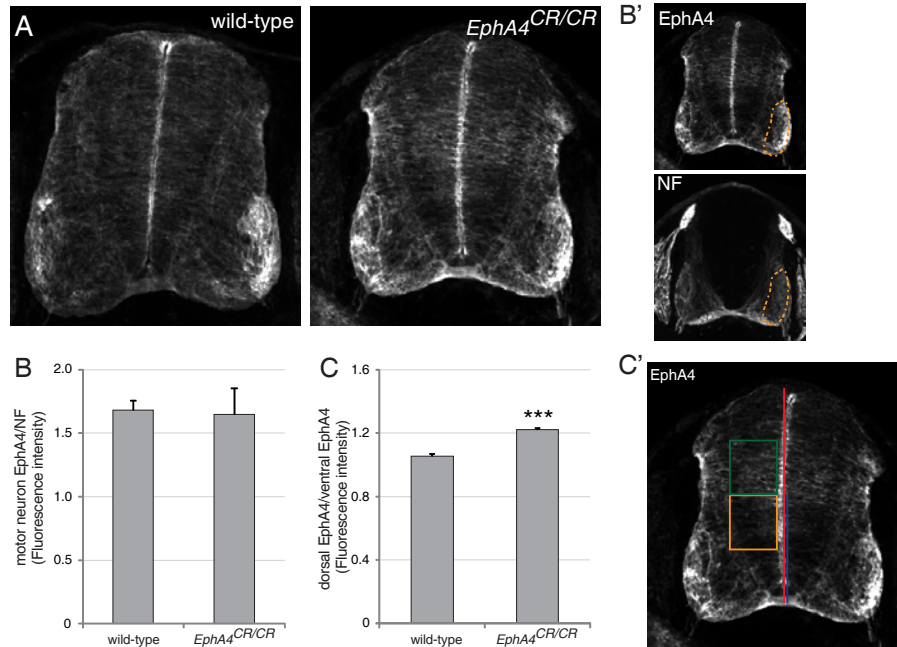


Figure 2-41. In *EphA4*^{CR/CR} embryos full-length EphA4 is up-regulated in the dorsal spinal cord but not on motor neurons.

(A) Immunostaining of E12.5 wild-type and *EphA4*^{CR/CR} spinal cord with EphA4-S20 antibody. (B) Graph representing mean±SEM of EphA4 staining intensity on motor neurons normalized to neurofilament staining (N=3 embryos per genotype). (B') Staining of EphA4 on motor neurons was analyzed in the area encircled by the orange dashed line. (C) Graph representing mean±SEM ratio of EphA4 staining intensity on the dorsal and ventral spinal cord (N=3 embryos per genotype). (C') Red and blue lines indicate the total and half length of the spinal cord, respectively. Two boxes (height equals one quarter of the total length of the spinal cord) were drawn beginning at the middle of the spinal cord. The green box represents the area considered dorsal, and the yellow the ventral one. Statistical analysis was done as for Figure 2-8.

2.2.7. *EphA4* shedding is required for LMC_L neuron axon guidance

Since EphA4 has been shown to be a key player in motor neuron axon guidance at the sciatic plexus [194], and the protein was up-regulated in the hindlimb mesenchyme, I next investigated the role of receptor shedding in LMC axon guidance.

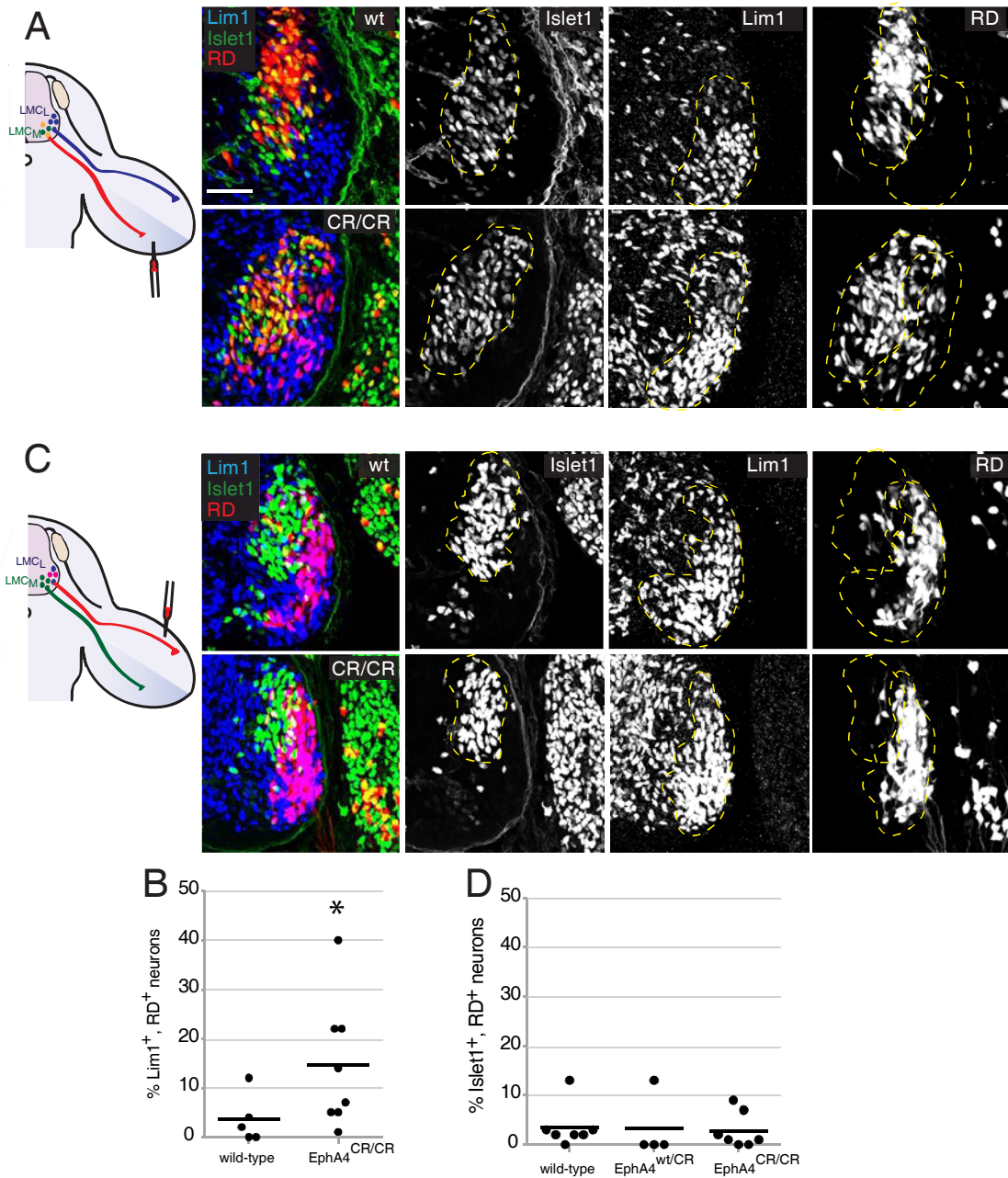


Figure 2-42. Hindlimb retrograde tracings show misguidance of LMC_L neurons in *EphA4*^{CR/CR} embryos

(A) Confocal pictures of ventral retrograde tracings in E12.5 embryos. Rhodamine dextran (RD) was injected in the ventral shank of the hindlimb and sections were stained with Islet1 and Lim1 to label LMC_M and LMC_L (populations are delineated by dashed lines), respectively. (B) Graph represents the percentage of misprojections (neurons positive for RD and Lim1 staining) in relation to all RD-labeled cells in ventral retrograde tracings of 5 wild-type embryos and 8 *EphA4*^{CR/CR} embryos. Each dot in the graphs represents one embryo. The black line represents the mean. (C) Confocal pictures of dorsal retrograde tracings in E12.5 embryos. Rhodamine dextran (RD) was injected in the dorsal shank of the hindlimb and sections were stained as above. (D) Graph represents the percentage of misprojections (neurons positive for RD and Islet1) in relation to all RD-labeled cells in dorsal retrograde tracings. The black line represents the mean. 7 wild-type embryos, 4 *EphA4*^{wt/CR} and 7 *EphA4*^{CR/CR} were analyzed. Each dot in the graphs represents one embryo. Scale bar is 50 μ m. Statistical analysis was done using the non-parametric Mann-Whitney test (* $p < 0.05$).

The two populations of LMC neurons, LMC_L and LMC_M, can be separately examined using ventral and dorsal retrograde tracings, respectively. As has already described for the PTPRO project, I injected Rhodamine Dextran (RD) in the dorsal and ventral shanks of E12.5 *EphA4*^{CR/CR} embryos, and labeled the two neuronal populations by staining for Islet1 and Lim1. Dorsal retrograde tracings did not show any misprojections, since all the labeled cells colocalized with Lim1 and there was no difference with wild-type embryos. However, ventral tracings showed 14% of mis-projecting axons in *EphA4*^{CR/CR} embryos (Figure 2-42). Unexpectedly, this mis-projection phenotype resembled qualitatively the *EphA4*^{-/-} phenotype.

Taken together these data suggest that abolishing cleavage *in vivo* impairs LMC_L axon guidance, re-routing them to the ventral mesenchyme. Further experiments will be required to uncover the mechanism underlying this phenotypic change in the *EphA4*^{CR/CR} embryos.

2.2.8. EphA4 shedding is dispensable for dorsal funiculus and anterior commissure formation

Since the phenotype observed in the hindlimb is similar to that of *EphA4*^{-/-} embryos, I decided to analyze other developmental processes dependent on EphA4 signaling: the morphology of the dorsal funiculus (DF) and the formation of the anterior commissure (AC). The DF is the structure in the dorsal spinal cord containing ascending and descending projections, including sensory afferents and CST axons. Formation begins at E14.5 and is completed by birth. In *EphA4*^{-/-} and *EphA4*^{KD} (kinase dead knock-in) mice the DF is shallower [150, 151]. In *EphA4*^{CR/CR} embryos full-length EphA4 is highly expressed in the dorsal spinal cord as compared to controls. I dissected spinal cords from

wild-type and *EphA4*^{CR/CR} adult mice and prepared vibratome sections from the lumbar region. To compare wild-type and *EphA4*^{CR/CR} I measured the length of the dorsal funiculus and normalized it to the distance between the dorsal tip of the spinal cord and the central canal. Although in the embryonic dorsal spinal cord EphA4 expression was increased and EphA4 cleavage abolished, I did not observe any alteration in the dorsal funiculus anatomy (Figure 2-43).

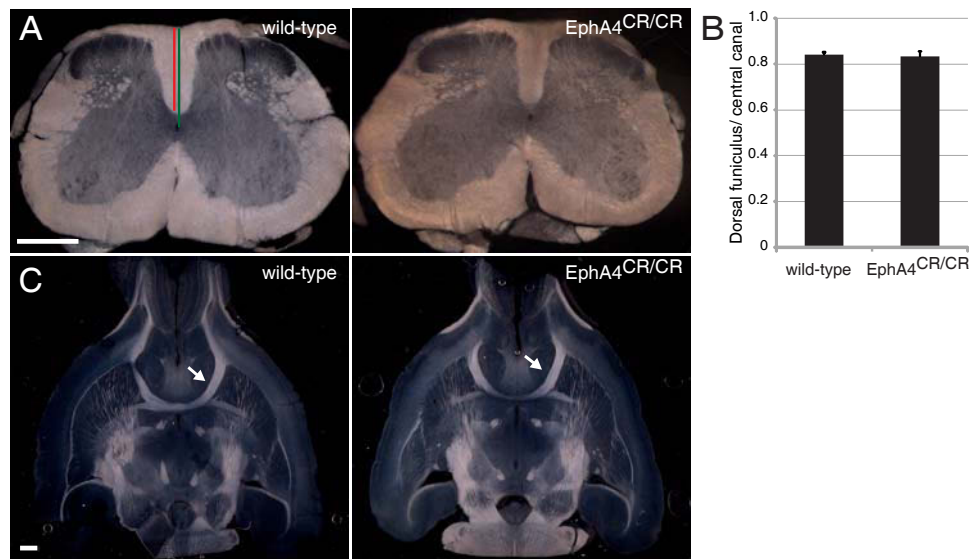


Figure 2-43 Dorsal funiculus morphology and anterior commissure formation are not affected in *EphA4*^{CR/CR} mice

(A) Cross-sections of adult spinal cord from wild-type and *EphA4*^{CR/CR} mice. Red line marks the dorsal funiculus length, and green, the distance between the dorsal tip of the spinal cord and the central canal. (B) Graph represents the mean±SEM ratio of the length of the dorsal funiculus (DF) and distance to central canal (N=3 mice per genotype). (C) Cross-sections of adult brain from wild-type and *EphA4*^{CR/CR}. Arrows point to the anterior tract of the anterior commissure (N=3 mice per genotype).

I next analyzed the formation of the anterior commissure. It has been shown that EphA4-mediated ephrin reverse signaling is required for the correct formation of the aAC tract. In *EphA4*^{-/-} mice the aAC tract is absent, while it is not affected in *EphA4*^{KD} [152]. I dissected brains from wild-type and *EphA4*^{CR/CR} adult mice and prepared vibratome sections. Although in embryonic forebrain lysates EphA4 expression was increased and EphA4 shedding abolished, the aAC tract was correctly formed. I compared 3 wild-type

and 3 *EphA4*^{CR/CR} brains and did not observe any morphological differences (Figure 2-43).

Taken together these data show that EphA4 is dispensable for the formation of the dorsal funiculus and of the aAC tract. Interestingly, the data on the anterior commissure suggest that EphA4 is capable of acting as a ligand, even as a membrane-bound protein.

2.3. Receptor cross-talk during development

2.3.1. *EphA4* and *Ret* do not interact in LMC neurons

As mentioned in the introduction, another way of regulating signaling and combining different stimuli in a great variety of outputs, is the cooperation of different receptors. In the hindlimb, as reported by Kramer et al. [196], *Ret* and *EphA4* cooperate in guiding LMC_L axons in the dorsal mesenchyme. In collaboration with Dr. Irina Dudanova, I assessed whether these two receptors converge on the same pathway or act independently.

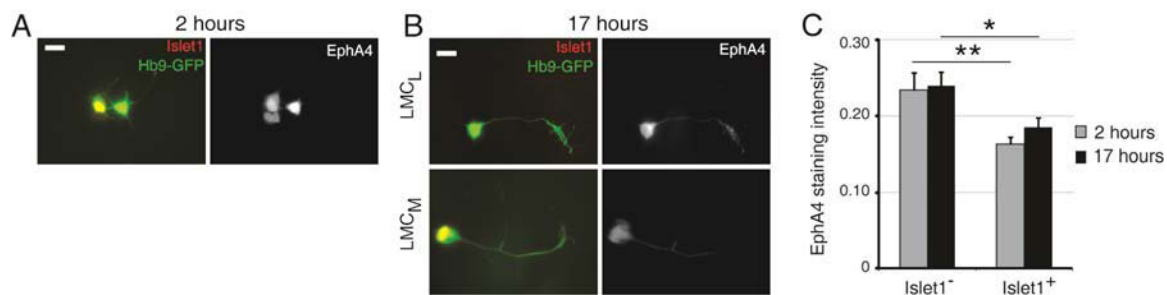


Figure 2-44 Characterization of dissociated LMC cultures

(A,B) The difference in EphA4 expression between LMC_M and LMC_L neurons is maintained in overnight cultures. Representative images of LMC_M and LMC_L neurons immunostained for Islet1 and EphA4, 2 hours (A) and 17 hours (B) after seeding. Islet1⁻ (LMC_L) neurons show stronger EphA4 staining than Islet1⁺ neurons. Scale bars are 12μm. (C) Quantification of fluorescence intensity of EphA4 staining. Data are presented as mean values (±SEM), the numbers of cells analyzed are: 13 neurons from 1 culture for Islet1⁻ 2 hours, 22 neurons from 1 culture Islet1⁺ 2 hours, 19 neurons from 2 cultures Islet1⁻ 17 hours, 20 neurons from 2 cultures for Islet1⁺ 17 hours. Statistical analysis was done as for Figure 2-8.

To identify a potential direct interaction between the two RTKs, I performed immunostaining on dissociated cultures of motor neurons and co-immunoprecipitation

experiments from spinal cord and hindlimb lysates. First, I characterized the E12.5 primary motor neuron culture system to make sure that LMC_L and LMC_M are equally represented. I cultured *Hb9-GFP*⁺ motor neurons for 2 or 17 hours and then did an immunostaining for EphA4 and Islet1 (marker of LMC_M). At both time points, as expected, EphA4 expression was higher on Islet1⁻ neurons (Figure 2-44), and the number of Islet1⁺ and Islet1⁻ neurons was roughly equal. Moreover, I prepared primary motor neuron dissociated cultures from E12.5 *Ret*^{-/-} and *EphA4*^{-/-} embryos, and tested the specificity of the Ret and EphA4 antibodies (Figure 2-45).

Having characterized the culture system and the antibodies, I did co-staining for Ret and EphA4, before and after stimulation with their respective ligands, and I did not observe a significant degree of colocalization between the two receptors in any of the conditions analyzed (Figure 2-46). Consistently, I was not able to co-immunoprecipitate EphA4 and Ret from the hindlimb or spinal cord lysates. As a positive control for the immunoprecipitation I used an antibody against FRS2, a known interactor of Ret [56] (Figure 2-46).

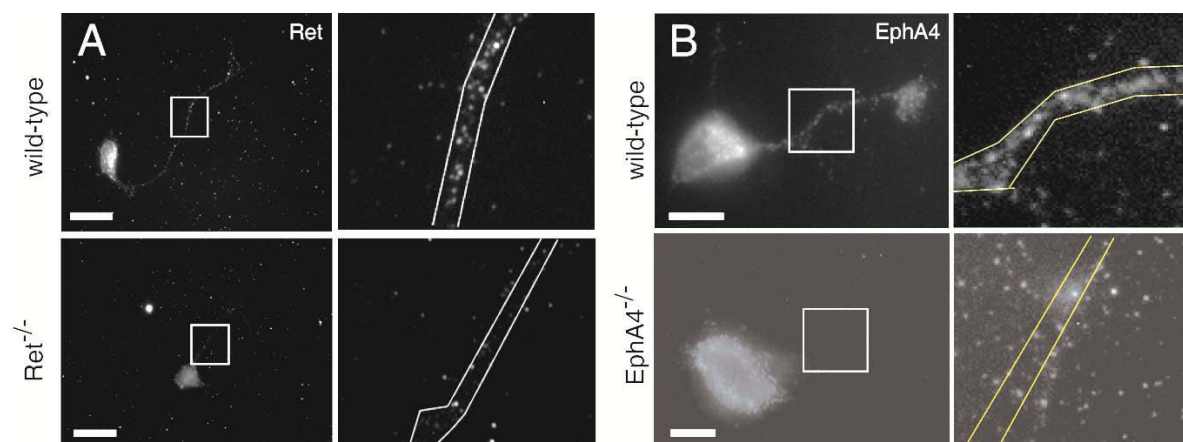


Figure 2-45 Specificity of Ret and EphA4 antibodies

(A,B) Dissociated cultures of LMC motor neurons from *Ret*^{-/-} (A), *EphA4*^{-/-} (B) and corresponding wild-type littermate embryos were immunostained for the respective proteins. Axons were outlined based on Hb9-GFP staining. Scale bars are 25 μ m.

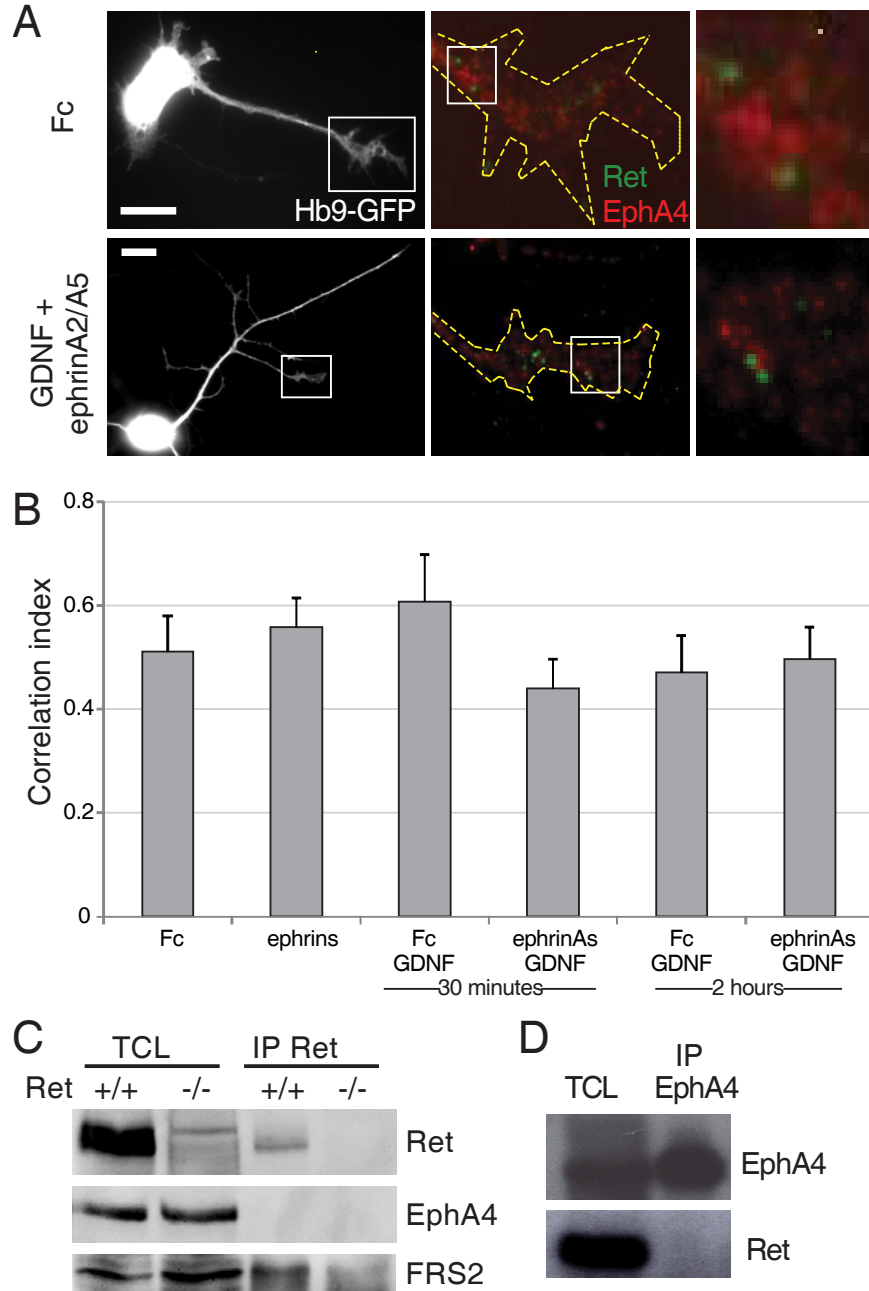


Figure 2-46 Ret and EphA4 do not directly interact in motor axons

(A) Immunodetection of endogenous Ret (green) and EphA4 (red) in dissociated LMC cultures from *Hb9-GFP*⁺ transgenic embryos stimulated with the indicated proteins. (B) Quantification of colocalization of Ret and EphA4 on motor neuron growth cones in the indicated stimulation conditions. The growth cone was manually selected based on the Hb9-GFP signal and the correlation between Ret and EphA4 staining was calculated as Pearson's correlation coefficient. Data are presented as mean values (±SEM), the numbers of cells analyzed are: 5-14 neurons from at least 2 cultures. Scale bars represent 10µm. (C) Lysates of E12.5 spinal cords were subjected to immunoprecipitation (IP) with the Ret antibody and examined by anti-Ret, anti-EphA4 and anti-FRS2 western blots as indicated. EphA4 does not coimmunoprecipitate with Ret. As a positive control, we observed coimmunoprecipitation of Ret and FRS2, a known interaction partner of Ret. TCL denotes total cell lysate. (D) Lysates of E12.5 spinal cords were immunoprecipitated with the EphA4 antibody and examined by anti-Ret and anti-EphA4 western blots. No Ret protein is detected in the precipitates.

These results suggest that the two receptors are unlikely to directly interact on motor neuron axons or growth cones, raising the possibility that they signal independently in an additive fashion.

2.3.2. *EphA4* signaling is not impaired in *Ret*^{-/-} mice

Although the two receptors do not interact directly, it is still possible that they influence each other's signaling. Therefore, I analyzed EphA4 phosphorylation and cleavage in spinal cord and hindlimb lysates in the presence and absence of Ret. I prepared spinal cord lysates from wild-type and *Ret*^{-/-} embryos, immunoprecipitated them with an EphA4 antibody and then probed the membrane with a phosphotyrosine antibody (4G10). As a control for the specificity of the immunoprecipitate, I also prepared lysates from *EphA4*^{-/-} embryos. EphA4 was not differentially phosphorylated in *Ret*^{-/-} lysates as compared to controls (Figure 2-47).

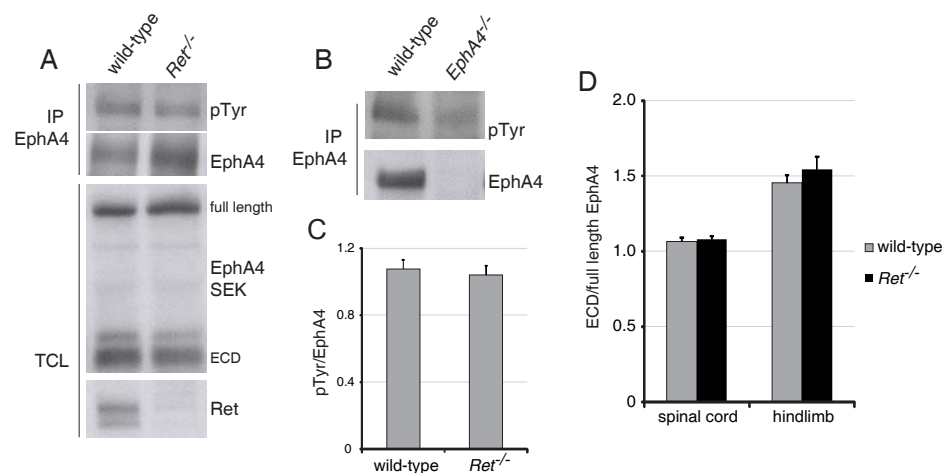


Figure 2-47 EphA4 phosphorylation and shedding are not altered in E12.5 *Ret*^{-/-} embryos

(A) E12.5 spinal cord lysates from wild-type and *Ret*^{-/-} embryos were immunoprecipitated with an antibody against EphA4, and probed with phosphotyrosine (pTyr) and EphA4 antibodies. Total cell lysates (TCL) were probed with EphA4-Sek and Ret antibodies. (B) E12.5 spinal cord lysates from wild-type and *EphA4*^{-/-} embryos were immunoprecipitated with an antibody against EphA4 and probed with phosphotyrosine (pTyr) and EphA4 antibodies. (C) Graph representing the mean±SEM ratio of pTyr and EphA4 staining. N=5 embryos per genotype. (D) Graph representing the mean±SEM ratio of shed ectodomain (ECD) of EphA4 and full length EphA4 in hindlimb and spinal cord lysates from wild-type and *Ret*^{-/-} embryos. N=5 embryos per genotype for the spinal cord, 5 wild-type and 4 *Ret*^{-/-} embryos for the hindlimb.

GDNF/NCAM signaling has been implicated in the proteolytic processing of PlexinA1 by calpain at the spinal cord midline [93]; and, GDNF/Ret signaling is involved in LMC_L guidance. Therefore, I addressed the potential involvement of Ret-dependent GDNF signaling in EphA4 shedding. I prepared lysates from E12.5 *Ret*^{-/-} spinal cords and hindlimbs and analyzed EphA4 cleavage using Western Blot. The ratio of EphA-ECD and EphA4 full-length was not affected in *Ret*^{-/-} spinal cord and hindlimb, excluding a modulatory role for Ret in EphA4 cleavage, similarly to what was reported for PlexinA1 cleavage at the midline [93] (Figure 2-47).

Consistent with these data, Dr. Irina Dudanova showed that EphA4-mediated growth cone collapse was not affected in *Ret*^{-/-} motor explants (Figure 2-48). Similar to as previously described for the PTPRO project (see Figure 2-22), she stimulated motor explants with pre-clustered Fc, as a control, or ephrinA2/A5 (1:1 mix) and then quantified the percentage of collapsed growth cones. Taken together these data demonstrate that genetic ablation of Ret does not impair EphA4 forward signaling.

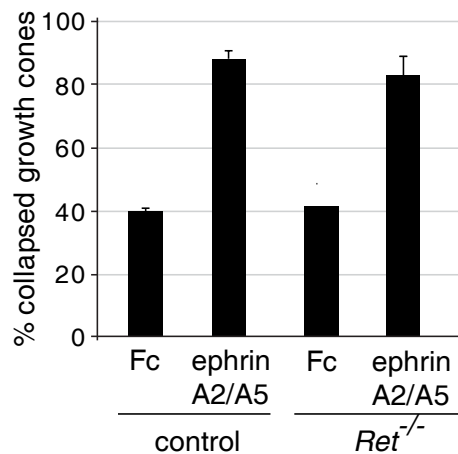


Figure 2-48 EphA4-induced growth cone collapse is not affected in *Ret*^{-/-} embryos (Dr. Irina Dudanova)

EphrinAs-induced growth cone collapse is not Ret dependent. Explants from *Ret* knockout embryos and control littermates were treated with 500ng/ml pre-clustered ephrinA2-Fc and ephrinA5-Fc or pre-clustered Fc. The graph represents mean values (\pm SEM) from two cultures (2–3 explants were counted per condition).

2.3.3. *GDNF and ephrinAs cooperate in Motor Axon Turning*

While it was already known how EphA4 guided motor axons, how Ret instructed axons upon binding to GDNF was still unclear. The expression pattern of GDNF, slightly dorsally to the dorsal/ventral choice point, suggested that it might act as a chemo-attractant cue. To test this hypothesis Dr. Irina Dudanova analyzed growth cone turning in response to a gradient of GDNF using the Dunn's chamber [245]. The Dunn's chamber consists of two concentric circular wells connected by a narrow bridge. If a guidance factor is added to the outer well it will slowly diffuse to the inner well, creating a gradient. To show the reliability of the assay, motor axons were exposed to a gradient of pre-clustered ephrinA5, and, as expected, they were repelled by high doses of the molecule. Interestingly, when motor neurons were challenged with a gradient of GDNF, they showed positive turning towards higher concentration of the neurotrophic factor. More interestingly, when they were challenged with opposing gradients of GDNF and ephrinA5 (such as to resemble the *in vivo* expression pattern of the two ligands in the hindlimb) the turning response was stronger than the response to either of the cues alone. However, if both ligands were applied in the same well, the attraction towards GDNF was neutralized by the repulsion away from ephrin, resulting in the absence of a net turning response (Figure 2-49). To further confirm that EphA4/ephrinAs and Ret/GDNF acted in an additive manner and that the receptors did not cross-talk, Dr. Dudanova repeated the turning assay in response to GDNF using wild-type and *EphA4*^{-/-} neurons, showing that EphA4 was dispensable for GDNF-induced turning (Figure 2-49).

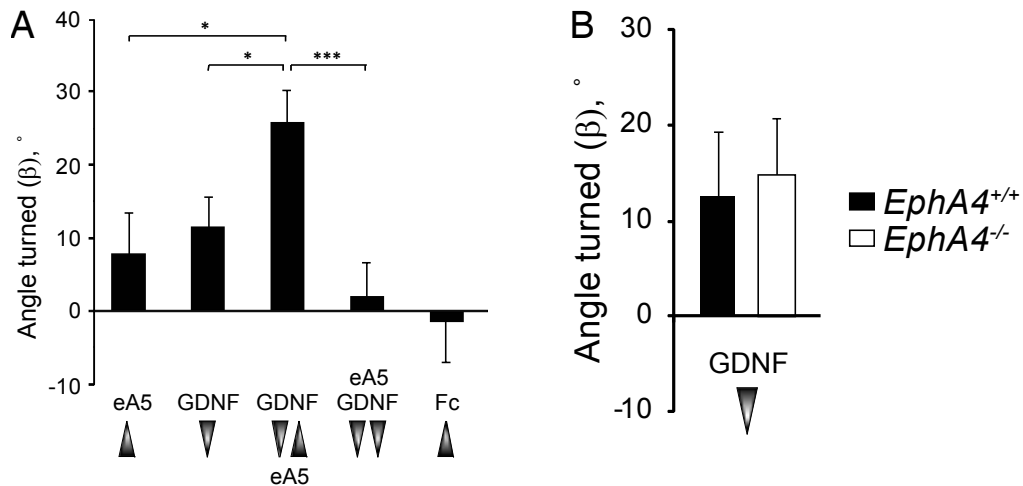


Figure 2-49 Cooperation between GDNF and ephrinA5 in motor axon turning (Dr. Irina Dudanova)
 (A) Quantification of LMC axon turning in the indicated gradients. Data are presented as mean values (\pm SEM). The numbers of axons analyzed are: ephrinA5-Fc, 65 axons from six cultures; GDNF, 145 axons from three cultures; GDNF and ephrinA5 in counter gradients, 66 axons from five cultures; GDNF and ephrinA5 in overlapping gradients, 43 axons from two cultures; Fc, 73 axons from five cultures. (B) The absence of EphA4 does not change the turning response to GDNF. Data are presented as mean values (\pm SEM). The numbers of axons analyzed are: *EphA4*^{+/+}, 44 axons from two cultures; *EphA4*^{-/-}, 44 axons from two cultures. The difference between wild-type and knockout cultures is not significant ($p = 0.80$, t test). Statistical analysis was done as for Figure 2-8.

Taken together these data suggest that *in vivo* LMC_L axons are guided by a push-and-pull mechanism, where GDNF pulls them towards the dorsal mesenchyme and ephrinAs push them away from the ventral side.

3. Discussion

The great variety of trajectories followed by neurons *in vivo* is due to the presence of modulatory cues that enlarge the spectrum of responses generated by a limited number of guidance molecules. In my thesis I focused on three different mechanisms of signal modulation: de-phosphorylation, cleavage and receptor cross-talk.

I demonstrated that PTPRO, previously shown as an Eph-specific phosphatase in chick, in mice does not act as an Eph-specific phosphatase, but rather regulates Ret and TrkB phosphorylation to modulate trigeminal neuron growth and branching.

Interestingly, PTPRO sets a functional threshold in response to BDNF and GDNF, and the genetic removal of the phosphatase sensitizes trigeminal neurons to a lower concentration of neurotrophic factors.

I generated a new mouse model to study the role of EphA4 cleavage during development and provided initial evidence for its requirement in LMC_L axon guidance. Using this mouse model I also showed that abolishing cleavage is sufficient to up-regulate the expression of the full-length protein, hinting that cleavage is a regulatory mechanism, fine tuning receptor expression during development.

Finally, I provided evidence that EphA4 and Ret signal independently and additively in LMC_L growth cones and thereby engage in a push-pull mechanism for LMC_L axon guidance. The two receptors do not co-localize on the growth cones of LMC neurons. Genetic removal of Ret does not affect EphA4 signaling, and vice versa. Stimulation of LMC axons with GDNF and ephrinAs in opposing gradients strengthens the turning response up the GDNF gradient.

3.1. Roles of RPTPs during development

Over the last years, the roles of RPTPs in regulating axon guidance in *Drosophila*, *C. elegans* and vertebrates have been clearly shown; however, the underlying molecular mechanisms have been poorly characterized. In particular, there is still sparse knowledge on how the specificity and enzymatic activity of RPTPs are regulated. Moreover, since RPTPs can act either as ligand or as receptor, independently of their phosphatase activity, there is an additional level of complexity in deciphering their molecular interactions.

3.1.1. Regulation and specificity of the phosphatase activity

To date it has not yet been clarified how the phosphatase activity of RPTPs is regulated, and how their substrate specificity is achieved. The current view is based on four hypothetical regulatory mechanisms: 1) dimerization, 2) binding to extracellular ligands, 3) *cis*-interactions with other transmembrane proteins, and 4) a combination of the above models (Figure 3-1). I will discuss these mechanisms in the following paragraphs.

PTPRO knockout mice display exuberant growth and branching of trigeminal but not motor nerves *in vivo*, although Ret, one of its potential substrates, is expressed in both neuronal populations. Moreover, E12.5 *PTPRO*^{-/-} cultured trigeminal neurons are more sensitive to BDNF and GDNF stimulation, but at P1, a similar behavior is not observed. These two observations raise the question of how PTPRO phosphatase activity and specificity is regulated in space and time.

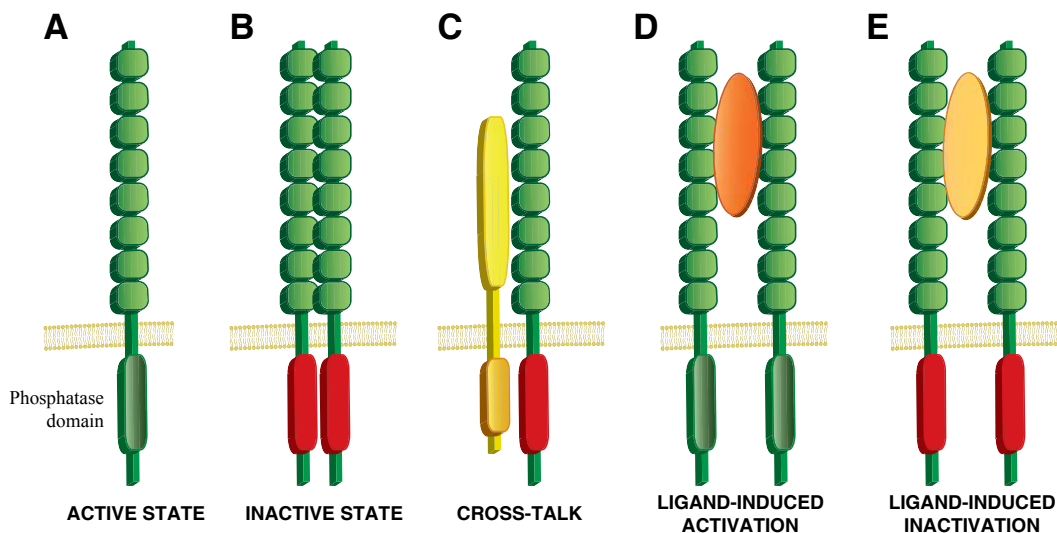


Figure 3-1. Models for the regulation of RPTP phosphatase activity

(A) Model of the active state of RPTP. The phosphate domain is catalytically active (green). (B) Model of the inactive state of RPTP. The phosphate domain is catalytically inactive (red) upon dimerization. (C) Model of potential cross-talk with other receptors or with other RPTP to silence the catalytic activity. (D) Model of ligand induced activation of the phosphatase domain. (E) Model of ligand induced inactivation of the phosphatase domain.

On one hand, this could be achieved by tightly controlled expression of the phosphatase, on the other hand it could be regulated by dimerization. *In vitro*, PTPRO can act on TrkC [220], TrkB and Ret, but *in vivo* PTPRO expression is restricted mainly to TrkB⁺ and Ret⁺ neurons, suggesting that *in vivo* the selective expression of the phosphatase might restrict the number of potential substrates. In newborn mice the percentage of TrkB⁺ and Ret⁺ neurons expressing PTPRO decreases, partially explaining the lack of increased sensitivity towards BDNF and GDNF in P1 *PTPRO*^{-/-} trigeminal neuron cultures compared to controls. Thus, PTPRO substrate specificity is partially achieved by restricted expression in space and time.

PTPRO phosphatase activity has been shown to be regulated by dimerization [220]. When PTPRO is dimerized it is catalytically inactive. How dimerization is normally induced is still unknown. The most accredited hypothesis is that dimerization is induced by an extracellular ligand. To date very few proteins have been identified as potential ligands for RPTPs. The interaction between PTP σ and proteoglycans is an example of how *trans*-interaction with an extracellular ligand leads to changes in phosphatase activity. If PTP σ binds to chondroitin sulfate proteoglycans, it inhibits DRG neuron outgrowth, however, if it binds to heparan sulfate proteoglycans, it triggers neurite extension [246]. Wnt3 has been shown to bind to PTPRO, however it has not yet been addressed whether this interaction has any effect on phosphatase activity [247]. Based on what has been reported for other RPTPs, it would be interesting to study a potential interaction of PTPRO with proteoglycans, and how this interaction might affect its enzymatic activity.

Another challenging question is to understand how RPTPs regulate developmental processes independently of their phosphatase activity. There is growing evidence that RPTPs can act as receptors, can be phosphorylated and can activate signaling cascades leading to cytoskeletal re-arrangements [248]. LAR has been reported to bind heparan sulfate proteoglycans mediating attractive guidance of sensory axons to the skin independently of its phosphatase activity [249]. In my thesis I showed that PTPRO can directly regulate TrkB and Ret phosphorylation *in vitro*, but this did not demonstrate a requirement of its phosphatase activity *in vivo*. The generation of a knock-in mouse expressing a trapping mutant isoform of PTPRO (in which the phosphatase activity is inhibited by a DA mutation [219]) would unequivocally prove this point.

Interestingly, I found a clear difference in substrate specificity between the mouse and chick isoforms of PTPRO. The chick, but not the mouse, isoform is able to dephosphorylate Eph receptors. Site-directed mutagenesis or domain swapping between the two isoforms could explain how this divergence in substrates has evolved. Direct comparison of the chick and mouse cDNA sequences points to a difference in the first 10 amino acids in the N-terminal region, raising the possibility that the two isoforms might have different extracellular regulation. From an evolutionary perspective, it will be intriguing to understand if and why the mouse isoform has restricted its substrate specificity.

3.1.2. Non cell-autonomous role of PTPRO

PTPRO^{-/-} mice were reported to have a reduced number of a subset of nociceptive (CGRP⁺) DRG neurons at birth and as adults [218]. Moreover, the central projections of the surviving nociceptive DRG neurons are abnormal and *PTPRO*^{-/-} mice perform

abnormally on behavioral tests to assess response to thermal stimuli [218]. My data on PTPRO expression in the spinal cord at different developmental stages show that PTPRO is rarely coexpressed with TrkA in DRG neurons, but is highly expressed at the spinal cord midline (CGRP⁺ fibers crossing the midline are absent in *PTPRO*^{-/-} mice [218]). In the TG, consistently with what has been reported by Gonzales-Britos *et al.* [218], there is a partial loss of TrkA⁺ neurons. As has been described for the DRG, in the TG PTPRO is rarely expressed in TrkA⁺ neurons at all the developmental stages analyzed. Thus, the defects observed in nociceptive neuron guidance and survival, are most likely caused by a non-cell autonomous function of PTPRO on TrkA⁺ neurons. Although the *ex vivo* experiments do not completely support a non cell-autonomous role of PTPRO in TrkA⁺ neurons, they do not rule it out. E12.5 *PTPRO*^{-/-} trigeminal neurons, although not more sensitive to low doses of NGF, have longer and more branched neurites at high doses of NGF. As discussed previously, these effects are likely to be independent of TrkA signaling, and could be due to NGF effects on different sub-populations of TG neurons. Although *PTPRO*^{-/-} P1 trigeminal neuron cultures are more branched in response to NGF, this might be a secondary effect due to the loss TrkA⁺ neurons observed in newborn *PTPRO*^{-/-} TG. A conditional knockout approach, specifically ablating PTPRO from TrkA⁺ neurons would unambiguously distinguish between cell-autonomous and non-cell autonomous roles of the phosphatase.

With respect to TrkC⁺ neurons, understanding PTPRO's role is more challenging. PTPRO expression in TrkC⁺ neurons increases during development and the loss of neurons observed is consistent with the number of neurons expressing the phosphatase. How the phosphatase leads to a post-natal loss of TrkC⁺ neurons and to misguidance of

DRG proprioceptive projections, as reported by the Bixby's group [218], is still unclear. Proprioceptive fibers develop in the spinal cord from E13.5 onward [236], and PTPRO at this stage is only expressed in 10% of TrkC⁺ neurons. At birth PTPRO is expressed in 35% of neurons, and the majority of parvalbumin⁺ fibers (a subpopulation of TrkC⁺ axons) do not reach their synaptic target: motor neuron cell bodies. Characterizing PTPRO expression in the different subsets of TrkC⁺ neurons would better clarify its role in proprioceptive fiber growth and guidance. Moreover, as described in the case of nociceptive fibers, PTPRO is also expressed on the synaptic target of proprioceptive axons (Figure 2-2). Conditional ablation of PTPRO in sensory axons versus their target fields should resolve whether PTPRO acts cell-autonomously regulating receptor kinase activity or non-cell autonomously as a ligand.

PTPRO acting as a target-derived ligand represents an intriguing possibility. This idea is supported by a study from 2001, showing that the PTPRO ectodomain acts as a chemorepulsive cue for chick RGC axons [250]. However, to date there is no evidence for such a function *in vivo*. Challenging DRG axons with the PTPRO ectodomain, either in axon turning or stripe assays, would shed light on PTPRO's chemorepellent properties towards nociceptive and proprioceptive fibers.

3.1.3. PTPRO as a potential therapeutic target

The activation of RTKs is a spatially and temporally well controlled process to avoid aberrant cellular behavior and diseases. The de-regulation of half of the RTK families has been associated with human tumors [251]. To ensure the fidelity of signaling, cells have evolved several regulatory mechanisms including ligand sequestration, receptor dephosphorylation, activation of inhibitory proteins or inhibitory feedback loops, receptor

endocytosis and degradation. Although several regulatory proteins have been identified *in vitro*, thus far their role *in vivo* has not been completely clarified.

To date, there is growing evidence supporting a role for PTPRO as a tumor suppressor, since its de-regulation has been associated with several human tumors [252-255]. Here, I presented evidence that PTPRO is expressed in the nervous system and that in *PTPRO*^{-/-} mice de-regulation of TrkB and Ret signaling causes excessive outgrowth and branching of trigeminal neurons *in vitro* and *in vivo*. In the future, it would be interesting to analyze the effects of PTPRO in the physiology and disease of other populations of neurons, where TrkB and Ret play a key role in development or maintenance. PTPRO is expressed in the substantia nigra of adult mice (Allen Brain Atlas staining), where Ret has been shown to prevent neurodegeneration in genetic or toxin-induced Parkinson models [79, 256, 257]. It would be intriguing to analyze if genetic ablation or pharmaceutical inhibition of PTPRO potentiates Ret signaling and prevent dopaminergic neuron degeneration. Since PTPRO is expressed in the adult hippocampus [235] it would be interesting to analyze PTPRO and TrkB interaction in synaptic plasticity. *TrkB*^{-/-} mice have impaired LTP, and a point mutation abolishing the PLC γ docking site on TrkB specifically affects hippocampal plasticity [19, 53]. Since in *PTPRO* knockout mice TrkB signaling is upregulated, it is possible that these mice have an enhanced LTP.

3.2. How does receptor cleavage regulate axon guidance decisions?

Work over the last decade has unraveled an important role for proteolytic processing of RTKs in neuronal development. Interestingly, cleavage can play versatile, and sometimes opposite functions. Cleavage can either inhibit or activate receptor signaling.

At the spinal cord midline the protease calpain is required to silence PlexinA1, by reducing its expression levels [93, 226]. By contrast, in *Drosophila* the protease kuzbanian is required to positively enhance Slit/Robo signaling [258, 259]. Cleavage can differentially regulate not only receptor activation, but also cell-cell contact. In the case of Eph/ephrin signaling cleavage has been proposed as a way to disrupt the initial adhesion and turn it into cell-cell repulsion [110, 123]. By contrast, work in *Drosophila* has shown that metalloproteases promote axon fasciculation, by enhancing adhesive interactions [260]. In summary, to date, it seems that receptor cleavage can mediate opposing functions in different neuronal populations and at different developmental stages. Considering the comprehensive literature on receptor cleavage in cultured cells it was surprising to learn that there are no reports addressing the question on how cleavage regulates the function of a single receptor *in vivo*. Genetic removal of metalloproteases or presenilin genes is likely to affect more than one receptor, and the resulting phenotypes can never be associated with the inhibition of the processing of a single protein. For example, a study from Sam Pfaff's group showed the requirement of presenilin1 in motor axon guidance [261]. In mammals, there are two highly homologous presenilin genes, presenilin-1 (PS1) and presenilin-2 (PS2) [262]. Two of the better known substrates are Notch and amyloid precursor protein (APP), but there are also several axon guidance molecules, including DCC and EphA4. If γ -secretase activity is impaired, DCC intracellular fragment (DCC-ICD) rapidly accumulates and enhances neurite outgrowth in cultured cells [263, 264]. Interestingly, in a mouse mutant called *Columbus*, identified by a ENU mutagenesis screen, motor axons do not leave the spinal cord through the ventral roots but converge towards the floor plate [261]. The mutation in *Columbus* mice

affects presenilin activity and therefore DCC processing. Normally, motor neurons are not attracted by Netrin1 since Robo interacts with DCC, silencing the receptor and preventing attraction towards the floor plate. In *Columbus* or *Presenilin1*^{-/-} mice, DCC-ICD accumulates in motor neurons and prevents Robo interaction with DCC, making motor axons inappropriately attracted to Netrin1, which is expressed at the floor plate [261]. Although this study characterized in much detail the role of a protease in axon guidance, it does not take into account the effects of presenilin1 removal on all the other potential substrates. A test of the proposed model would be the generation of a DCC cleavage-resistant knock-in mouse. Difficulties in generating such a knock-in mouse arise from the fact that even once the cleavage sites have been identified, deleting or mutating them is often not sufficient to inhibit receptor shedding. The *EphA4*^{CR} represents the first example of a knock-in mouse carrying a mutation in a guidance receptor that completely prevents its cleavage. By Western Blot and immunostaining, I demonstrated that inhibiting EphA4 shedding is sufficient to up-regulate EphA4 full-length expression *in vivo* in several tissues. Moreover, abolishing EphA4 cleavage is also sufficient to re-route LMC_L axons into the ventral mesenchyme of the hindlimb.

I showed that the extent of EphA4 cleavage differs among tissues and during development, but how this is achieved and why cleavage is required only for some EphA4-mediated cellular processes remain unanswered questions. Identifying the molecules involved in EphA4 cleavage, e.g. metalloproteases, would reveal new players in the regulation of LMC axon guidance. Once this analysis will be completely and the underlying mechanism discovered (see below), the results from this knock-in mouse will

provide a significant contribution to our understanding of receptor shedding in development.

3.2.1. Potential molecular mechanisms leading to LMC_L misguidance in EphA4^{CR/CR} embryos

EphA4 is expressed on the growing LMC axons and in the hindlimb mesenchyme. Although I showed the requirement of EphA4 cleavage at the sciatic plexus choice point, further experiments are required to unravel the molecular mechanisms. There are three possible scenarios: 1) EphA4 forward signaling is impaired, 2) EphA4 up-regulation in the hindlimb mesenchyme initiates aberrant ephrinA reverse signaling 3) EphA4 up-regulation in the hindlimb masks ephrinAs *in cis* (Figure 3-2).

Cleavage could be required on the axons to achieve cell-cell repulsion. LMC_L axons express high levels of EphA4, and upon entering the ventral mesenchyme are repelled by ephrinA2 and ephrinA5 [187, 188, 196]. Inhibiting EphA4 cleavage might abolish the ability of LMC_L axons to leave the ventral mesenchyme, because they could be unable to switch from the initial adhesion to repulsion (Figure 3-2). The easiest explanation is that in EphA4^{CR/CR} mice, axons remain “glued” to the ephrinA-expressing mesenchyme. However, to compensate for the absence of cleavage, other repulsive mechanisms, such as bi-directional endocytosis, could be activated *in vivo*. In support of this theory, HeLa cells transfected with EphA4^{CR} displayed a higher rate of reverse-endocytosis when compared to controls. Another possibility is that EphA4 signaling is affected by the lack of cleavage. EphA4^{CR} cannot generate the EphA4-ICD and EphA4-ECD fragments, and it has been shown that the EphA4-ICD specifically enhances Rac1 activation [192]. Rac1-activation triggers Eph-dependent growth cone collapse [102, 265, 266]. Therefore,

it is possible that in the absence of the EphA4-ICD, Rac1 activation is reduced, and cell-cell repulsion could be impaired.

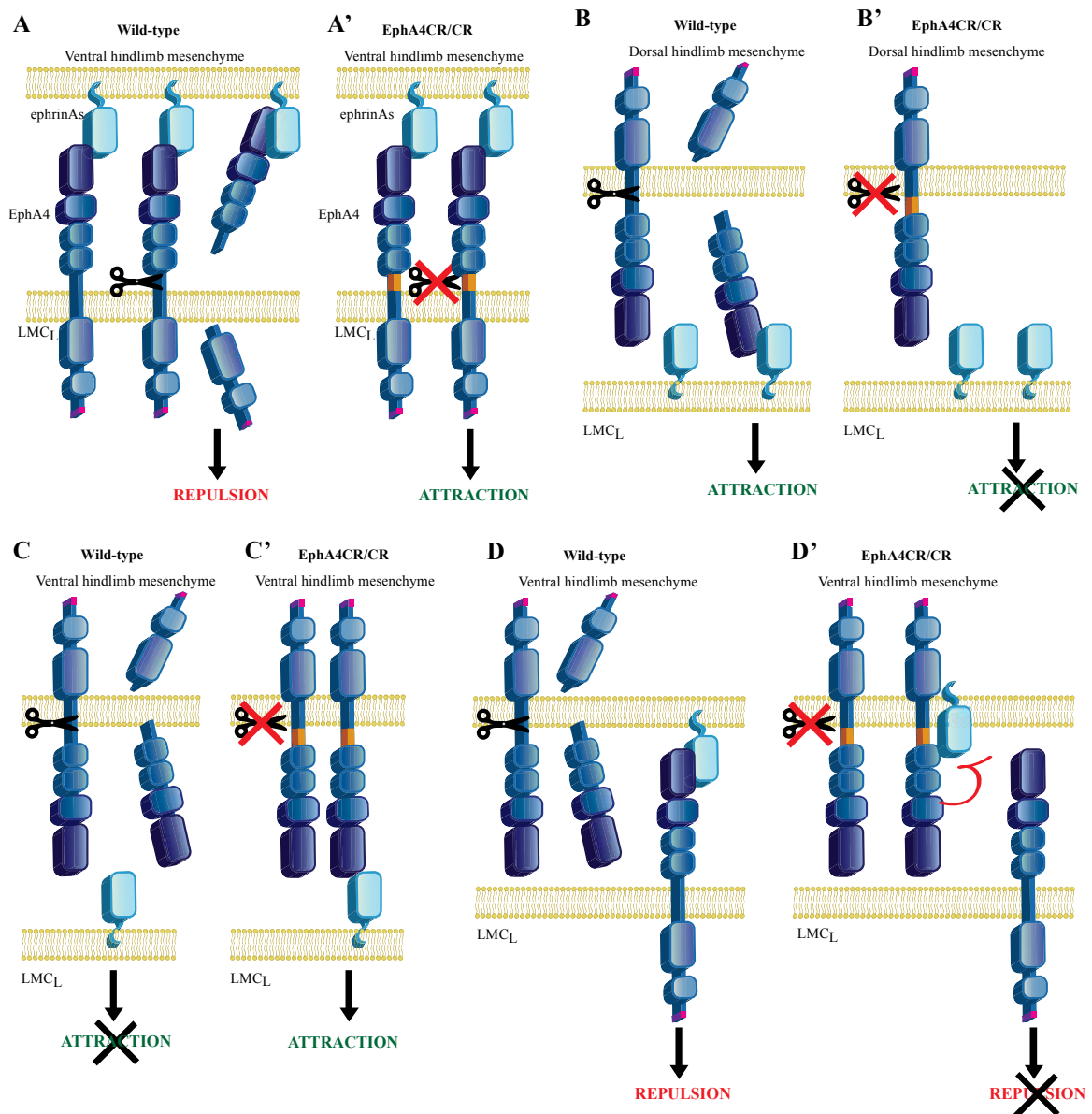


Figure 3-2. Hypothetical molecular mechanisms leading to LMC_L misguidance in *EphA4^{CR/CR}* mice

(A,A') EphA4 cleavage is necessary to trigger repulsion. If EphA4 expressed on LMC_L axons is not cleaved, these axons are no longer repelled by ephrinA-expressing ventral mesenchyme. (B,B') EphA4 shed ectodomain acts as a chemoattractant. If EphA4 expressed on the dorsal mesenchyme is not shed, it is unable to bind to ephrinAs, expressed on LMC_L axons, and initiate reverse signaling. (C-D') EphA4 cleavage reduces EphA4 expression in the ventral mesenchyme (C). In *EphA4^{CR/CR}* embryos EphA4 expression is up-regulated in the ventral mesenchyme, and attracts ephrinAs-expressing LMC_L axons (C'). EphA4 cleavage reduces EphA4 expression in the ventral mesenchyme and prevents *cis*-interactions with ephrinAs (D). In *EphA4^{CR/CR}* embryos, EphA4 full-length protein over-expression in the ventral mesenchyme masks ephrinAs. The increased *cis*-interactions reduce the availability of mesenchymal ephrinAs for *trans*-interactions with EphA4-expressing LMC_L axons, thus impairing repulsion (D').

The generation of a transgenic mouse expressing the EphA4-ICD in an inducible manner could clarify this mechanistic issue. This hypothetical lack of EphA4-mediated repulsion raises the question of whether axons would stall in the ephrinA-expressing mesenchyme or continue accumulating errors at secondary choice points. Staining of whole-mount *Hb9-GFP*⁺, *EphA4*^{CR/CR} embryos to selectively visualize motor axons at different developmental stages would provide more insights.

The second scenario is that cleavage is required for ephrinA reverse signaling. On one hand it is possible that EphA4 has to be shed to act as a chemo-attractant for ephrinA-expressing LMC_L axons. Inhibiting the cleavage could prevent the chemo-attraction in the dorsal mesenchyme and, thus re-route LMC_L axons in the ventral shank. On the other hand, the increase in EphA4 full-length protein in the *EphA4*^{CR/CR} ventral mesenchyme might erroneously attract LMC_L axons (Figure 3-2). *In vivo* it is very difficult to discriminate between these two scenarios, however, genetic evidence hints at the second hypothesis. Genetic ablation of EphA4 in the hindlimb is not sufficient to cause a phenotype, whereas EphA4 over-expression in the chick ventral hindlimb is sufficient to re-route 15% of LMC_L neurons [191]. Moreover, in *EphA4*^{CR/CR} mice the aAC tract develops normally, suggesting that the ability of the receptor to mediate reverse signaling is not affected. Over-expressing EphA4^{CR} in the ventral mesenchyme would unequivocally clarify whether ectodomain shedding is a requirement for the protein to act as a chemoattractant.

Finally, the observed phenotype could be due to the *cis*-interaction of EphA4 and ephrinAs in the ventral mesenchyme. Up-regulation of EphA4 expression in the *EphA4*^{CR/CR} hindlimb could favor binding to coexpressed ephrinAs, thus limiting ligand

availability for *trans*-interactions. This reduced propensity for interacting with EphA4 *in trans* would enable EphA4-expressing axons to grow into the ventral mesenchyme. If this is the case, it would be possible to observe a significant difference in the amount of free ephrinAs detected by EphA4-Fc overlay, as done in the paper from Dudanova *et al.* [191]. Cross-sections of the hindlimb could be incubated with pre-clustered EphA4 protein that should bind to free ephrinAs (not bound *in cis*), and then stained using a fluorescent antibody raised against the Fc region.

In conclusion, further *in vitro* and *in vivo* experiments are required to shed light on the molecular mechanisms underlying LMC_L misguidance. However, the above described scenarios are not mutually exclusive; indeed, it is possible that the phenotype is due to the combination of two or more of them.

3.2.2. What triggers EphA4 cleavage?

Interestingly, EphA4 seems to have a different proteolytic regulation compared to EphB2. While EphB2 shedding is dependent on both ligand stimulation and calcium influx, EphA4 seems to be dependent on expression levels and neuronal activity [122, 192, 228]. Motor neuron guidance and spinal circuit formation are dependent on electrical activity, at all stages of development [267]. How activity shapes the circuits and the connections is not yet known, however it has been shown that reduction in the frequency *in ovo* causes misguidance of LMC axons in the hindlimb [268]. One of the suggested mechanisms is that reducing the neuronal firing frequency leads to down-regulation of EphA4 and EphB1 expression on LMC axons. However, an increase in the frequency, although sufficient to impair the guidance of some motor pools, has no effect on the level of EphA4 [268]. To date the molecular mechanisms by which activity

instructs Eph expression are unknown. Activity-dependent expression of Eph receptor is independent of Islet1 and Lim1, but may be dependent on proteins like c-Jun and MEK/ERK [268-271]. In addition to regulating Eph receptor expression, neuronal activity could also modulate downstream signaling, possibly by controlling cyclic nucleotide dynamics, i.e. cAMP. *In vitro*, growth cone collapse of RGC axons stimulated with ephrinA5 is inhibited when activity is acutely blocked, and rescued by the induction of cAMP oscillations [272].

In summary, two models have been proposed by which activity regulates Eph/ephrin signal transduction: regulation of receptor expression and modulation of the signaling cascade. Interestingly, EphA4 cleavage could be the molecular mechanism to achieve both types of regulation. Abolishing cleavage is sufficient to increase EphA4 expression and in hippocampal neurons, the EphA4-ICD can initiate an independent signaling cascade [192]. However, further experiments are required to show that cleavage is the mechanism by which electrical activity instructs EphA4 signaling. A key experiment would be to assess whether in *EphA4^{CR/CR}* embryos a reduction in the frequency is still able to down-regulate the expression levels of the receptor.

3.2.3. EphA4 cleavage in neurodegenerative diseases

EphA4 is cleaved consecutively by metalloproteases and γ -secretase. The latter is the enzyme that cleaves APP to generate A β -fragments. In Alzheimer's mouse models and patients, the generation of A β -oligomers leads to cognitive impairment [273, 274]. EphA4 cleavage by γ -secretase is dependent on synaptic activity and generates the EphA4-ICD, which does not translocate to the nucleus but stays in the cytosol to promote Rac1 activation [192]. Over-expressing the EphA4-ICD in hippocampal neurons

potentiates the Rac1 pathway and induces the formation of dendritic spines [192]. Interestingly, when EphA4 is co-transfected in presenilin knockout cells, with presenilin1 carrying Alzheimer's disease-related familial mutations, the generation of the EphA4-ICD is severely impaired [192]. This would suggest that the synaptic failure observed in the Alzheimer's mouse model could be due to the reduced generation of the EphA4-ICD, which would lead to a decrease in the formation of dendritic spines. Interestingly, two downstream effectors of Rac1, PAK1 and cofilin, seem also to be altered in Alzheimer's disease patients and mouse models. PAK1 is less active and cofilin forms pathological aggregates, consistent with the idea that impairing EphA4 cleavage may negatively regulate the Rac1 pathway [275]. Crossing *EphA4^{CR/CR}* mice with an Alzheimer mouse model would unravel whether inhibiting the generation of the EphA4-ICD worsens the disease.

Moreover, as described previously EphA4 and ephrinA3 are required for modulation of hippocampal LTP, a critical component of the cellular mechanisms underlying certain aspects of learning and memory [276]. ephrinA3, expressed in astrocytes, upon binding to EphA4, expressed in post-synaptic CA1 neurons, regulates the levels of glial glutamate transporters. Impairing ephrinA3 reverse signaling leads to the up-regulation of glial glutamate transporters and to defects in LTP. *ephrinA3^{-/-}* mice perform abnormally in behavioral tasks requiring the hippocampus, implying that abundance of glial glutamate transport and regulation of synaptic plasticity could be essential for certain forms of hippocampal learning [276]. Several neurological and neurodegenerative diseases, such as epilepsy and amyotrophic lateral sclerosis (ALS), are correlated with defects in the glial glutamate transporters [277, 278]. Since EphA4 has been shown to be cleaved in

hippocampal neurons, in response to change in electrical activity, it would be interesting to analyze LTP and glial glutamate transporter levels in *EphA4*^{CR/CR} mice. If reverse signaling is impaired in these mice, then this mutation would be sufficient to phenocopy EphA4 and ephrinA3 knockouts. If abolishing cleavage leads to an up-regulation of EphA4 and enhancement of reverse signaling, the phenotype would be similar to that which has been observed in mice over-expressing ephrinA3 in glia [158].

3.3. Guidance cue integration

Axons, while navigating towards their final target, are challenged by multiple cues that can act either independently or synergistically. Two cues are defined as additive, if the net effect of their cooperation is the sum of the effects they generate when acting singularly. If two cues trigger a final effect bigger or smaller than the effects they generate separately, they are defined as non-additive. Non-additive effects are generally due to receptor or ligand cross-talk.

3.3.1. Additive and non-additive effects of guidance cues

The spinal cord midline represents a nice model system to analyze how multiple cues are integrated by growth cones of commissural axons. Upon crossing the midline multiple repulsive cues act simultaneously to drive the axons away from the midline, and removing any of these proteins results in the same stalling or ipsilateral recrossing phenotype [226, 230]. Conversely, Netrin/DCC and Slit/Robo signaling cross-talk and cooperate in a non-additive manner. Upon crossing the midline, the activation of the Slit/Robo signaling pathway, on one hand promotes repulsion away from the midline, and on the other hand silences netrin-mediated attraction to the midline [233].

In my thesis, I presented data in a different model system, the hindlimb where Ret and EphA4 act in an additive manner. Moreover, this represents a remarkable example, since in this case, the two cues have opposing effects on the growth cone. Ret promotes attraction towards the GDNF source, whereas EphA4 mediates repulsion from the ephrinA-expressing mesenchyme. In addition, our work combined with what has been reported by Kramer *et al.* [196] provided evidence for an additive effect of these two cues *in vivo* and *in vitro*. *In vivo* the Ret and EphA4 double knockout has a more severe phenotype than the single knockout, and *in vitro* stimulation with an opposing gradient of ephrinA5 and GDNF has a net effect comparable to the sum of the effects of the two molecules applied individually.

Interestingly, GDNF cooperates additively with ephrinAs, when ephrinAs act as ligands. But GDNF acts synergistically (non-additively) when ephrinAs act as receptors [279]. To attract LMC_L axons in the dorsal mesenchyme, both GDNF and EphAs signal via Ret. However, GDNF binds to a receptor complex, formed by Ret and GFR α 1, and EphAs to a complex, formed by Ret and ephrinAs [279]. When applied in combination with EphAs, GDNF strengthens their growth-promoting activity [279]. LMC axons are not responsive to lower doses (subthreshold doses) of GDNF and EphAs applied individually, but show a robust turning response to the two ligands when applied together [279]. Thus, Ret acts as a coincidence detector, which, when activated by both EphAs and GDNF, ensures a stronger response of LMC_L axons [279].

4. Materials and Methods

4.1. Chemicals and drugs

Chemicals were purchased from Millipore, Merck, Roth and Sigma. Enzymes and relative buffers were purchased from New England Biolabs (NEB) or Roche. Kits for plasmid and PCR purification and gel-extraction were purchased from Qiagen. All water solutions were filtered using the Milli-Q-Water System (Millipore).

4.2. Reagents

4.2.1. Plasmids

Insert	Species	Backbone	Use	Reference
EphA4-wt Flag	Mouse	p3XFlag-CMV	Mammalian expression	Sónia Paixão
EphA4ΔN Flag	Mouse	p3XFlag-CMV	Mammalian expression	Sónia Paixão
EphA4ΔC-GFP Flag	Mouse	p3XFlag-CMV	Mammalian expression	Sónia Paixão
EphA4ΔLBD Flag	Mouse	p3XFlag-CMV	Mammalian expression	Sónia Paixão
EphA4ΔFN3 Flag	Mouse	p3XFlag-CMV	Mammalian expression	Sónia Paixão
EphA4Δ10 Flag	Mouse	p3XFlag-CMV	Mammalian expression	
EphA4Δ2 Flag	Mouse	p3XFlag-CMV	Mammalian expression	
EphA4Δ4 Flag	Mouse	p3XFlag-CMV	Mammalian expression	
EphA4Δ6 Flag	Mouse	p3XFlag-CMV	Mammalian expression	
EphA4Δ8 Flag	Mouse	p3XFlag-CMV	Mammalian expression	
EphA4 ^{CR} Flag	Mouse	p3XFlag-CMV	Mammalian expression	
EphA4 mCherry	Mouse	pcDNA3.1	Mammalian expression	Irina Dudanova

EphA3 Flag	Mouse	pCMV3-3xFlag	Mammalian expression	Uwe Drescher
Ret51wt	Human	pcDNA3.1	Mammalian expression	Carlos Ibañez
TrkB	Mouse	pMEXneo	Mammalian expression	Rüdiger Klein
PTPRO-Flag	Mouse	pFlag-CMV5	Mammalian expression	Eek-hoon Jho
PTPRO-Flag	Chick	p3XFlag-CMV14	Mammalian expression	John Bixby
GFP		pcDNA3.1	Mammalian expression	
mCherry		pcDNA3.1	Mammalian expression	
EphA4 ^{CR}	Mouse	TOPO-IIA	Subcloning	
EphA4 ^{CR}	Mouse	pKSII+	Targeting vector	
EphB2	Mouse	pcDNA3.1	Mammalian expression	Jenny Köhler
EphA4 3' probe		TOPO-IIA	Southern Blot probe 3'	Christine Hassler
EphA4 5' probe		TOPO-IIA	Southern Blot probe 3'	Christine Hassler

4.2.2. Oligonucleotides

Oligonucleotides were purchased from MWG as HPSF purified.

4.2.3. Cloning primers

Name	Sequence
A4FlagΔ2-Fw	5'-CGCATCATTGGCGATCTCGAGAACTCCACT-3'
A4FlagΔ2-Rev	5'-GCCAATGATGCGGGAAGGCACTGTATTAGT-3'
A4FlagΔ4-Fw	5'-CCTTCCCGCATCATTGGCGAGAACTCCACT-3'
A4FlagΔ6-Fw	5'-GGAAGTCACTACTAGTCCAGTGCCTTCCCG-3'
A4FlagΔ6-Rev	5'-AGTAGTGACTTCCAGGGGCTCGCTGAAGTC-3'

A4Flag Δ 8-Fw	5'-GTCACTACTAGCCCAGACTCTTCCCGCATC-3'
A4CR-Fw	5'-CTACTAGCCCAGACTCTTTCAGCATCTCTGGC-3'
A4CR-Rev	5'-AGAGTCTGGGCTAGTAGTGACTTCCAGGGG-3'
A4mCherry Δ 2-Fw	5'-GTCGACGTCCTGCTGGTCTCCGTCTCTG-3'
A4mCherry Δ 2-Rev	5'-GGCACTGTATTAGTCGACAGTAGTGACTTCC-3'

4.2.4. Genotyping primers

Name	Sequence
PTPROwt-Fw	5' AAA CCT TAA ACT CCT GAT CCT CCT GCC TCC 3'
PTPROko-Fw	5' GCC TTC TAT CGC CTT CTT GAC GAG TTC TTC 3'
PTPRO-Rev	5' CAC TGA ATC AAA ATG TCC CAC CCA TGT TTC 3'
Retgeno5	5'CCA ACA GTA GCC TCT GTG TAA CCC C 3'
Retgeno7	5'GCA GTC TCT CCA TGG ACA TGG TAG 3'
Retgeno6	5'CGA GTA GAG AAT GGA CTG CCA TCT CCC 3'
Ret3E	5' ATG AGC CTA TGG GGG GGT GGG CAC 3'
A4WT-Fw	5' CAAGCCGGCTGGGATCTAAGTGCCTGTTAGC 3'
A4WT-Rev	5'ACCGTTGCAAATCTAGCCAGT 3'
A4KO-Fw	5' GACTCTAGAGGATCCACTAGTGTCGA 3'
A4KO-Rev	5'-TTTTCTGCCCTCTTTAAGCAAGGATCAAGC 3'
A4KIGG-Fw	5' GCCCAGACTCTTTCAGCATCTCTGGCGAG 3'
A4KIGG-Rev	5' GCCAGCTTTCAGAGTCTTGATGGCCACAC 3'
A4wtKI-Fw	5' GACTCTAGAGGATCCACTAGTGTCGA 3'
A4wtKI-Rev	5' TTTTCTGCCCTCTTTAAGCAAGGATCAAGC 3'
GFP-F	5'GCA CGA CTT CTT CAA GTC CGC CAT 3'

GFP-R	5`GCG GAT CTT GAA GTT CAC CTT GAT 3`
GDNF wt – Fw	5`TCT GCC TCC GCC ATC TTG GTC CTT ATC 3`
GDNF ko – Fw	5`CAG ATA AAC AAG CGG CAG CGC TTC C 3`
GDNF - Rev	5`CGC ATC GTA ACC GTG CAT CTG CCA GTT TGA 3`

4.2.5. Primary antibodies

Antibody	Species	Company	Dilution	Application
EphA4S20	Rabbit	Sigma	1:100	WB, IF
EphA4SEK	Mouse	Sigma	1:1000	WB
EphA4-1383	Mouse	Homemade	1:1000	IP
EphA4-Zymed	Mouse	Zymed	1:1000	WB, IP
Ret	Goat	Fitzgerald	1:1000	WB, IP
Ret	Goat	R&D	1:100	IF
TrkA	Rabbit	Millipore	1:500	WB, IF
TrkB	Goat	R&D	1:500	WB, IP, IF
TrkC	Goat	R&D	1:500	IF
NeuN	Mouse	Millipore	1:500	IF
Islet1	Mouse	DHSB, clone	1:50	IF
Lim-1	Rabbit	Homemade, gift from A. Huber	1:1000	IF
PTPRO	Rat	Homemade, gift from T. Matosaki	1:200	IF
Flag	Rabbit	Sigma	1:1000	WB, IF
Tubulin	Mouse	Sigma	1:20000	WB
Tuj1	Mouse	Covalence	1:500	IF

NF-160	Mouse	Sigma	1:300 or 1:500	Whole-mount staining, IF
FRS2	Rabbit	Santa Cruz	1:1000	WB
phosphotyrosine	Mouse	Upstate	1:500, 1:1000	IF, WB
Phalloidin-594		Molecular Probes	1:200	IF

4.2.6. Secondary antibodies

Antibody	Species	Company	Dilution	Application
Rabbit-cy2	Donkey	Jackson Immunoresearch	1:200	IF
Rabbit-cy3	Donkey	Jackson Immunoresearch	1:200	IF
Rabbit-cy5	Donkey	Jackson Immunoresearch	1:200	IF
Mouse-cy2	Donkey	Jackson Immunoresearch	1:200	IF
Mouse-cy3	Donkey	Jackson Immunoresearch	1:200	IF
Mouse-cy5	Donkey	Jackson Immunoresearch	1:200	IF
Goat-cy2	Donkey	Jackson Immunoresearch	1:200	IF
Goat-cy3	Donkey	Jackson Immunoresearch	1:200	IF
Goat-cy5	Donkey	Jackson Immunoresearch	1:200	IF
Mouse-HRP	Sheep	GE Healthcare	1:5000	WB
Rabbit-HRP	Donkey	GE Healthcare	1:5000	WB
Goat-HRP	Donkey	DAKO	1:5000	WB

4.2.7. Cell lines

Hela: Human epithelial adenocarcinoma cell line.

HEK293: Human embryonic kidney cell line.

SKN-TG2: Human neuroblastoma cell line expressing Histone2B-tagged with RFP.
Generated by Dr. Thomas Gaitanos.

4.2.8. Media

4.2.8.1. Luria-Bertani (LB) medium

Bacto-Tryptone 10g

Bacto-Yeast extract 5g

NaCl 5g

Distilled water up to 1L.

Solution was prepared, pH was adjusted to 7.5, autoclaved and stored at RT.

4.2.8.2. LB plates

15 g of Bacto Agar was dissolved in 1 L of LB media and autoclaved. After cooling down, antibiotics were added (Ampicillin 100mg/ml or Kanamycin monosulfate 50mg/ml), solution was poured in 10 cm dishes, and stored at 4°C.

4.2.8.3. Cell culture media

Hela and HEK293: DMEM, 10% FBS (1% FBS for starving medium), 1% Glutamine, 1% Penicillin-Streptomycin

SK-N-TG2: OptiMEM with Glutamax, 10% FBS, 1% Penicillin-Streptomycin, 1% zeocin

ES cells: DMEM+HEPES, 1% Pyruvate, 1% Penicillin-Streptomycin, 1% Non-essential amino acids, 1% nucleosides, 0.2% β -mercaptoethanol, 15% fetal bovine serum, 1000 units LIF.

4.2.9. Primary culture reagents

BSA 4% (w/v) in L15:

20 g of BSA was dissolved in 500 ml of L15 medium. Solution was then dialysed against PBS, using Spectra/Por membranes (MWCO: 25 000, Spectrum) overnight at RT. After washing with water membranes were dialysed against L15 medium. After 3 days, the solution was filtered (22 μ m) and stored at -20°C.

Dnase I 1 mg/ml in L15, stored at -20°C.

Glucose 72 mg/ml in L15; filtered and stored at -20°C.

Poly-D,L-ornithine 3 mg/ml in water; stored at -20°C.

Glutamate 25 mM in L15; stored at -20°C.

2-mercaptoethanol 25 mM in L15; stored at -20°C.

Poly-D-Lysine 1 mg/ml in Borate Buffer (Boric Acid 1.24g, 1.9g Sodium Borate in 400ml of H₂O pH=8.5); sterilized by filtration. Prepared fresh each time.

Papain 20 mg/ml in PBS, stored at -20°C.

Trypsin inhibitor 10 mg/ml in dissociation media, filtrate and pre-warm at 37°C.

4.2.10. Primary culture media

Complete Neurobasal medium; prepared freshly (50 ml)

NeuroBasal™ (Invitrogen) 47.5 ml

Glutamine 125 µl

Glutamate 50 µl

β-Mercaptoethanol 50 µl

Horse serum 500 µl

B27 supplement 500 µl

MN culture medium 500 ml (modified from Garces *et al.* 2000, J. Neurosci. 20: 4992)

Neurobasal medium 450 ml

B-27 supplement to 1x from 50x stock

L-Glutamate 0.5 mM

L-Glutamine 25 mM

Penicillin-Streptomycin to 1x from 100x stock

Dissociation medium

HBSS 500 ml

HEPES (pH 7.5) 3.5 ml
1 M MgCl 5 ml
Penicillin-Streptomycin to 1x from 100x stock

4.2.11. Buffers and Solutions

50x TAE

2 M Tris acetate
50 mM EDTA

Gel loading buffer

Glycerol 25 ml
50x TAE 1 ml
Orange G 0.1 g
H₂O 24 ml

Lysis buffer (Cell lysate for protein extraction)

50 mM Tris pH 7.5
150 mM NaCl
50 mM EDTA
1% Triton
Distilled water.

Stored at 4°C. Before use, 1 tablet of Protease Inhibitor (Roche) was added to 50 ml of Buffer and 1 tablet of PhosphoSTOP (Roche) to 10 ml of Buffer.

SDS PAGE separating gel 7.5% (10 ml)

H₂O 4.85 ml
1.5M Tris pH 8.8, 0.4% SDS 2.6 ml
30% (w/v) Acrylamide : 0.8% (w/v) Bis-Acrylamide 2.5 ml
10% APS 50 µl
TEMED 5 µl

SDS PAGE stacking gel 4% (5 ml)

H₂O 3.05 ml

1.5M Tris pH 6.8, 0.4% SDS 1.3 ml

30% (w/v) Acrylamide : 0.8% (w/v) Bis-Acrylamide 0.65 ml

10% APS 50 µl

TEMED 5 µl

6x Sample buffer for reducing conditions

12% SDS

300 mM Tris-HCl, pH 6.8

600 mM DTT

0.6% BPB

60% Glycerol

Distilled water.

Stored at -20°C.

5x Electrophoresis buffer

Tris base 154.5 g

Glycine 721 g

SDS 50 g

Distilled water was added to 10 L. Stored at RT.

Protein transfer buffer

Tris base 3.03 g

Glycine 14.4 g

Methanol 200 ml

Approximately 650 ml of distilled water were added. Mixed to dissolve and made up to a final volume of 1 L. Stored at 4°C.

Sodium phosphate buffer, pH 7.2

1M Na₂HPO₄ 60.5 g

1M NaH₂PO₄ 31.6 g

2% SDS

Distilled water was added to 1 L. Stored at RT.

PBS-Tween (PBS-T)

1x PBS

0.1% Tween[®] 20

Stored at RT.

BABB 100%

1 part Benzyl alcohol

2 parts Benzyl benzoate

Protected from light and stored at RT.

BABB 50%

50% BABB

50% MetOH

Protected from light and stored at RT.

Blocking solution

0.2% Gelatine

0.5% Tritonx100

50% NCS

in PBS.

PGT and TGT buffer

0.2% Gelatine

0.5% Tritonx100

in PBS or TBS, respectively.

Dextrantetramethylrhodamine 3000MW, lysine fixable 20 mg/ml in PBS (Molecular Probes)

Lysis buffer (Cell lysate for DNA extraction)

10mM Tris pH 8.0

10mM NaCl

10mM EDTA

0.1% SDS

0.2-0.4mg/ml Proteinase K

0.1mg/ml RNaseA

Distilled water

TNE

100mM Tris pH 8

5mM EDTA

200mM NaCl

Distilled water.

Church Buffer

1% (w/v) BSA

1 mM EDTA

0.5 M Phosphate Buffer

7% (w/v) SDS

Denaturing Buffer

0.4 M NaOH

1M NaCl

Neutralizing Buffer

0.5 M Tris pH7.5

1M NaCl

Phosphate Buffer

134g Na₂HPO₄-7H₂O

4 ml of 85% H₃PO₄

H₂O to 1 L

Washing Buffer I

5% SDS

40 mM Phosphate Buffer

1mM EDTA

0.5% BSA

Washing Buffer II

1% SDS

40 mM Phosphate Buffer

1mM EDTA

4.2.12. Mouse lines

Ret knockout mice were generated by Edgar Kramer [196] and maintained in a C57Bl6/J genetic background.

EphA4 knockout mice were generated in Andrew W. Boyd laboratory [150], and maintained in a mixed 129 x C57Bl6/J genetic background.

EphA4^{CR} knock-in mice were generated by me, and maintained in a C57Bl6/J genetic background.

PGK-Cre transgenic mice were generated by Yvan Lallemand [280]. The mice were used to remove the neo-cassette in the EphA4^{CR} knock-in mice.

PTPRO knockout mice were generated by Wiggins [281], received by the John Bixby laboratory and maintained in a mixed 129/P3J x C57Bl6/J genetic background.

Hb9-GFP transgenic mice were generated by Hynek Wichterle [243] and received from the Jackson Laboratory.

GDNF knockout mice were generated by Mark Moore [67], and maintained in a C57Bl6/J genetic background

4.3. Methods

4.3.1. Molecular Biology

4.3.1.1. Preparation of plasmid DNA

Cultures of a single colony of transformed bacteria were grown overnight at 37°C in LB containing 100µg/ml ampicillin or kanamycin. Using the Qiagen Plasmid kits DNA was purified from small-scale (Miniprep) or large-scale (MaxiPrep) bacterial cultures. DNA concentration was measured using the Nanodrop.

4.3.1.2. Transformation of competent *E. coli* by electroporation

1-2 µl of plasmid DNA was added to 50µl of electrocompetent bacteria (DH5α from Invitrogen), and the mix was transferred to pre-chilled 0.2 cm cuvettes. Cuvettes were placed in the electroporation chamber and a pulse of 25 µF (2.5 k, 200 Ω) was given. After the pulse, cells were resuspended in 200µl of LB medium and placed at 37°C to recover for 45 minutes. Bacteria were then plated on LB plates with the required antibiotics for selection. Plates were incubated overnight at 37°C.

4.3.1.3. Site-direct mutagenesis

Mutations were introduced in the EphA4 over-expression construct using specific primers (mentioned in the cloning primers table, section 4.2.2.1) and high-fidelity PFU-Phusion polymerase (NEB). After the PCR reaction, the restriction enzyme DpnI was added to the reaction to digest methylated DNA (template) for 1 hour at 37°C. DNA was then purified using the PCR purification kit and transformed in DH5α bacteria. Positive

mutants were screened by digestion (since site-direct mutagenesis created new restriction sites) or sequencing.

4.3.1.4. TOPO cloning

Specific primers were used to amplify EphA4 cDNA with Pfu Turbo DNA polymerase (Invitrogen) and cloned into the pCRII TOPO vector. 4µl of linearized DNA (PCR product), 1µl of 1:4 diluted salt solution and 1µl of TOPO vector were mixed and incubated at RT for 15 min. DH5α cells were transformed with this mix. Bacterial clones were screened by digestion to determine the orientation of the inserted DNA.

4.3.1.5. Tail DNA preparation and genotyping using PCR

To genotype mice or embryos, DNA was extracted from tail, forelimb or yolk sac biopsies. Tissues were incubated with 100µl of 50mM NaOH for 45 minutes at 95°C and afterward the solution was neutralized with the addition of 10µl 1.5mM Tris-HCl (pH 8.8) and stored at 4°C.

For the PCR reaction:

2µl of DNA

2.5mM dNTPs,

50mM primers

1X PCR Buffer (NEB)

0.5µl of Taq polymerase (NEB)

Distilled water to 50µl

Program	Denaturing	Denaturing	Annealing	Extension	N. cycles
Cre	94°C for 2'	94°C for 1'	67°C for 1'	72°C for 2'	40
EphA4 WT	95°C for 2'	95°C for 30''	60°C for 1'20''	72°C for 1'15''	30
EphA4 KO	95°C for 3'	94°C for 1'	65°C for 1'	72°C for 1'	38
EphA4KI-GG	95°C for 1'	95°C for 1'	60°C for 1'	72°C for 1'	38
EphA4GG	95°C for 1'	95°C for 1'	60°C for 1'	72°C for 1'	38
Ret WT	94°C for 1'	94°C for 20''	62°C for 20''	72°C for 40''	35
Ret KO	94°C for 1'	94°C for 20''		72°C for 1'	35
HB9-GFP	94°C for 1'	94°C for 1'	68°C for 1'	72°C for 1'	36
PTPRO	94°C for 2'	94°C for 30''	56°C for 45''	72°C for 45''	36
GDNF	94°C for 3'	94°C for 15''	56°C for 30''	72°C for 30''	40

4.3.1.6. Agarose gel electrophoresis

PCR or enzymatic digestion products were loaded on 1% or 2% agarose gels. Agarose was dissolved in 1X TAE and boiled. Once cooled, ethidium bromide (1:20000 Roth) was added, the solution was poured into a gel chamber, and combs were added. Combs

were removed after the gel was solidified. Gel was then placed into an electrophoresis chamber filled with 1X TAE. Samples were loaded into the wells and separated for 10-30 minutes at ~200V. DNA was then visualized under UV light using a gel documentation system (BioRad).

4.3.2. Cell culture

4.3.2.1. Propagation, thawing and freezing of mammalian cells

Hela, HEK293 or SKN cells were grown at 37°C with 5% CO₂ in appropriate growth medium. Confluent cells were washed with warm 1X PBS before splitting, and then incubated at 37°C with 1ml of Trypsine/EDTA (Invitrogen) for ~2 minutes. Fresh medium was added and cells were harvested and centrifuged at 1200 rpm for 3 minutes at RT. Supernatant was then discarded and cells were gently resuspended and seeded. Cells were frozen in 10%DMSO and 90% FBS. They were first kept at -80°C overnight and then transferred to the liquid nitrogen tank. Cells were thawed in warm medium, centrifuged at 1200 rpm for 3 minutes at RT to remove DMSO, resuspended and seeded.

4.3.2.2. Transfection of cell lines using Lipofectamine

Cells were transiently transfected using Lipofectamine2000 (Invitrogen) according to the manufacturer protocol. Briefly, Lipofectamine was mixed with DMEM in an eppendorf tube and incubated for 5 minutes at RT. DNA was then added to this mix (3 µl Lipofectamine per 1 µg DNA) and the reaction was incubated for 15 minutes at RT. The mix was then added to the cells, and medium was changed after 5-6 hours. For Hela and SKN cells, growth medium was changed to OPTIMEM Glutamax, just before transfection.

4.3.2.3. Primary culture of dissociated mouse trigeminal neurons

4-well plates were coated with poly-ornithine (diluted 1:1000 from stock) overnight at RT. Plates were then washed 3 times with water, air dried for 2 hours at RT, and incubated with 20 μ g/ml laminin for at least 3 hours at 37°C and 5% CO₂. Pregnant females were sacrificed by cervical dislocation, and uteri were removed from the abdomen. Embryos were taken out of the uteri and placed in ice-cold L15 medium (Invitrogen). Two coronal cuts were made through the head using tungsten needles, in order to dissect the region delineated by the area just above the eye and the area between the maxillary and mandibular processes. The trigeminal ganglia were then exposed by cutting in front of the hindbrain curvature and behind the eyes. Adherent mesenchymal tissues surrounding the ganglia were removed with tungsten needles and ganglia collected in L15 medium with a 1 ml pipette tip in a falcon tube. L15 medium was replaced with 1ml of HBSS (Invitrogen), and 50 μ l of trypsin were added, and ganglia were incubated for 5 minutes at 37°C. Medium was the removed and ganglia washed twice with 10ml of F12 (Invitrogen) supplemented with 10% of horse serum. Neurons were then centrifuged at 2000rpm for 2 minutes and resuspended in F12 medium supplemented with 10ng/ml NGF (R&D) or as indicated in the result section. Using a Pasteur pipette neurons were dissociated by triturating them for at least 20 times. Dissociated trigeminal neurons were then seeded onto 4-well plates and put in the incubator at 37°C and 5% CO₂. Neurons were grown for 18 hours in F12 medium supplemented with 10ng/ml NGF, and where indicated, 5ng/ml BDNF (R&D) or 5ng/ml GDNF (R&D) were added to the culture medium. Neurons were fluorescently labelled with calcein-AM (Invitrogen) and imaged using an Axiovert 200M microscope (Zeiss)

with a 10X objective. Neurite length and number of branches were quantified as described in [238]. For culture in the presence of caspase inhibitors, neurons were grown on coverslips. Coverslips were smoothed with nitric acid for 24-36 hours at RT, and then extensively washed for 2-3 days in water, dried and autoclaved. Coverslips were then coated as above described for 4-well plates. E12.5 dissociated trigeminal neurons were then seeded on the coverslips and grown for 18 hours in F12 supplemented with 10 μ M Q-VD-Oph (Calbiochem) and NGF, BDNF or GDNF as indicated. Neurons were stained with Cell Tracker Green (Invitrogen), fixed 5 minutes with 4% PFA on ice, and coverslips were mounted using Dako fluorescent medium. Images were acquired using a Zeiss epifluorescent microscope. Explant cultures of trigeminal neurons from E12.5 embryos were grown on poly-D-lysine/laminin coated coverslips for 15 hours in F12 medium supplemented with 10ng/ml NGF at 37°C and 5% CO₂.

4.3.2.4. Explant of trigeminal neurons

Lysine pre-coated coverslips (BD Bioscience) were incubated with 50 μ g/ml laminin for at least 3 hours at 37°C and 5% CO₂. Trigeminal ganglia were dissected as mentioned above and cut in 4 pieces. 2-3 trigeminal explants were placed onto the coverslips and grown in F12 medium supplemented with 10ng/ml NGF for 18 hours at 37°C and 5% CO₂.

4.3.2.5. Primary culture of dissociated mouse motor neurons

Coverslips were then coated with poly-ornithine (diluted 1:1000 in water from stock) for 30 minutes at RT, air dried for another 30 minutes and incubated with 5 μ g/ml laminin at 37°C and 5% CO₂ for at least 3 hours before seeding the neurons. Hb9-GFP⁺ E12.5 embryos were dissected in ice cold 1X HBSS. Embryos were decapitated and the spinal

cord was opened along the dorsal side along its length. The spinal cord was then separated from the embryo. Open book preparation of the spinal cord was then pinned on an agarose plate and using a fluorescent microscope (to detect Hb9-GFP expression) motor neuron were identified. The lower half of the lumbar LMC was dissected using fine scissors and a scalpel. The lower half was then cut into small pieces. Using a 1 ml pipette tip the spinal cord fragments were transferred into 1 ml of HAM-F10 (Invitrogen), later replaced with 1 ml of fresh HAM-F10 plus 10 μ l of trypsin (2.5% w/v). The mix was incubated at 37°C with frequent shaking. After 10 minutes, the supernatant was discarded and fragments were triturated in a mix of 0.8ml L15 complete medium without bicarbonate (medium M) + 100 μ l BSA (4% w/v in L15) + 100 μ l DNase (1 mg/ml in L15). After leaving the mix to settle for 2 minutes, the supernatant was collected in another tube, and the residual fragments were triturated again in a mix of 0.9 ml of L15 complete medium without bicarbonate + 100 μ l of BSA (4% w/v) + 20 μ l of DNase (1 mg/ml in L15 medium). After 2 minutes, the supernatant was again collected and transferred to the same tube as before. A 2ml BSA (4% w/v) cushion was dispensed to the bottom of the tube containing the pooled supernatants using a long Pasteur pipette. The dissociated cells were centrifuged for 5 minutes at 1500 rpm and resuspended 4 times with a 1 ml pipette tip in 1 ml of Neurobasal complete. Approximately one half of a spinal cord was seeded per coverslip. Growth factors [BDNF (1ng/ml), CNTF (10ng/ml) and GDNF (1ng/ml)] were added to NB medium just before seeding.

4.3.2.6. Explant culture of mouse motor neurons

Lysin pre-coated coverslips were coated under sterile conditions with 50 μ g/ml laminin for at least 3 hours at 37°C or alternatively overnight at 4°C. Open book

preparation of the spinal cord was done as previously described, however in this case the spinal cord fragments were smaller (around 10 per lower half of lumbar LMC). 3 to 6 explants were seeded onto coated cover slips and incubated at 37°C and 5% CO₂.

4.3.2.7. Primary culture of dissociated cortical neurons

Coverslips were coated overnight with poly-lysine at 37°C. The day after, they were washed and incubated with laminin for at least 3 hours at 37°C. Forebrain neurons were dissected from E16 embryos. Embryos were collected in HBSS, decapitated, and brains were dissected from the opened skull. Samples were placed in dissociation medium, forebrains were isolated and meninges removed. Samples were incubated at 37°C with 1mg/ml pre-activated (incubated 20 minutes at 37°C) Papain (Sigma) in HBSS for 10-15 minutes, washed 3 times at RT with 10mg/ml Trypsin inhibitor solution (Roche) and then resuspended in Neurobasal medium (Invitrogen). Neurons were dissociated with a round glass Pasteur pipette, counted and plated onto coated coverslips. Cultures were incubated at 37°C and 5% CO₂ for 1 to 7 days, according to the experimental design.

4.3.3. Biochemistry

4.3.3.1. Cell lysis and immunoprecipitation of proteins

Transfected cells were washed in PBS and then incubated with Lysis Buffer for 20 minutes on ice. Lysates were then transferred in eppendorf tubes and centrifuged at 4°C for 15 minutes at 13000rpm. Spinal cords or other tissues were lysed in 100 µl of Lysis Buffer. Protein concentration was measured using the DC Protein Assay (BioRad). Equal amount of protein from different samples were incubated in a final volume of 1ml with 2 µl of the specific antibody overnight on the rotating wheel at 4°C. 40µl Protein-A coupled sepharose beads were added to each tube and incubated on the rotating wheel for two

hours at 4°C. For immunoprecipitation of proteins with a Flag-tag, lysates were added to M2-Flag beads (Sigma), already conjugated with the antibody. Supernatant was discarded and beads were then washed 3 times with Lysis Buffer. Beads were then resuspended in 25µl of 2X SDS sample buffer and boiled at 95°C for 10 minutes before loading on a 7.5% SDS-PAGE gel.

4.3.3.2. Immunoblotting

Proteins were separated by SDS-PAGE on a 7.5% gel, running at 124V for 1 hour and 30 minutes. Proteins were then transferred onto a nitrocellulose membrane (Whatman) by semi-dry blotting (10V for 2 hours). Nitrocellulose membranes were then blocked in 5% BSA in PBS (for phospho-antibodies) or in 5% Milk in PBS for at least 30 minutes at RT. Primary antibodies were applied in 1% BSA in TBS or in TBS-T (for phospho-antibodies) or in PBS overnight at 4°C while rocking on a shaker. The membranes were washed with PBS-T for 5 minutes at least 3 times before incubation with the secondary antibodies for 1 hour at RT. After at least 3 washes of 5 minutes with PBS-T, the membranes were incubated with 1 ml of ECL solution (Amersham) and exposed to X-ray films (Amersham). If subsequent detection of another protein was necessary the next antibody (raised in a different species) was applied in 0.03% Na-Azide.

4.3.4. Immunofluorescence

Hela cells or neurons grown on glass coverslips (Marienfeld) were stimulated according to experimental design, and rinsed with ice-cold PBS. Hela cells were fixed with 4% PFA/8% sucrose 20 minutes on ice, while neurons with 4% PFA for 2 minutes at RT. After rinsing with PBS, they were incubated with 50mM Ammoniumchloride for

10 minutes at RT, rinsed again and permeabilised with PBS-0.1% TritonX-100 for 5 minutes on ice. Cells were washed 3 times for 5 minutes in PBS and then incubated with blocking solution (2% BSA, 4% Donkey serum in PBS) for 30 minutes at RT. Samples were incubated with the specific primary antibodies diluted in blocking solution for 2 hours at RT, washed 3x with PBS and incubated for 1 hour at RT with secondary antibodies conjugated to fluorophores, also diluted in blocking solution. Coverslips were washed 3 times for 5 minutes at RT with PBS and incubated with a 1:10000 dilution of Cell Mask Blue in PBS for 10 minutes at RT. Coverslips were then washed in PBS and mounted using DAKO fluorescent medium or with “Antifade Prolong” mounting medium (Molecular Probes).

4.3.5. Mouse work

Cultures from Hb9-GFP⁺ embryos were done using CD1 females. Mice were genotyped using DNA from tail biopsies and ear-tagged. The morning after setting up the breeding, vaginal plugs were checked and counted as day 0.5 of pregnancy.

4.3.6. Histology

4.3.6.1. Cryostat sections

The lower half (hindlimbs+tail) of PFA fixed embryos was embedded in OCT medium (Tissue Tek) and left in dry ice for few minutes to harden. 25 µm to 40 µm sections were cut using a Leica Cryotome and collected on coated glass slides (Menzel-Gläser). Sections were left to dry for at least 2 hours at RT and later stored at -20°C.

4.3.6.2. Whole mount Neurofilament staining

E11.5 and E12.5 embryos were fixed overnight in Dent's solution (1 part DMSO; 4 parts methanol). Then, they were bleached in one part 30% H₂O₂ – two parts Dent's Solution for several hours at RT. Three washing steps (1 hour each at RT) in PBS containing 0.2% Gelatin and 1% Triton X-100 (SIGMA) were followed by incubation with the anti-neurofilament antibody (NF-160 from Sigma 1:300 in 4 parts newborn calf serum, 1 part DMSO) overnight at RT. Five washing steps in TBS containing 1% Triton X-100 and 0.2% gelatin for 1 hour each were followed by incubation with anti-mouse HRP-conjugated antibody (1:300 in 4 parts newborn calf serum, 1 part DMSO) overnight at RT. Finally, embryos were washed and incubated with diaminobenzidine working solution followed by dehydration in methanol and clearing in BABB. Images were acquired using the DC150 camera from Leica and analyzed using ImageJ or NeuronJ. The ophthalmic nerve phenotype at E11.5 was quantified as the ratio between the area of the ophthalmic nerve arbor and the area of the maxillary nerve arbor. The ophthalmic nerve arbor complexity at E12.5 was analyzed using the Sholl analysis plug-in of NeuronJ. The hindlimb phenotype at E11.5 was quantified as the ratio between the length of the tibial nerve and the length of the peroneal nerve. The bifurcation of the sciatic nerve was considered as the origin and the distal termination of each nerve was considered as the end point. The hindlimb phenotype at E12.5 was quantified as the ratio between the diameter of the tibial nerve and the diameter of the peroneal nerve.

4.3.6.3. Staining of tissue sections

E10.5, E11.5, E12.5, E15.5 embryos and newborn pups were fixed in 4% PFA for 2 hours or overnight at 4°C, and then incubated overnight in 30% sucrose at 4°C. 30 µm

cryostat sections were blocked in 4% Goat Serum, 4% Donkey Serum, 2% BSA, 0.3% triton in PBS. Primary antibodies were applied overnight in 4% Goat Serum, 4% Donkey Serum, 2% BSA, 0.1% triton at 4°C. After 3 washes of 15 minutes in PBS, sections were incubated with secondary antibodies (1:200) for 1 hour at RT. After 3 washes of 15 minutes in PBS, cryosections were mounted using Dako fluorescent medium. Images were acquired using the Axioplan epifluorescent microscope (Zeiss). For analysis of colocalization and to count neurons, images were acquired using the confocal microscope (Spinning Zeiss Axio Observer Z1 with a Yokagawa Spinning Disk Confocal Unit and a Cool SNAP HQ² CCD Camera).

4.3.6.4. Labeling of explant cultures and dissociated motor neurons

Trigeminal explants were stimulated for 30 minutes with 0.5µg/ml pre-clustered ephrinA5 or with 0.5µg/ml pre-clustered human IgG Fc-fragments as a control. Motor neuron explants were stimulated for 30 minutes with 0.1µg/ml and 0.5µg/ml pre-clustered ephrinA2/A5 (mixed 1:1), or with 0.1µg/ml and 0.5µg/ml pre-clustered ephrinB2, or with 0.1µg/ml and 0.5µg/ml pre-clustered human IgG Fc-fragments as a control. Explants were fixed twice for 30 minutes in 2% PFA-15% sucrose, blocked and permeabilised in 0.5% Triton X-100, 1% BSA in PBS and then stained using anti-Phalloidin568. Coverslips were mounted using Dako fluorescent medium and images acquired with an Axioplan epifluorescence microscope (Zeiss).

4.3.6.5. Motor neuron retrograde tracings

E12.5 embryos were eviscerated and the lower halves were kept in DMEM/F-12 medium (Invitrogen) aerated with 5% CO₂/95% O₂. The lower halves were pinned on an agarose plate and injected in the ventral or dorsal shank of the hindlimb with a solution of

6% lysine-fixable tetramethylrhodamine-dextran (MW 3000, Invitrogen) in PBS with 0.4% Triton X-100. After injection, they were left bubbling in 5% CO₂/95% O₂ for 5-6 hours at RT. They were then fixed for 1 hour at 4°C with 4% PFA, and incubated overnight in 30% sucrose at 4°C. The day after, they were washed in PBS and embedded in OCT medium.

4.3.7. Generating *EphA4*^{CR/CR} knock-in mouse

4.3.7.1. Cloning

A knock-in targeting construct for *ephA4* was generated by Klas Kullander by fusing the wild-type EphA4 cDNA in frame to exon III within the 5.5 kb long arm of the vector. At the 3' site the construct contained a poly(A) tail, a PGK-driven *neo* cassette flanked by loxP sites and a 1.2 kb short arm. *EphA4*^{CR} cDNA was cloned into this targeting vector. This construct encodes EphA4 with 15 amino acids in the extracellular juxtamembrane domain replaced by the correspondent 13 amino acids of the EphA3 sequence.

4.3.7.2. ES cells culture and DNA electroporation

ES cells were maintained in an undifferentiated status in ES cell medium and cultured them on a monolayer of feeder cells [mouse embryonic fibroblast (MEF)] on gelatinized plates. ES cells were seeded in a 10cm dish and when confluent, cells were electroporated with 35 µg of linearized target vector (linearized using NheI overnight at 37°C) by the application of a 0.24kV/375µF pulse. After electroporation cells were removed from the cuvette, diluted in 50ml of ES cell medium supplemented with 150µg/ml neomycin (G418) and seeded in five 10cm dishes, pre-coated with MEFs. After a week, cells were washed with PBS and single colonies were picked, trypsinised and seeded in a 96 well plate containing feeder cells.

4.3.7.3. DNA extraction

96 well plate: ES cells clones were grown in three 96 well plates until confluent. $\frac{3}{4}$ of the trypsinised cells were frozen down and $\frac{1}{4}$ were expanded to extract DNA. Briefly, media was removed completely and 100 μ l of Lysis Buffer were added to each well. The plate was sealed, placed in a “wet chamber” and incubated for 1 day at 55°C. DNA was then precipitated by adding 12 μ l of 8M LiCl and 110 μ l isopropanol to each well, and incubated for 2 days at 4°C. Samples were then centrifuged for 40 minutes at 4000rpm at 4°C. The supernatant was discarded and DNA was washed with 70% ethanol. DNA was then air-dried, and resuspended in 110 μ l TE (10 mM Tris, 1 mM EDTA, pH=8).

6 well plate: When cells reached high confluency, they were detached by adding 0.5 ml PBS-5 mM EDTA for 10 minutes at 37°C. Cells were harvested and centrifuged for 10 minutes at 10000rpm at RT. Supernatant was discarded, 300 μ l of TNE were added before vortexing. Then 300 μ l of TNE supplemented with 0.4% SDS and 400 μ g/ml Proteinase K were added and solution incubated overnight at 55°C. The day after, 600 μ l of isopropanol were added and samples were centrifuged at 13200 rpm for 15 minutes. Supernatant was discarded and DNA pellet washed with 70% ethanol. DNA was air-dried and resuspended in 500 μ l TE overnight at 55°C.

4.3.7.4. Southern Blot

To screen for positive clones 80ng of DNA were digested overnight with BamHI (1 μ l) at 37°C. Digestion was checked on a 1% Agarose gel and if not completed, 1 μ l of enzyme was added and reaction was carried on for one more hour at 37°C. Samples were then loaded on a 0.8% Agarose gel and run at 80-100V for 3 hours. The gel was washed twice for 20 minutes in Denaturing Buffer, while the membrane was washed in H₂O and

Denaturing Buffer for 20 minutes. DNA was transferred by capillarity onto the membrane overnight at RT. The day after, the membrane was washed twice for 20 minutes in Neutralizing Buffer, and then pre-hybridized with Church Buffer for 2 hours at 65°C. Meanwhile, the probe was labeled using an Amersham labeling kit. 50 ng of probe were denatured at 95°C for 5 minutes and then put on ice. Probe was then mixed with 5 µl of ³²P, water was added to the final volume (50 µl) and the reaction was incubated at 37°C for 30 minutes. The labeled probe was then purified by passing it through a gel separation column (Amersham). It was then added to the membrane in 20 ml of Church Buffer, and hybridization was carried overnight at 65°C. The day after, the membrane was washed 4 times for 20 minutes in Wash Buffer I, and 4 times for 20 minutes in Wash Buffer II at 65°C. The membrane was then wrapped in Saran Wrap paper and exposed for 1-5 days using a PhosphorImager.

5. Bibliography

1. Raper, J., and Mason, C. (2010). Cellular strategies of axonal pathfinding. *Cold Spring Harb Perspect Biol* 2, a001933.
2. Kolodkin, A.L., and Tessier-Lavigne, M. (2011). Mechanisms and molecules of neuronal wiring: a primer. *Cold Spring Harb Perspect Biol* 3.
3. Yu, T.W., and Bargmann, C.I. (2001). Dynamic regulation of axon guidance. *Nat Neurosci* 4 *Suppl*, 1169-1176.
4. Alberts, B. (2008). *Molecular Biology of The Cell*. Garland Science.
5. Lemmon, M.A., and Schlessinger, J. (2010). Cell signaling by receptor tyrosine kinases. *Cell* 141, 1117-1134.
6. Bibel, M., Hoppe, E., and Barde, Y.A. (1999). Biochemical and functional interactions between the neurotrophin receptors trk and p75NTR. *EMBO J* 18, 616-622.
7. Hempstead, B.L., Martin-Zanca, D., Kaplan, D.R., Parada, L.F., and Chao, M.V. (1991). High-affinity NGF binding requires coexpression of the trk proto-oncogene and the low-affinity NGF receptor. *Nature* 350, 678-683.
8. Reichardt, L.F. (2006). Neurotrophin-regulated signalling pathways. *Philos Trans R Soc Lond B Biol Sci* 361, 1545-1564.
9. Clary, D.O., and Reichardt, L.F. (1994). An alternatively spliced form of the nerve growth factor receptor TrkA confers an enhanced response to neurotrophin 3. *Proc Natl Acad Sci U S A* 91, 11133-11137.
10. Strohmaier, C., Carter, B.D., Urfer, R., Barde, Y.A., and Dechant, G. (1996). A splice variant of the neurotrophin receptor trkB with increased specificity for brain-derived neurotrophic factor. *EMBO J* 15, 3332-3337.
11. Esteban, P.F., Yoon, H.Y., Becker, J., Dorsey, S.G., Caprari, P., Palko, M.E., Coppola, V., Saragovi, H.U., Randazzo, P.A., and Tessarollo, L. (2006). A kinase-deficient TrkC receptor isoform activates Arf6-Rac1 signaling through the scaffold protein tamalin. *J Cell Biol* 173, 291-299.

12. Rose, C.R., Blum, R., Pichler, B., Lepier, A., Kafitz, K.W., and Konnerth, A. (2003). Truncated TrkB-T1 mediates neurotrophin-evoked calcium signalling in glia cells. *Nature* 426, 74-78.
13. Chao, M.V. (2003). Neurotrophins and their receptors: a convergence point for many signalling pathways. *Nat Rev Neurosci* 4, 299-309.
14. Inagaki, N., Thoenen, H., and Lindholm, D. (1995). TrkA tyrosine residues involved in NGF-induced neurite outgrowth of PC12 cells. *Eur J Neurosci* 7, 1125-1133.
15. Kao, S., Jaiswal, R.K., Kolch, W., and Landreth, G.E. (2001). Identification of the mechanisms regulating the differential activation of the mapk cascade by epidermal growth factor and nerve growth factor in PC12 cells. *J Biol Chem* 276, 18169-18177.
16. Wu, C., Lai, C.F., and Mobley, W.C. (2001). Nerve growth factor activates persistent Rap1 signaling in endosomes. *J Neurosci* 21, 5406-5416.
17. Xing, J., Kornhauser, J.M., Xia, Z., Thiele, E.A., and Greenberg, M.E. (1998). Nerve growth factor activates extracellular signal-regulated kinase and p38 mitogen-activated protein kinase pathways to stimulate CREB serine 133 phosphorylation. *Mol Cell Biol* 18, 1946-1955.
18. Medina, D.L., Sciarretta, C., Calella, A.M., Von Bohlen Und Halbach, O., Unsicker, K., and Minichiello, L. (2004). TrkB regulates neocortex formation through the Shc/PLCgamma-mediated control of neuronal migration. *EMBO J* 23, 3803-3814.
19. Minichiello, L., Calella, A.M., Medina, D.L., Bonhoeffer, T., Klein, R., and Korte, M. (2002). Mechanism of TrkB-mediated hippocampal long-term potentiation. *Neuron* 36, 121-137.
20. Minichiello, L., Casagrande, F., Tatche, R.S., Stucky, C.L., Postigo, A., Lewin, G.R., Davies, A.M., and Klein, R. (1998). Point mutation in trkB causes loss of NT4-dependent neurons without major effects on diverse BDNF responses. *Neuron* 21, 335-345.
21. MacDonald, J.I., Gryz, E.A., Kubu, C.J., Verdi, J.M., and Meakin, S.O. (2000). Direct binding of the signaling adapter protein Grb2 to the activation loop tyrosines on the nerve growth factor receptor tyrosine kinase, TrkA. *J Biol Chem* 275, 18225-18233.

22. Qian, X., Riccio, A., Zhang, Y., and Ginty, D.D. (1998). Identification and characterization of novel substrates of Trk receptors in developing neurons. *Neuron* *21*, 1017-1029.
23. Robinson, K.N., Manto, K., Buchsbaum, R.J., MacDonald, J.I., and Meakin, S.O. (2005). Neurotrophin-dependent tyrosine phosphorylation of Ras guanine-releasing factor 1 and associated neurite outgrowth is dependent on the HIKE domain of TrkA. *J Biol Chem* *280*, 225-235.
24. Yano, H., Cong, F., Birge, R.B., Goff, S.P., and Chao, M.V. (2000). Association of the Abl tyrosine kinase with the Trk nerve growth factor receptor. *J Neurosci Res* *59*, 356-364.
25. Oppenheim, R.W. (1991). Cell death during development of the nervous system. *Annu Rev Neurosci* *14*, 453-501.
26. Purves, D., Snider, W.D., and Voyvodic, J.T. (1988). Trophic regulation of nerve cell morphology and innervation in the autonomic nervous system. *Nature* *336*, 123-128.
27. Crowley, C., Spencer, S.D., Nishimura, M.C., Chen, K.S., Pitts-Meek, S., Armanini, M.P., Ling, L.H., McMahon, S.B., Shelton, D.L., Levinson, A.D., et al. (1994). Mice lacking nerve growth factor display perinatal loss of sensory and sympathetic neurons yet develop basal forebrain cholinergic neurons. *Cell* *76*, 1001-1011.
28. Minichiello, L., Piehl, F., Vazquez, E., Schimmang, T., Hokfelt, T., Represa, J., and Klein, R. (1995). Differential effects of combined trk receptor mutations on dorsal root ganglion and inner ear sensory neurons. *Development* *121*, 4067-4075.
29. Silos-Santiago, I., Molliver, D.C., Ozaki, S., Smeyne, R.J., Fagan, A.M., Barbacid, M., and Snider, W.D. (1995). Non-TrkA-expressing small DRG neurons are lost in TrkA deficient mice. *J Neurosci* *15*, 5929-5942.
30. Smeyne, R.J., Klein, R., Schnapp, A., Long, L.K., Bryant, S., Lewin, A., Lira, S.A., and Barbacid, M. (1994). Severe sensory and sympathetic neuropathies in mice carrying a disrupted Trk/NGF receptor gene. *Nature* *368*, 246-249.
31. Bianchi, L.M., Conover, J.C., Fritsch, B., DeChiara, T., Lindsay, R.M., and Yancopoulos, G.D. (1996). Degeneration of vestibular neurons in late

- embryogenesis of both heterozygous and homozygous BDNF null mutant mice. *Development* 122, 1965-1973.
32. Ernfors, P., Lee, K.F., and Jaenisch, R. (1994). Mice lacking brain-derived neurotrophic factor develop with sensory deficits. *Nature* 368, 147-150.
 33. Jones, K.R., Farinas, I., Backus, C., and Reichardt, L.F. (1994). Targeted disruption of the BDNF gene perturbs brain and sensory neuron development but not motor neuron development. *Cell* 76, 989-999.
 34. Klein, R., Smeyne, R.J., Wurst, W., Long, L.K., Auerbach, B.A., Joyner, A.L., and Barbacid, M. (1993). Targeted disruption of the trkB neurotrophin receptor gene results in nervous system lesions and neonatal death. *Cell* 75, 113-122.
 35. Liu, X., Ernfors, P., Wu, H., and Jaenisch, R. (1995). Sensory but not motor neuron deficits in mice lacking NT4 and BDNF. *Nature* 375, 238-241.
 36. Ernfors, P., Lee, K.F., Kucera, J., and Jaenisch, R. (1994). Lack of neurotrophin-3 leads to deficiencies in the peripheral nervous system and loss of limb proprioceptive afferents. *Cell* 77, 503-512.
 37. Farinas, I., Jones, K.R., Backus, C., Wang, X.Y., and Reichardt, L.F. (1994). Severe sensory and sympathetic deficits in mice lacking neurotrophin-3. *Nature* 369, 658-661.
 38. Klein, R., Silos-Santiago, I., Smeyne, R.J., Lira, S.A., Brambilla, R., Bryant, S., Zhang, L., Snider, W.D., and Barbacid, M. (1994). Disruption of the neurotrophin-3 receptor gene trkC eliminates Ia muscle afferents and results in abnormal movements. *Nature* 368, 249-251.
 39. Kucera, J., Fan, G., Jaenisch, R., Linnarsson, S., and Ernfors, P. (1995). Dependence of developing group Ia afferents on neurotrophin-3. *J Comp Neurol* 363, 307-320.
 40. Tessarollo, L., Vogel, K.S., Palko, M.E., Reid, S.W., and Parada, L.F. (1994). Targeted mutation in the neurotrophin-3 gene results in loss of muscle sensory neurons. *Proc Natl Acad Sci U S A* 91, 11844-11848.
 41. Tojo, H., Kaisho, Y., Nakata, M., Matsuoka, K., Kitagawa, M., Abe, T., Takami, K., Yamamoto, M., Shino, A., Igarashi, K., et al. (1995). Targeted disruption of the neurotrophin-3 gene with lacZ induces loss of trkC-positive neurons in sensory ganglia but not in spinal cords. *Brain Res* 669, 163-175.

42. Nikolettou, V., Lickert, H., Frade, J.M., Rencurel, C., Giallonardo, P., Zhang, L., Bibel, M., and Barde, Y.A. (2010). Neurotrophin receptors TrkA and TrkC cause neuronal death whereas TrkB does not. *Nature* 467, 59-63.
43. Mehlen, P., and Bredesen, D.E. (2004). The dependence receptor hypothesis. *Apoptosis* 9, 37-49.
44. Patel, T.D., Jackman, A., Rice, F.L., Kucera, J., and Snider, W.D. (2000). Development of sensory neurons in the absence of NGF/TrkA signaling in vivo. *Neuron* 25, 345-357.
45. Levi-Montalcini, R. (1964). Growth Control of Nerve Cells by a Protein Factor and Its Antiserum: Discovery of This Factor May Provide New Leads to Understanding of Some Neurogenetic Processes. *Science* 143, 105-110.
46. Davies, A.M., Thoenen, H., and Barde, Y.A. (1986). The response of chick sensory neurons to brain-derived neurotrophic factor. *J Neurosci* 6, 1897-1904.
47. Paves, H., and Saarma, M. (1997). Neurotrophins as in vitro growth cone guidance molecules for embryonic sensory neurons. *Cell Tissue Res* 290, 285-297.
48. Ernsberger, U. (2009). Role of neurotrophin signalling in the differentiation of neurons from dorsal root ganglia and sympathetic ganglia. *Cell Tissue Res* 336, 349-384.
49. Ming, G., Lohof, A.M., and Zheng, J.Q. (1997). Acute morphogenic and chemotropic effects of neurotrophins on cultured embryonic *Xenopus* spinal neurons. *J Neurosci* 17, 7860-7871.
50. Cohen-Cory, S., Kidane, A.H., Shirkey, N.J., and Marshak, S. (2010). Brain-derived neurotrophic factor and the development of structural neuronal connectivity. *Dev Neurobiol* 70, 271-288.
51. Schinder, A.F., and Poo, M. (2000). The neurotrophin hypothesis for synaptic plasticity. *Trends Neurosci* 23, 639-645.
52. Korte, M., Carroll, P., Wolf, E., Brem, G., Thoenen, H., and Bonhoeffer, T. (1995). Hippocampal long-term potentiation is impaired in mice lacking brain-derived neurotrophic factor. *Proc Natl Acad Sci U S A* 92, 8856-8860.

53. Minichiello, L., Korte, M., Wolfer, D., Kuhn, R., Unsicker, K., Cestari, V., Rossi-Arnaud, C., Lipp, H.P., Bonhoeffer, T., and Klein, R. (1999). Essential role for TrkB receptors in hippocampus-mediated learning. *Neuron* 24, 401-414.
54. Chen, K.S., Nishimura, M.C., Armanini, M.P., Crowley, C., Spencer, S.D., and Phillips, H.S. (1997). Disruption of a single allele of the nerve growth factor gene results in atrophy of basal forebrain cholinergic neurons and memory deficits. *J Neurosci* 17, 7288-7296.
55. Airaksinen, M.S., and Saarma, M. (2002). The GDNF family: signalling, biological functions and therapeutic value. *Nat Rev Neurosci* 3, 383-394.
56. Takahashi, M. (2001). The GDNF/RET signaling pathway and human diseases. *Cytokine Growth Factor Rev* 12, 361-373.
57. Myers, S.M., Eng, C., Ponder, B.A., and Mulligan, L.M. (1995). Characterization of RET proto-oncogene 3' splicing variants and polyadenylation sites: a novel C-terminus for RET. *Oncogene* 11, 2039-2045.
58. de Graaff, E., Srinivas, S., Kilkenny, C., D'Agati, V., Mankoo, B.S., Costantini, F., and Pachnis, V. (2001). Differential activities of the RET tyrosine kinase receptor isoforms during mammalian embryogenesis. *Genes Dev* 15, 2433-2444.
59. Iwamoto, T., Taniguchi, M., Asai, N., Ohkusu, K., Nakashima, I., and Takahashi, M. (1993). cDNA cloning of mouse ret proto-oncogene and its sequence similarity to the cadherin superfamily. *Oncogene* 8, 1087-1091.
60. Jing, S., Wen, D., Yu, Y., Holst, P.L., Luo, Y., Fang, M., Tamir, R., Antonio, L., Hu, Z., Cupples, R., et al. (1996). GDNF-induced activation of the ret protein tyrosine kinase is mediated by GDNFR-alpha, a novel receptor for GDNF. *Cell* 85, 1113-1124.
61. Kawamoto, Y., Takeda, K., Okuno, Y., Yamakawa, Y., Ito, Y., Taguchi, R., Kato, M., Suzuki, H., Takahashi, M., and Nakashima, I. (2004). Identification of RET autophosphorylation sites by mass spectrometry. *J Biol Chem* 279, 14213-14224.
62. Jijiwa, M., Fukuda, T., Kawai, K., Nakamura, A., Kurokawa, K., Murakumo, Y., Ichihara, M., and Takahashi, M. (2004). A targeting mutation of tyrosine 1062 in Ret causes a marked decrease of enteric neurons and renal hypoplasia. *Mol Cell Biol* 24, 8026-8036.

63. Wong, A., Bogni, S., Kotka, P., de Graaff, E., D'Agati, V., Costantini, F., and Pachnis, V. (2005). Phosphotyrosine 1062 is critical for the in vivo activity of the Ret9 receptor tyrosine kinase isoform. *Mol Cell Biol* 25, 9661-9673.
64. Drosten, M., and Putzer, B.M. (2006). Mechanisms of Disease: cancer targeting and the impact of oncogenic RET for medullary thyroid carcinoma therapy. *Nat Clin Pract Oncol* 3, 564-574.
65. Cacalano, G., Farinas, I., Wang, L.C., Hagler, K., Forgie, A., Moore, M., Armanini, M., Phillips, H., Ryan, A.M., Reichardt, L.F., et al. (1998). GFRalpha1 is an essential receptor component for GDNF in the developing nervous system and kidney. *Neuron* 21, 53-62.
66. Enomoto, H., Araki, T., Jackman, A., Heuckeroth, R.O., Snider, W.D., Johnson, E.M., Jr., and Milbrandt, J. (1998). GFR alpha1-deficient mice have deficits in the enteric nervous system and kidneys. *Neuron* 21, 317-324.
67. Moore, M.W., Klein, R.D., Farinas, I., Sauer, H., Armanini, M., Phillips, H., Reichardt, L.F., Ryan, A.M., Carver-Moore, K., and Rosenthal, A. (1996). Renal and neuronal abnormalities in mice lacking GDNF. *Nature* 382, 76-79.
68. Pichel, J.G., Shen, L., Sheng, H.Z., Granholm, A.C., Drago, J., Grinberg, A., Lee, E.J., Huang, S.P., Saarma, M., Hoffer, B.J., et al. (1996). Defects in enteric innervation and kidney development in mice lacking GDNF. *Nature* 382, 73-76.
69. Sanchez, M.P., Silos-Santiago, I., Frisen, J., He, B., Lira, S.A., and Barbacid, M. (1996). Renal agenesis and the absence of enteric neurons in mice lacking GDNF. *Nature* 382, 70-73.
70. Schuchardt, A., D'Agati, V., Larsson-Blomberg, L., Costantini, F., and Pachnis, V. (1994). Defects in the kidney and enteric nervous system of mice lacking the tyrosine kinase receptor Ret. *Nature* 367, 380-383.
71. Hellmich, H.L., Kos, L., Cho, E.S., Mahon, K.A., and Zimmer, A. (1996). Embryonic expression of glial cell-line derived neurotrophic factor (GDNF) suggests multiple developmental roles in neural differentiation and epithelial-mesenchymal interactions. *Mech Dev* 54, 95-105.

72. Kim, D., and Dressler, G.R. (2007). PTEN modulates GDNF/RET mediated chemotaxis and branching morphogenesis in the developing kidney. *Dev Biol* 307, 290-299.
73. Sainio, K., Suvanto, P., Davies, J., Wartiovaara, J., Wartiovaara, K., Saarma, M., Arumae, U., Meng, X., Lindahl, M., Pachnis, V., et al. (1997). Glial-cell-line-derived neurotrophic factor is required for bud initiation from ureteric epithelium. *Development* 124, 4077-4087.
74. Airaksinen, M.S., Titievsky, A., and Saarma, M. (1999). GDNF family neurotrophic factor signaling: four masters, one servant? *Mol Cell Neurosci* 13, 313-325.
75. Parisi, M.A., and Kapur, R.P. (2000). Genetics of Hirschsprung disease. *Curr Opin Pediatr* 12, 610-617.
76. Plaza-Menacho, I., Burzynski, G.M., de Groot, J.W., Eggen, B.J., and Hofstra, R.M. (2006). Current concepts in RET-related genetics, signaling and therapeutics. *Trends Genet* 22, 627-636.
77. Lin, L.F., Doherty, D.H., Lile, J.D., Bektesh, S., and Collins, F. (1993). GDNF: a glial cell line-derived neurotrophic factor for midbrain dopaminergic neurons. *Science* 260, 1130-1132.
78. Grondin, R., and Gash, D.M. (1998). Glial cell line-derived neurotrophic factor (GDNF): a drug candidate for the treatment of Parkinson's disease. *J Neurol* 245, P35-42.
79. Kramer, E.R., Aron, L., Ramakers, G.M., Seitz, S., Zhuang, X., Beyer, K., Smidt, M.P., and Klein, R. (2007). Absence of Ret signaling in mice causes progressive and late degeneration of the nigrostriatal system. *PLoS Biol* 5, e39.
80. Gould, T.W., and Enomoto, H. (2009). Neurotrophic modulation of motor neuron development. *Neuroscientist* 15, 105-116.
81. Henderson, C.E., Phillips, H.S., Pollock, R.A., Davies, A.M., Lemeulle, C., Armanini, M., Simmons, L., Moffet, B., Vandlen, R.A., Simpson, L.C., et al. (1994). GDNF: a potent survival factor for motoneurons present in peripheral nerve and muscle. *Science* 266, 1062-1064.
82. Markus, A., Patel, T.D., and Snider, W.D. (2002). Neurotrophic factors and axonal growth. *Curr Opin Neurobiol* 12, 523-531.

83. Oppenheim, R.W., Houenou, L.J., Johnson, J.E., Lin, L.F., Li, L., Lo, A.C., Newsome, A.L., Prevette, D.M., and Wang, S. (1995). Developing motor neurons rescued from programmed and axotomy-induced cell death by GDNF. *Nature* 373, 344-346.
84. Oppenheim, R.W., Houenou, L.J., Parsadanian, A.S., Prevette, D., Snider, W.D., and Shen, L. (2000). Glial cell line-derived neurotrophic factor and developing mammalian motoneurons: regulation of programmed cell death among motoneuron subtypes. *J Neurosci* 20, 5001-5011.
85. Haase, G., Dessaud, E., Garces, A., de Bovis, B., Birling, M., Filippi, P., Schmalbruch, H., Arber, S., and deLapeyriere, O. (2002). GDNF acts through PEA3 to regulate cell body positioning and muscle innervation of specific motor neuron pools. *Neuron* 35, 893-905.
86. Enomoto, H., Heuckeroth, R.O., Golden, J.P., Johnson, E.M., and Milbrandt, J. (2000). Development of cranial parasympathetic ganglia requires sequential actions of GDNF and neurturin. *Development* 127, 4877-4889.
87. Fundin, B.T., Mikaelis, A., Westphal, H., and Ernfors, P. (1999). A rapid and dynamic regulation of GDNF-family ligands and receptors correlate with the developmental dependency of cutaneous sensory innervation. *Development* 126, 2597-2610.
88. Nguyen, Q.T., Parsadanian, A.S., Snider, W.D., and Lichtman, J.W. (1998). Hyperinnervation of neuromuscular junctions caused by GDNF overexpression in muscle. *Science* 279, 1725-1729.
89. Luo, W., Wickramasinghe, S.R., Savitt, J.M., Griffin, J.W., Dawson, T.M., and Ginty, D.D. (2007). A hierarchical NGF signaling cascade controls Ret-dependent and Ret-independent events during development of nonpeptidergic DRG neurons. *Neuron* 54, 739-754.
90. Luo, W., Enomoto, H., Rice, F.L., Milbrandt, J., and Ginty, D.D. (2009). Molecular identification of rapidly adapting mechanoreceptors and their developmental dependence on ret signaling. *Neuron* 64, 841-856.

91. Ledda, F., Paratcha, G., Sandoval-Guzman, T., and Ibanez, C.F. (2007). GDNF and GFR α 1 promote formation of neuronal synapses by ligand-induced cell adhesion. *Nat Neurosci* *10*, 293-300.
92. Paratcha, G., Ledda, F., and Ibanez, C.F. (2003). The neural cell adhesion molecule NCAM is an alternative signaling receptor for GDNF family ligands. *Cell* *113*, 867-879.
93. Charoy, C., Nawabi, H., Reynaud, F., Derrington, E., Bozon, M., Wright, K., Falk, J., Helmbacher, F., Kindbeiter, K., and Castellani, V. (2012). gdnf activates midline repulsion by Semaphorin3B via NCAM during commissural axon guidance. *Neuron* *75*, 1051-1066.
94. Tsui-Pierchala, B.A., Milbrandt, J., and Johnson, E.M., Jr. (2002). NGF utilizes c-Ret via a novel GFL-independent, inter-RTK signaling mechanism to maintain the trophic status of mature sympathetic neurons. *Neuron* *33*, 261-273.
95. Bordeaux, M.C., Forcet, C., Granger, L., Corset, V., Bidaud, C., Billaud, M., Bredesen, D.E., Edery, P., and Mehlen, P. (2000). The RET proto-oncogene induces apoptosis: a novel mechanism for Hirschsprung disease. *EMBO J* *19*, 4056-4063.
96. Egea, J., and Klein, R. (2007). Bidirectional Eph-ephrin signaling during axon guidance. *Trends Cell Biol* *17*, 230-238.
97. Noren, N.K., and Pasquale, E.B. (2004). Eph receptor-ephrin bidirectional signals that target Ras and Rho proteins. *Cell Signal* *16*, 655-666.
98. Sahin, M., Greer, P.L., Lin, M.Z., Poucher, H., Eberhart, J., Schmidt, S., Wright, T.M., Shamah, S.M., O'Connell, S., Cowan, C.W., et al. (2005). Eph-dependent tyrosine phosphorylation of ephexin1 modulates growth cone collapse. *Neuron* *46*, 191-204.
99. Shamah, S.M., Lin, M.Z., Goldberg, J.L., Estrach, S., Sahin, M., Hu, L., Bazalakova, M., Neve, R.L., Corfas, G., Debant, A., et al. (2001). EphA receptors regulate growth cone dynamics through the novel guanine nucleotide exchange factor ephexin. *Cell* *105*, 233-244.
100. Fawcett, J.P., Georgiou, J., Ruston, J., Bladt, F., Sherman, A., Warner, N., Saab, B.J., Scott, R., Roder, J.C., and Pawson, T. (2007). Nck adaptor proteins control the

- organization of neuronal circuits important for walking. *Proc Natl Acad Sci U S A* *104*, 20973-20978.
101. Wegmeyer, H., Egea, J., Rabe, N., Gezelius, H., Filosa, A., Enjin, A., Varoqueaux, F., Deininger, K., Schnutgen, F., Brose, N., et al. (2007). EphA4-dependent axon guidance is mediated by the RacGAP alpha2-chimaerin. *Neuron* *55*, 756-767.
102. Cowan, C.W., Shao, Y.R., Sahin, M., Shamah, S.M., Lin, M.Z., Greer, P.L., Gao, S., Griffith, E.C., Brugge, J.S., and Greenberg, M.E. (2005). Vav family GEFs link activated Ephs to endocytosis and axon guidance. *Neuron* *46*, 205-217.
103. Murai, K.K., and Pasquale, E.B. (2005). New exchanges in eph-dependent growth cone dynamics. *Neuron* *46*, 161-163.
104. Smalla, M., Schmieder, P., Kelly, M., Ter Laak, A., Krause, G., Ball, L., Wahl, M., Bork, P., and Oschkinat, H. (1999). Solution structure of the receptor tyrosine kinase EphB2 SAM domain and identification of two distinct homotypic interaction sites. *Protein Sci* *8*, 1954-1961.
105. Stapleton, D., Balan, I., Pawson, T., and Sicheri, F. (1999). The crystal structure of an Eph receptor SAM domain reveals a mechanism for modular dimerization. *Nat Struct Biol* *6*, 44-49.
106. Wimmer-Kleikamp, S.H., Janes, P.W., Squire, A., Bastiaens, P.I., and Lackmann, M. (2004). Recruitment of Eph receptors into signaling clusters does not require ephrin contact. *J Cell Biol* *164*, 661-666.
107. Seiradake, E., Harlos, K., Sutton, G., Aricescu, A.R., and Jones, E.Y. (2010). An extracellular steric seeding mechanism for Eph-ephrin signaling platform assembly. *Nat Struct Mol Biol* *17*, 398-402.
108. Halford, M.M., Armes, J., Buchert, M., Meskenaite, V., Grail, D., Hibbs, M.L., Wilks, A.F., Farlie, P.G., Newgreen, D.F., Hovens, C.M., et al. (2000). Ryk-deficient mice exhibit craniofacial defects associated with perturbed Eph receptor crosstalk. *Nat Genet* *25*, 414-418.
109. Janes, P.W., Griesshaber, B., Atapattu, L., Nievergall, E., Hii, L.L., Mensinga, A., Chheang, C., Day, B.W., Boyd, A.W., Bastiaens, P.I., et al. (2011). Eph receptor function is modulated by heterooligomerization of A and B type Eph receptors. *J Cell Biol* *195*, 1033-1045.

110. Janes, P.W., Saha, N., Barton, W.A., Kolev, M.V., Wimmer-Kleikamp, S.H., Nievergall, E., Blobel, C.P., Himanen, J.P., Lackmann, M., and Nikolov, D.B. (2005). Adam meets Eph: an ADAM substrate recognition module acts as a molecular switch for ephrin cleavage in trans. *Cell* *123*, 291-304.
111. Trivier, E., and Ganesan, T.S. (2002). RYK, a catalytically inactive receptor tyrosine kinase, associates with EphB2 and EphB3 but does not interact with AF-6. *J Biol Chem* *277*, 23037-23043.
112. Lim, Y.S., McLaughlin, T., Sung, T.C., Santiago, A., Lee, K.F., and O'Leary, D.D. (2008). p75(NTR) mediates ephrin-A reverse signaling required for axon repulsion and mapping. *Neuron* *59*, 746-758.
113. Marler, K.J., Becker-Barroso, E., Martinez, A., Llovera, M., Wentzel, C., Poopalasundaram, S., Hindges, R., Soriano, E., Comella, J., and Drescher, U. (2008). A TrkB/EphrinA interaction controls retinal axon branching and synaptogenesis. *J Neurosci* *28*, 12700-12712.
114. Cowan, C.A., and Henkemeyer, M. (2001). The SH2/SH3 adaptor Grb4 transduces B-ephrin reverse signals. *Nature* *413*, 174-179.
115. Segura, I., Essmann, C.L., Weinges, S., and Acker-Palmer, A. (2007). Grb4 and GIT1 transduce ephrinB reverse signals modulating spine morphogenesis and synapse formation. *Nat Neurosci* *10*, 301-310.
116. Xu, N.J., and Henkemeyer, M. (2009). Ephrin-B3 reverse signaling through Grb4 and cytoskeletal regulators mediates axon pruning. *Nat Neurosci* *12*, 268-276.
117. Makinen, T., Adams, R.H., Bailey, J., Lu, Q., Ziemiecki, A., Alitalo, K., Klein, R., and Wilkinson, G.A. (2005). PDZ interaction site in ephrinB2 is required for the remodeling of lymphatic vasculature. *Genes Dev* *19*, 397-410.
118. Bruckner, K., Pablo Labrador, J., Scheiffele, P., Herb, A., Seeburg, P.H., and Klein, R. (1999). EphrinB ligands recruit GRIP family PDZ adaptor proteins into raft membrane microdomains. *Neuron* *22*, 511-524.
119. Lu, Q., Sun, E.E., Klein, R.S., and Flanagan, J.G. (2001). Ephrin-B reverse signaling is mediated by a novel PDZ-RGS protein and selectively inhibits G protein-coupled chemoattraction. *Cell* *105*, 69-79.

120. Marston, D.J., Dickinson, S., and Nobes, C.D. (2003). Rac-dependent trans-endocytosis of ephrinBs regulates Eph-ephrin contact repulsion. *Nat Cell Biol* 5, 879-888.
121. Zimmer, M., Palmer, A., Kohler, J., and Klein, R. (2003). EphB-ephrinB bidirectional endocytosis terminates adhesion allowing contact mediated repulsion. *Nat Cell Biol* 5, 869-878.
122. Lin, K.T., Sloniowski, S., Ethell, D.W., and Ethell, I.M. (2008). Ephrin-B2-induced cleavage of EphB2 receptor is mediated by matrix metalloproteinases to trigger cell repulsion. *J Biol Chem* 283, 28969-28979.
123. Hattori, M., Osterfield, M., and Flanagan, J.G. (2000). Regulated cleavage of a contact-mediated axon repellent. *Science* 289, 1360-1365.
124. Carvalho, R.F., Beutler, M., Marler, K.J., Knoll, B., Becker-Barroso, E., Heintzmann, R., Ng, T., and Drescher, U. (2006). Silencing of EphA3 through a cis interaction with ephrinA5. *Nat Neurosci* 9, 322-330.
125. Hornberger, M.R., Dutting, D., Ciossek, T., Yamada, T., Handwerker, C., Lang, S., Weth, F., Huf, J., Wessel, R., Logan, C., et al. (1999). Modulation of EphA receptor function by coexpressed ephrinA ligands on retinal ganglion cell axons. *Neuron* 22, 731-742.
126. Kao, T.J., and Kania, A. (2011). Ephrin-mediated cis-attenuation of Eph receptor signaling is essential for spinal motor axon guidance. *Neuron* 71, 76-91.
127. Yin, Y., Yamashita, Y., Noda, H., Okafuji, T., Go, M.J., and Tanaka, H. (2004). EphA receptor tyrosine kinases interact with co-expressed ephrin-A ligands in cis. *Neurosci Res* 48, 285-296.
128. Klein, R. (2012). Eph/ephrin signalling during development. *Development* 139, 4105-4109.
129. Cheng, H.J., and Flanagan, J.G. (1994). Identification and cloning of ELF-1, a developmentally expressed ligand for the Mek4 and Sek receptor tyrosine kinases. *Cell* 79, 157-168.
130. Cheng, H.J., Nakamoto, M., Bergemann, A.D., and Flanagan, J.G. (1995). Complementary gradients in expression and binding of ELF-1 and Mek4 in development of the topographic retinotectal projection map. *Cell* 82, 371-381.

131. Drescher, U., Kremoser, C., Handwerker, C., Loschinger, J., Noda, M., and Bonhoeffer, F. (1995). In vitro guidance of retinal ganglion cell axons by RAGS, a 25 kDa tectal protein related to ligands for Eph receptor tyrosine kinases. *Cell* 82, 359-370.
132. Lewin, B. (1994). On neuronal specificity and the molecular basis of perception. *Cell* 79, 935-943.
133. Udin, S.B., and Fawcett, J.W. (1988). Formation of topographic maps. *Annu Rev Neurosci* 11, 289-327.
134. Feldheim, D.A., and O'Leary, D.D. (2010). Visual map development: bidirectional signaling, bifunctional guidance molecules, and competition. *Cold Spring Harb Perspect Biol* 2, a001768.
135. Brown, A., Yates, P.A., Burrola, P., Ortuno, D., Vaidya, A., Jessell, T.M., Pfaff, S.L., O'Leary, D.D., and Lemke, G. (2000). Topographic mapping from the retina to the midbrain is controlled by relative but not absolute levels of EphA receptor signaling. *Cell* 102, 77-88.
136. Feldheim, D.A., Kim, Y.I., Bergemann, A.D., Frisen, J., Barbacid, M., and Flanagan, J.G. (2000). Genetic analysis of ephrin-A2 and ephrin-A5 shows their requirement in multiple aspects of retinocollicular mapping. *Neuron* 25, 563-574.
137. Frisen, J., Yates, P.A., McLaughlin, T., Friedman, G.C., O'Leary, D.D., and Barbacid, M. (1998). Ephrin-A5 (AL-1/RAGS) is essential for proper retinal axon guidance and topographic mapping in the mammalian visual system. *Neuron* 20, 235-243.
138. Monschau, B., Kremoser, C., Ohta, K., Tanaka, H., Kaneko, T., Yamada, T., Handwerker, C., Hornberger, M.R., Loschinger, J., Pasquale, E.B., et al. (1997). Shared and distinct functions of RAGS and ELF-1 in guiding retinal axons. *EMBO J* 16, 1258-1267.
139. Pfeiffenberger, C., Yamada, J., and Feldheim, D.A. (2006). Ephrin-As and patterned retinal activity act together in the development of topographic maps in the primary visual system. *J Neurosci* 26, 12873-12884.

140. Feldheim, D.A., Nakamoto, M., Osterfield, M., Gale, N.W., DeChiara, T.M., Rohatgi, R., Yancopoulos, G.D., and Flanagan, J.G. (2004). Loss-of-function analysis of EphA receptors in retinotectal mapping. *J Neurosci* 24, 2542-2550.
141. Rashid, T., Upton, A.L., Blentic, A., Ciossek, T., Knoll, B., Thompson, I.D., and Drescher, U. (2005). Opposing gradients of ephrin-As and EphA7 in the superior colliculus are essential for topographic mapping in the mammalian visual system. *Neuron* 47, 57-69.
142. Roskies, A.L., and O'Leary, D.D. (1994). Control of topographic retinal axon branching by inhibitory membrane-bound molecules. *Science* 265, 799-803.
143. Sakurai, T., Wong, E., Drescher, U., Tanaka, H., and Jay, D.G. (2002). Ephrin-A5 restricts topographically specific arborization in the chick retinotectal projection in vivo. *Proc Natl Acad Sci U S A* 99, 10795-10800.
144. Yates, P.A., Roskies, A.L., McLaughlin, T., and O'Leary, D.D. (2001). Topographic-specific axon branching controlled by ephrin-As is the critical event in retinotectal map development. *J Neurosci* 21, 8548-8563.
145. Lom, B., Cogen, J., Sanchez, A.L., Vu, T., and Cohen-Cory, S. (2002). Local and target-derived brain-derived neurotrophic factor exert opposing effects on the dendritic arborization of retinal ganglion cells in vivo. *J Neurosci* 22, 7639-7649.
146. Hindges, R., McLaughlin, T., Genoud, N., Henkemeyer, M., and O'Leary, D. (2002). EphB forward signaling controls directional branch extension and arborization required for dorsal-ventral retinotopic mapping. *Neuron* 35, 475-487.
147. McLaughlin, T., Hindges, R., Yates, P.A., and O'Leary, D.D. (2003). Bifunctional action of ephrin-B1 as a repellent and attractant to control bidirectional branch extension in dorsal-ventral retinotopic mapping. *Development* 130, 2407-2418.
148. Mann, F., Ray, S., Harris, W., and Holt, C. (2002). Topographic mapping in dorsoventral axis of the *Xenopus* retinotectal system depends on signaling through ephrin-B ligands. *Neuron* 35, 461-473.
149. Stanfield, B.B. (1992). The development of the corticospinal projection. *Prog Neurobiol* 38, 169-202.
150. Dottori, M., Hartley, L., Galea, M., Paxinos, G., Polizzotto, M., Kilpatrick, T., Bartlett, P.F., Murphy, M., Kontgen, F., and Boyd, A.W. (1998). EphA4 (Sek1)

- receptor tyrosine kinase is required for the development of the corticospinal tract. *Proc Natl Acad Sci U S A* *95*, 13248-13253.
151. Kullander, K., Butt, S.J., Lebret, J.M., Lundfald, L., Restrepo, C.E., Rydstrom, A., Klein, R., and Kiehn, O. (2003). Role of EphA4 and EphrinB3 in local neuronal circuits that control walking. *Science* *299*, 1889-1892.
152. Kullander, K., Mather, N.K., Diella, F., Dottori, M., Boyd, A.W., and Klein, R. (2001). Kinase-dependent and kinase-independent functions of EphA4 receptors in major axon tract formation in vivo. *Neuron* *29*, 73-84.
153. Butt, S.J., Lundfald, L., and Kiehn, O. (2005). EphA4 defines a class of excitatory locomotor-related interneurons. *Proc Natl Acad Sci U S A* *102*, 14098-14103.
154. Goulding, M., and Pfaff, S.L. (2005). Development of circuits that generate simple rhythmic behaviors in vertebrates. *Curr Opin Neurobiol* *15*, 14-20.
155. Henkemeyer, M., Orioli, D., Henderson, J.T., Saxton, T.M., Roder, J., Pawson, T., and Klein, R. (1996). Nuk controls pathfinding of commissural axons in the mammalian central nervous system. *Cell* *86*, 35-46.
156. Leighton, P.A., Mitchell, K.J., Goodrich, L.V., Lu, X., Pinson, K., Scherz, P., Skarnes, W.C., and Tessier-Lavigne, M. (2001). Defining brain wiring patterns and mechanisms through gene trapping in mice. *Nature* *410*, 174-179.
157. Contractor, A., Rogers, C., Maron, C., Henkemeyer, M., Swanson, G.T., and Heinemann, S.F. (2002). Trans-synaptic Eph receptor-ephrin signaling in hippocampal mossy fiber LTP. *Science* *296*, 1864-1869.
158. Filosa, A., Paixao, S., Honsek, S.D., Carmona, M.A., Becker, L., Feddersen, B., Gaitanos, L., Rudhard, Y., Schoepfer, R., Klopstock, T., et al. (2009). Neuron-glia communication via EphA4/ephrin-A3 modulates LTP through glial glutamate transport. *Nat Neurosci* *12*, 1285-1292.
159. Grunwald, I.C., Korte, M., Adelman, G., Plueck, A., Kullander, K., Adams, R.H., Frotscher, M., Bonhoeffer, T., and Klein, R. (2004). Hippocampal plasticity requires postsynaptic ephrinBs. *Nat Neurosci* *7*, 33-40.
160. Grunwald, I.C., Korte, M., Wolfer, D., Wilkinson, G.A., Unsicker, K., Lipp, H.P., Bonhoeffer, T., and Klein, R. (2001). Kinase-independent requirement of EphB2 receptors in hippocampal synaptic plasticity. *Neuron* *32*, 1027-1040.

161. Henderson, J.T., Georgiou, J., Jia, Z., Robertson, J., Elowe, S., Roder, J.C., and Pawson, T. (2001). The receptor tyrosine kinase EphB2 regulates NMDA-dependent synaptic function. *Neuron* 32, 1041-1056.
162. Erzurumlu, R.S., Chen, Z.F., and Jacquin, M.F. (2006). Molecular determinants of the face map development in the trigeminal brainstem. *Anat Rec A Discov Mol Cell Evol Biol* 288, 121-134.
163. Davies, A.M. (1997). Studies of neurotrophin biology in the developing trigeminal system. *J Anat* 191 (Pt 4), 483-491.
164. Buchman, V.L., and Davies, A.M. (1993). Different neurotrophins are expressed and act in a developmental sequence to promote the survival of embryonic sensory neurons. *Development* 118, 989-1001.
165. Pinon, L.G., Minichiello, L., Klein, R., and Davies, A.M. (1996). Timing of neuronal death in trkA, trkB and trkC mutant embryos reveals developmental changes in sensory neuron dependence on Trk signalling. *Development* 122, 3255-3261.
166. Davies, A.M. (1989). Intrinsic differences in the growth rate of early nerve fibres related to target distance. *Nature* 337, 553-555.
167. Arumae, U., Pirvola, U., Palgi, J., Kiema, T.R., Palm, K., Moshnyakov, M., Ylikoski, J., and Saarma, M. (1993). Neurotrophins and their receptors in rat peripheral trigeminal system during maxillary nerve growth. *J Cell Biol* 122, 1053-1065.
168. Davies, A.M., Bandtlow, C., Heumann, R., Korsching, S., Rohrer, H., and Thoenen, H. (1987). Timing and site of nerve growth factor synthesis in developing skin in relation to innervation and expression of the receptor. *Nature* 326, 353-358.
169. Harper, S., and Davies, A.M. (1990). NGF mRNA expression in developing cutaneous epithelium related to innervation density. *Development* 110, 515-519.
170. Ulupinar, E., Jacquin, M.F., and Erzurumlu, R.S. (2000). Differential effects of NGF and NT-3 on embryonic trigeminal axon growth patterns. *J Comp Neurol* 425, 202-218.
171. Trupp, M., Ryden, M., Jornvall, H., Funakoshi, H., Timmusk, T., Arenas, E., and Ibanez, C.F. (1995). Peripheral expression and biological activities of GDNF, a new

- neurotrophic factor for avian and mammalian peripheral neurons. *J Cell Biol* 130, 137-148.
172. Luukko, K., Saarma, M., and Thesleff, I. (1998). Neurturin mRNA expression suggests roles in trigeminal innervation of the first branchial arch and in tooth formation. *Dev Dyn* 213, 207-219.
173. Golden, J.P., DeMaro, J.A., Osborne, P.A., Milbrandt, J., and Johnson, E.M., Jr. (1999). Expression of neurturin, GDNF, and GDNF family-receptor mRNA in the developing and mature mouse. *Exp Neurol* 158, 504-528.
174. Schwarz, Q., Vieira, J.M., Howard, B., Eickholt, B.J., and Ruhrberg, C. (2008). Neuropilin 1 and 2 control cranial gangliogenesis and axon guidance through neural crest cells. *Development* 135, 1605-1613.
175. Taniguchi, M., Yuasa, S., Fujisawa, H., Naruse, I., Saga, S., Mishina, M., and Yagi, T. (1997). Disruption of semaphorin III/D gene causes severe abnormality in peripheral nerve projection. *Neuron* 19, 519-530.
176. Kitsukawa, T., Shimizu, M., Sanbo, M., Hirata, T., Taniguchi, M., Bekku, Y., Yagi, T., and Fujisawa, H. (1997). Neuropilin-semaphorin III/D-mediated chemorepulsive signals play a crucial role in peripheral nerve projection in mice. *Neuron* 19, 995-1005.
177. Ma, L., and Tessier-Lavigne, M. (2007). Dual branch-promoting and branch-repelling actions of Slit/Robo signaling on peripheral and central branches of developing sensory axons. *J Neurosci* 27, 6843-6851.
178. Luukko, K., Loes, S., Kvinnsland, I.H., and Kettunen, P. (2005). Expression of ephrin-A ligands and EphA receptors in the developing mouse tooth and its supporting tissues. *Cell Tissue Res* 319, 143-152.
179. North, H.A., Karim, A., Jacquin, M.F., and Donoghue, M.J. (2010). EphA4 is necessary for spatially selective peripheral somatosensory topography. *Dev Dyn* 239, 630-638.
180. Bentley, C.A., and Lee, K.F. (2000). p75 is important for axon growth and schwann cell migration during development. *J Neurosci* 20, 7706-7715.

181. Lance-Jones, C., and Landmesser, L. (1981). Pathway selection by chick lumbosacral motoneurons during normal development. *Proc R Soc Lond B Biol Sci* *214*, 1-18.
182. Landmesser, L. (1978). The development of motor projection patterns in the chick hind limb. *J Physiol* *284*, 391-414.
183. Kania, A., and Jessell, T.M. (2003). Topographic motor projections in the limb imposed by LIM homeodomain protein regulation of ephrin-A:EphA interactions. *Neuron* *38*, 581-596.
184. Luria, V., Krawchuk, D., Jessell, T.M., Laufer, E., and Kania, A. (2008). Specification of motor axon trajectory by ephrin-B:EphB signaling: symmetrical control of axonal patterning in the developing limb. *Neuron* *60*, 1039-1053.
185. Kania, A., Johnson, R.L., and Jessell, T.M. (2000). Coordinate roles for LIM homeobox genes in directing the dorsoventral trajectory of motor axons in the vertebrate limb. *Cell* *102*, 161-173.
186. Eberhart, J., Swartz, M.E., Koblar, S.A., Pasquale, E.B., and Krull, C.E. (2002). EphA4 constitutes a population-specific guidance cue for motor neurons. *Dev Biol* *247*, 89-101.
187. Helmbacher, F., Schneider-Maunoury, S., Topilko, P., Tiret, L., and Charnay, P. (2000). Targeting of the EphA4 tyrosine kinase receptor affects dorsal/ventral pathfinding of limb motor axons. *Development* *127*, 3313-3324.
188. Eberhart, J., Swartz, M., Koblar, S.A., Pasquale, E.B., Tanaka, H., and Krull, C.E. (2000). Expression of EphA4, ephrin-A2 and ephrin-A5 during axon outgrowth to the hindlimb indicates potential roles in pathfinding. *Dev Neurosci* *22*, 237-250.
189. Iwamasa, H., Ohta, K., Yamada, T., Ushijima, K., Terasaki, H., and Tanaka, H. (1999). Expression of Eph receptor tyrosine kinases and their ligands in chick embryonic motor neurons and hindlimb muscles. *Dev Growth Differ* *41*, 685-698.
190. Marquardt, T., Shirasaki, R., Ghosh, S., Andrews, S.E., Carter, N., Hunter, T., and Pfaff, S.L. (2005). Coexpressed EphA receptors and ephrin-A ligands mediate opposing actions on growth cone navigation from distinct membrane domains. *Cell* *121*, 127-139.

191. Dudanova, I., Kao, T.J., Herrmann, J.E., Zheng, B., Kania, A., and Klein, R. (2012). Genetic evidence for a contribution of EphA:ephrinA reverse signaling to motor axon guidance. *J Neurosci* 32, 5209-5215.
192. Inoue, E., Deguchi-Tawarada, M., Togawa, A., Matsui, C., Arita, K., Katahira-Tayama, S., Sato, T., Yamauchi, E., Oda, Y., and Takai, Y. (2009). Synaptic activity prompts gamma-secretase-mediated cleavage of EphA4 and dendritic spine formation. *J Cell Biol* 185, 551-564.
193. Oricchio, E., Nanjangud, G., Wolfe, A.L., Schatz, J.H., Mavrakis, K.J., Jiang, M., Liu, X., Bruno, J., Heguy, A., Olshen, A.B., et al. (2011). The Eph-receptor A7 is a soluble tumor suppressor for follicular lymphoma. *Cell* 147, 554-564.
194. Bonanomi, D., and Pfaff, S.L. (2010). Motor axon pathfinding. *Cold Spring Harb Perspect Biol* 2, a001735.
195. Ebens, A., Brose, K., Leonardo, E.D., Hanson, M.G., Jr., Bladt, F., Birchmeier, C., Barres, B.A., and Tessier-Lavigne, M. (1996). Hepatocyte growth factor/scatter factor is an axonal chemoattractant and a neurotrophic factor for spinal motor neurons. *Neuron* 17, 1157-1172.
196. Kramer, E.R., Knott, L., Su, F., Dessaud, E., Krull, C.E., Helmbacher, F., and Klein, R. (2006). Cooperation between GDNF/Ret and ephrinA/EphA4 signals for motor-axon pathway selection in the limb. *Neuron* 50, 35-47.
197. Huber, A.B., Kania, A., Tran, T.S., Gu, C., De Marco Garcia, N., Lieberam, I., Johnson, D., Jessell, T.M., Ginty, D.D., and Kolodkin, A.L. (2005). Distinct roles for secreted semaphorin signaling in spinal motor axon guidance. *Neuron* 48, 949-964.
198. Kao, T.J., Palmesino, E., and Kania, A. (2009). SRC family kinases are required for limb trajectory selection by spinal motor axons. *J Neurosci* 29, 5690-5700.
199. O'Donnell, M., Chance, R.K., and Bashaw, G.J. (2009). Axon growth and guidance: receptor regulation and signal transduction. *Annu Rev Neurosci* 32, 383-412.
200. Boutilier, J., Ceni, C., Pagdala, P.C., Forgie, A., Neet, K.E., and Barker, P.A. (2008). Proneurotrophins require endocytosis and intracellular proteolysis to induce TrkA activation. *J Biol Chem* 283, 12709-12716.
201. Sadowski, L., Pilecka, I., and Miaczynska, M. (2009). Signaling from endosomes: location makes a difference. *Exp Cell Res* 315, 1601-1609.

202. Bernadskaya, Y.Y., Wallace, A., Nguyen, J., Mohler, W.A., and Soto, M.C. (2012). UNC-40/DCC, SAX-3/Robo, and VAB-1/Eph polarize F-actin during embryonic morphogenesis by regulating the WAVE/SCAR actin nucleation complex. *PLoS Genet* 8, e1002863.
203. Mandai, K., Guo, T., St Hillaire, C., Meabon, J.S., Kanning, K.C., Bothwell, M., and Ginty, D.D. (2009). LIG family receptor tyrosine kinase-associated proteins modulate growth factor signals during neural development. *Neuron* 63, 614-627.
204. Ledda, F., Bieraugel, O., Fard, S.S., Vilar, M., and Paratcha, G. (2008). Lrig1 is an endogenous inhibitor of Ret receptor tyrosine kinase activation, downstream signaling, and biological responses to GDNF. *J Neurosci* 28, 39-49.
205. Johnson, K.G., and Van Vactor, D. (2003). Receptor protein tyrosine phosphatases in nervous system development. *Physiol Rev* 83, 1-24.
206. Pot, D.A., Woodford, T.A., Remboutsika, E., Haun, R.S., and Dixon, J.E. (1991). Cloning, bacterial expression, purification, and characterization of the cytoplasmic domain of rat LAR, a receptor-like protein tyrosine phosphatase. *J Biol Chem* 266, 19688-19696.
207. Streuli, M., Krueger, N.X., Thai, T., Tang, M., and Saito, H. (1990). Distinct functional roles of the two intracellular phosphatase like domains of the receptor-linked protein tyrosine phosphatases LCA and LAR. *EMBO J* 9, 2399-2407.
208. Pot, D.A., and Dixon, J.E. (1992). Active site labeling of a receptor-like protein tyrosine phosphatase. *J Biol Chem* 267, 140-143.
209. Kurihara, D., and Yamashita, T. (2012). Chondroitin sulfate proteoglycans downregulate spine formation in cortical neurons by targeting tropomyosin-related kinase B (TrkB). *J Biol Chem*.
210. Yang, T., Massa, S.M., and Longo, F.M. (2006). LAR protein tyrosine phosphatase receptor associates with TrkB and modulates neurotrophic signaling pathways. *J Neurobiol* 66, 1420-1436.
211. Faux, C., Hawadle, M., Nixon, J., Wallace, A., Lee, S., Murray, S., and Stoker, A. (2007). PTPsigma binds and dephosphorylates neurotrophin receptors and can suppress NGF-dependent neurite outgrowth from sensory neurons. *Biochim Biophys Acta* 1773, 1689-1700.

212. Wallace, M.J., Batt, J., Fladd, C.A., Henderson, J.T., Skarnes, W., and Rotin, D. (1999). Neuronal defects and posterior pituitary hypoplasia in mice lacking the receptor tyrosine phosphatase PTPsigma. *Nat Genet* 21, 334-338.
213. Yeo, T.T., Yang, T., Massa, S.M., Zhang, J.S., Honkaniemi, J., Butcher, L.L., and Longo, F.M. (1997). Deficient LAR expression decreases basal forebrain cholinergic neuronal size and hippocampal cholinergic innervation. *J Neurosci Res* 47, 348-360.
214. Shintani, T., and Noda, M. (2008). Protein tyrosine phosphatase receptor type Z dephosphorylates TrkA receptors and attenuates NGF-dependent neurite outgrowth of PC12 cells. *J Biochem* 144, 259-266.
215. Poliakov, A., Cotrina, M.L., Pasini, A., and Wilkinson, D.G. (2008). Regulation of EphB2 activation and cell repulsion by feedback control of the MAPK pathway. *J Cell Biol* 183, 933-947.
216. Harrington, R.J., Gutch, M.J., Hengartner, M.O., Tonks, N.K., and Chisholm, A.D. (2002). The *C. elegans* LAR-like receptor tyrosine phosphatase PTP-3 and the VAB-1 Eph receptor tyrosine kinase have partly redundant functions in morphogenesis. *Development* 129, 2141-2153.
217. Stepanek, L., Sun, Q.L., Wang, J., Wang, C., and Bixby, J.L. (2001). CRYP-2/cPTPRO is a neurite inhibitory repulsive guidance cue for retinal neurons in vitro. *J Cell Biol* 154, 867-878.
218. Gonzalez-Brito, M.R., and Bixby, J.L. (2009). Protein tyrosine phosphatase receptor type O regulates development and function of the sensory nervous system. *Mol Cell Neurosci* 42, 458-465.
219. Shintani, T., Ihara, M., Sakuta, H., Takahashi, H., Watakabe, I., and Noda, M. (2006). Eph receptors are negatively controlled by protein tyrosine phosphatase receptor type O. *Nat Neurosci* 9, 761-769.
220. Hower, A.E., Beltran, P.J., and Bixby, J.L. (2009). Dimerization of tyrosine phosphatase PTPRO decreases its activity and ability to inactivate TrkC. *J Neurochem* 110, 1635-1647.
221. Stepanek, L., Stoker, A.W., Stoeckli, E., and Bixby, J.L. (2005). Receptor tyrosine phosphatases guide vertebrate motor axons during development. *J Neurosci* 25, 3813-3823.

222. Puente, X.S., Sanchez, L.M., Overall, C.M., and Lopez-Otin, C. (2003). Human and mouse proteases: a comparative genomic approach. *Nat Rev Genet* 4, 544-558.
223. Bai, G., and Pfaff, S.L. (2011). Protease regulation: the Yin and Yang of neural development and disease. *Neuron* 72, 9-21.
224. Galko, M.J., and Tessier-Lavigne, M. (2000). Function of an axonal chemoattractant modulated by metalloprotease activity. *Science* 289, 1365-1367.
225. Chedotal, A. (2011). Further tales of the midline. *Curr Opin Neurobiol* 21, 68-75.
226. Nawabi, H., Briancon-Marjollet, A., Clark, C., Sanyas, I., Takamatsu, H., Okuno, T., Kumanogoh, A., Bozon, M., Takeshima, K., Yoshida, Y., et al. (2010). A midline switch of receptor processing regulates commissural axon guidance in vertebrates. *Genes Dev* 24, 396-410.
227. Deheuninck, J., Foveau, B., Goormachtigh, G., Leroy, C., Ji, Z., Tulasne, D., and Fafeur, V. (2008). Caspase cleavage of the MET receptor generates an HGF interfering fragment. *Biochem Biophys Res Commun* 367, 573-577.
228. Litterst, C., Georgakopoulos, A., Shioi, J., Ghersi, E., Wisniewski, T., Wang, R., Ludwig, A., and Robakis, N.K. (2007). Ligand binding and calcium influx induce distinct ectodomain/gamma-secretase-processing pathways of EphB2 receptor. *J Biol Chem* 282, 16155-16163.
229. Charron, F., Stein, E., Jeong, J., McMahon, A.P., and Tessier-Lavigne, M. (2003). The morphogen sonic hedgehog is an axonal chemoattractant that collaborates with netrin-1 in midline axon guidance. *Cell* 113, 11-23.
230. Long, H., Sabatier, C., Ma, L., Plump, A., Yuan, W., Ornitz, D.M., Tamada, A., Murakami, F., Goodman, C.S., and Tessier-Lavigne, M. (2004). Conserved roles for Slit and Robo proteins in midline commissural axon guidance. *Neuron* 42, 213-223.
231. Ruiz de Almodovar, C., Fabre, P.J., Knevels, E., Coulon, C., Segura, I., Haddick, P.C., Aerts, L., Delattin, N., Strasser, G., Oh, W.J., et al. (2011). VEGF mediates commissural axon chemoattraction through its receptor Flk1. *Neuron* 70, 966-978.
232. Serafini, T., Colamarino, S.A., Leonardo, E.D., Wang, H., Beddington, R., Skarnes, W.C., and Tessier-Lavigne, M. (1996). Netrin-1 is required for commissural axon guidance in the developing vertebrate nervous system. *Cell* 87, 1001-1014.

233. Stein, E., and Tessier-Lavigne, M. (2001). Hierarchical organization of guidance receptors: silencing of netrin attraction by slit through a Robo/DCC receptor complex. *Science* *291*, 1928-1938.
234. Gore, B.B., Wong, K.G., and Tessier-Lavigne, M. (2008). Stem cell factor functions as an outgrowth-promoting factor to enable axon exit from the midline intermediate target. *Neuron* *57*, 501-510.
235. Kotani, T., Murata, Y., Ohnishi, H., Mori, M., Kusakari, S., Saito, Y., Okazawa, H., Bixby, J.L., and Matozaki, T. (2010). Expression of PTPRO in the interneurons of adult mouse olfactory bulb. *J Comp Neurol* *518*, 119-136.
236. Marmigere, F., and Ernfors, P. (2007). Specification and connectivity of neuronal subtypes in the sensory lineage. *Nat Rev Neurosci* *8*, 114-127.
237. Beltran, P.J., Bixby, J.L., and Masters, B.A. (2003). Expression of PTPRO during mouse development suggests involvement in axonogenesis and differentiation of NT-3 and NGF-dependent neurons. *J Comp Neurol* *456*, 384-395.
238. Gutierrez, H., and Davies, A.M. (2007). A fast and accurate procedure for deriving the Sholl profile in quantitative studies of neuronal morphology. *J Neurosci Methods* *163*, 24-30.
239. Conti, A.M., Brimijoin, S., Miller, L.J., and Windebank, A.J. (2004). Suppression of neurite outgrowth by high-dose nerve growth factor is independent of functional p75NTR receptors. *Neurobiol Dis* *15*, 106-114.
240. Huang, E.J., Wilkinson, G.A., Farinas, I., Backus, C., Zang, K., Wong, S.L., and Reichardt, L.F. (1999). Expression of Trk receptors in the developing mouse trigeminal ganglion: in vivo evidence for NT-3 activation of TrkA and TrkB in addition to TrkC. *Development* *126*, 2191-2203.
241. Huang, E.J., Zang, K., Schmidt, A., Saulys, A., Xiang, M., and Reichardt, L.F. (1999). POU domain factor Brn-3a controls the differentiation and survival of trigeminal neurons by regulating Trk receptor expression. *Development* *126*, 2869-2882.
242. Encinas, M., Rozen, E.J., Dolcet, X., Jain, S., Comella, J.X., Milbrandt, J., and Johnson, E.M., Jr. (2008). Analysis of Ret knockin mice reveals a critical role for

- IKKs, but not PI 3-K, in neurotrophic factor-induced survival of sympathetic neurons. *Cell Death Differ* *15*, 1510-1521.
243. Wichterle, H., Lieberam, I., Porter, J.A., and Jessell, T.M. (2002). Directed differentiation of embryonic stem cells into motor neurons. *Cell* *110*, 385-397.
244. Yamagishi, S., Hampel, F., Hata, K., Del Toro, D., Schwark, M., Kvachnina, E., Bastmeyer, M., Yamashita, T., Tarabykin, V., Klein, R., et al. (2011). FLRT2 and FLRT3 act as repulsive guidance cues for Unc5-positive neurons. *EMBO J* *30*, 2920-2933.
245. Yam, P.T., Langlois, S.D., Morin, S., and Charron, F. (2009). Sonic hedgehog guides axons through a noncanonical, Src-family-kinase-dependent signaling pathway. *Neuron* *62*, 349-362.
246. Coles, C.H., Shen, Y., Tenney, A.P., Siebold, C., Sutton, G.C., Lu, W., Gallagher, J.T., Jones, E.Y., Flanagan, J.G., and Aricescu, A.R. (2011). Proteoglycan-specific molecular switch for RPTPsigma clustering and neuronal extension. *Science* *332*, 484-488.
247. Kim, M., Kim, H., and Jho, E.H. (2010). Identification of ptpro as a novel target gene of Wnt signaling and its potential role as a receptor for Wnt. *FEBS Lett* *584*, 3923-3928.
248. Murata, Y., Mori, M., Kotani, T., Supriatna, Y., Okazawa, H., Kusakari, S., Saito, Y., Ohnishi, H., and Matozaki, T. (2010). Tyrosine phosphorylation of R3 subtype receptor-type protein tyrosine phosphatases and their complex formations with Grb2 or Fyn. *Genes Cells* *15*, 513-524.
249. Wang, F., Wolfson, S.N., Gharib, A., and Sagasti, A. (2012). LAR receptor tyrosine phosphatases and HSPGs guide peripheral sensory axons to the skin. *Curr Biol* *22*, 373-382.
250. Stepanek, L., Sun, Q.L., Wang, J., Wang, C., and Bixby, J.L. (2001). CRYP-2/cPTPRO is a neurite inhibitory repulsive guidance cue for retinal neurons in vitro. *The Journal of cell biology* *154*, 867-878.
251. Blume-Jensen, P., and Hunter, T. (2001). Oncogenic kinase signalling. *Nature* *411*, 355-365.

252. Motiwala, T., Ghoshal, K., Das, A., Majumder, S., Weichenhan, D., Wu, Y.Z., Holman, K., James, S.J., Jacob, S.T., and Plass, C. (2003). Suppression of the protein tyrosine phosphatase receptor type O gene (PTPRO) by methylation in hepatocellular carcinomas. *Oncogene* 22, 6319-6331.
253. Motiwala, T., Kutay, H., Ghoshal, K., Bai, S., Seimiya, H., Tsuruo, T., Suster, S., Morrison, C., and Jacob, S.T. (2004). Protein tyrosine phosphatase receptor-type O (PTPRO) exhibits characteristics of a candidate tumor suppressor in human lung cancer. *Proc Natl Acad Sci U S A* 101, 13844-13849.
254. van Doorn, R., Zoutman, W.H., Dijkman, R., de Menezes, R.X., Commandeur, S., Mulder, A.A., van der Velden, P.A., Vermeer, M.H., Willemze, R., Yan, P.S., et al. (2005). Epigenetic profiling of cutaneous T-cell lymphoma: promoter hypermethylation of multiple tumor suppressor genes including BCL7a, PTPRG, and p73. *J Clin Oncol* 23, 3886-3896.
255. Wang, Z., Shen, D., Parsons, D.W., Bardelli, A., Sager, J., Szabo, S., Ptak, J., Silliman, N., Peters, B.A., van der Heijden, M.S., et al. (2004). Mutational analysis of the tyrosine phosphatome in colorectal cancers. *Science* 304, 1164-1166.
256. Aron, L., Klein, P., Pham, T.T., Kramer, E.R., Wurst, W., and Klein, R. (2010). Pro-survival role for Parkinson's associated gene DJ-1 revealed in trophically impaired dopaminergic neurons. *PLoS Biol* 8, e1000349.
257. Kowsky, S., Poppelmeyer, C., Kramer, E.R., Falkenburger, B.H., Kruse, A., Klein, R., and Schulz, J.B. (2007). RET signaling does not modulate MPTP toxicity but is required for regeneration of dopaminergic axon terminals. *Proc Natl Acad Sci U S A* 104, 20049-20054.
258. Coleman, H.A., Labrador, J.P., Chance, R.K., and Bashaw, G.J. (2010). The Adam family metalloprotease Kuzbanian regulates the cleavage of the roundabout receptor to control axon repulsion at the midline. *Development* 137, 2417-2426.
259. Schimmelpfeng, K., Gogel, S., and Klambt, C. (2001). The function of leak and kuzbanian during growth cone and cell migration. *Mech Dev* 106, 25-36.
260. Miller, C.M., Page-McCaw, A., and Broihier, H.T. (2008). Matrix metalloproteinases promote motor axon fasciculation in the *Drosophila* embryo. *Development* 135, 95-109.

261. Bai, G., Chivatakarn, O., Bonanomi, D., Lettieri, K., Franco, L., Xia, C., Stein, E., Ma, L., Lewcock, J.W., and Pfaff, S.L. (2011). Presenilin-dependent receptor processing is required for axon guidance. *Cell* *144*, 106-118.
262. Donoviel, D.B., Hadjantonakis, A.K., Ikeda, M., Zheng, H., Hyslop, P.S., and Bernstein, A. (1999). Mice lacking both presenilin genes exhibit early embryonic patterning defects. *Genes Dev* *13*, 2801-2810.
263. Parent, A.T., Barnes, N.Y., Taniguchi, Y., Thinakaran, G., and Sisodia, S.S. (2005). Presenilin attenuates receptor-mediated signaling and synaptic function. *J Neurosci* *25*, 1540-1549.
264. Taniguchi, Y., Kim, S.H., and Sisodia, S.S. (2003). Presenilin-dependent "gamma-secretase" processing of deleted in colorectal cancer (DCC). *J Biol Chem* *278*, 30425-30428.
265. Hall, A., and Lalli, G. (2010). Rho and Ras GTPases in axon growth, guidance, and branching. *Cold Spring Harb Perspect Biol* *2*, a001818.
266. Journey, W.M., Gallo, G., Letourneau, P.C., and McLoon, S.C. (2002). Rac1-mediated endocytosis during ephrin-A2- and semaphorin 3A-induced growth cone collapse. *J Neurosci* *22*, 6019-6028.
267. Spitzer, N.C. (2006). Electrical activity in early neuronal development. *Nature* *444*, 707-712.
268. Hanson, M.G., and Landmesser, L.T. (2004). Normal patterns of spontaneous activity are required for correct motor axon guidance and the expression of specific guidance molecules. *Neuron* *43*, 687-701.
269. Kastanenka, K.V., and Landmesser, L.T. (2010). In vivo activation of channelrhodopsin-2 reveals that normal patterns of spontaneous activity are required for motoneuron guidance and maintenance of guidance molecules. *J Neurosci* *30*, 10575-10585.
270. Marek, K.W., Kurtz, L.M., and Spitzer, N.C. (2010). cJun integrates calcium activity and *tlx3* expression to regulate neurotransmitter specification. *Nat Neurosci* *13*, 944-950.
271. Nateri, A.S., Raivich, G., Gebhardt, C., Da Costa, C., Naumann, H., Vreugdenhil, M., Makwana, M., Brandner, S., Adams, R.H., Jefferys, J.G., et al. (2007). ERK

- activation causes epilepsy by stimulating NMDA receptor activity. *EMBO J* 26, 4891-4901.
272. Nicol, X., Voyatzis, S., Muzerelle, A., Narboux-Neme, N., Sudhof, T.C., Miles, R., and Gaspar, P. (2007). cAMP oscillations and retinal activity are permissive for ephrin signaling during the establishment of the retinotopic map. *Nat Neurosci* 10, 340-347.
273. De Strooper, B. (2003). Aph-1, Pen-2, and Nicastrin with Presenilin generate an active gamma-Secretase complex. *Neuron* 38, 9-12.
274. Walsh, D.M., and Selkoe, D.J. (2004). Deciphering the molecular basis of memory failure in Alzheimer's disease. *Neuron* 44, 181-193.
275. Zhao, L., Ma, Q.L., Calon, F., Harris-White, M.E., Yang, F., Lim, G.P., Morihara, T., Ubeda, O.J., Ambegaokar, S., Hansen, J.E., et al. (2006). Role of p21-activated kinase pathway defects in the cognitive deficits of Alzheimer disease. *Nat Neurosci* 9, 234-242.
276. Morris, R.G., Moser, E.I., Riedel, G., Martin, S.J., Sandin, J., Day, M., and O'Carroll, C. (2003). Elements of a neurobiological theory of the hippocampus: the role of activity-dependent synaptic plasticity in memory. *Philos Trans R Soc Lond B Biol Sci* 358, 773-786.
277. Beart, P.M., and O'Shea, R.D. (2007). Transporters for L-glutamate: an update on their molecular pharmacology and pathological involvement. *Br J Pharmacol* 150, 5-17.
278. Halassa, M.M., Fellin, T., and Haydon, P.G. (2007). The tripartite synapse: roles for gliotransmission in health and disease. *Trends Mol Med* 13, 54-63.
279. Bonanomi, D., Chivatakarn, O., Bai, G., Abdesselem, H., Lettieri, K., Marquardt, T., Pierchala, B.A., and Pfaff, S.L. (2012). Ret is a multifunctional coreceptor that integrates diffusible- and contact-axon guidance signals. *Cell* 148, 568-582.
280. Lallemand, Y., Luria, V., Haffner-Krausz, R., and Lonai, P. (1998). Maternally expressed PGK-Cre transgene as a tool for early and uniform activation of the Cre site-specific recombinase. *Transgenic Res* 7, 105-112.
281. Wharram, B.L., Goyal, M., Gillespie, P.J., Wiggins, J.E., Kershaw, D.B., Holzman, L.B., Dysko, R.C., Saunders, T.L., Samuelson, L.C., and Wiggins, R.C. (2000).

Altered podocyte structure in GLEPP1 (P_tpro)-deficient mice associated with hypertension and low glomerular filtration rate. *J Clin Invest* *106*, 1281-1290.

6. Curriculum vitae

PERSONAL DATA

Name Graziana Gatto
Nationality Italian
Date of birth September 22nd, 1984
Place of birth Vallo della Lucania, Italy

EDUCATION

Sep 2008 - Present International Max Planck Research School for Molecular and Cellular Life Sciences, Munich, Germany.

Sep 2008 - Present PhD student position at the Max Planck Institute of Neurobiology, Martinsried, Germany.

July 2008 Master degree in Medical Biotechnology, *summa cum laude*, University of Naples “Federico II”, Italy.

July 2006 Bachelor degree in Biotechnology for healthcare, *summa cum laude*, University of Naples “Federico II”, Italy.

RESEARCH EXPERIENCE

Sep 2008 - Present

Max Planck Institute of Neurobiology, Martinsried, Germany
Position PhD student
PI Prof. Rüdiger Klein
Project Molecular mechanisms of axon guidance

Sep 2006 – August 2008

Department of Biochemistry and Molecular Biology (DBBM), University of Naples, Italy
Position Master student
PI Prof. Stefano Bonatti
Dr. Massimo Mallardo
Project The Epstein-Barr Virus Latent Membrane Protein 1 (LMP1) trans-activates miR-155 expression through NF- κ B

July 2007 – October 2007

MRC-Laboratory of Molecular Biology, Cell Biology Division, Cambridge, United Kingdom
Position Summer student
PI Dr. Simon Bullock
Project Elucidate the molecular function of the mRNA transport machinery in *Drosophila*

Sep 2005 – Jul 2006

Department of Biochemistry and Molecular Biology (DBBM), University of Naples, Italy

Position Bachelor student

PI Prof. Stefano Bonatti

Dr. Massimo Mallardo

Project Northern Blot validation of microarray data from a promyelocytic cell line treated and untreated with retinoic acid

TEACHING EXPERIENCE

Feb 2012 – Mar 2012 Supervisor of an undergraduate student taking part in the exchange program “Münchener Halbjahr” organized by the Max Planck Institute of Biochemistry

Aug 2011 – Sep 2011 Supervisor of an intern student

PUBLICATIONS

Gatto G, Dudanova I, Suetterlin P, Davies AM, Drescher U, Bixby JL, Klein R (2013) “Protein Tyrosine Phosphatase Receptor Type O Inhibits Trigeminal Axon Growth and Branching by Repressing TrkB and Ret Signaling”. *J.Neurosci* 33(12):5399-410

Dudanova I, **Gatto G**, Klein R (2010) “GDNF acts as a chemoattractant to support ephrinA-induced repulsion of limb motor axons”. *Current Biology* 20: 2150-6

Bianco A, Dienstbier M, Salter HK, **Gatto G**, Bullock SL (2010) “Bicaudal-D regulates fragile X mental retardation protein levels, motility, and function during neuronal morphogenesis”. *Current Biology* 16: 1487-92

Rossi A, D’Urso OF, **Gatto G**, Poltronieri P, Ferracin M, Remondelli P, Negrini M, Caporaso MG, Bonatti S, Mallardo M (2010) “Non-coding RNAs change their expression profile after Retinoid induced differentiation of the promyelocytic cell line NB4”. *BMC research note* 3: 24

Gatto G*, Rossi A*, Rossi D, Kroening S, Bonatti S, Mallardo M (2008) “Epstein-Barr virus latent membrane protein 1 trans-activates miR-155 transcription through the NF-kappaB pathway” *Nucleic Acid Research* 20: 6608-6619 *equal contribution